



**LOW DIMENSIONAL Ti-OXIDE BASED
STRUCTURES: SURFACES, INTERFACES
AND ULTRATHIN FILMS OF
SrTiO₃ AND TiO₂**

Milan Radović

**Supervisor:
Dr Fabio Miletto Granozio**



TABLE OF CONTENTS

<u>I INTRODUCTION</u>	1
1.1 BACKGROUND, MOTIVATIONS AND AIMS.....	1
References.....	7
1.2 PROPERTIES OF STO.....	9
1.2.1 Crustal Structure of SrTiO ₃	7
1.2.2 Defects in STO.....	10
1.2.3 STO Electronic Structure.....	12
1.2.3.1 Optical properties of STO.....	15
1.2.4 Surface structure and properties of STO.....	16
1.2.4.1 (001) Surface.....	21
1.2.4.2 (110) Surface.....	27
References.....	30
1.3: PROPERTIES OF TiO ₂	32
1.3.1 Crystal structures of TiO ₂	34
1.3.2 Anatase electronic structure	33
1.3.3 Thin films of TiO ₂ anatase grown on different substrates.....	37
1.3.4 Surface structure, reconstruction and properties of anatase	39
References.....	48
 <u>II THIN FILM GROWTH AND ANALYTIC TECHNIQUES AT MODA SYSTEM</u>	 50
2.1 THE GROWTH CHAMBER.....	51
2.1.1 Overview of the PLD technique.....	53
2.1.1.1 Growth modes.....	55
2.1.1.2 Growth kinetics.....	57
2.1.2 Reflection high-energy electrons diffraction – RHEED.....	60
2.1.2.1 High pressure RHEED.....	62
2.1.2.2 Growth monitoring by RHEED.....	63
2.2 THE ANALYTIC CHAMBER.....	65
2.2.1 X-ray Photoemission Spectroscopy-XPS.....	65
2.2.2 Low Energy Electrons Diffraction-LEED.....	67
2.2.3 SPM microscopy.....	74
References.....	76

III RESULTS OF STO	78
3.1: THE SURFACES TERMINATIONS OF STO (001) SINGLE CRYSTAL, AND HOMOEPITAXIAL FILMS.....	78
3.1.1 Homoepitaxial STO film on as received STO (001).....	81
3.1.2 Homoepitaxial STO film on TiO ₂ terminated STO (001).....	83
References.....	88
3.2 GROWTH AND CHARACTERIZATION OF STABLE SrO-TERMINATED SrTiO SURFACES.....	89
References.....	97
3.3 THE TiO ₂ TERMINATED (001) STO SURFACES UNDER THERMAL TREATMENTS.....	98
3.3.1 High temperature UHV (1x2) reconstructed surface of TiO ₂ -terminated STO.....	98
3.3.2 Low temperature annealing of TiO ₂ terminated (001) STO.....	105
3.3.3 The model of (1x2) reconstruction.....	107
References.....	110
3.4 THE STUDY OF (6X4) RECONSTRUCTION OF (110) SrTiO ₃ SURFACES.....	111
References.....	118
IV RESULTS OF TiO₂-ANATASE THIN FILM	119
4.1 THE STABILIZATION OF TiO ₂ ANATASE THIN FILMS GROWN ON DIFFERENT SUBSTRATES, STO (100), SLAO (100) AND LAO (100), AND THEIR CHARACTERISATION.....	120
4.2 Sr DIFFUSION AND SEGREGATION DURING UHV ANNEALING IN ANATASE THIN FILMS GROWN ON STO (001) AND SLAO (001) SUBSTR.....	131
References.....	136
4.3 <i>IN SITU</i> INVESTIGATION OF THE EARLY STAGES OF TiO ₂ EPITAXY ON SrTiO ₃	137
References.....	150
Appendix : Properties of STO/LAO interface.....	151
V GENERAL CONCLUSIONS	154

I THE INTRODUCTION

1.1 BACKGROUND, MOTIVATIONS AND AIMS

Transition metal oxides (TMO) form altogether a very wide class of materials, which has attracted since decades the attention of scientists for showing highly diversified and unusual electronic properties. The building blocks of TMO are typically octahedral structures (BO_6) where a transition metal atom (B) is embedded in a cage composed of six oxygen atoms (Figure 1.1.1). The electronic properties of such oxides are typically dominated by the narrow d-bands of the TMs, where the physics is dominated by strong electronic correlations, often hybridized with O p-bands. The crystal field of the six neighboring O-atoms (BO_6) cause five initially degenerate d orbitals to split into an energetically lower, 3-fold degenerate t_{2g} (d_{xy} , d_{xz} , and d_{yz}) set and in a higher 2-fold degenerate e_g ($d_{x^2-y^2}$ and $d_{3z^2-r^2}$). The splitting energy is in the order of a few eV which is comparable to the energy of a chemical bond.

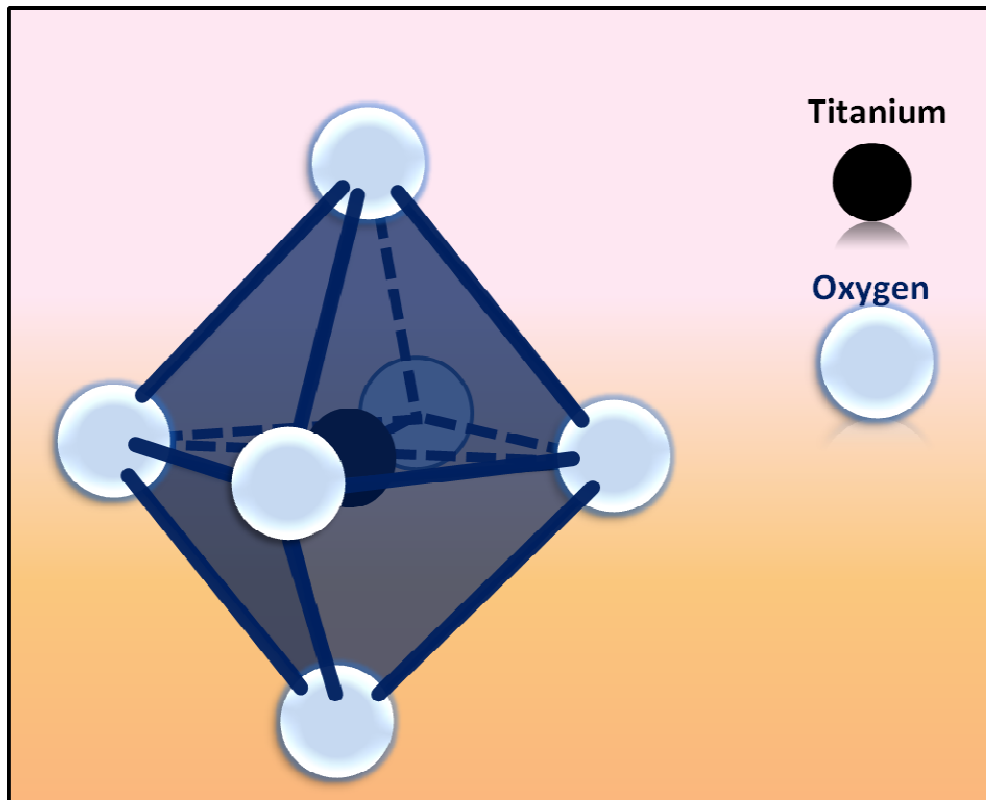


Figure 1.1.1: TiO_6 octahedral as structural block in SrTiO_3 and anatase unit cell.

The Introduction

According to the specific properties of the single materials, the “ideal” octahedra are often found to be distorted, rotated, elongated, or even to show unoccupied oxygen planes (as in layered materials), thus further affecting the single orbitals and the resulting bands, and eventually the overall electronic properties.

Depending on the specific transition metal which is employed, a wide variety of physical phenomena take place, including a) high T_c superconductivity in cuprates, b) a wealth of different magnetic behaviors in manganites, nickelates, ferrites and other compounds, c) high-k-dielectric, ferroelectric and piezoelectric properties in titanates, and so on.

Strontium titanate (SrTiO_3) belongs to the class of particularly important TMO materials with the general formula ABO_3 . These materials have the perovskite structure named by the mineral “perovskite” CaTiO_3 in which this atomic arrangement was discovered. In perovskites structure the A-site is, usually, occupied by an alkaline earth or rare-earth metal, while the B-site normally contains a transition metal surrounded by six oxygen atoms forming an octahedron.

Strontium titanate (STO) is an excellent model of TMO and its bulk, thin film, and small particle structure, as well as its electronic properties has been extensively investigated. Moreover, the surface of strontium titanate, which at first glance might seem to be simple, still challenges science experimentally, methodically and theoretically. Strontium titanate is a widely used substrate material for electronic oxide thin film devices and it has been used as a lattice matched substrate for the growth of high temperature superconductors ^{1, 2}. STO was also successfully used as a support for metal thin film and nanocrystal growth for Au, Pd, Pt, Co, Ag ^{3, 7}, as well as a support for the formation of TiO_x islands ⁸, Sr ⁹, SrO rich islands ¹⁰ and perovskite nanodots ¹¹. SrTiO_3 is one of the few stable materials that can decompose water into hydrogen and oxygen with the assistance of light (photoelectrolysis) ¹². STO could be a good candidate for a crystalline gate dielectric in silicon based devices ^{13, 14}. Also, it exhibits several unexpected and intriguing properties, such as quantum paraelectricity, record-high permittivity (up to 10^4 at 10K)¹⁵ and ferroelectricity (induced by compressive biaxial strain ¹⁶ or by isotopic substitution ¹⁷). Mentioned properties make this oxide a promising candidate in technological

applications. Moreover, STO surface and the region below the surface, strongly influence the macroscopic properties of SrTiO₃, such as the electrical conductivity or dielectric phenomena at elevated temperatures.

Truncation of STO bulk lattice along [001] can result in two possible, no charged, terminations: stoichiometric composition SrO or stoichiometric composition TiO₂. The type of termination will strongly affect the stacking of hetero-epitaxial perovskite thin films. Heteroepitaxial growth on SrTiO₃ has highlighted the importance of the nature of a film surface. Generally, the presence of a TiO₂- or the SrO-terminated surface can give completely different properties of interfaces, ultrathin films as well as their final termination. The detailed descriptions of physical properties of STO are presented in **Chapter 1.2**.

Technological applications of SrTiO₃ require the optimization of the processes that can reproducibly produce a given surface. However, polishing and etching of STO as a substrate (usually named "as received"), lead to several kinds of defects on the surface and cannot be successfully used as a proper substrate in above mentioned manner. This fact is demonstrated in **Chapter 3.1.1**. Obtaining of TiO₂-terminated STO (001) with ultra-flat and molecularly layered steps by chemical etching in an NH₄F–HF buffer solution in combination with thermal treatment^{18,19} is already established as common way for the surface preparation. On contrary, surface sensitive techniques such as Ion Scattering¹⁸ or Photoelectron Spectroscopy²⁰ have shown that even atomically flat TiO₂-terminated surfaces, that have been annealed at above 800 °C, can have significant levels of segregated SrO. Having in mind these facts and established way for obtaining the TiO₂ termination, which is usually done *ex situ*, I have performed small modification in the thermal treatment. This work and its consequences on the growth are presented in **Chapter 3.1.2**.

The A-site termination of STO is by far less investigated, in spite of the potential interest for catalytic processes²¹ and for the realization of specific functional heterostructures and interfaces. Additionally, obtaining of SrO-terminated STO (001) surface is not developed as much as the B-site termination. This could be the consequence of the instability of A termination. The **Chapter 3.2** describes the way to achieve A termination. Presented results in this chapter suggest that a high

quality SrO termination can be achieved by resorting of STO heteroepitaxial growth on the A-site terminated (110) NdGaO₃ substrates.

A good illustrative example of the importance of the termination type of STO (001) surface is interface between STO and LaAlO₃. Although both of these materials are insulators the electron gas is present in the interface but only in the case of TiO₂-terminated STO, whereas for SrO-termination, this effect is not observed²². Some of results of experiments on this interface are presented at the end of Chapter 4.3.

One of the methods to modify the material properties is to reduce the stoichiometric SrTiO₃ and introduce oxygen deficiencies (δ in SrTiO_{3- δ}). The simple way to obtain oxygen deficiencies is to anneal the stoichiometric crystal at high temperature (800°C – 1200°C) in vacuum²³. It is well known, that depending on the annealing conditions different surface reconstructions occur. However, the atomic surface structure is still matter of debate. For example, most studies agree that these reconstructions are formed by oxygen vacancies^{24, 25}, while some studies²⁶ proposed a model in which an ordered Sr adatom occurs on the surface. (1x2) reconstruction, which often appears during the specific UHV thermal treatment was subject of my studies. The obtained results are presented in **Chapter 3.3**.

While there is an increasing number of studies of SrTiO₃ (001), there are only few reports about the detailed topographic and electronic structure of the SrTiO₃ (110) surface. These types of substrates are of special importance for the fabrication of superconducting/normal-conducting/superconducting Josephson junctions²⁷, (110) or (103)/(013)-oriented RBa₂Cu₃O_{7-x} thin films²⁸ for Grain Boundary Josephson Junctions²⁹ etc. The ideal bulk truncated SrTiO₃ (110) surface consists either of a positively charged SrTiO or of a negatively charged O₂ terminating layer. The preparation of the STO (110) surface is not developed as well as for STO (001). To provide new information of a termination, morphology and chemical composition of the surface immediately before of a deposition in the **Chapter 3.4** new results of STO (110) surface after light annealing are presented.

Titanium dioxide, another representative of TMO materials, occurs in several forms such as rutile, anatase and brookite. **Anatase** is a TiO_2 polymorph which is less stable than rutile (it is a low-temperature phase), but more efficient for several applications such as catalysis³⁰ and dye-sensitized solar cells³¹. Anatase is actively investigated for its utility in photocatalytic water splitting³²⁻³³ as well as oxidative destruction of organic pollutants³⁴⁻³⁵. The excellent dielectric features (high dielectric constant) of TiO_2 have been exploited for dielectric layers in thin film capacitors and memory devices³⁶. Moreover, anatase titanium dioxide doped with cobalt, ($\text{Ti}_{1-x}\text{Co}_x\text{O}_2$), in thin film form, has ferromagnetic properties even above 400 K³⁷. This anatase became popular material because of its possible technological applications by exploring both the semiconductor physics and the ferromagnetism. This material may be useful as a room-temperature spin injector for semiconductor heterostructures (spintronics devices)³⁸. Anatase is commercially available in powder form but, in principal, if anatase is in a form of a thin solid film is more suitable for photocatalyses as well as for the heterostructures based on multilayers. Therefore, the improvement of the production technique of the anatase TiO_2 thin film is of great importance. Physical properties of anatase (in general), electronic structure and (001) surface are extensively described in **Chapter 1.2**.

According to the phase diagram of TiO_2 , the rutile phase is thermodynamically preferred at high temperature and is expected that no pure anatase phase can exist at temperatures higher than 650 °C. Having in mind this fact and that almost all growth techniques require high temperature in the process, obtaining of pure anatase phase seems very ambitious. However, at present many procedures for preparing titanium dioxide films, such as coating, chemical vapour deposition, sputtering, anode oxidation of titanium and pulsed laser deposition (PLD) are developed. PLD is a suitable method for preparing titanium dioxide films in basic research, since the films properties are easily controlled by adjusting deposition parameters. One of the aims of this study was also to obtain stable and poor epitaxial anatase films on the various substrates with pulsed laser deposition (PLD) by considering the lattice mismatch. The best candidate for the substrate seems to be LaAlO_3 . The crystal structure of LaAlO_3 is rhombohedral, which can be considering as a perovskite. In this case the lattice mismatch with anatase is rather

The Introduction

small (0.2%). The considerable lattice mismatch between SrTiO₃, as mostly used substrates in thin film technology, and anatase (-3.1%), however, makes difficult obtaining the high-quality epitaxial films. Additional substrate was used, SrLaAlO₄, where the mismatch is less than 1% and causes the compressive strain while the film grown on STO expansively strained. The high-quality anatase thin films with flat surfaces are advantageous not only for practical application to optical and electronics devices but also for basic studies on electric, optical, and photocatalytic properties of TiO₂ since the fundamental properties of anatase are less known than those of rutile. The anatase structure can be pictured as stoichiometric TiO₂ planes stacked in the [001] direction. Thus the bulk-terminated anatase (001) surface is autocompensated, or non-polar, and therefore was not expected to reconstruct. Many studies, however, revealed a two-domain (1x4) reconstruction³⁹⁻⁴¹.

The study dedicated to optimization of anatase thin film growth, surface properties, the (1x4) reconstruction and chemical composition of as grown and UHV annealed samples are presented in **Chapter 4.1**.

In the case of heteroepitaxial growth, there always exists an unavoidable compressive or tensile strain in the films, due to the lattice mismatch between film and substrate and/or the thermal expansion misfit between the film and the substrate compounds. The strain effect induces a deformation of the unit cell of the film, thus inter-diffusion between a substrate and a film during growth could be expected. Since the STO (001) is commonly used substrate and the mismatch with anatase is large, this heterostructure seems to be an excellent model to study Sr inter-diffusion. Results of the Sr inter-diffusion and the anatase/STO (001) interface are presented in **Chapter 4.2** and **Chapter 4.3**.

One part of my activities was setup a new facility for oxides deposition and analysis - MODA (Modular facility for Oxides Deposition and Analysis) at Coherentia Institute, INFN-CNR, Naples. The facility allows modification of the surface properties by a highly controlled growth process, or by proper thermal annealing and their analysis by a number of complementary surface sensitive techniques. The MODA facility is described in details in **Chapter 2**.

References:

- 1 R. Sum, H.P. Lang, H. J. Guntherodt, *Physica C* **242**, 174 (1995).
- 2 K. Endo, P. Badica, J. Itoh, *Physica C* **386** 292 (2003).
- 3 M.R. Castell, F. Silly, *Phys. Rev. Lett.* **96**, 086104. (2006).
- 4 G. Richter, T. Wagner, *J. Appl. Phys.* **98**, 094908 (2005).
- 5 X. Chen, T. Garrent, S.W. Liu, Y. Lin, Q.Y. Zhang, C. Dong, C.L. Chen, *Surf. Sci* **542**, L655 (2003).
- 6 F. Silly, M.R. Castell, *Appl. Phys. Lett.* **87**, 053106 (2005).
- 7 F. Silly, M.R. Castell, *Appl. Phys. Lett.* **87** 213107 (2005).
- 8 A. Gunhold, L. Beuermann, M. Frerichs, V. Kempter, K. Goßmann, G. Borchardt, W. Maus-Friedrichs, *Surf. Sci.* **523**, 80 (2003).
- 9 T. Matsumoto, H. Tanaka, K. Kouguchi, T. Kawai, S. Kawai, *Surf. Sci.* **312**, 21 (1994).
- 10 B. Rahmati, J. Fleig, W. Sigle, E. Bischoff, J. Maier, M. Ruhle, *Surf. Sci.* **595**, 115 (2005).
- 11 D. Ruzmetov, Y. Seo, L.J. Belenky, D.-M. Kim, X. Ke, H. Sun, V. Chandrasekhar, C.-B. Eom, M.S. Rzchowski, X. Pan, *Adv. Mater.* **17**, 2869 (2005).
- 12 J.G. Mavroides, J.A. Kafalas, D.F. Kolisar, *Appl. Phys.Lett.* **28**, 241 (1976).
- 13 R.A. McKee, F.J. Walker, M.F. Chisholm, *Phys. Rev. Lett.* **81**, 3014 (1998).
- 14 R.A. McKee, F.J. Walker, M.F. Chisholm, *Science* **293**, 468 (2001).
- 15 K.A. Muller, *Phys. Rev. B* **19**, 3593 (1979).
- 16 J. H. Haeni et al., *Nature* **430**, 758 (2004).
- 17 M.Itoh et al., *Phys.Rev.Lett.* **82**, 3540 (1999).
- 18 M. Kawasaki, K. Takahashi, T. Maeda, R. Tsuchiya, M. Shinohara, O. Ishiyama, T. Yonezawa, M. Yoshimoto, and H. Koinuma, *Science* **266**, 1540 (1994).
- 19 Gertjan Koster, Guus Rijnders, Dave H.A. Blank , Horst Rogalla, *Physica C* **339**, 215 (2000).
- 20 Z. Szot, W. Speier, U. Breuer, R. Meyer, J. Szade, and R. Waser, *Surf. Sci.* **460**, 112 (2000).
- 21 Y. Matsumoto et al., *Thin Solid Films* **11**, 486 (2005).
- 22 A. Ohtomo and H. Y. Hwang, *Nature* **427**, 423 (2004).
- 23 Tufte O. N., Chapman P. W., *Phys. Rev* **155**, 796 (1967).
- 24 Q. Jiang, J. Zegenhagen, *Surf. Sci.* **425**, 343 (1999).
- 25 N. Erdman, L.D. Marks, *Surf. Sci.* **526**, 107 (2003).
- 26 T. Kubo, H. Nozoye, *Surf. Sci.* **542**, 177 (2003).
- 27 R.B. Laibowitz, R.H. Koch, A. Gupta, G. Koren, W.J. Gallagher, W. Foglietti, B. Oh, J.M. Viggiano, *Appl. Phys. Lett.* **56** 686 (1990).
- 28 F. Miletto Granozio, F.R., U. Scotti di Uccio, J. C. Villegier, *PHYS. REV. B*, **57**, 6173 (1998).
- 29 Thilo Bauch, T.L., Francesco Tafuri, Giacomo Rotoli, Per Delsing, Tord Claeson and Floriana Lombardi, *SCIENCE* **311**, 57 (2006).
- 30 K. I. Hadjiivanov and D. G. Klissurski, *Chem. Soc. Rev.* **25**, 61 (1996).
- 31 B. O'Regan and M. Gratzel, *Nature* **353**, 737 (1991).
- 32 V.E. Henrich, G. Dresselhaus, H.J. Zeiger, *Phys. Rev. Lett.* **36**, 1335 (1976).
- 33 W.J. Lo, Y.W. Chung, G.A. Somorjai, *Surf. Sci.* **71**, 199 (1978).

The Introduction

- 34 J. Schwitzgebel, J.G. Ekerdt, H. Gerischer, A. Heller, J. Phys. Chem. **99**,
5633 (1995).
- 35 L. Zang, C. Lange, I. Abraham, S. Storck, W.F. Maier, H. Kisch, J. Phys.
Chem. B **102**, 10765 (1998).
- 36 A. I. Kingon, J.P. Maris, S. K. Steiffer, Nature **406**, 1032 (2000).
- 37 Y. Matsumoto et al., Science **291**, 854 (2001).
- 38 R. Fiederling et al., Nature **402**, 787 (1999).
- 39 G.S. Herman, Y. Gao, T.T. Tran, J. Osterwalder, Surf. Sci. **447**, 201
(2000).
- 40 Y. Liang, S. Gan, S.A. Chambers, E.I. Altman, Phys. Rev.B **63**, 5402
(2001).
- 41 R. Hengerer, B. Bolliger, M. Erbudak, M. Gratzel, Surf. Sci. **460**, 162
(2000).

1.2 PROPERTIES OF STO

1.2.1 Crustal Structure of SrTiO₃

At room temperature SrTiO₃ has an ideal cubic perovskite structure in which Strontium-Sr is an alkaline earth metal and Titanium-Ti is a transition metal. The crystal structure may be described as a network of the basic structural unit of Ti⁺⁴-O₆⁻² octahedron with Sr⁺² ions as icosahedral interstices (Figure 1.2.1).

The lattice, actually, has a simple cubic symmetry and crystallographic space group is Pm3m.

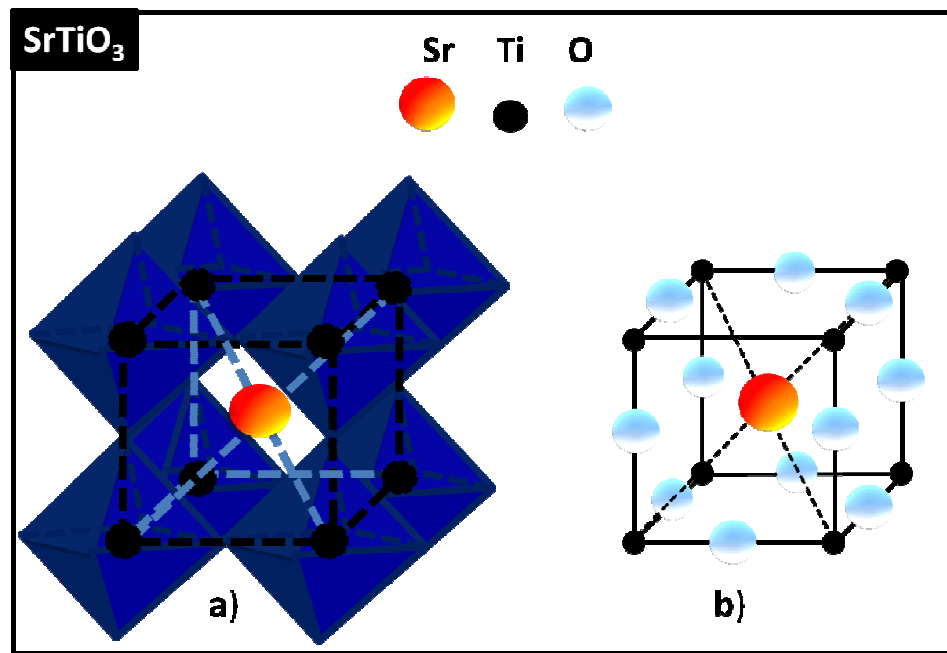


Fig 1.2.1: Schematic diagrams of STO crystal structure: a) with presentation of the Ti⁴⁺-O₆²⁻ octahedron basic as structural unit, b) with positioned the atoms in the lattice.

Observing oxygen atoms, it can be seen that all of them are coordinated by two Ti⁴⁺ ions and four Sr²⁺ ions. The Ti-O bond length is smaller than the Sr-O bond length. Each oxygen atom is surrounded by the other eight oxygen ions and their bond length is equivalent to Sr-O bond. The bond lengths are approximately: 1.95Å for the Ti-O bonds and for the 2.76Å Sr-O (O-O) bonds¹. Consequently, the unit cell dimensions are 3.905Å.

STO is chemically a very stable material up to the melting point of 2353 K, but during cooling down its cubic structure transforms to tetragonal at 105 K.

1.2.2 Defects in STO

Even though it is generally accepted that STO is a highly stable material, often it is defective in stoichiometrical point of view. Depending on fabrication, preparation, or thermal treatment this material can have: a) excess of or deficiency of strontium, b) oxygen deficiency and c) Ti excess.

a) Oxygen vacancies

SrTiO_3 as a pure crystal is an electronic insulator at room temperature. However, integration of above mentioned point defects into the lattice can produce free charge carriers or charged ionic type material leading to conducting effect. The charge carriers are predominantly electrons introduced by donors. Impurity doping or heating in a reducing atmosphere alter STO into semiconducting phase at room temperature. Potent annealing treatment can introduce an approximately equivalent density of oxygen vacancies which is comparable with donor mechanism². The creation of oxygen vacancies with annealing is a quite simple procedure. The stoichiometric crystal has to be at high temperature (800°C – 1200°C) in vacuum³ or in the titanium or hydrogen rich environment for some hours⁴.

The other way to create oxygen vacancies is incorporation of acceptor-type impurities or intrinsic acceptor defects. Acceptor-type impurities, such as Al or Fe, are present in oxides at levels typically no less than 10–100 ppma (parts per million atomic)⁵. Otherwise, reduced STO can be fabricated by deposition as a film at low oxygen pressure which consequently creates intrinsically oxygen depleted SrTiO_{3-x} . Some authors demonstrated that it is possible to make oxygen deficient layers of SrTiO_{3-x} by Ar-ion etching⁶⁻⁹.

The structural arrangement of oxygen vacancies in STO is schematically depicted in Figure 1.2.2.

The left part of the figure represents stoichiometric SrTiO_3 in an octahedral scheme. The thermal treatment leads to lattice change, i.e. two Ti^{+4} are reduced to two Ti^{+3} by removal of one oxygen, as shown in the right figure. This causes the replacement of two octahedra, shown in the scheme, by two square-pyramids.

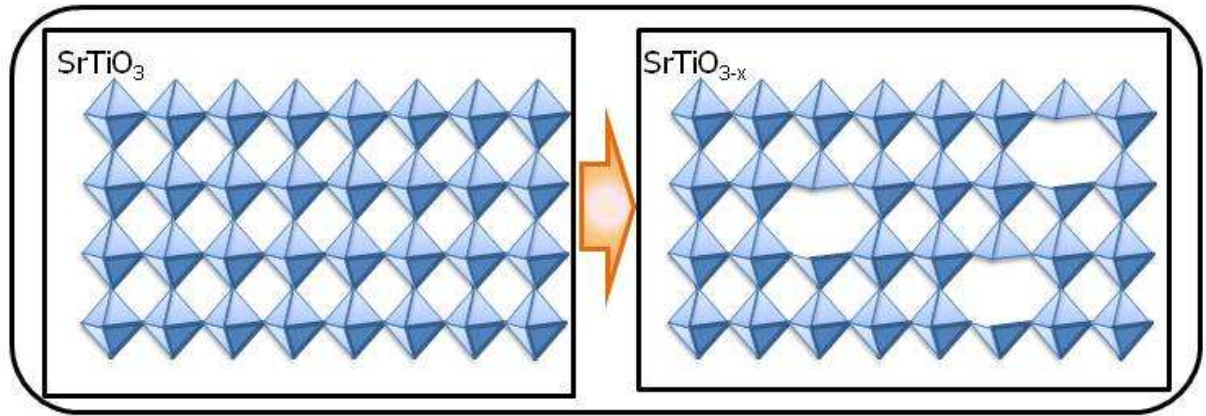
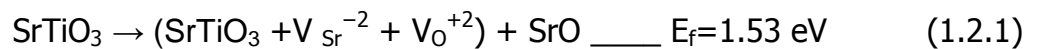


Fig. 1.2.2: Positions of Oxygen vacancies using the octahedron presentation.

The oxygen vacancy density, measured on a sample reduced in the oxygen partial pressure in the order of 10^{-13} Torr, is in the range of $2.0\text{--}7.6 \times 10^{19} \text{ cm}^{-3}$ ¹⁰. This value corresponds to the one oxygen vacancy per 500 unit cells, or chemically presented as $\text{SrTiO}_{2.998}$ ¹¹.

b) Strontium and Titanium excesses

The existence of strontium vacancies is intrinsic defect and can be formed during high temperature processes of fabrication or annealing. With the vacancies, the crystal has the dominant ionic disorder and the formation of vacancies can be described with three reactions known as Schottky or "Schottky-like" defect reactions¹².



E_f represents the formation energy.

The product of the above reaction is SrO, and this could be connected with the formation of Ruddlesden-Popper (R-P) phases¹³ which do not change conductivity behavior.

A second reaction, actually, leading to the creation of the TiO_2 in SrTiO_3 and their segregation:



This reduction of the surface results in the formation of TiO₂-rich phases, known as Magneli phases, with R-P phases forming in the sub-surface region¹⁴.

One of the reaction products, V_{Ti}⁻⁴ vacancy, is highly charged and it is energetically unstable in the ionic structure. Some researchers¹⁵ suggested that the excess of TiO₂ can be compensated with the formation of neutral coupled vacancy pairs - V_{Sr}⁻²- V_O⁺². Also, these processes do not change the conductivity behavior¹⁶.



The stability of the strontium vacancies together with the formation of Magneli phases have been proven both into bulk¹⁷ and thin film STO samples¹⁸.

1.2.3 STO Electronic Structure

One of the most complete theoretical studies of STO electronic band structure was done by E. Heifets et al.^{19, 20}. Their calculations lightened the electrical and optical properties of SrTiO₃ and their work encouraged theoretical and experimental scientists to further study the material. E. Heifets et al. compared results of *ab initio* Hartree–Fock method with electron correlation corrections and density functional theory (DFT) with different exchange-correlation functional. Short overview of their results which can be used as basic model for electronic structure of STO will be presented.

But before presenting the electronic structure, Fig 1.2.3 shows sketch of high symmetry point's positions in a cubic lattice. These points are mainly used in all theoretical and experimental approaches to describe electronic band structure of crystals.

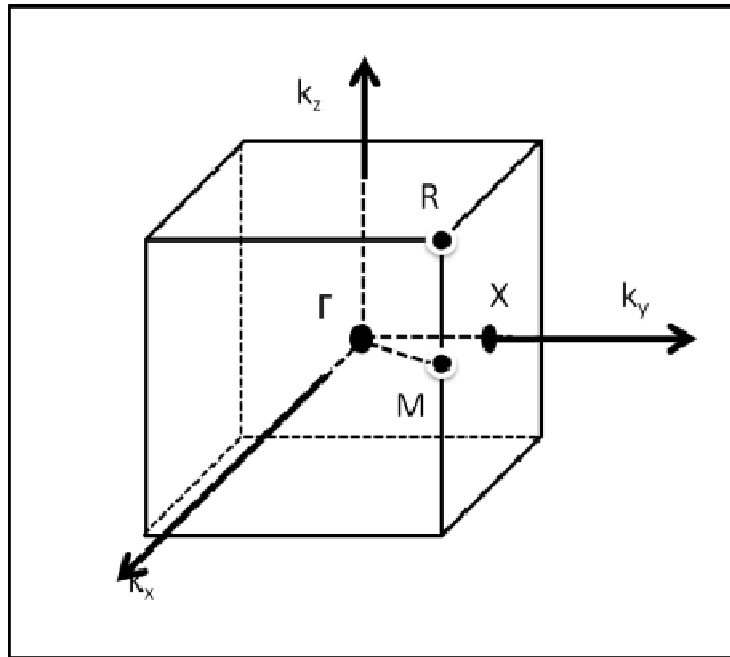


Fig 1.2.3: The Brillouin zone for a simple cubic lattice (the symmetry points and directions are labeled in terms of the Bouckaert-Smoluchowski-Wigner symbols²¹).

Fig. 1.2.4 presents the theoretically calculated band structures of the bulk (a), TiO₂ (b) and SrO (c)-terminated surfaces.

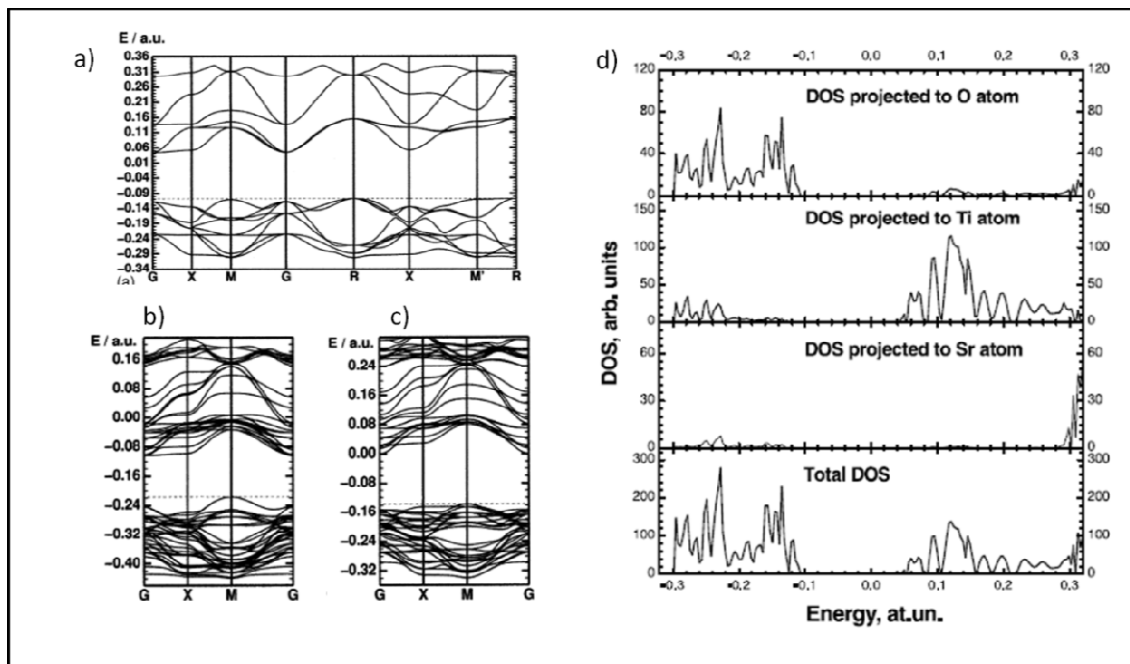


Fig. 1.2.4: The band structure of SrTiO₃: a) bulk, b) TiO₂ terminated surface c) and SrO terminated surface, d) total and projected DOS for the bulk SrTiO₃.

Properties of STO

Calculation of the surface Brillouin Zone corresponds to the square 2D lattice. Full DOS calculations for the bulk SrTiO₃ and contributions of all kind of the atoms are presented in Fig 1.2.4d. From Figure 1.2.4 it is possible to see that the upper valence band of bulk SrTiO₃ is quite flat, with the local maximums at M and R points of the Brillouin zone. The bottom of the conduction band drops at the G point and the X point, where the energies are very similar. The dispersion curve between these G and X points is very flat. Such flat bands could make possible hole and exciton self-trapping²². The optical bulk gap obtained with their theoretical approach is 4.16 eV. This result is in disagreement with the experimental value of 3.2 to 3.3 eV. However, their value of the gap is in better agreement in respect to the other theoretical calculations based on different models, for example "pure" HF calculations or LDA calculations²³.

The upper valence band is formed by O2p atomic orbitals with a small contribution from Ti atomic orbitals. The top of the upper valence band for the TiO₂-terminated surface is located at the M point of the Brillouin zone (Fig.1.2.4b). Analysis of the atomic orbital contributions to the DOS shows that this band consists mainly of the atomic orbitals near or in the surface. Due to this fact the band can be considered as a band of surface states. Bottom of conduction band consists essentially of Ti orbitals. Contribution from strontium atomic orbitals is insignificant in this energy range. Actually, the Sr orbitals give an important contribution to the DOS only at energies much higher in the conduction band.

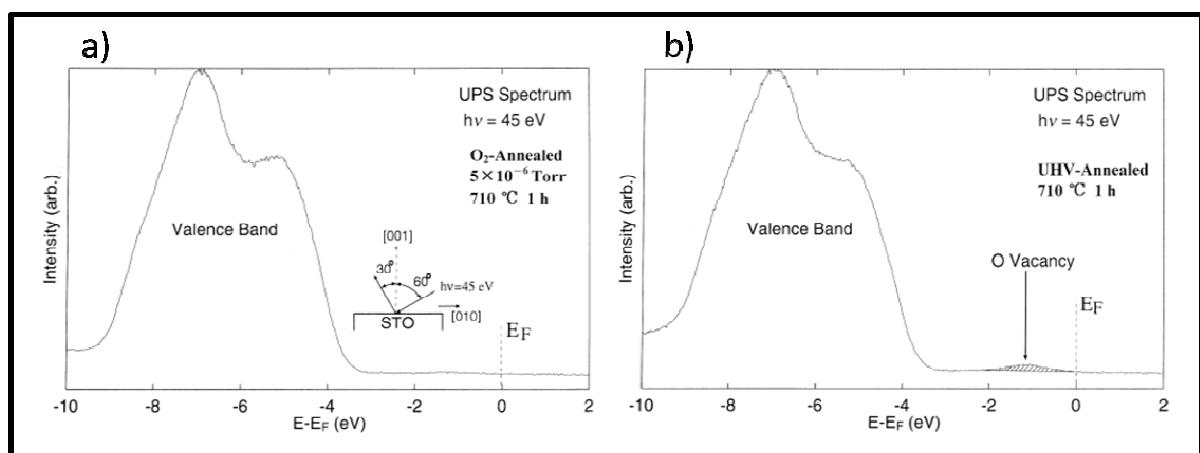


Fig. 1.2.5: UPS spectrum from STO (001) annealed for 1h at: a) 710°C in O₂ atmosphere (5 × 10⁻⁶ Torr) and b) annealed in UHV at 710°C²⁴.

Experimental Ultraviolet Photoemission Spectroscopy (UPS) data on STO crystal²⁴ are shown on the Fig. 1.2.5. Fig. 1.2.5 shows the UPS spectrum from the non-bonding O2p (~5 eV) and bonding O2p and Ti mixed orbital, 3d+4p(4s) (~7 eV). The authors demonstrated that the annealing in O₂ atmosphere gives an atomically clean and stoichiometric surface. On the contrary, when the sample was annealed in UHV at temperatures from 570 up to 1020°C for 1 hour, additional surface state near the Fermi edge was observed. This small peak about 1.2 eV below the Fermi edge was explained as the creation of oxygen vacancies in the top TiO₂-terminated STO. The new band inside the gap was described theoretically using a tight-binding model including the effects of lattice relaxation²⁵.

1.2.3.1 Optical properties of STO

Optical properties and activity of STO depend strongly on a sample preparation and degree of the reduction. Pure stoichiometric SrTiO₃ is a transparent in visibly range of light. Moreover, regarding to the optical studies, it has a transparency window in the energy range of 0.25– 3.1 eV^{26, 27}.

Furthermore, under the introduction of n-type dopants, including, in a generalized sense, oxygen vacancies V_O²⁻, STO turns from a transparent insulator into an black/dark-blue material²⁸⁻³⁰. A totally new field of interest and application has emerged from recent papers^{9, 31} reporting a previously unnoticed fascinating optical feature of n-doped STO: a room temperature broadband blue light emission occurring under exposure to UV light of 3.8 eV. In those works, the authors doped crystalline STO with electrons, by substitution of Nb⁴⁺ for Ti³⁺, La³⁺ for Sr²⁺, or creation of V_O²⁻ impurities irradiating crystal by Ar⁺ ions. These procedures transform stoichiometric STO samples into blue light emitters at room temperature³¹.

A. Rubano, M. Radović et al. in order to understand real potential of STO as light emitter focus their attention on two questions³². First issue was to understand relation of presence of impurities or vacancies as donors on reported blue emitting properties of n-doped STO. Rationale for this question was that Kan et al.^{9, 31} provided conclusive evidence that it is indeed the “oxygen vacancies shining blue”³³, according to other reports blue light emission is also found in intrinsic STO³⁴. Second question was how suitable the discovered luminescence is for high

frequency applications, and what is the intrinsic limit to the bandwidth of the potential future devices. In order to investigate these issues, authors performed time resolved photoluminescence (PL) measurements on “intrinsic” “I”, Nb-doped “Nb” and oxygen deficient “O” STO samples prepared at MODA lab. With regard to the first mentioned issue, time resolution complements spectral resolution thus allowing the comparison of the mechanisms which are present in different samples. While the spectral analysis allows comparing the energy of the electronic states involved in the luminescence, the analysis of the temporal profiles allows evaluating the radiative and non radiative mechanisms causing the decay of the excited plasma. With regard to the second issue, the intrinsic bandwidth limit can be trivially estimated to be of the order of the inverse of the decay half-life.

However, we found strong overall similarities in the emission spectrum, the yield and the decay dynamics of the photoluminescent response of pure, oxygen deficient, and Nb-doped STO. This results point to a very minor role of donors and doping-induced electrons both on the states involved in the transition, and at least on the most relevant decay mechanism, i.e., the BD. The results seem to be in disagreement with the results which quote that in intrinsic STO there is not blue light emission. Obtained results set the upper bandwidth limit of STO-based emitting devices above 1 GHz, opening some interesting prospects on the fabrication of integrated optoelectronic devices based on titanates, where the growth of epitaxial heterostructures allows integrating emitting elements with tunable filters, optical switches, and ultrawide bandwidth modulators.

1.2.4 Surface structure and properties of STO

Appreciation of the SrTiO₃ surface crystallography and the morphology is critical for the understanding and the interpretation of an observed a electrical, an optical and achemical properties. After many published data and a lot of debates, it turned out that the resulting chemical composition and morphology of surface significantly depends on the history of the sample including chemical treatment, annealing temperature, oxygen partial pressure, annealing time, cooling rate etc. ^{14, 35-42}.

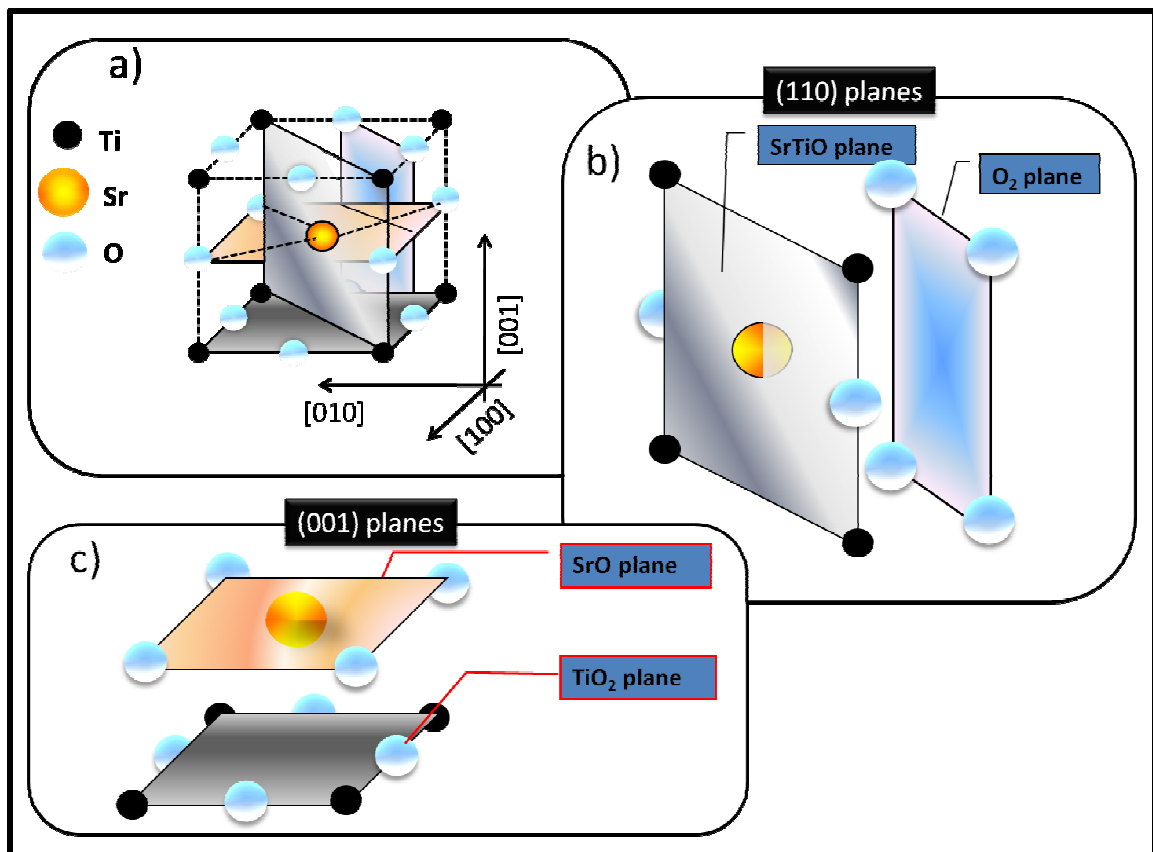


Fig. 1.2.6: The crystal planes of STO a) The crystal lattice, b) (110) plane with double termination and c) (001) plane with double termination.

This subchapter provides introductions of two surface planes of STO, (001) and (110) which are schematically depicted in Fig. 1.2.6. Both planes were subjects of this study.

In order to understand the relative stability of the surface planes, the charge redistribution at the surface and how this give rise to the rearrangement of atoms have to be established. However, the mechanism of charge redistribution depends on the surface type. P. W. Tasker established a classification of surface types using basic electrostatic principles⁴³. His classification is shown schematically in Fig. 1.2.7.

In the type I surface the charge in each plane is spread in the way that these planes are charged neutrally.

If planes are arranged with repeating units and are charged, but without dipole moment, the surface is called type II.

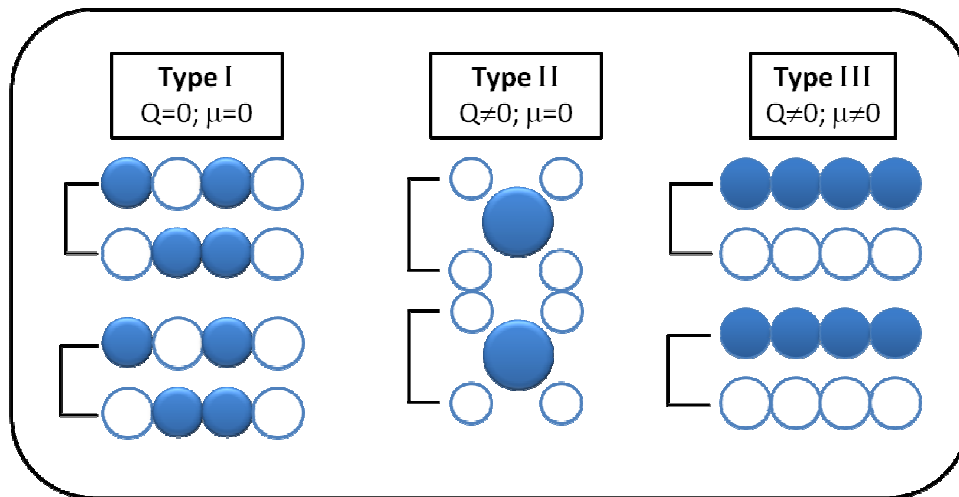


Fig. 1.2.7: The surface types according to Tasker classification.

Finally, type III surface is characterized by that each layer parallel to the surface has a charge σ and the dipole moment. To which type a surface belongs depends mostly on: the surface orientation \mathbf{n} , the characteristics of the polarization in the bulk unit cell, and on the crystal termination.

The surface orientation determines the coordination numbers and organization of ions on the surface.

Bulk electric polarization (\mathbf{P}) of insulating crystals is defined by the centers of charge of the Wannier functions of the occupied bands. If the surface orientation is \mathbf{n} , the bound charge density on the surface (σ_b), is described with equation $\sigma_b = \mathbf{P} \cdot \mathbf{n}$. The polarization as vector has modulo as q/A , where A is the surface cell area. If condition that modulo q/A is equal to zero ($\sigma_b = 0$) is satisfied, the surface is non-polar⁴⁴.

The polarization, \mathbf{P} , can be estimated from the information of the ground-state electronic distribution in the bulk unit cell by high-resolution x-ray diffraction experiments, or theoretically, by first-principles methods based on the density functional theory (DFT).

Actually, in most cases, simple models for the electronic structure can easily indicate when a surface is a polar or not. In this way it is necessary just to use the sign of the ions charge in the plane. For example, SrTiO_3 (110) contain SrTiO and O_2 layers as repeated units which are charged. If formal charges are assigned to the ions as: Sr^{2+} , Ti^{4+} , and O^{2-} the SrTiO has charge $+4e$ and O_2 has -4 per unit cells in the plane.

Properties of STO

Generally speaking polar surfaces have low stability. Next few sentences explain the origin of this instability. Claudine Noguera gives very simple presentation of a the crystalline compound cut along a polar direction ⁴⁵. Fig.1.2.8a. presents schematically inequivalent layers with equal but opposite charge densities ($\pm\sigma$), with interlayer spacing R_1 and R_2 . The unit cell has a dipole moment density equal to $\mu=\sigma R_1$. With increasing number of the layers, the electrostatic potential increases monotonically across the system by an amount $\delta V = 4\pi\sigma R_1$ per double layer as shown in Fig. 1.2.8b. A potential, δV , is actually large, and could be of the order of several tens of eV in a pure ionic material like MgO ⁴⁶ or a partially ionic material like LaAlO₃. The total dipole moment $M=N\sigma R_1$ of N bilayers is proportional to the thickness, and the electrostatic energy amounts to $E=2\pi N R_1 \sigma^2$.

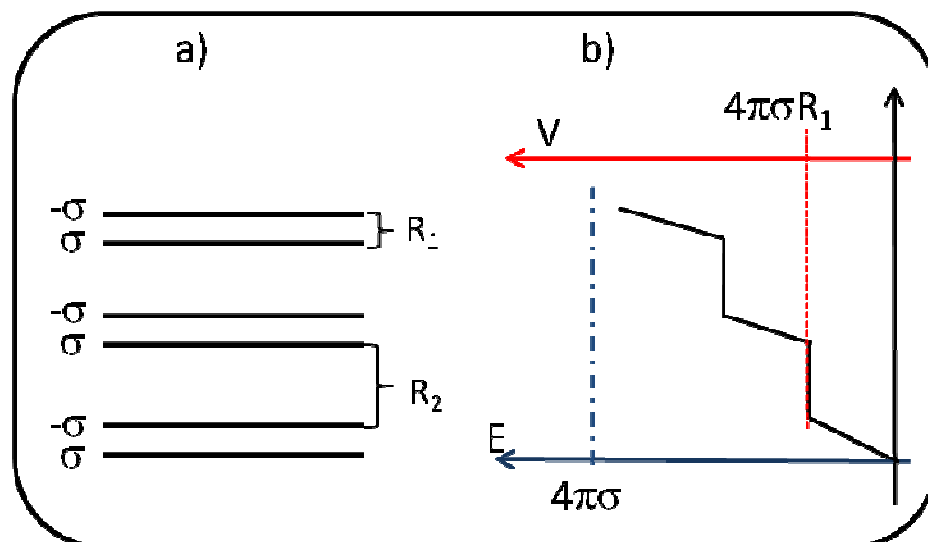


Fig. 1.2.8: a) Structured material with inequivalent charged layers, b) Energy and potential dependences of the number of layers.

With increase of a thickness ($N \rightarrow \infty$), the electrostatic contribution to the surface energy per unit area diverges and surface cannot exist and will collapse.

However, several scenarios that would cancel the polarity and stabilize the surface are likely. One possibility is that one or several surface layers change chemical compositions respect to the bulk. This effect can be followed by reconstruction depending on order of the vacancies or adatoms which could be created.

Properties of STO

Second scenario is connected with the environment where adsorbed atoms or ions may provide the charge compensation.

Third situation for charge compensation can be due to the electron redistribution which can cancel out the macroscopic component of the dipole moment in response to the polar electrostatic field and this scenario can happen only on stoichiometric surfaces and this effect is presented in Fig. 1.2.9.

If the value ($\sigma' = \sigma R_2 / (R_1 + R_2)$) of the charge density is transferred on the external layers of the crystal this results that a total dipole moment is not any more proportional to the thickness of crystal ($M = \sigma R_1 R_2 / (R_1 + R_2)$). Increasing of the electrostatic potential is also suppressed and, moreover, saturates.

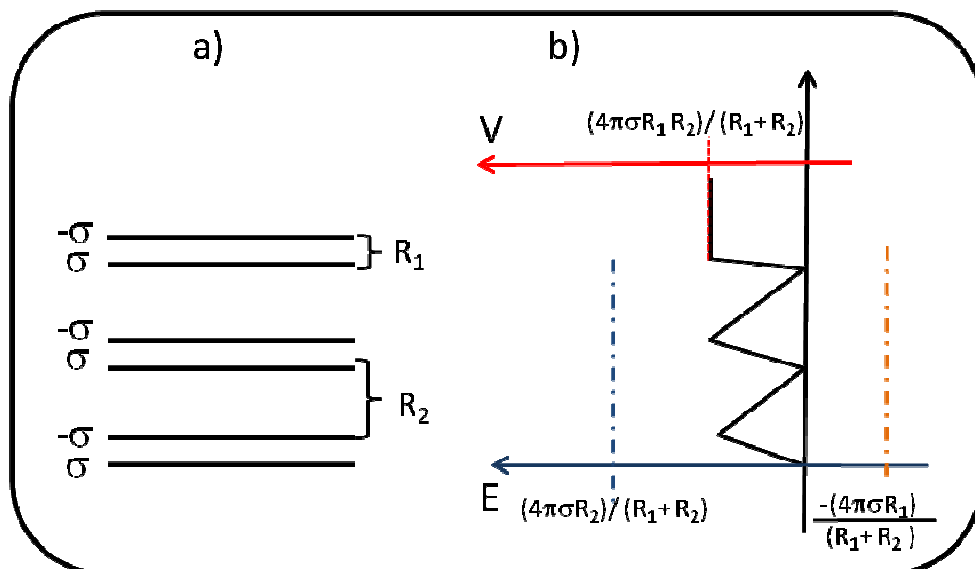


Fig. 1.2.9: Structured material with inequivalent charged layers, b) Energy and potential dependencies of the number of layers with charge redistribution.

Which process for stabilization of the surface will take place depends strongly on energetic considerations. However, the resulting surface energy, considering the process of depolarization, has to be as lowest as possible. If crystal is in conditions of thermodynamic equilibrium, additional condition has to be satisfied-the lowest thermodynamical potential because the surface is in contact with the environment. If thermodynamic equilibrium cannot be reached, the final surface configuration is that of the lowest kinetically available energy ⁴⁷.

1.2.4.1 (001) Surface

As mentioned previously, cutting down the bulk lattice along [001] direction results two possible terminations of the surface:

- SrO; the oxygen coordination of Sr ions decreases from the bulk value of 12 to a surface value of 8.
- TiO₂: where oxygen coordination of Ti decreases from the bulk value of 6 to a surface value of 5.

The double termination of the surface is schematically presented in Fig. 1.2.10.

In order to understand the relative stability of these two possible terminations, prerequisite is a determination of the charge redistribution on the surface and consequent shifts in atomic positions.

By the surface classification described above, both terminated (001) surfaces of SrTiO₃ are considered as type I. On the other hand, SrTiO₃ is not fully ionic because its gap width (3.2 eV) is not large enough. Due to this and the fact that the Ti–O bond has a small covalent contribution, STO acts as semiconductor. These causes existence of $Q_{\text{Sr}} + Q_{\text{O}}$ and $Q_{\text{Ti}} + 2Q_{\text{O}}$ charges; thus SrTiO₃ (100) should be considered as a polar surface. All this can cause some of the following surface modifications: charge redistribution, the ramping, the relaxation, the reconstruction or even segregation.

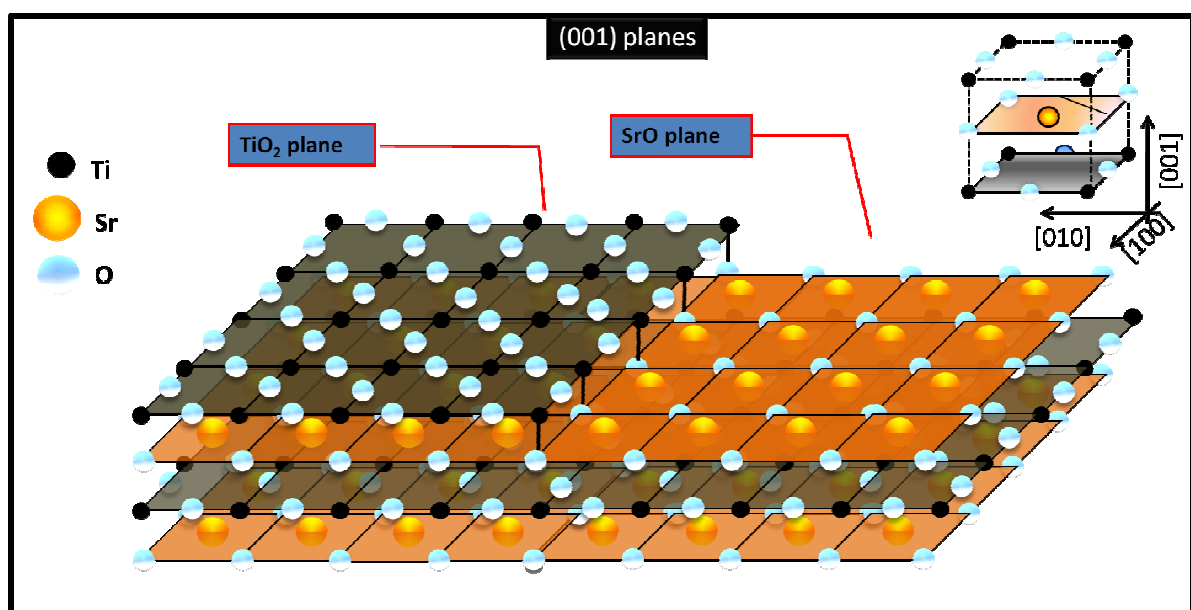


Fig. 1.2.10: Double terminated (001) STO surface.

Considering the way of the SrO and TiO₂ surfaces formation, due to the breaking of the bonds between the planes, and the fact that difference in covalency between surface and subsurface layers and layers in the bulk does not exist⁴⁸ large modification in the electronic structure is not expected.

Anyway, some reduction of the surface ionic charges with respect to the bulk was demonstrated by X-ray photoemission studies^{49, 50}. Since the SrO and TiO₂ terminations have less coordinated atoms than bulk, one might expect a contraction of the outer layers of both surface terminations. The attractive forces in the lattice is due to the electrostatic interactions and estimating is possible using the formal charges Z by an equation 1.2.4⁵¹.

$$E_{coh} = \frac{1}{2N_c} \sum_i \sum_{j \neq i} \frac{Z_i Z_j e^2}{r_{ij}} \quad (1.2.4)$$

i, j - vary independently over all ions in the crystal, r - the distance between two ions, N_c - number of unit cells in the crystal.

This energy, known as the Madelung potential, describes the cohesion of the solid a short-range regime. Moreover, it gives possibility for determination of the equilibrium inter-atomic separation, r_{ij}^{eq} .

The relaxation was predicted by theoretical calculations⁵² and it was confirmed experimentally with LEED study by Bickel et al.⁵³. Another structural modification, rumpling, was observed in the measurements by Bickel et al. Rumpling is, actually, a consequence of the differences in polarizability of the anions and the cations. The anions and cations are, in fact, in the field generated by the surface dipole moment but cations sustain stronger force than the anions do. This provokes surface rumpling. The other reason for the rumpling could be in surface relaxation inhomogeneity where the cations are more relaxed respect to the anions.

Reconstruction of the STO (001), as a way of the surface stabilization is one of the mostly studied phenomena on the surface. One of the subjects of this thesis is the understanding of the surface reconstruction nature with the accent on (1x2) type of reconstruction. Actually, many types of the surface reconstruction were observed on (001) and they are presented in the Table 1.1.1^{14, 36-40, 42, 54-57}.

Table 1.1.1 Observed surface reconstructions of STO (001)

Observed reconstruction	Sample preparation of STO(100)	Techniques
(1x1)	1.UHV annealing, T= 827 ⁰ C, t=60min 2. Annealing, P=10 ⁻⁵ mbar O ₂	AES, LEED,SPM, UPS, RHEED
(2x1)	1. Annealing, P=10 ⁻⁵ mbar O ₂ 2. UHV annealing, T= 950 ⁰ C, t=120min 3. UHV annealing,T= 600-800 ⁰ C, t=30min	LEED, AES, STM
(2x2)	Annealing, P=10 ⁻⁵ mbar O ₂	LEED, AES, MEIS,UPS,
C(4x2)	1.UHV annealing in P=10 ⁻⁵ mbar H ₂ , T=950 ⁰ C, t=120min	LEED, STM, AES
C(6x2)	O ₂ annealing T=1100 ⁰ C, t=180min, then UHV annealing T=950 ⁰ C, t=120min	LEED, AES, STM
(6x2)	O ₂ annealing T=1100 ⁰ C, t=180min, then UHV annealing T=950 ⁰ C, t=120min	LEED, STM
(√5x √5)R26.6 ⁰	1.UHV annealing, T= 900 ⁰ C, t=15h, then flashing at T=1200 ⁰ C, t=2min 2. UHV annealing, T=1830 ⁰ C,t=120min	AES,LEED, STM,XPS,RHEED

Note from the table that the similar preparation conditions can cause different types of reconstruction. On the contrary, different recipes raise the same reconstruction. Some researchers often claim that the observed structure actually represents an equilibrium structure. Generally speaking, combined data obtained by high resolution surface sensitive tools (STM-AFM, XPS-UPS, LEED-RHEED, TEM), provide basics for the three theories for the (001) surface reconstructions.

One explanation is that the reconstruction is related to an arrangement of oxygen vacancies³⁸.

Second explanation is that reconstruction may be due to Sr diffusion from the bulk and the segregation on the surface^{54, 57} and the last explanation is that the surface reconstruction occurs from the formation of new oxides^{14, 35, 36}.

a) The surface reconstruction due to the ordering of oxygen vacancies

When it comes to the SrTiO₃ (100) surface reconstruction, the proposed model includes that the oxygen vacancies on the surface are coupled with Ti³⁺ ions leading to the titanium-oxygen vacancy complex (Ti³⁺-V_O)³⁸. The ordering of the Ti³⁺-V_O

complexes causes some types of surface reconstruction. J. Goniakowski and C. Noguera ⁴⁸ used the electrostatic principles to qualitatively describe of this effect.

For the TiO_2 terminated surface, creation of a single oxygen vacancy redistributes q charge in a way that a quadrupole is formed in the plane with $-q$ on the two linearly coordinated Ti ions and $+2q$ on the vacancy site. Numerical simulations suggested that aligned quadrupoles on the TiO_2 -terminated surface have a higher attractive interaction while the interaction is repulsive when two quadrupoles are normal to each other. In the case when Ti-Vo-Ti quadrupoles are present in high density they will preferentially order in the parallel row-like structure. With this ordering, the structure maximizes the attractive energy while minimizing the repulsive energy. It should be noted, however, that this simple explanation ignores relaxation effects. Some varieties of row-like superstructures are observed with LEED, RHEED and AFM-STM ³⁹ and they are included in Table 1.1.1. Some examples of reconstruction varieties are presented in Figure 1.2.11.

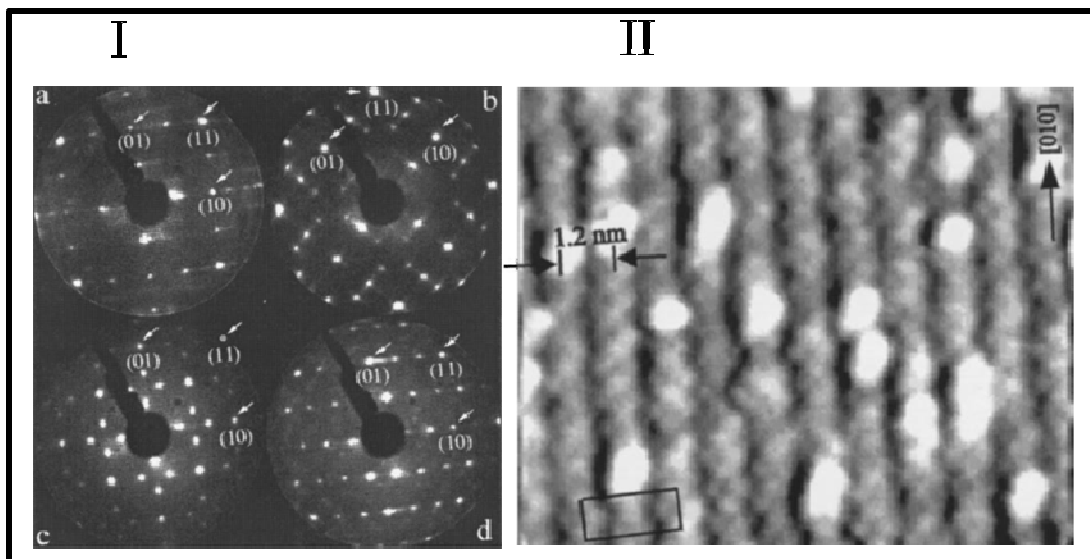


Fig.1.2.11: I) LEED pattern of $\text{SrTiO}_3(001)$ surfaces prepared by different procedures (a) double domain (2×1) reconstruction, (b) double domain $c(4 \times 2)$ reconstruction, (c) double domain $c(6 \times 2)$ reconstruction, (d) a single domain $c(6 \times 2)$ (preparation conditions as in (c)), reconstruction is stabilized on a vicinal (001) SrTiO_3 surface, II) High resolution STM image of $c(6 \times 2)$ ³⁹.

The creation of the oxygen vacancies on the TiO₂-terminated surface raised an interesting question: if the Oxygen vacancies creation on the SrO-terminated surface is possible? Following the electrostatic argument used by J. Goniakowski and C. Noguera, it is clear that Oxygen vacancies creation on the SrO-terminated surface does not occur. The charge redistribution for a single oxygen vacancy shifts electron density towards the titanium in the subsurface plane, thus creating the dipole oriented normally to the surface. Finally, the oxygen defect formation energy on the SrO surface is higher than on the TiO₂ surface. This is further supported by the absence of the surface states on the SrO-terminated samples annealed under UHV conditions ⁵⁶.

b) The surface reconstruction due to Sr adatoms

A new structural model for (001) SrTiO₃ reconstruction - ($\sqrt{5} \times \sqrt{5}$)-R26.6⁰ was proposed by Kubo et al. ⁵⁴. The model is based on the existence of Sr adatom and their ordering at the oxygen fourfold site of a TiO₂-terminated layer. Kubo et al. used STM and the first-principles total-energy calculation to study atomic and electronic structures of the SrTiO₃ (100) surface. Moreover, they proposed this model for the other types of surface reconstruction. The c(4x2) phase and the series of the structural phase transitions, c(2x2), c(4x4), p(2x2), p(4x4) and ($\sqrt{13} \times \sqrt{13}$)-R33.7⁰ were observed ⁵⁷. Kubo et al. claimed that their model for the SrTiO₃ (100) surface reconstructions, based on ordered Sr ad-atoms can explain the obtained experimental results very well.

c) The surface reconstruction due to the formation of non perovskite phases

Some studies on STO were devoted to understand if the stabilization of the (001) surface could be due to formation of new surface oxides. One possibility is that the heating in a reducing atmosphere lead to surface alteration, in a way that various orders of the sub-oxide Sr_{n+1}Ti_nO_{3n+1} known as Ruddlesden-Popper (R-P) phases are formed (n = 1 or 2 depend on the level of reduction) ^{35, 36}. While the second possibility is that the reduction of the surface results in the formation of TiO-rich phases, known as Magneli phases, with R-P phases forming in the sub-surface region ¹⁴. One of the studies was based on the results obtained by Transmission

Properties of STO

Electron Microscopy (TEM) showing that the crystal contains non-perovskite phases including Ruddlesden–Popper phases. These measurements showed that in the regions where TiO_2 layers have been removed, SrO on SrO layers appear^{58, 59}.

Moreover, Castell et al. showed that on the STO (001) many varieties of nanostructures, as nanolines and nanodots, can be formed^{40, 59, 60}. These structures were created by the combination of Ar^+ ion sputtering and annealing in UHV. M.R. Castell speculated that these structures are due to either SrO or TiO_x enrichment of the surface region giving rise to nanocrystalline growth of non-perovskite phases on the surface. Nanostructured surfaces obtained by Martin R. Castell are shown in Figure 1.2.12.

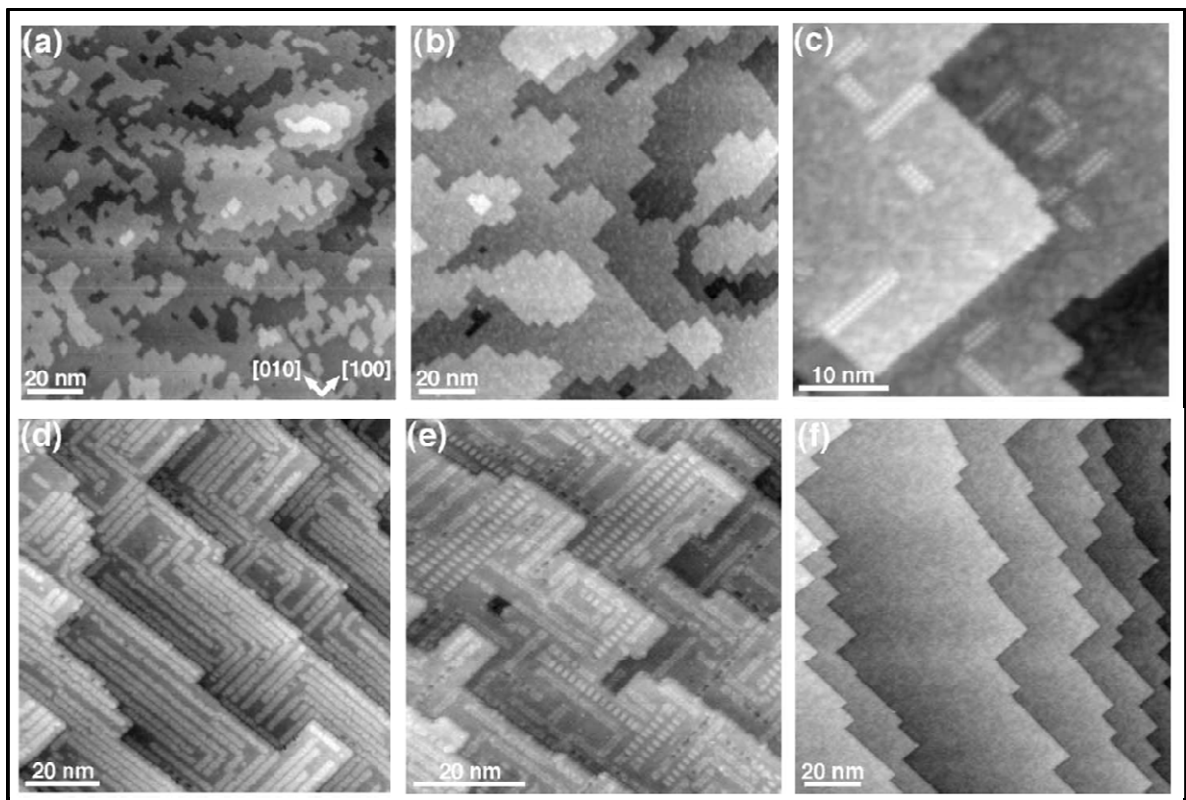


Fig. 1.2.12: Sequence of STM images showing the SrTiO_3 (0 0 1) surface morphology evolution following Ar ion sputtering and annealing in UHV. (a) terrace evolution at 750°C , (b) step edge straightening at 860°C , (c) nanoline appearance at 950°C , (d) nanoline self-assembly at 975°C , (e) nanolines breaking up into ordered nanodot arrays with additional annealing at 900°C , (f) disappearance of all nanostructures at 1235°C .⁵⁹

Auger Electron Spectroscopy (AES) measurements of this surface shown that the Ti/Sr peak ratio, compared with the ratio of stoichiometric SrTiO_3 , increased. This result supported the conclusion that nanostructured surfaces are TiO_2 -based⁶¹. M.R. Castell suggested that these TiO_2 -based surface phases on SrTiO_3 may also be useful for the development of the photocatalytic technologies.

1.2.4.2 (110) surface

The STO (110), as already mentioned, is the polar surface and the most “open”, it has the lowest surface density. The surface was experimentally studied using several different techniques. Low-energy electron diffraction-LEED shows different kinds of surface reconstruction after thermal treatments. Atomic force microscopy also confirmed surface adaptation of the STO⁶²⁻⁶⁴. Similarly to the (001) surface, the atomic and electronic structure of the (110) surface strongly depend on the preparation procedures, especially on the annealing temperature and O_2 partial pressure.

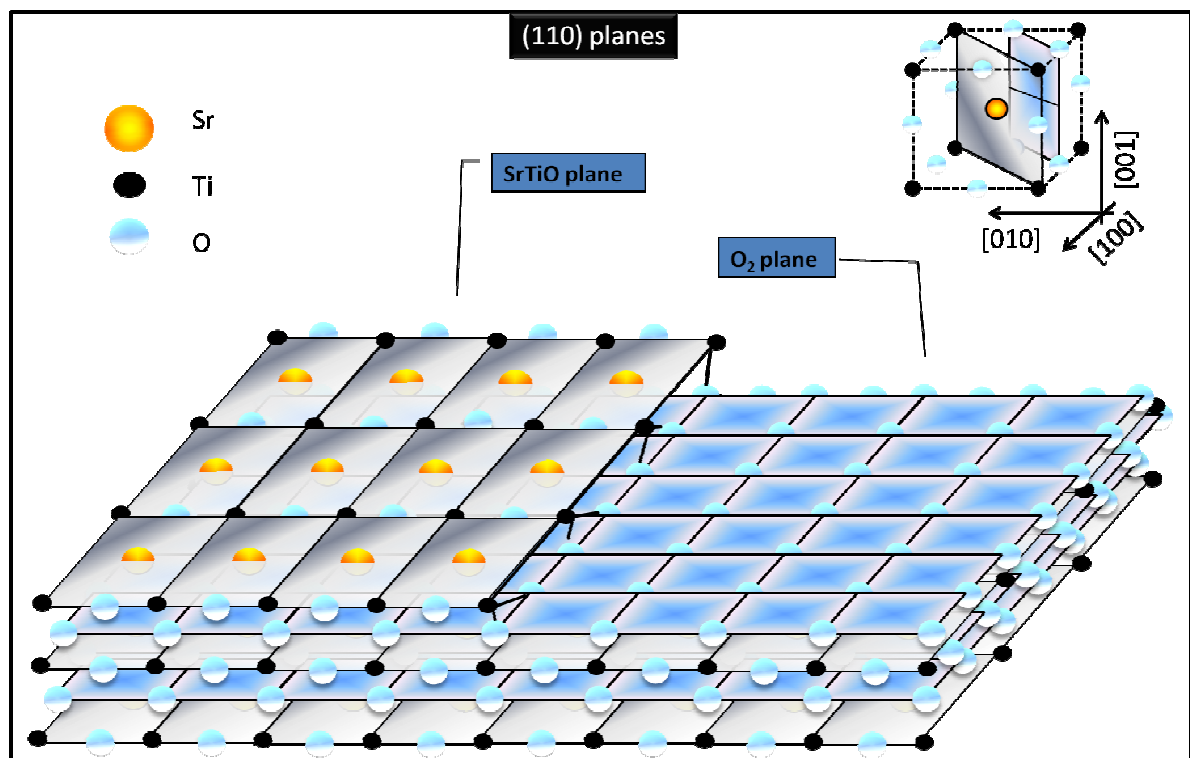


Fig. 1.2.13: Schematic view of the two (110) STO surface termination.

Also some theoretical studies were carried out to understand the nature of the (110) surface reconstructions^{46, 65}. In agreement with the fully ionic model, the layer charge densities amount for 2D unit cell is ± 4 electrons. Moreover, the repeat unit has a dipole moment leading to the system electrostatic instability. For complete stabilization, the macroscopic component of the total dipole moment has to be compensated. There are two ways to overcome the instability: the spontaneous electron redistribution with the surface perturbation, or the modification of the atomic concentrations at the surface⁴⁶.

Here the second way for depolarization is explained in more details.

For the SrTiO-terminated (110) surface orientation, the charge compensation can be achieved by the transfer of Sr atom from the SrTiO face to the opposite face. For O₂- termination, the removal an oxygen atom from the O₂ termination and adding one oxygen atom above the SrTiO layer on the other side can solve instability. Both processes may produce (1x1) structured surfaces. Of course, the other configurations of the surface could also exist, but they are more complex and result in 2D unit cells larger than (1x1). E. Heifets et al. used *ab initio* calculations for (1x1) surface⁶⁶ and obtained results indicate a significant increase of the covalent behavior of the Ti-O bonds near the surface respect to the bulk. This should have an impact on the electronic structure of the surface defects and should affect the adsorption and a surface diffusion of atoms and small molecules relevant for catalysis. They claimed that the O-terminated (1x1) surface has the lowest surface energy among all the (110) terminations studied. They also noted that the formation of O vacancies is much more efficient than a strong electronic-density redistribution for the depolarization. A. Kotomin et al. studied the (2x1) surface reconstruction, where O atoms are removed in pairs in a "zig-zag" way⁶⁷. They found that this reconstruction has the surface energy only slightly lower than the (1x1) reconstruction.

Based on the idea that the transition-metal (110) surfaces have to be stabilized as faceted surface due to the stress of the missing-rows⁶⁸ additional model for the STO (110) surface reconstruction appeared. Brunen and Zegenhagen studied undoped SrTiO₃ (110) single-crystal surfaces treated with annealing at 1000 °C in ultrahigh vacuum⁶⁴. They observed the sample with Scanning Tunneling Microscopy (STM) and the results showed that the surfaces contained TiO₂ (100)

Properties of STO

and TiO_2 (010) microfaceted planes. The planes are consequences of the Sr and O desorption from the SrTiO - terminated surface. A. Gunhold et al. performed similar experiment on STO (110) and their results confirmed the coexistence of two periodicities⁶⁹. Actually, the removal of Sr and O atoms from the surface leads to the periodicity of (1x1) while the removal of the additional Sr, Ti and O atoms provokes to the reconstruction with (1x2) periodicity. For the (1x1) periodicity the spacing between the rows has to be 0.55 nm, whereas for the (1x2) periodicity is 1.1 nm. These were in good agreement with their AFM measurement and it is presented in Figure 1.2.14.

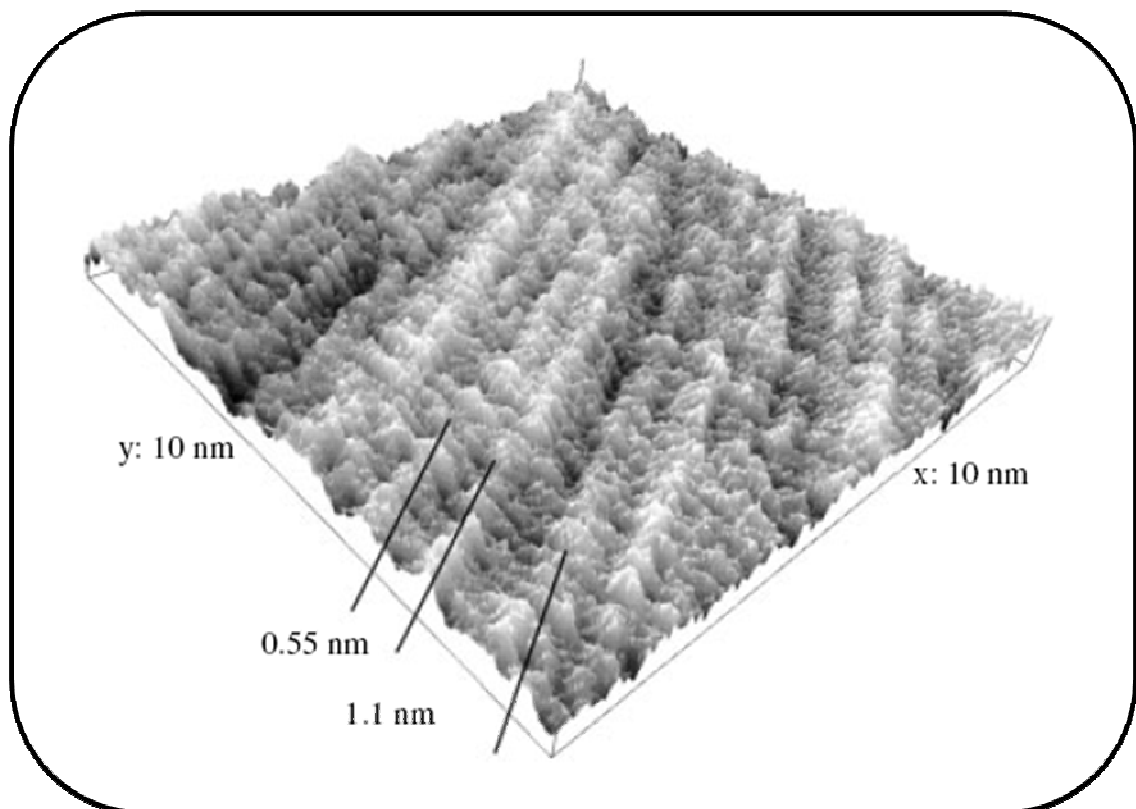


Fig1.2.14: The AFM image $10 \times 10 \text{ nm}^2$ of the SrTiO_3 (110) surface heated at $900 \text{ }^\circ\text{C}$ for 1 h in synthetic air (20% O_2 , 80% N_2).⁶⁹

Since the other types of the reconstruction, such as (4x6), and at the same time, morphological changes on (110) surface often appear during the thermal treatment, analysis of this kind of the reconstruction was one of the subjects of the studies performed during the course of this PhD thesis. The obtained results are presented in subchapter 3.4.

References:

- 1 H. Yamada and G. R. Miller, J. Solid State Chem. **6**, 169 (1973).
- 2 J. Blanc and D. L. Staebler, Phys. Rev. B **4**, 3548 (1971).
- 3 H. P. R. Frederikse, W. R. Thurber, E. R. Hosler Phys. Rev. **134**, A442 (1964).
- 4 Muller, D. A., Nakagawa, N., Ohtomo, A., Grazul, J. L. & Hwang, H. Y, Nature **430**, 657 (2004).
- 5 D. M. Smyth, Prog. Solid St. Chem. **15**, 145 (1984).
- 6 V. E. Henrich, G. Dresselhaus, H. J. Zeiger, Phys. Rev. B **17**, 4908 (1978)
- 7 M. R. Castell, Surf. Science **516**, 33 (2002)
- 8 Reagor, D. W. & Butko, V. Y Nature Materials **4**, 593 (2005)
- 9 D. Kan, T. Terashima, R. Kanda, A. Masuno, K. Tanaka, S. Chu, H. Kan, A. Ishizumi, Y. Kanemitsu, Y. Shimakawa, and M. Takano, Nat. Mater. **4**, 816 (2005)
- 10 E. B. Várhegyi, I. V. Perczel, J. Gerblinger, M. Fleischer, H. Meixner and J. Giber, Sensors and Actuators B **18-19**, 569 (1994).
- 11 Z. Liu, Appl. Phys. Lett. **90**, 201104 (2007).
- 12 M. J. Akhtar, Z. Akhtar, R. A. Jackson and C. R. A. Catlow J. Am. Ceram. Soc. **78**, 421 (1995).
- 13 S. Ruddlesden and R. Popper, Acta Crystallogr. **11**, 54 (1958).
- 14 K. Szot, W. Speier, J. Herion and Ch. Freiburg Appl. Phys. A **64**, 55 (1997).
- 15 U. Balachandran and N. G. Eror, J. Mat. Sci. **17**, 2133 (1982).
- 16 S. Witek, D. M. Smyth and H. Pickup J. Am. Ceram. Soc. **67**, 372 (1984).
- 17 Peter Blennow, Kent K. Hansen, L. Reine Wallenberg, Mogens Mogensen, Electrochimica Acta **52**, 1651 (2006).
- 18 A. Tsuzuki, K. Kato, K. Kusimoto, Y. Torii, J. Of Mat. Sc. Lett. **16** 1652 (1997).
- 19 E. Heifets, R.I. Eglitis, E.A. Kotomin, J. Maier, G. Borstel, Phys. Rev. B **64**, 235417 (2001).
- 20 E. Heifets, R.I. Eglitis, E.A. Kotomin, J. Maier, G. Borstel, Surface Science **513**, 211 (2002).
- 21 M. J. Lax, *Symmetry Principles in Solid State and Molecular Physics* (Wiley, New York, 1974).
- 22 V. Vixnina, R. Eglitis, E.A. Kotomin, S. Kapphann, G. Borstel, Mater. Res. Soc. Symp. Proc. **677**, AA4.15.11-AA14.15.16 (2001).
- 23 A. Reller, J. M. Thomas, F. R. S., D.A. Jefferson and M. K. Uppal, Proc. R. Soc. Lond. A **394**, 223 (1984).
- 24 T. Nishimura, A. Ikeda, H. Namba, T. Morishita, Y. Kido, Surface Science **421**, 273 (1999).
- 25 M. O. Selme and P. Pêcheur, J. Phys C: Solid State Phys. **16**, 2559 (1983).
- 26 Field Levin, Plock and Merker J. Opt. Soc. Am. **45** 737 (1955);
- 27 J. A. Noland, Phys. Rev. **94**, 724 (1954).
- 28 O. N. Tufte, Phys. Rev. **155**, 796 (1967).
- 29 S J. F. Schooley, Phys. Rev. Lett. **12**, 474 (1964);
- 30 K. Szot, W. Speier, G. Bihlmayer, and R. Waser, Nat. Mater. **5**, 312 (2006).
- 31 D. Kan, R. Kanda, Y. Kanemitsu, Y. Shimakawa, M. Takano, T. Terashima, and A. Ishizumi, Appl. Phys. Lett. **88**, 191916 (2006).
- 32 A. Rubano, D. Paparo, M. Radović, A. Sambri, F. Miletto Granozio, U. Scotti di Uccio, and L. Marrucci, Appl. Phys. Lett. **92**, 021102 (2008).
- 33 H. Hwang, Nat. Mater. **4**, 803 (2005).

- 34 S. Mochizuki, F. Fujishiro, and S. Minami, *J. Phys.: Condens. Matter* **17**, 923 (2005).
- 35 Y. Liang and D. A. Bonnell, *Surface Science Lett.* **285**, 510 (1993).
- 36 Y. Liang and D. Bonnell, *J. Am. Ceram. Soc.* **78**, 2633 (1995).
- 37 T. Matsumoto, H. Tanaka, T. Kawai and S. Kawai, *Surface Science Lett.* **278**, 153 (1992).
- 38 Q.D. Jiang, J. Zegenhagen, *Surf. Science* **425**, 343 (1999).
- 39 Q. Jiang and J. Zegenhagen, *Surface Science* **367**, 42 (1996).
- 40 Fabien Silly, David T. Newell, Martin R. Castell, *Surface Science* **600**, 219 (2006).
- 41 N. Erdman, L.D. Marks, *Surface Science* **526**, 107 (2003).
- 42 B. Stäuble-Pümpin, B. Ilge, V. C. Matijasevic, P. M. L. O. Scholte, A. J. Steinfort and F. Tuinstra *Surface Science* **369**, 313 (1996).
- 43 P. W. Tasker, *J. Phys. C* **12**, 4977 (1979).
- 44 Vanderbilt D., King-Smith R. D., *Phys. Rev. B* **48**, 4442 (1993).
- 45 Claudine Noguera, *J. Phys: Condens. Matter* **12**, 367 (2000).
- 46 Ariana Pojani, Fabio Finocchi, Claudine Noguera, *Surface Science* **442**, 179 (1999).
- 47 C.Duke, *Chem. Rev.* **96**, 1237 (1996).
- 48 J. Goniakowski and C. Noguera, *Surface Science* **365**, 65 (1996).
- 49 N. B. Brookes, F. M. Quinn and G. Thornton, *Physica Scripta* **36**, 711 (1987).
- 50 R. Courths, J. Noffke, H. Wern and R. Heise, *Phys. Rev. B* **42**, 9127 (1990).
- 51 W. A. Harrison, *Electronic Structure and the Properties of Solids*. (W. H. Freeman and Company, San Francisco 1980).
- 52 V. Ravikumar, D. Wolf and V. P. Dravid, *Phys. Rev. Lett.* **74**, 960 (1995).
- 53 N. Bickel, G. Schmidt, K. Heinz and K. Müller, *Phys. Rev. Lett.* **62**, 2009 (1989).
- 54 T. Kubo, H. Nozoye, *Phys. Rev. Lett.* **86**, 1801 (2001).
- 55 K. Szot, W. Speier, *Phys. Rev. B* **60**, 5909 (1999).
- 56 A. Hirata, A. Ando, K. Saiki and A. Koma, *Surface Science* **310**, 89 (1994).
- 57 T. Kubo and H. Nozoye, *Surf. Sci.* **42**, 177 (2003).
- 58 K. Hawkins, T.J. White, *Phys. Eng. Sci.* **336**, 541 (1991).
- 59 M.R. Castell, *Surface Science* **516**, 33 (2002).
- 60 Martin R. Castell, *Surface Science* **505**, 1 (2002).
- 61 David S. Deak, Fabien Silly, David T. Newell, and Martin R. Castell, *J. Phys. Chem. B* **110**, 9246 (2006).
- 62 K. Szot and W. Speier, *Phys. Rev. B* **60**, 5909(1999).
- 63 H. Bando, Y. Ochiai, Y. Aiura, Y. Haruyama, T. Yasue, and Y. Nishihara, *J. Vac. Sci. Technol. A* **19**, 1938 (2001).
- 64 J. Brunen and J. Zegenhagen, *Surf. Sci.* **389**, 349 (1997).
- 65 Francois Bottin, Fabio Finocchi, and Claudine Noguera, *Phys. Rev. B.* **68**, 035418 (2003).
- 66 E. Heifets, W. A. Goddard III, E. A. Kotomin, R. I. Eglitis and G. Borstel, *Phys. Rev. B* **69**, 035408, (2004).
- 67 E. A. Kotomin, E. Heifets, S. Dorfman, D. Fuks, A. Gordon and J. Maier, *Surf. Sci.* **566–568**, 231 (2004).
- 68 Alessio Filippetti and Vincenzo Fiorentini, *Phys. Rev. B* **60**: 14366 (1999).
- 69 A. Gunhold, L. Beuermann, K. Gomann, G. Borchardt, V. Kempster, W. Maus-Friedrichs, S. Piskunov, E. A. Kotomin and S. Dorfman, *Surf. Interface Anal.* **35**, 998 (2003).

1.3 PROPERTIES OF TiO₂

TiO₂ has wide palette of applications and great effort has been put to understand TiO₂ properties and the obtained knowledge becomes basic stone in understanding metal oxide surfaces. Moreover, the surface plays major role in catalysis, photo-catalysis, solar cells, etc. and in all these TiO₂ anatase as one of polymorphous represents one of the most important materials. In the following chapter is description of TiO₂ crystals, electronic and surface structure with strong accents on anatase.

1.3.1 Crystal structures of TiO₂

Titanium dioxide TiO₂, commercially named titania, is typically found in three allotropic modifications with different crystal structures ¹.

1. rutile, with a tetragonal crystal structure;
2. anatase - also with a tetragonal crystal structure;
3. brookite with a rhombohedral structure.

It is worth mentioning that other TiO₂ structures exist as well but they are either unstable or their synthesis is more than difficult ².

Rutile, anatase and brookite, all contain 6 coordinate titanium (Ti- octahedra) as basic structural block. The crystal structures of rutile, anatase and brookite are presented in Fig 1.3.1. All of them are presented in two ways, on the left positions of Ti- octahedra in crystal lattice are shown, while on the right lattice representation with titanium and oxygen atoms positions are depicted. For rutile and anatase, Ti-octahedras are slightly distorted, the two bonds between Ti and O atoms are longer at the apices of octahedron. These facts lead to deviation from 90 degrees angle bond in anatase phase.

All of these phases of TiO₂ have wide band gaps which potentially enable the introduction of both, deep donor and deep acceptor levels. Thus TiO₂ can be doped heavily with both n- and p- type carriers ³. All these materials are transparent in the visible region and with a high refractive index, which allows several optical applications. TiO₂ also has a high dielectric constant and can be a good candidate as the gate material in Field-Effect Transistor (FET) logic devices ⁴.

Properties of TiO₂

Doped with Co or Fe, TiO₂ is believed to be diluted magnetic semiconductors (DMS) oxide, and could possibly play a key role in semiconductor based spintronics technology⁵.

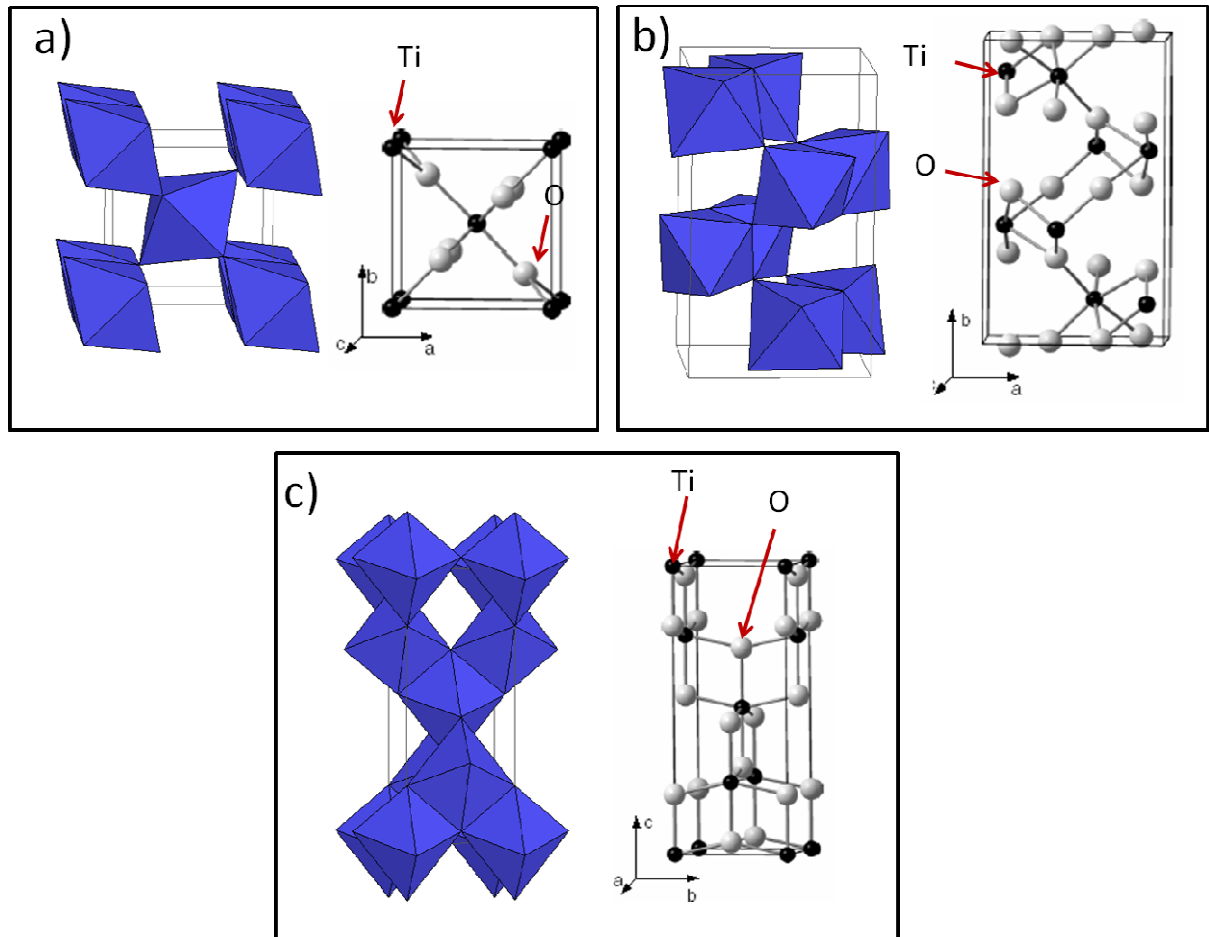


Fig.1.3.1: Schematic diagrams of the polymorphs of TiO₂: a) rutile, b) anatase and c) brookite.

The physical properties of TiO₂ polymorphs are given in the Table 1.3.1. With regards to anatase, which is the allotropic form studied in thin film form in the present work, it is worth mentioning that it has the lowest density among the three main allotropic forms.

Table 1.3.1: Physical properties of three phases of TiO₂.

TiO ₂	Rutile	Brookite	Anatase
Lattice constants (Å)	a=b=4.59; c=2.953	a=9.18;b=5.45 c=5.15	a=b=3.782 c=9.502
Space group	P4 ₂ /mnm	Pbca	I4 ₁ /amd
Molecule/cell	2	8	4
Ti-O bond length(Å)	1.95(4), 1.98(2)	1.87 ~ 2.04	1.94(4), 1.97(2)
O-Ti-O bond angle	81.2°, 90.0°	77.0° ~ 105°	77.7°, 92.6°
Volume/molecule(Å³)	31.22	32.17	34.06
Density(g/cm³)	4.13	3.99	3.79

Moreover, anatase is meta-stable phase and it can be transformed easily in rutile at relatively low temperature (below 700⁰ C) while brookite is instead unstable ⁶.

Anatase surface science is relatively recent due to the difficulty in producing large enough monocrystals. Additionally, commercially available titania is a mixture of rutile and anatase phases, so to obtain clean anatase measurements is very difficult. As shown bellow, large anatase surfaces can now be produced by resorting to epitaxial thin film growth.

1.3.2 Anatase electronic structure

Both polymorphisms with a tetragonal crystal structure, anatase and rutile, are wide band-gap insulators with band gaps of 3.1 eV for rutile and 3.2 eV for anatase ⁷. Although rutile can absorb UV light almost down to the upper edge of visible light, anatase exhibits higher photo activity (for catalysis) due to the difference in the position of the conduction band.

The analysis of the electronic structure of anatase is fundamental for understanding of its catalytic and optical properties and the following text brings the description of that.

The valence band of anatase is created, mainly, of O2p states, with some Ti3d and Ti4sp character acquired through hybridization with the empty Ti 3d/4sp conduction-band states. Formation of the valence band is shown on Fig 1.3.a.

R. Asahi et al. used First-principles calculations of the full-potential linearized augmented plane-wave method to investigate the detailed electronic and optical properties of TiO₂ in the anatase structure⁸. Calculated band structure of the anatase is presented in Fig 1.3.b. A minimum direct band gap was found at Γ point. The energy difference in the valence-band maxima at Γ and Z was, however, only 2 meV but the band gap obtained, 2.0 eV, is much smaller than experimentally obtained 3.2 eV⁹. This difference could be due to the well known shortcoming of Local Density Approximation -LDA¹⁰.

Anatase loses oxygen easily from the surface and bulk during annealing at temperatures of around 500–700 °C in HV or UHV conditions. As consequence of the annealing, anatase becomes an n-type semiconductor (TiO_{2-x}) containing oxygen vacancies. The presence of O vacancies at the surface and the connected defect electrons, which remain localized as Ti³⁺ ions, results in the appearance of a defect peak or band-gap state at around 1 eV binding energy, between the valence band and the Fermi energy^{1, 11-14}.

The low-binding energy states may be accessed during a catalytic redox cycle, in the case of unreduced surfaces, the atomic character of the states close to the valence-band maximum (VBM) may be of importance in determining the catalytic activity of the surface. For reduced surfaces, the presence of defect states at around 1 eV from the Fermi energy is likely to have a substantial influence on the reactivity of the surface, through changes in both the electronic structure of the surface and in the geometric structure caused by the presence of oxygen defects.

The resonant behavior of anatase TiO₂ (101) and (001) surfaces has been investigated using synchrotron photoemission spectroscopy by A. G. Thomas et al¹¹. The results obtained are shown in Fig 1.3.2.c.

The data for the (101) surface are in agreement with the bulk band-structure calculations. At the same time, they noticed deviations of the data from the bulk band structure in the case of the (001) surface. Explanation for this could be that in the case of (001) surface the reconstruction plays important role. Since the sample was annealed in order to get the conducting sample, a small peak is observed at around 1 eV binding energy for both surfaces.

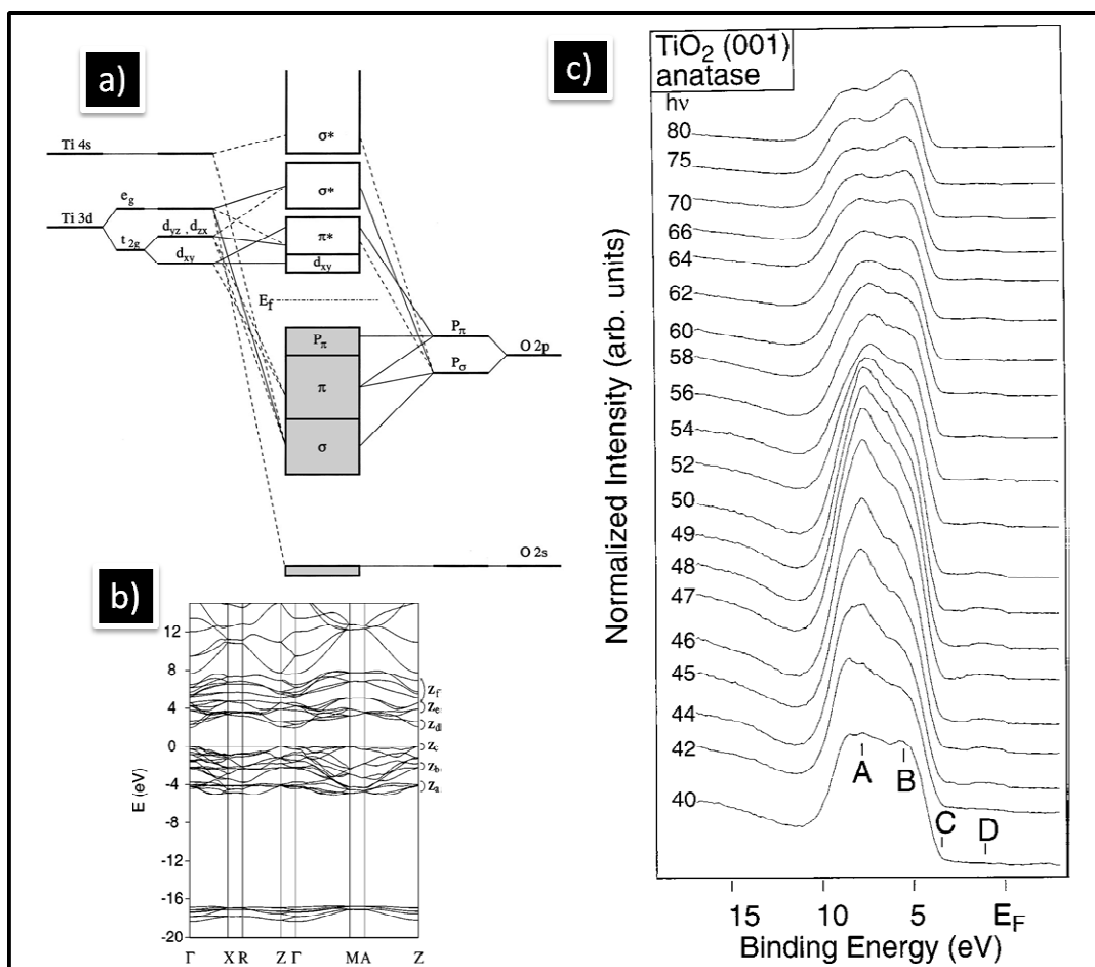


Fig. 1.3.2: Electronic structure of anatase: a) Molecular-orbital bonding structure for anatase TiO₂; b) Calculated band structure of the anatase TiO₂ structure; c) Energy distribution curves from the clean TiO₂ anatase (001) surface at increasing photon energies. The points marked as A, B, C, and D refer to the binding energies. A=58.2 eV, B=5.4 eV, C=4.0 eV, D=1.1 eV^{8, 11}.

These results are concordant with well known effect of the creation of surface defects O vacancies which is connected with Ti³⁺ generation on the surface. Mostly, the Ti³⁺ peak in XPS spectra is hard to detect even though the samples were strongly treated (ion spattering and UHV annealing). Creation of oxygen vacancies on anatase surface sufficient for XPS detection is more difficult than, for example, in the case of STO. This may be consequence of strong surface reconstruction in the case of anatase.

1.3.3 Thin films of TiO₂ anatase grown on different substrates

In order to avoid impurities which are often found in mineral samples (Iron, Calcium...) and mixed phases (anatase and rutile) the great effort is put in figuring out out successfully growth methods for anatase growth. Developed growth methods resulted in high-purity anatase single crystals and films of dimensions sufficiently large for applicative and fundamental studies. In industry, more specific in catalysis, photo-catalysis, and dye-sensitized solar cells, there is significant interest in the synthesis of phase-pure anatase thin films because this polymorphism is proven to be more advantageous over the rutile phase.

In this section, a brief overview about a deposition of anatase thin films will be presented.

As already mentioned, according to the phase diagram of TiO₂, the rutile phase is thermodynamically preferred at high temperature and is expected that no pure anatase phase can exist at temperatures higher than 650 °C¹⁵. As a consequence of this fact, and if we keep in mind that almost all growth techniques require high temperature in the process, obtaining of pure anatase phase seems very ambitious. As an illustration of this, most commercial TiO₂ powder catalysts are mixture of 80-90% anatase and rest of rutile¹⁶.

The deposition of TiO₂ thin films by pulsed laser deposition (PLD) has been reported previously¹⁷⁻¹⁹. The structural properties, crystallinity, and the surface morphology of the TiO₂ films deposited on Si, MgO, and sapphire substrates under various deposition conditions such as oxygen partial pressure PO₂ and substrate temperature were investigated.

Generally speaking, the structure of the obtained films is strongly dependent on the substrate and in their cases the quality of the films was not satisfied.

However, Chen et al. used the metallorganic chemical vapor deposition technique (MCVD) to prepare mono-phasic anatase and rutile films on SrTiO₃ (STO) and sapphire substrates, respectively²⁰. They showed that the pure anatase phase can be grown on STO (100) even when the substrate temperature (Ts) is higher than 900 °C. This indicates that substrate structure can play a significant role in controlling the heteroepitaxial growth of TiO₂ films.

STO as a substrate for anatase growth might not seem as an optimal choice considering relatively big mismatch (about 3%) between their lattices. TiO₂ anatase

heteroepitaxial growth is, however, possible without big a structural tension on interface. It should be pointed out again, that in both cases the building blocks are identical, Ti octahedra. Heteroepitaxial growth of TiO₂ anatase film could be explained as continuous formation of oxygen atom network with additional extension from STO substrate into the film. Within this oxygen sublattice, the relatively small Ti cations arrange in their correct sites. Formation of the interfaces in this way is common model for hetero epitaxial growth of metal oxides and could be implemented in the case of anatase growth on STO ²¹.

In any case, to have a successful heteroepitaxial growth, the mismatch between the substrate and film lattices has to be as small as possible. In the instance of TiO₂ anatase LaAlO₃ (001) can be seen as optimal substrate candidate. Although the crystal structure of LaAlO₃ is rhombohedral, it can be accepted as a pseudocubic cell (as perovskite) with displaced O ions. If so, the unit cell parameter is 0.379 nm. In such case the mismatch is very small, about 0.2% and the starting condition for the epitaxial growth is satisfied.

Another advantage which results from this solution of growth is that it is possible to evaluate optical properties of these anatase thin films because of wider a gap of LAO then STO. In the case of STO substrate there are difficulties in optical properties measurements because of the overlapping band gap energies (3.2 eV for both anatase and SrTiO₃). Indeed, M. Murakami et al. demonstrated possibility to fabricate epitaxial anatase thin films on lattice-matched LaAlO₃ (001) substrates in the layer-by-layer growth by laser molecular-beam epitaxy. X-ray diffraction and transmission electron microscope performed on the films show evidence of high crystallinity and atomically defined interfaces ²².

Current studies on epitaxially-stabilized anatase are focused on pulsed-laser deposition or molecular beam epitaxy. These techniques enable simple fabrication with full control of deposition parameters and reproducibility of the films quality.

The research performed during this PhD studies and reported in the Chapter IV aimed at stabilizing the growth of the anatase phase in epitaxial thin films, by resorting to three different substrates, SrTiO₃, SrLaAlO₄ and LaAlO₃. It is widely noticed that during sample deposition or preparation for the measurement of anatase growth on STO by the techniques which are charge sensitive, on the

surface appear Strontium^{23, 24}. This was also goal of this thesis and study regarding the presence of Sr into anatase thin film is presented in the subchapter 4.3.

1.3.4 Surface structure, reconstruction and properties of anatase (001)

Surface of materials has, usually, different physical and chemical properties than bulk. For metal oxide system such SrTiO₃ or TiO₂, because of their mixed ionic covalent bonding, the surface structure has higher influence on surface properties than for example metals or semiconductors. As a consequence of above mentioned property and the fact that TiO₂ has wide palette of application great effort has been put to understand TiO₂ properties and the obtained knowledge becomes basic stone in understanding metal oxide surface. The surface plays major role in catalysis, photocatalysis, solar cells, etc. and in all this TiO₂ anatase represents one of the most important materials.

Describing surface with condensed bulk models is almost impossible because these models totally neglect the impressive change in the atoms coordination and crystal potential due to the rapid bulk to vacuum change in the direction normal to the surface. For the complex materials which include several different kinds of atoms in crystal structure bulk-vacuum discontinuity can be even more dramatical. These discontinuities can provoke surfaces change in two ways, relaxation and reconstruction. Relaxation phenomenon is presented on Figure 1.3a and represents a change in the distances between the first few layers of crystal with respect to the bulk values. For the most surfaces the distance d_1 is smaller than the corresponding bulk value. A more rigorous change of structure is the phenomenon of surface reconstruction. This change of the surface is presented on Figure 1.3b. A reconstruction means that the periodicity parallel to the surface is changed in respect to that of the bulk. This phenomenon can be very drastic, it can elicit strong morphological change, it can even create planes with different orientation than cut surface plane, for example microfacets. Surfaces of some materials are completely unstable if exposed to environment and cannot exist as unreconstructed and unrelaxed.

If the material is composed by two or more different kinds of atoms, also the chemical composition at the surface can be different than in the bulk. This effect is called segregation and is presented in Fig 1.3.4.

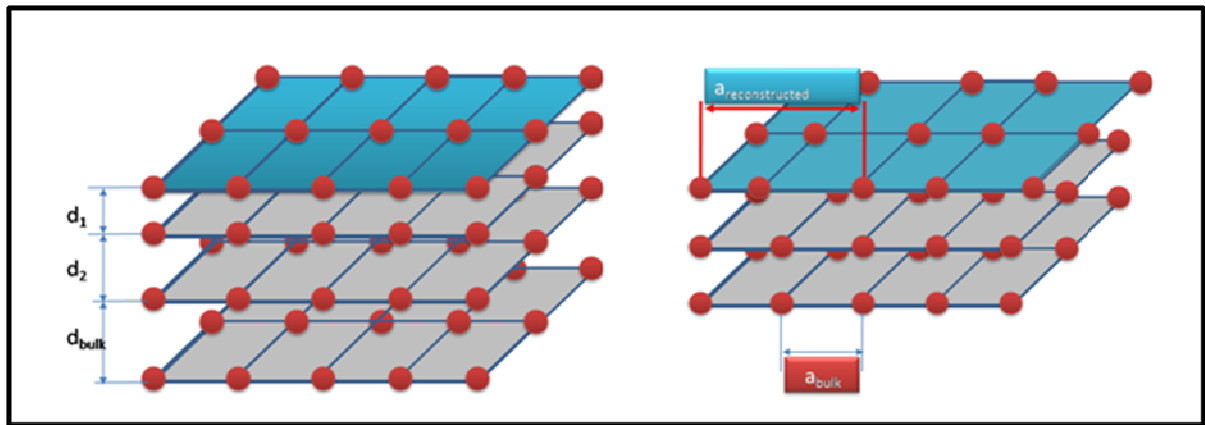


Fig 1.3.3: Schematic presentation of surface: a) relaxation; b) reconstruction.

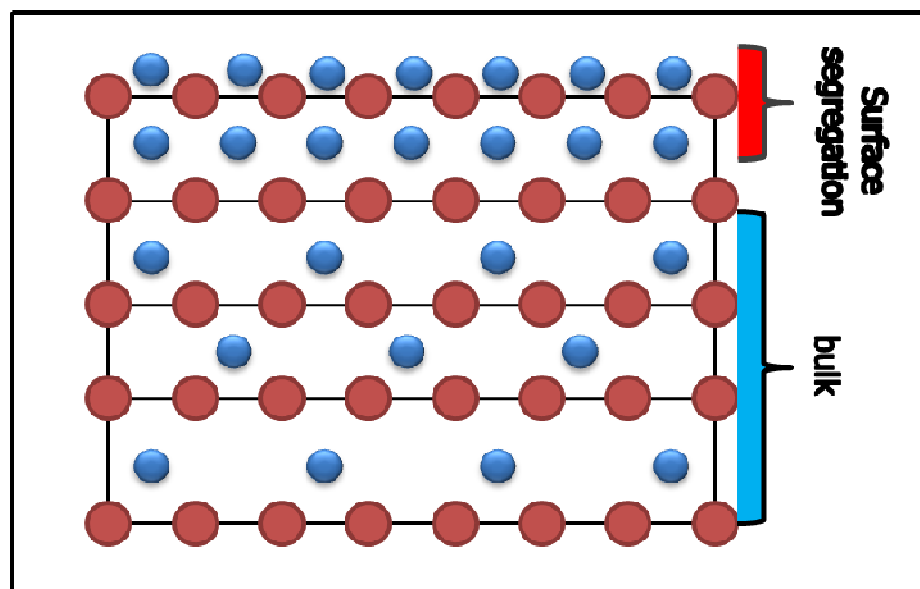


Fig 1.3.4: Schematic presentation of surface segregation.

All of the above mentioned effects appear in complex structures; such crystal of transition metal oxides including TiO₂ and this thesis describe obtained data during the analysis of anatase reconstruction and segregation processes.

Crystal planes, in general, are not equal with respect of energy minimization. For TiO₂ mono crystal Michele Lazzeri et al. calculated formation energies for all of crystallographic planes which are stable ²⁵. Figure 1.3.5 represented Wulffs equilibrium shape of anatase according to theoretical calculation of surface energies from Table 1.3.2.

Table 1.3.2: Calculated surface formation energy (J/m²) for relaxed TiO₂ surfaces²⁵.

Rutile	Anatase					
(110)	(101)	(100)	(103)f	(001)	(103)s	(110)
0.31	0.44	0.53	0.84	0.90	0.93	1.09

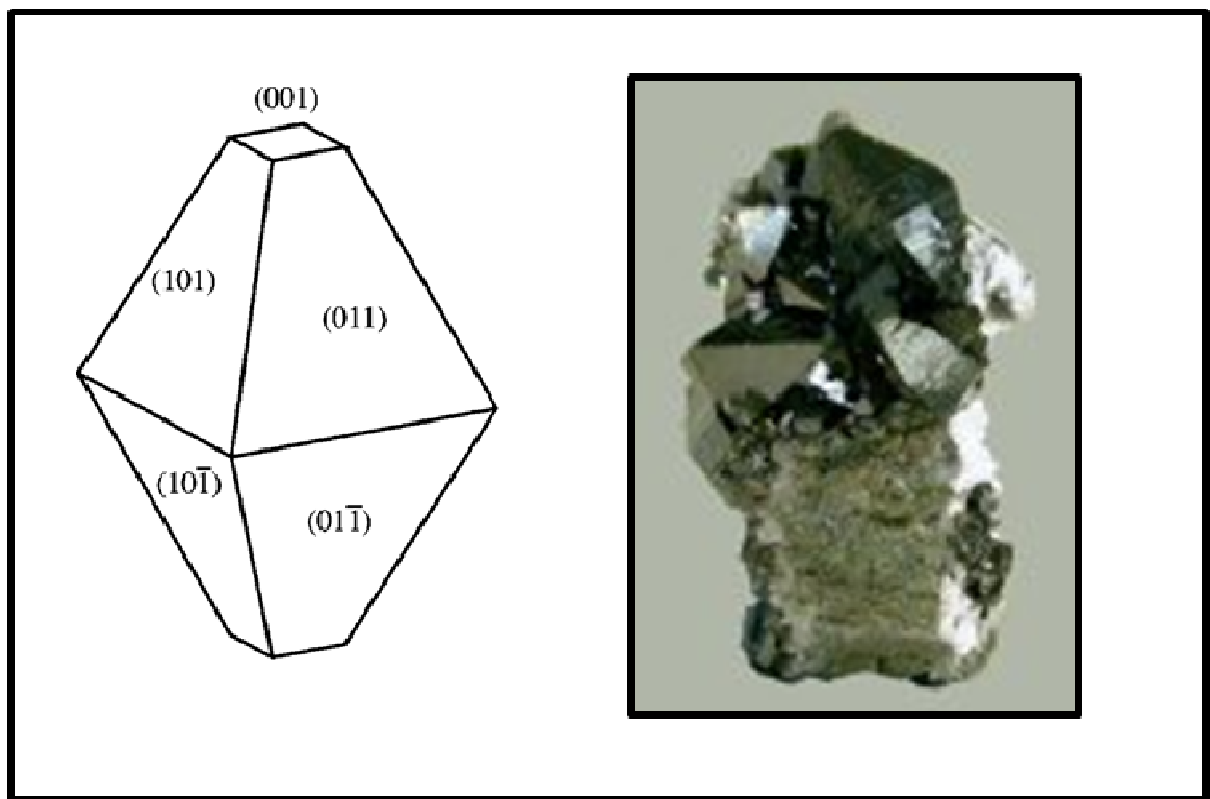


Fig 1.3.5 a) The equilibrium shape of a TiO₂ crystal in the anatase phase, according to the Wulff construction and the calculated surface energies^{1,25}, b) shape of mineral anatase crystal.

From the data presented in Table 1.3.2 is clear that (001) anatase surface is not favorable to form. The (001) surface of anatase exhibits fivefold coordinated Ti atoms, as well as twofold and threefold coordinated oxygen atoms. The corrugation increases leading by relaxation, according calculation, from 0.82 Å to 0.92 Å²⁶.

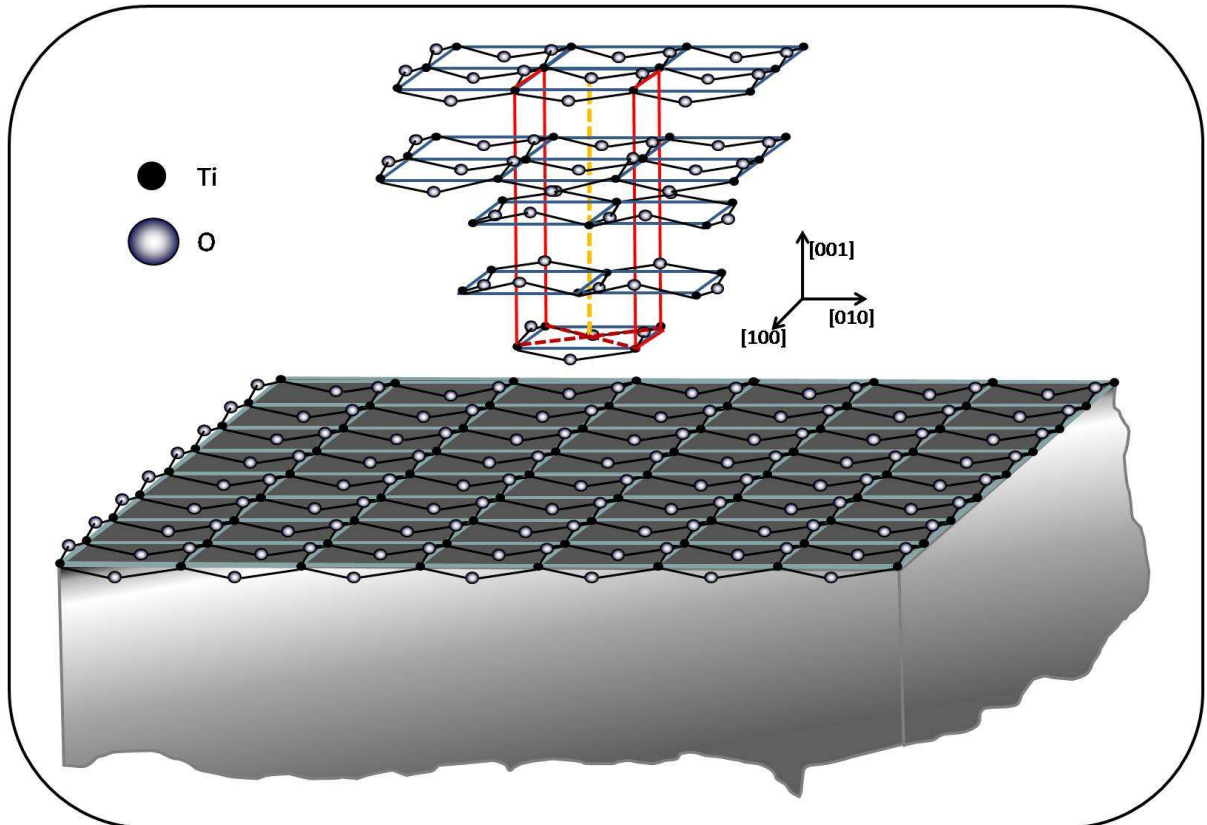


Fig. 1.3.6: Scheme of unreconstructed (001) anatase surface.

The unreconstructed (001) anatase surface is schematically presented in Fig. 1.3.6. The surface, as (1x1) motive, of natural anatase is not very stable and reconstructs when heated for a long enough time at elevated temperature^{23,27}. Only on fabricated sample which was slightly contaminated by carbon²⁸ (1x1) reconstruction surface was observed. Moreover, (001) surface of mineral anatase treated with few cycles of ion sputtering and annealing is always stabilized as (1x4) motives reconstructed like two-domain surface. Detailed structural analysis on this surface so far have been performed on thin film, mainly grown on STO (001) substrate^{23, 29, 30}. Herman and et al. were the first ones to point out that the (1x1) surface of TiO₂ thin film grown on STO (001) after sputtering and annealing under UHV condition transforms in to two domains (1x4) reconstructed surface²³. The initial explanation of this reconstruction was based on ideas of arrangement Oxygen's vacancies. Vacancies can be arranged into rows and finally can create "missing oxygen rows". This model was proposed by Hengerer et al. and the proposed schematic view of (1x4) reconstructed anatase surface is presented in Fig

1.3.7²⁷. This model, actually, can hardly explain the stability of the reconstruction during annealing in the oxygen environment. Anatase films are, in fact grown in an activated oxygen environment with relatively high oxygen partial pressure (approximately in the mbar range). Under these conditions, the (1x4) reconstruction was observed only during the anatase growth by RHEED by several groups including ours^{29, 31-33}. When it became clear that the surface is already (1x4) reconstructed during the growth the interpretation of it as missing oxygen rows was dismissed.

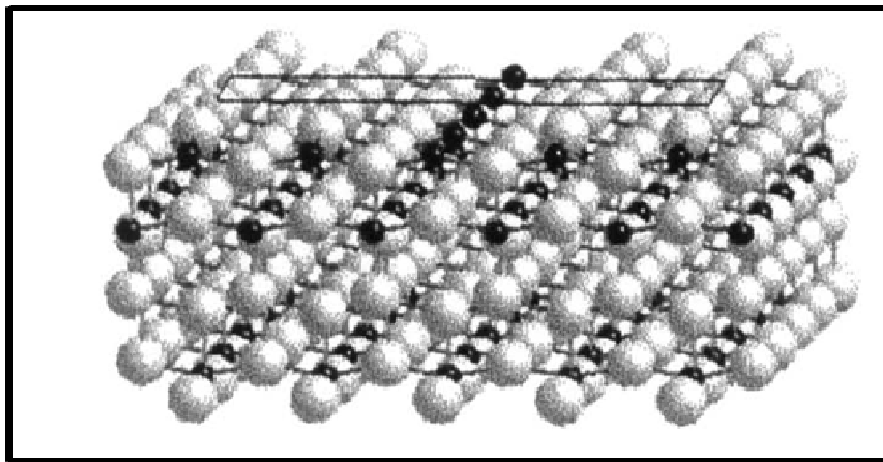


Fig 1.3.7: The missing row model (MRM). Ions are represented by dark circles (Ti) and light circles (O)²³.

In addition, XPS spectra of the (1x4) surface showed none or very weak evidence of Ti³⁺ at the surface. Furthermore, post-growth annealing of the TiO₂ (001)-(1x4) under reduction and oxidation conditions showed no substantial differences in STM, LEED, and XPS results. These experimental evidences suggest that the (1x4) reconstruction is fully oxidized and remains stable under these annealing conditions.

Second model, micro-faceting model, was proposed soon after the first model and it was based on angle resolved mass spectroscopy of recoiled atoms (AR-MRSI). According to this model, (103) planes of anatase with higher stability than (001) are exposed to environment²³. From Table 1.3.2, where the data of surface formation energy are shown, is seen that (103) surface (0.84 J/m²) is more stable than (001) surface (0.90 J/m²). Of course the total energy is higher because the surface increases by a factor SQRT(2). The microfaceting model is schematically

presented in Figure 1.3.8. This model clearly shows that the reconstruction involves half of anatase unit cell, which means that a corrugation of the rows has to be about 4 Å and should be easily detected by microscopy techniques. However, the microfacets model for (1x4) reconstruction surface is not in agreement with the high-resolution STM measurements.

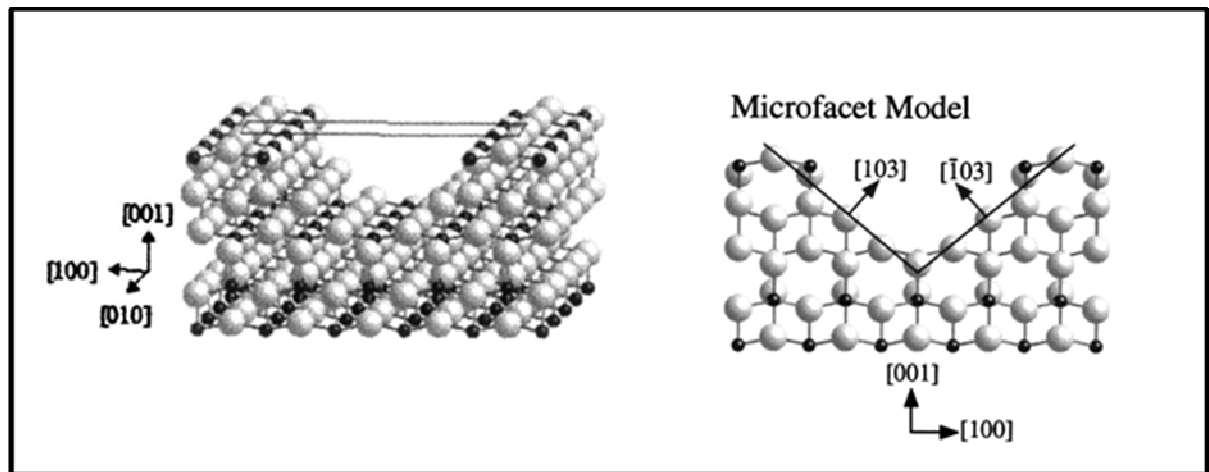


Fig. 1.3.8: a) Model of the microfacet; b) side view along [010] direction (large balls are oxygen atoms and small are Ti).

The STM images of (1x4) anatase reconstructed surface are shown in Figure 1.3.9³⁴. There are domains with rows structures in [100] or [010] directions. The space between the rows corresponds to 4 times the lateral dimension of the unit cell. Steps between the domains on the surface are about 2.4Å high, which corresponds to the distance between two layers of anatase phase. The model is not nevertheless in quantitative agreement with the above mentioned measurements, where the corrugation varied from 0.8 to 1.7 Å²⁹. Similar value and ratio in the corrugation variation in STM measurements were also obtained by the other authors³⁴.

However, the opinion that overpowered is that reconstructed (1x4) surface, in any case, is a structural property of anatase and that it is not due to the formation of any non-anatase phases such as Ti₂O₃ or rutile on the surface.

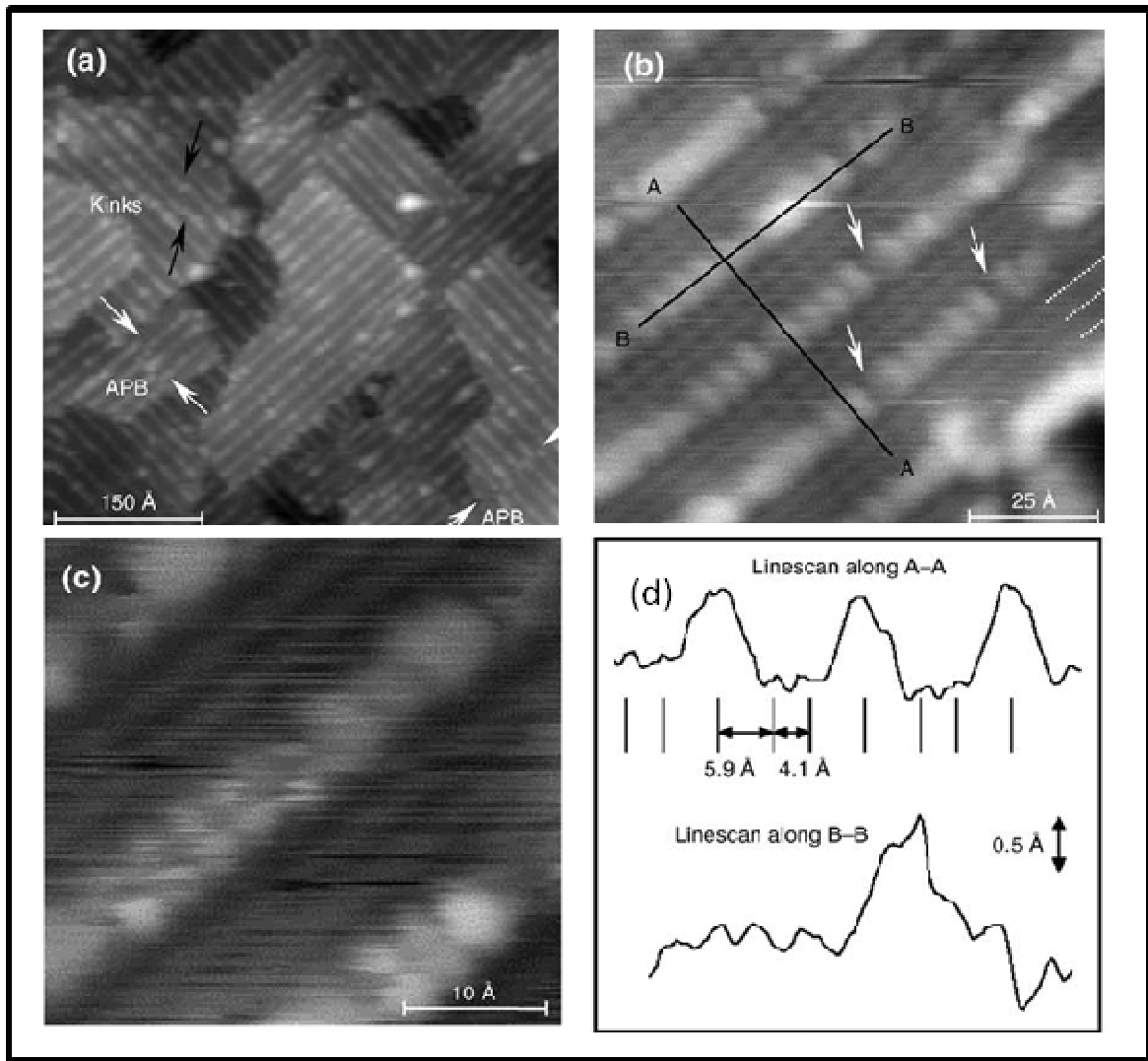


Fig 1.3.9: STM and NC-AFM images of the reconstructed 1x4 anatase (001) films. a) the film after re-annealing in oxygen atmosphere, b) the zoom of a terrace c) high resolution STM shows two parallel rows, d) the profiles of liner scan³⁴.

Nevertheless, the third model has pointed out the above mentioned fact and it conciliate with all collected data about the reconstruction. This model was already mentioned by G. S. Herman and et al. but in a simple form as add row model (ARM)²³.

Consequently, some authors published articles using this model as base with aim to better explain morphological or electronic nature of the reconstruction. One of the first models, based on ARM model, that reconciled with experimental data, was proposed by Yong Liang and et al.²⁹

This model is based on the (1x1) surface structure, involving “added” and “missing” rows. All atoms in this model derive from their bulk positions. Each surface unit cell consists of one added Ti-O row, two added oxygen rows, and one missing oxygen row. The resulting surface is stoichiometric and auto-compensated in charge; thus not only is it energetically favorable, but it also contains no Ti³⁺ states, consistent with XPS results. This model is presented in Figure 1.3.10.

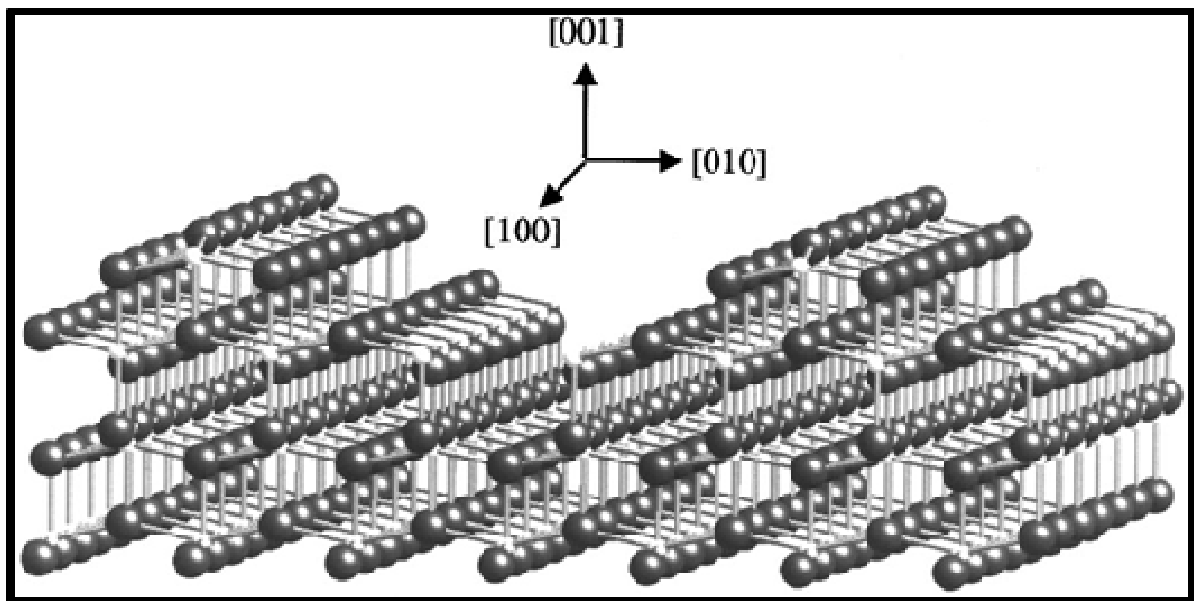


Fig 1.3.10: A ball and stick model of (1x4) reconstruction of (001) anatase (large balls are Oxygen atoms and small are titanium²⁹).

In the subchapter 4.3, representing one of the main goals of this thesis, the experimental work designed to explain formation of (1x4) reconstruction during anatase growth is presented, and it is based on the Yong Liang et al. model.

Finally, also (1x4) reconstruction model proposed by Lazzeri and Selloni²⁵ should be mentioned. The scheme of this model is presented in Figure 1.3.11. Their model is based on the DFT total energy calculations. Moreover, they claim that the model is not energetically favored, but it is in agreement with STM data including the observation of less frequent (1x3) and (1x6) periodicities. According to them, the primary mechanism of this reconstruction is the relief of the surface stress.

This mechanism is familiar in the context of metal and semiconductor surface reconstructions³⁵.

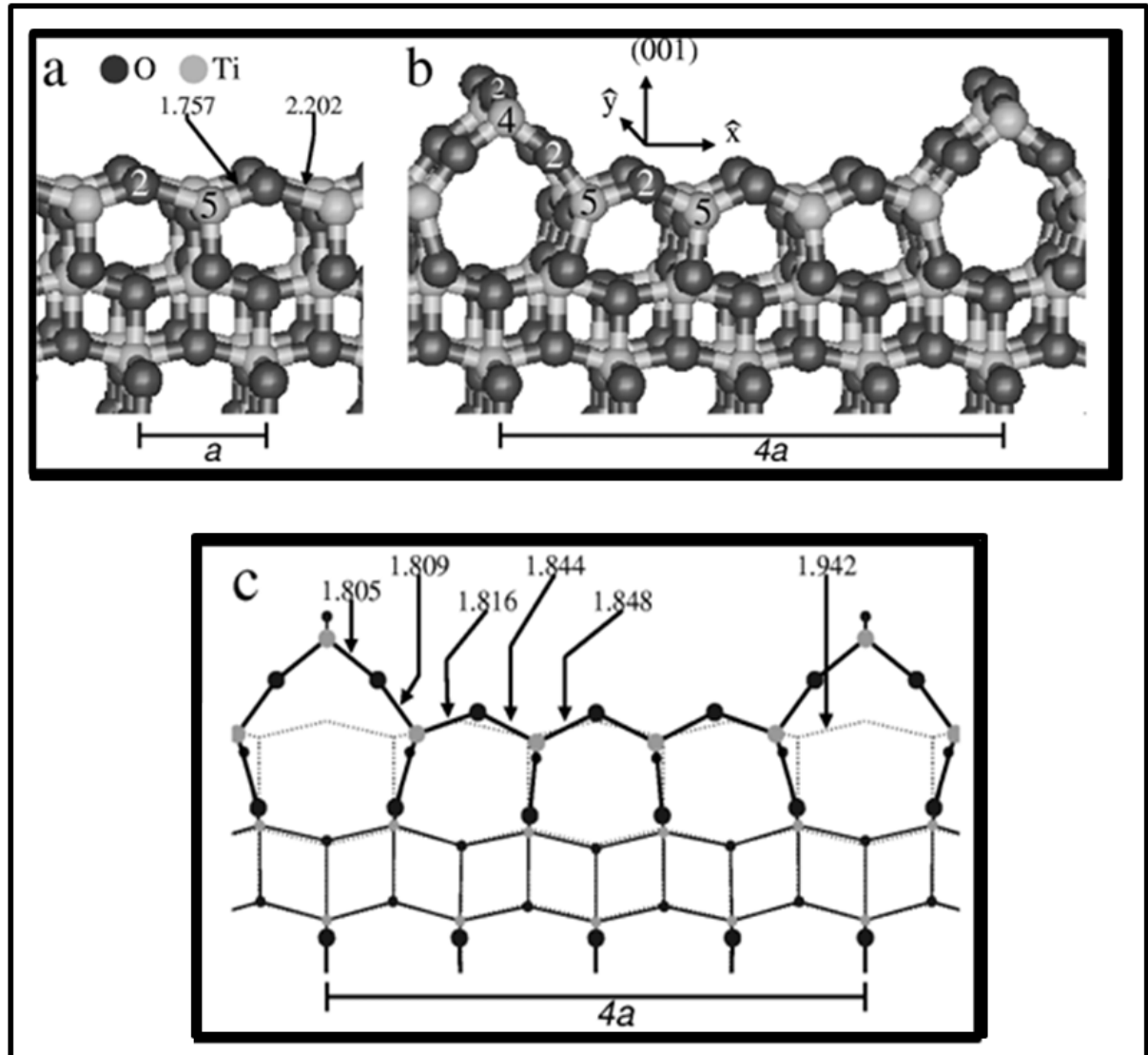


Fig 1.3.11: (1×4) reconstruction model of (001) anatase: a) (1×1) relaxed (001) surface of TiO_2 anatase; b) Relaxed structure of the ADM (1×4) reconstruction; c) Projection of the atomic positions of the ADM model²⁵.

In their model, the (1×4) periodicity of reconstruction, compare with the other $(1 \times n)$ reconstructions, is the most favorable, but the predicted surface energy differences between this and the other are very small.

References:

- 1 U. Diebold, Surf. Sci. Rep. **48**, 53 (2003).
- 2 L.S Dubrovinsky, et all. , Nature **410**, 653 (2001).
- 3 Angus I. Kingon, Jon-Paul Maria and S. K. Streiffer, NATURE **406** (2000).
- 4 Campbell, S. A. et al. , IEEE Trans. Electron Devices **44**, 104 (1997).
- 5 Yuji Matsumoto, Makoto Murakami, Tomoji Shono, Tetsuya Hasegawa,
Tomoteru Fukumura, Masashi Kawasaki, Parhat Ahmet, Toyohiro Chikyow,
Shin-ya Koshihara, Hideomi Koinuma, SCIENCE **291** (2001).
- 6 J.M.G. Amores, et. all, J.Mater. Chem. **5**, 1245 (1995).
- 7 L. Kavan, M. Grätzel, S. E. Gilbert, C. Klemenz, and H. J.Scheel, J. Am.
Chem. Soc. **118**, 6716 (1996).
- 8 Y. Taga R. Asahi , W. Mannstadt and A. J. Freeman, Phys. Rev. B **61**,
7459 (2000).
- 9 H. Tang, H. Berger, P.E. Schmid, F. Le´vy, and G. Burri, SolidState
Commun **23**, 161 (1977).
- 10 R.M. Dreizler, and E.K.U. Gross, *Density Functional Theory, An Approach
to the Quantum Many-Body Problem* (Springer- Verlag, Berlin, 1990).
- 11 A. G. Thomas, W. R. Flavell, A. R. Kumarasinghe, A. K. Mallick, D.
Tsoutsou, G. C. Smith, R. Stockbauer, S. Patel, M. Grätzel, and and R.
Hengerer, Phys. Rev. B **67**, 035110 (2003).
- 12 Z. Zhang, S.P. Jeng, and V. E. Henrich, Phys. Rev. B **43**, 12004 (1991);
- 13 J. Nerlov, Q. Ge, and P. J. Møller, Surf. Sci. Rep. **348** 28 (1996);
- 14 R. Heise, R. Courths, and S. Witzel, Solid State Commun. **84**, 599 (1992).
- 15 F. Dache, P. Y. Simons, and R. Roy, Am. Mineral. **53**, 1929 (1968).
- 16 C.N. Satterfield, *Heterogeneous Catalysis in Industrial Practice*, 2nd ed.
(McGraw-Hill, New York, 1991).
- 17 H. A. Durand, J. H. Brimaud, O. Hellman, H. Shibata, Y. Makita, D.Gesbert,
and P. Meyrueis, Appl. Surf. Sci. **86**, 122 (1995);
- 18 C. Garapon, C. Champeaux, J. Mugnier, G. Panczer, P. Marchet, A.
Catherijot and B. Jacquier, Appl. Surf. Sci. **96-98**, 836 (1996);
- 19 J. H. Kim, S. Lee, and H. S. Im, Appl. Surf. Sci. **151**, 6 (1999).
- 20 S. Chen, M. G. Mason, H. J. Gysling, G. R. Paz-Pujalt, T. N. Blanton, T., K.
M. Chen Castro, C. P. Fictorie, W. L. Gladfelter, A. Franciosi, P. I., and and
J. F. Evans Cohen, J. Vac. Sci. Technol. A **11**, 2419 (1993).
- 21 D.S. Lind, et. all, Phys. Rev. B **45**, 1838 (1992).
- 22 M. Murakami, M. Matsumoto, K. Nakajima, T. Makino, Y. Segawa, T.
Chikyow, P. Ahmet, M. Kawasaki, and H. Koinuma, Appl. Phys. Lett. **78**,
2664 (2001).
- 23 M. R. Seivers and Y.Gao G.S. Herman, Phys. Rev. Lett. **84**, 3354 (2000).
- 24 M. R. Seivers and Y.Gao G.S. Herman, Phys. Rev. Lett. **84**, 3354
(2000).
- 25 Michele Lazzeri, Andrea Vittadini, and Annabella Selloni, Phys. Rev. B **63**,
155409 (2001).
- 26 A. Vittadini, A. Selloni, F. P. Rotzinger, and M. Gratzel, Phys. Rev. Lett **81**,
2954 (1998).
- 27 R. Hengerer, B. Bolliger, M. Erbudak, M. Grätzel, Surf. Sci. **460**, 162
(2000).
- 28 G.S. Herman, Y. Gao, T.T. Tran, J. Osterwalde, Surf. Sci **447**, 201 (2000).

- ²⁹ Yong Liang, Shupan Gan and Scott A. Chambers, *Phys. Rev. B* **63**, 235402 (2001).
- ³⁰ W. Hebenstreit, N. Ruzycki, G. S. Herman, Y. Gao, and U. Diebold, *Phys. Rev. B* **62**, 16334 (2000).
- ³¹ S.A. Chambers, C.M. Wang, S. Thevuthasan, T. Droubay, D.E. McCready, A.S. Lea, V. Shutthanandan, C.F. Windisch Jr, *Thin Solid Films* **418**, 197 (2002);
- ³² Patrick Fisher, Oleg Maksimov, Hui Du, Volker D. Heydemann, and Paul A. Salvador Marek Skowronski, *Microelectronics Journal* **37**, 1493 (2006);
- ³³ M. Radović, G. M. De Luca, R. Di Capua, N. Lampis, P. Perna, M. Salluzzo, A. Sambri, U. Scotti Di Uccio, F. Miletto Granozio and R. Vaglio, presented at the Thin Films for Novel Oxide Devices -THIOX Barcelona (Spain), 2007 (unpublished).
- ³⁴ R.E. Tanner, A. Sasahara, Y. Liang, E.I. Altman, H. Onishi, *J. Phys. Chem. B* **106**, 8211 (2002).
- ³⁵ H.Ibach, *Surf. Sci. Rep.* **29**, 195 (1997).

2. THIN FILM GROWTH AND ANALYTIC TECHNIQUES AT MODA SYSTEM

The experimental results presented in this thesis are obtained using a particularly complex experimental set-up named MODA, which is the acronym for Modular facility for Oxides Deposition and Analysis. The photo and the scheme of the MODA system are shown in Figure 2.1.

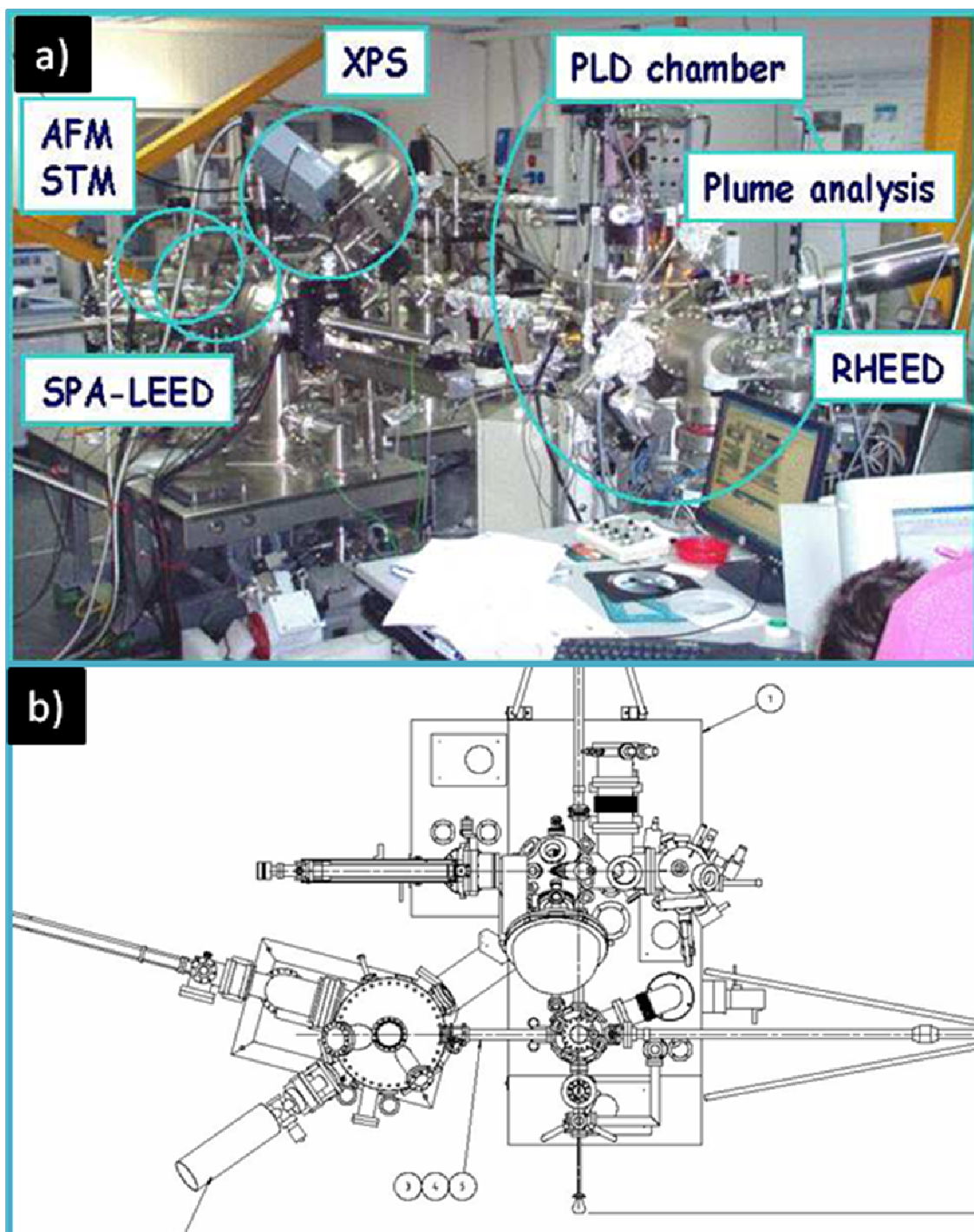


Fig. 2.1: a) the photo of the MODA facility, b) the scheme of the system - top view.

The facility is a system for pulsed laser deposition (PLD) of thin films oxides and *in situ* analysis of their properties. Several surface science techniques have been set up, such as *Reflection high-energy electrons diffraction* - RHEED, fast *Intensified Charge Couple Device* - ICCD camera, *Spot Profile Analysis* - Low energy electrons diffraction – SPA-LEED, *X-ray Photoemission Spectroscopy* - XPS, *Scanning Tunnel Microscopy* - STM and *Atomic Force Microscopy* - AFM. The ablation plasma is produced by focusing the output beam of a KrF excimer laser on stoichiometric targets.

Details of the instrumentations and of the experimental techniques are described in the following sections.

2.1 THE GROWTH CHAMBER

Thin film growth takes place in a vacuum chamber devoted to the pulsed laser deposition process (PLD chamber). The base pressure in the chamber is in the range of 10^{-9} mbar. A multitarget carousel situated in such chamber can allow the deposition of thin film multilayer or superlattices by using different targets, simply by changing the position of the target holder by means of a step motor. The analysis of the expanding plume produced during the pulsed laser ablation is performed by a fast ICCD camera, while the film deposition process is monitored *in situ* by a high pressure RHEED (Reflection High Energy Electron Diffraction). The peculiarity of the MODA systems consists in the UHV connections (load-locks) between all the chambers of the system that allows a transfer of the sample and the carousel using transfers rods. This allows the analysis of the film surface properties avoiding any contamination. The scheme of the chamber is presented in Figure 2.2.

The multi-target holder and the substrate holder can be inserted in the deposition chamber via a load-lock system without breaking the vacuum. The body of the heater is resistively heated using platinum wire and the deposition temperature, read by a thermocouple (calibrated by pyrometer), and is controlled by means of an electronic feedback system. Depositions is performed in a fully software controlled mode. The software controls the motion of the heater, the pressure, the laser, the temperature, the loading and motion of the carousel and a selection of the

Thin Film Growth and Analytic Techniques at MODA System

targets. The degrees of freedom of the substrate holder (the heater), equipped with five independent software controlled stepper motors (XYZ-rotation stage, tilt angle and the azimuth angle), allow varying at any time, even during the experiments, the positioning of the substrate in the plume. The pulsed laser deposition of complex oxides is performed using oxygen (99.999%) as a deposition gas. The deposition atmosphere was maintained by increasing a vacuum resistance between the turbo pump and the chamber (controlling the opening of the valve) and introducing flowing oxygen gas by means of a mass flow meter into the chamber to attain overall dynamic pressures of 1×10^{-5} mbarr–1mbar O_2 .

Each target, mounted on a holder, rotates during ablation in aim to prevent the degradation of the target surface.

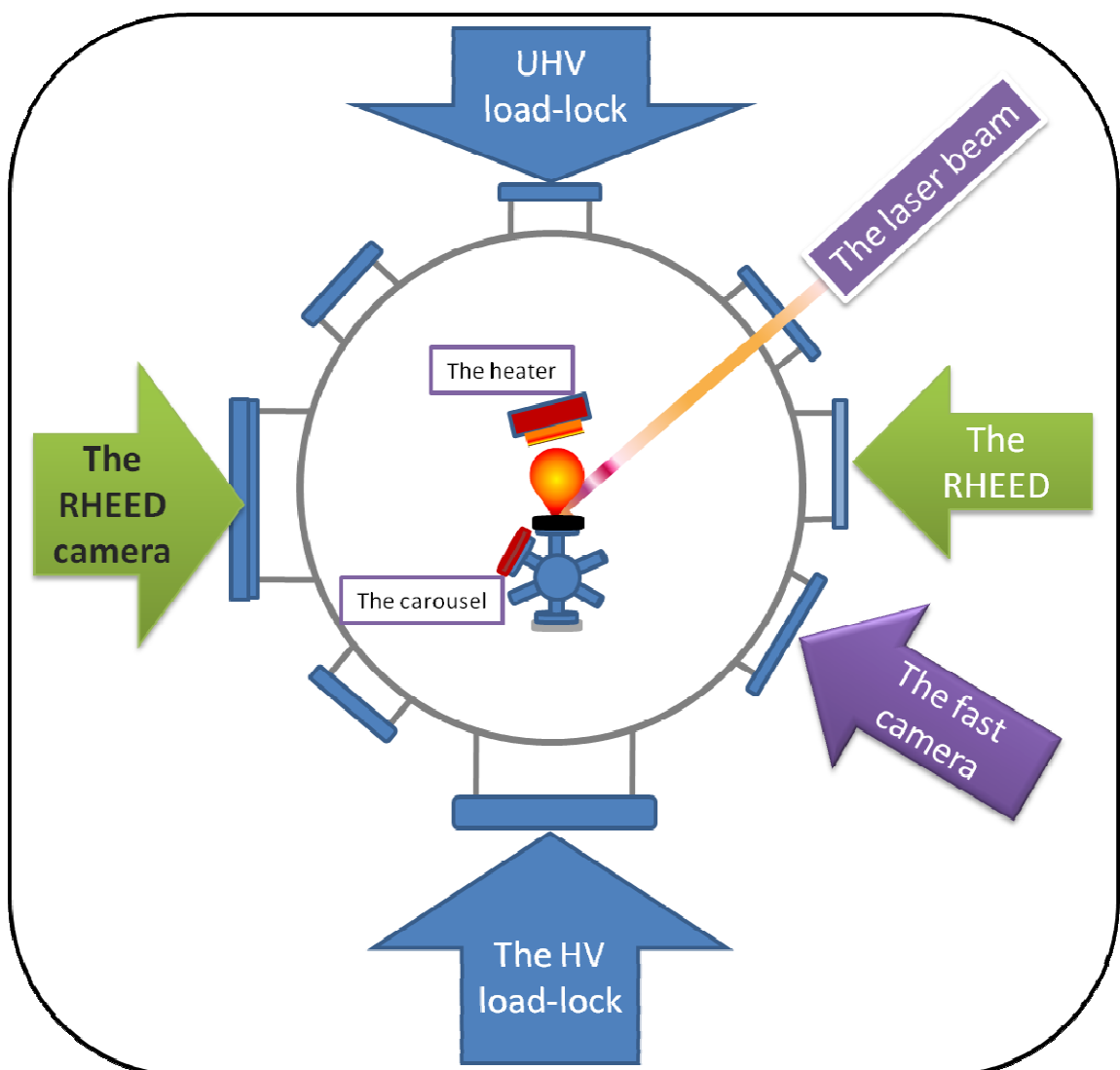


Fig 2.2: The scheme of the growth chamber.

For the ablation MODA system uses KrF excimer laser. The KrF excimer laser has following parameters: $\lambda=248$ nm, $\tau\approx 25$ ns full width half maximum and 45° incidence angle. A mask is used to select the homogeneous part of the laser beam. The mask is projected at an inclination of 45° on the target by means of a focusing lens (the focal length is 50 mm). The energy density on the target is controlled by adjustment of, both, mask size and demagnification. Substrates can be attached with silver paste or clamped in the centre of a large metal substrate holder, which was heated from the back side resistively and controlled at temperatures up to 1000°C . The films can be deposited at various substrate temperatures by adjusting the current applied to the resistive heating filament, or at various oxygen pressures.

2.1.1 Overview of the PLD technique

The first experiment with PLD was performed by Smith and Turner in 1965 using a ruby laser¹. The development of the technique was quite slow and followed the improvements in laser technology. The reason is that it is important to have short laser pulses with high power density to achieve congruent ablation of the target material. In a dielectric target the laser pulse creates an electromagnetic field inside the material and cause electrical breakdown. If the target is metallic, the energy in the laser pulse will be absorbed by the free electrons and transferred to the lattice and the material will be vaporized, if the energy is above threshold. In both cases particles which are produced by ablation form plasma. The plume consists of a mixture of atoms, molecules, electrons, ions, clusters and micron-sized particulates. Successful process of ablation occurs when layers of the material are vaporized without heating the layers below. If the layer below is heated into a liquid the process, termed splashing, occurs. Consequently, droplets will be formed inside of the plume which significantly lowers the quality of the film. Increasing the power density from zero, the ablation does not occur until the power reaches some threshold. The other problem - the ablation of the elements in the target with a lower temperature required for vaporization, before the other elements - can appear. Solution to this problem is to have short pulses with a high power density or to use a laser with shorter wavelength. The reason is that most materials used for deposition have absorption coefficients that increase with decreasing wavelength causes that shorter wavelengths reduce the absorption depth and thus splashing.

The laser-target interaction is a highly complex process and there is at present no model based on first principles that can describe the whole process.

The main deposition parameters are: 1) laser power density, 2) repetition rate (time between laser pulses), 3) substrate temperature, 4) background gas pressure and 5) distance between target and substrate.

1. The laser power density for standard ablation is, typically, between 10^6 and 10^8 W/cm². With increasing power the ablated atoms will have higher kinetic energy. This can be an advantage because the atoms can heat the substrate or hit a cluster of already deposited atoms, transfer energy to these atoms, making them rearrange in a more ordered way². On the other hand, highly energetic atoms may also cause defects in the substrate and deposited film.

2. The repetition rate can affect the quality of the epitaxial film. The argument is that one should allow time for the last deposited material to settle in a good way on the substrate before ablating the next layer³.

3. The substrate temperature is very important parameter. Heating the substrate will give additional energy to deposited atoms. This can rise to a more homogeneous, relaxed and defect-free film. However, higher temperatures do not automatically produce better films. The substrate temperature cannot be too high because in an oxygen background, materials that are heated too much can burn or start to decompose. Also, high substrate temperature can lead to interdiffusion between a substrate and a film.

4. The pressure of the background gas influences the quality of the film. The velocity of the impinging atoms also depends on the background gas pressure⁴, which causes resputtering effect on the film or smooth a surface. For deposition of oxide material, it is necessary to have a background of oxygen to obtain the right stoichiometry of the film. Oxide films made in vacuum are, usually, oxygen deficient. In contrary, a high gas pressure increases the amount of large particulates in the plume, since larger gas pressure causes higher scattering frequency inside of the plume and the ablated material loses energy and becomes thermalized. This increases probability for the species to collide with each other and form larger particulates, which usually, decreases a film quality.

5. The target-substrate distance has similar effect on the film as the background gas pressure. It is even better to say that the effects of target-substrate distance

are closely related to the background gas pressure. If the distance is large, the time to reach the film is longer and there is more time to form large particulates. A large pressure will decrease the size of the plume ⁴ which requires to consider also the angular spread of the plume. At different distances from the target the shape and angular spread of the plume is different.

2.1.1.1 Growth modes

In the following paragraphs a description of the possible ways of a growth, determined by the thermodynamic approach of the balance between the free energies of film - γ_f and substrate - γ_s and the interface between film and substrate γ_i , is given. When the total free energy of the film surface and the interface is less than the free energy of the substrate surface ($\gamma_f + \gamma_i < \gamma_s$), significant wetting is expected. This leads to layer-by-layer growth as described by Frank and Van der Merwe ⁵.

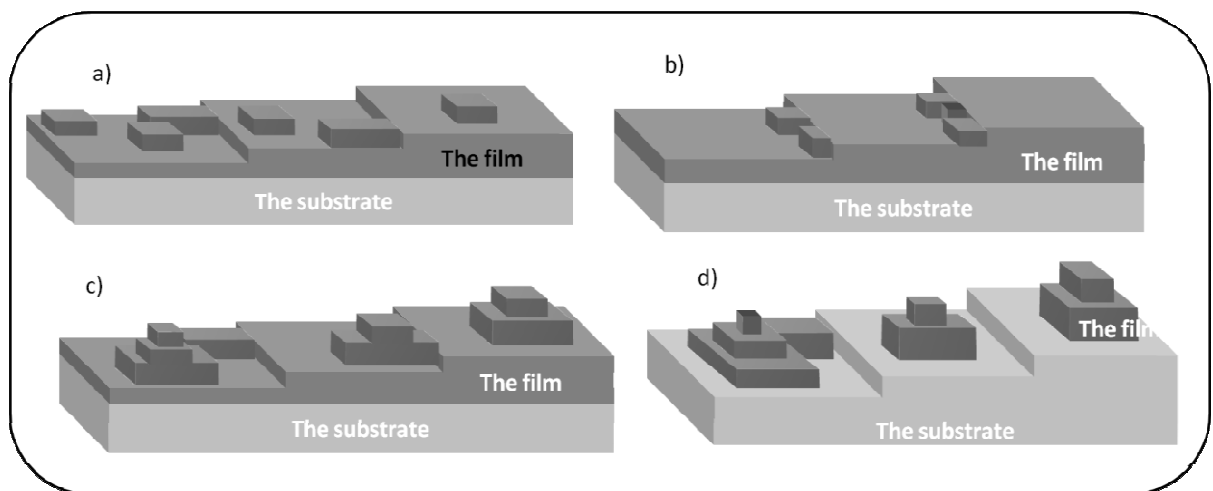


Fig. 2.3: *The growth modes : a) Frank-Van der Merwe or 2D- layer-by-layer growth, b) step-flow growth, c) Stranski-Krastanov growth, (d) 3D or Volmer-Weber growth.*

In the opposite case, wetting is energetically unfavourable and the deposit will take place minimizing the film substrate interface due to islands growth (3D). In this growth mode (named as Volmer-Weber mechanism ⁶) the energy is higher, due to

the creation of interface, than the surface energy of the substrate and film ($\gamma_f + \gamma_i > \gamma_s$). At the intermediate case, a transition from the Frank and Van der Merwe to the Volmer-Weber growth mode can be observed. Here, a crucial role is played by the mismatch between the film and the substrate, inducing a strain on the growing film. A layer-by-layer growth takes place in the first stage. Then, the thicker becomes the film, the higher is the elastic energy due to the strain. Such large strain energy can be lowered by forming islands in which strain is relaxed. This mechanism results in a continuous film of one or two monolayers onto which successively discrete islands are formed. This way of growth is the so-called Stranski-Krastanov⁷. The previous approach does not take into account the effect on the growth kinetic of the deposition parameters, such as the value of supersaturation in the gas phase, the substrate vicinality and the crystallographic misfit between the film and substrate unit cells. For the effect of such parameters, different growth modes have been observed for the same film-substrate system, thus clearly indicating that growth techniques and parameters are crucial to determine the final film morphology.

The biggest difference should be between homoepitaxy and heteroepitaxy growth. In the first case the film and substrate compounds are deposited the same and the substrate crystalline structure extends into the film during the growth. In case of heteroepitaxy, materials of the film and the substrate are different, with different lattice parameters. Such lattice mismatch gives rise to a strain, tensile or compressive, that can be calculated as the ratio between the lattice parameters of the substrate and the film:

$$\delta = (a_{\text{sub}} - a_{\text{film}}) / a_{\text{film}} \quad (2.1)$$

where a_{film} and a_{sub} are the unstrained crystal bulk lattice parameters in plane of film and substrate, respectively. In order to satisfy Poisson ratio a deformation, the plane lattice parameters produce an out of plane deformation of the cell. When $\delta > 0$, it means that tensile strain on the deposited film is in plane while strain is compressed out of plane. For $\delta < 0$, the strain is compressive, causing the lattice to be compressed in plane, but expanded out of plane. During the growth an elastic energy increases with increasing of the film thickness. When the thickness reaches a value, called critical thickness (h_c), the accumulated elastic energy becomes

comparable with the interfacial energy and the strained film tends to relax by creating misfit dislocations near the film-substrate interface. The misfit, usually, induces Volmer-Weber growth, except for large interface energies between substrate and deposited film, which cause the Stranski-Krastanov growth from the beginning.

The substrate vicinality provides terrace surface separated by steps. The steps heights and the terraces length depend on the angle and the direction of the miscut. On a vicinal substrate, including the growth modes described above, a fourth way of growth can occur, called the step-flow mode. This growth can occur on vicinal surface with high steps density and in some deposition conditions. During this growth the steps take action as a sink where the adatoms diffuse towards the substrate steps preventing the nucleation on the terraces, resulting that steps will propagate during the growth. If the terraces keep the same width and the step ledges remain almost straight, this growing mode will go on indefinitely causing no significant change in the starting substrate surface morphology. If not, step bunching can occur. In this case, a high density of steps moves with large velocities over the growth surface. By fluctuation, higher steps catch up with lower ones and then move together as double or triple steps. Consequently, the distribution in the terrace length (l_t) becomes broadened⁸. All of mode growths discussed above are depicted in Figure 2.3.

2.1.1.2 Growth kinetics

In next sentences kinetic of growth processes is briefly described.

The following effects can happen to an ablated atom. It can be deposited on the substrate or on clusters of atoms which are already deposited. There is a possibility that the atom can re-evaporate from there. If the atom is on the substrate surface, it can diffuse until becomes attached to a cluster or form a new cluster with other disusing atoms. In contrary, if the atom is attached to a cluster, it can dissociate from it. All these processes are shown in Figure 2.4. Once adsorbed on the surface, adatom may change adsorption site, in which case it can diffuse on the surface for several (even some hundreds) atomic lengths, before being detached and incorporated in the crystal structure. The molecule-surface interaction is described

by a potential that is a periodic function of the two coordinates parallel to the surface and a decreasing function of a third coordinate normal to it.

However, the average distance, l_D , that atom has moved on a flat surface before being trapped, can be given as:

$$l_D = \sqrt{D_s \tau} \quad (2.2)$$

D_s is the surface diffusion coefficient of the adatoms, and τ is the time before the reevaporation.

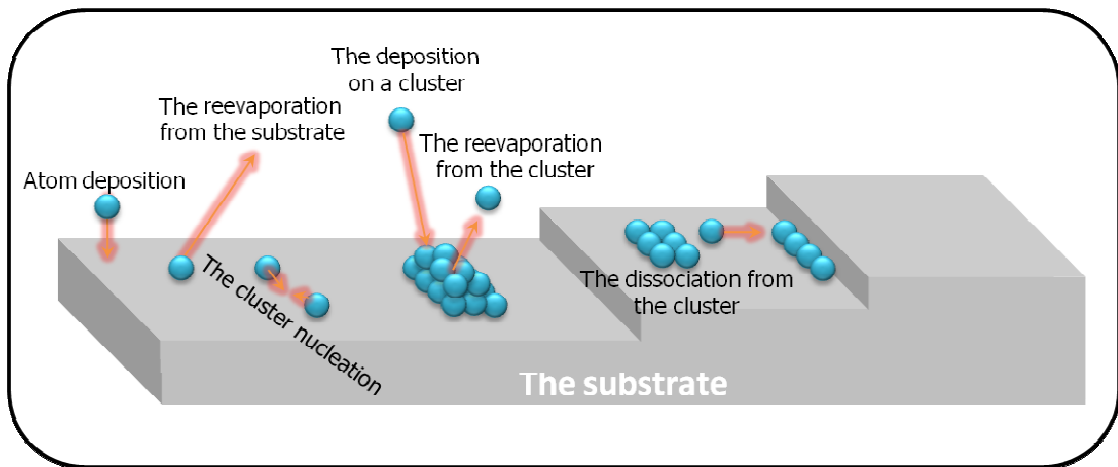


Fig. 2.4: Possible processes during deposition.

Typical values of the D_s for metal oxides are between 10^{-4} and 10^{-8} cm^2/s ⁹. The surface diffusion coefficient D_s is generally expressed as:

$$D_s = a^2 \nu e^{-\frac{E_A}{k_B T}} \quad (2.3)$$

where E_A is the activation energy for diffusion, a is the characteristic jump distance and ν is the sticking coefficient.

The sticking coefficient expresses the probability that a molecule can be captured, once impacting on the substrate surface and it is given by the ratio of the number of captured molecules to the total number of molecule hitting the surface. From the equation 2.3 the importance of the deposition temperature in the PLD technique becomes evident, since it controls the diffusivity of the adatoms. Nevertheless, the adatom's mobility on the surface is determined not only by the

deposition temperature. An important contribution in the nucleation process comes from the redistribution of the kinetic energy of the incoming flux of impinging atoms. The diffusion process is a crucial phenomenon that determines how the deposited materials rearrange itself on the surface and by a careful control of these parameters it is possible to obtain 2D growth modes not only during homoepitaxial growth but, also, in heteroepitaxy.

Growth on vicinal substrates has some particularities and to understand this, two diffusion process determined by kinetic parameters have to be considered ⁹:

1. the diffusion of atoms on terrace, the intralayer mass transport;
2. the diffusion of atoms to a lower step, the interlayer mass transport.

In the case of fast intralayer mass transport, the mobility of the adatoms is high enough to enable atoms to reach the edges of the substrate steps, i.e. the diffusion length (l_D) is larger than the average terrace width (l_t), the nucleation on the terraces is prevented and the step-flow growth takes place ($l_D > l_t$). Otherwise, if the terraces distribution (l_t) of the surface broadens, $l_D < l_t$, the nucleation on the terraces will occur. After that, the probability for atoms to attach to an existing nucleus reaches the probability to form a new nucleus. In this case the interlayer mass transport plays a big role to determine the growth mode. To obtain a layer-by-layer growth mode in this situation, an interlayer mass transport should be present allowing that atoms deposited on top of a growing island can reach the island edge and then diffuse to a lower layer. In the ideal case, the nucleations start after completion of a layer, but if there is no interlayer mass transport, the nucleation will occur on top of 2D islands before these have coalesced. This process is called second layer nucleation and probability for it is related to the mean island radius at the time of stable clusters nucleation on top of the islands, R_C . The value of R_C is related to the parameter E_S , which presents the energy barrier for an atom to descend across the step edge to a lower terrace. The larger is the value of E_S , smaller will be the value of R_C , since the additional energy barrier lead to accumulation of the adatoms on top of the islands, with subsequently increase of second layer nucleation rate. In the real system the growth mode is in between these growth modes described here. In some cases, even a transition from a layer-by-layer to a step flow growth on vicinal substrate can happen when the diffusion length of adatoms becomes comparable to the terrace width, i.e. when $l_D \approx l_t$. This

can happen because either the substrate temperature, determining the surface diffusion length l_D or the vicinal angle, which determines the terrace width l_t , is changed.

2.1.2 Reflection high-energy electrons diffraction –RHEED

RHEED is a powerful tool for in situ analysis of thin film deposition and it has been installed at the MODA growth chamber. In the following chapter an introduction to the technique is presented.

The first RHEED experiment was conducted by Nishikawa and Kikuchi in 1928. After them, several RHEED experiments were carried out for polished metal surfaces and on thin metallic films evaporated on metal substrates (Kirchner, 1932). In these experiments, many kinds of RHEED patterns were observed. The origin of these patterns, especially the streaks and transmission patterns, were explained in details by using kinematic diffraction theory (Kirchner and Raether, 1932).

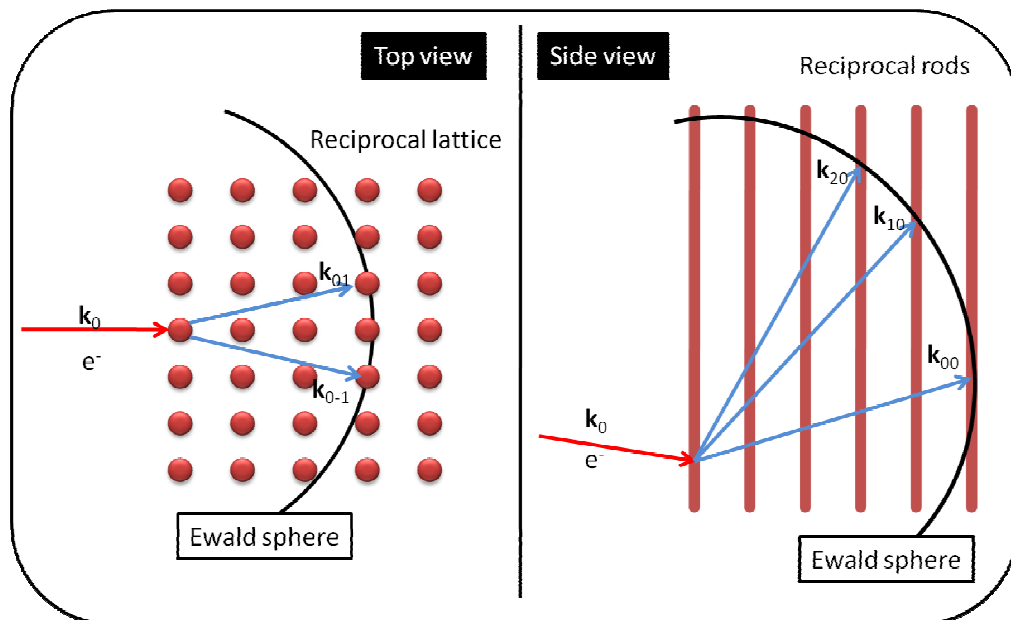


Fig. 2.5: RHEED diffraction on the cubic lattice.

RHEED is based on the reflection of electrons with high kinetic energy (typically in the range of 5-100 keV) and low impact angle Θ (typically less than 5°) from the

solid surface. Below is the brief illustration of the operation principle of RHEED for a sample with a cubic lattice.

If incoming electrons, with a momentum of \mathbf{k}_0 , have a very small incident angle with respect to the sample surface, they will only be scattered from atoms of the top sample layer. In the Figure 2.5 the surface of the sample is shown in reciprocal space. This reciprocal lattice builds a surface with a quadratic array of atoms. Assuming elastic scattering, no energy transfer is allowed from the electrons to the sample, the scattered wave vector \mathbf{k}_{ij} lies on the surface of the sphere of constant energy, the so-called Ewald sphere. In reciprocal space, the two-dimensional array of the surface atoms turns into vertical lines, the reciprocal rods. Wherever these rods cross the Ewald sphere, the condition for constructive interference of the elastically scattered electron beams from the surface is satisfied, while these crossing points in k-space determine the directions of constructive interference for the electrons in real space.

The RHEDD pattern is very particular because it contains elongated points which are placed on cycle and generally, the pattern depends on the morphology and roughness of the sample surface.

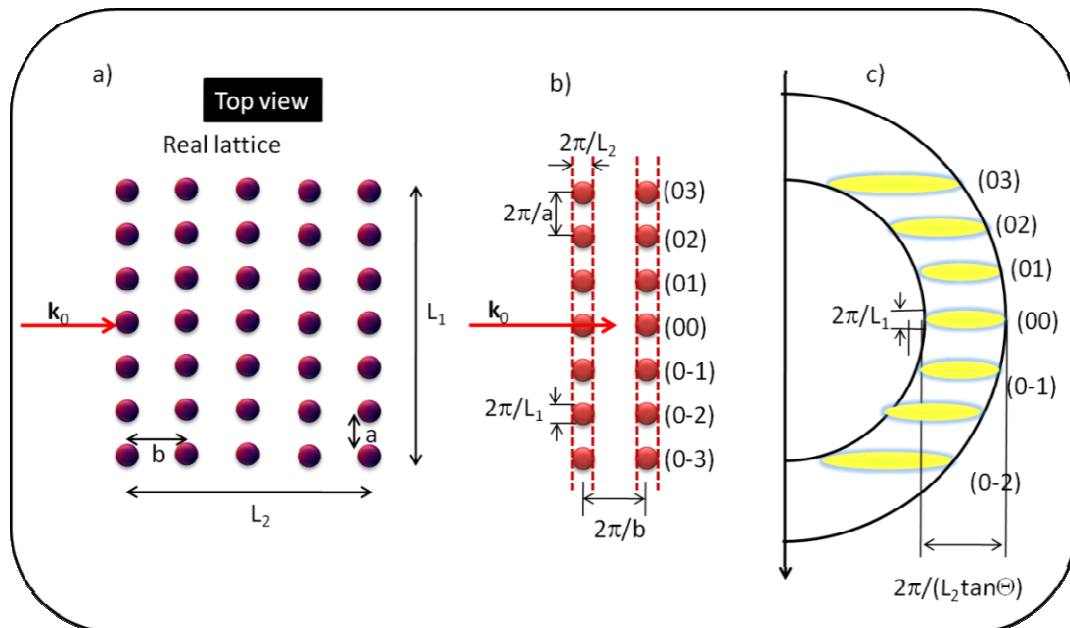


Fig. 2.5: Explanation of the origin of RHEED streaks: a) arrangement of the two-dimensional array of lattice points, b) Reciprocal lattice for the arrangement in (a), c) RHEED construction for (b) ¹⁰.

The patterns could be explained in a very elegant way, according to which RHEED streaks arise from small domains on the surface, as shown in Figure 2.5. The finite sizes of the lattice, L_1 and L_2 (Figure 2.5), are perpendicular and parallel to the incident direction, respectively, where the incident direction is indicated by the arrow. Reciprocal lattice of the domain is presented in Figure 2.5b. These scattered electron beams hit a fluorescent RHEED screen in certain RHEED spots, laying on so-called Laue circles which are numbered starting from zero (2.5c). The lengths of the streaks depend on the glancing angle of incidence- Θ .

2.1.2.1 High pressure RHEED

As the RHEED intensity depends on the film roughness, the growth process leads to characteristic intensity oscillations of the RHEED spots during the growth process with a single oscillation usually corresponding to the completion of a single monolayer.

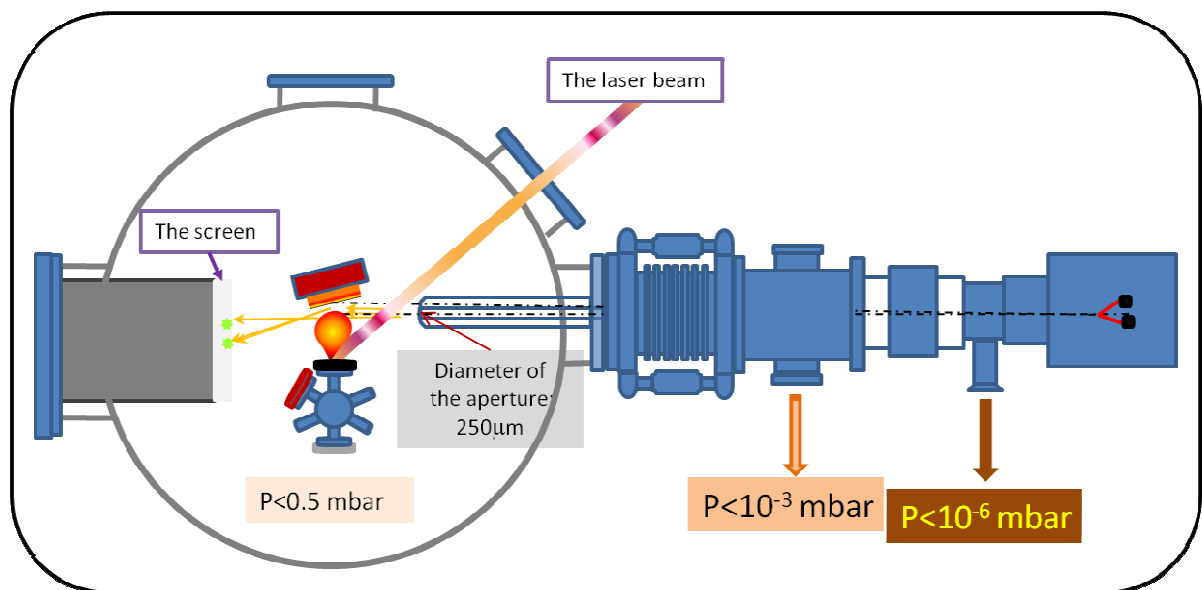


Fig. 2.6: The scheme of the High Pressure RHEED set up mounted in MODA-lab.

However, with the typical pressure values used in oxides films deposition, it is not possible to use the "standard" RHEED system, due to its incompatibility with environmental pressure higher than 10^{-4} mbar. In fact, the heated tungsten wire,

used as electron source in the RHEED gun, requires an environmental pressure below 10^{-4} mbar to avoid breakage or a short lifetime. Furthermore, the electrons' elastic and inelastic scattering with gas molecules, on high deposition pressure, gives rise to the attenuation of the e-beam intensity and, consequently, to very diffuse RHEED pattern. In order to overcome this problem, several groups tried to find alternative experimental conditions in RHEED-assisted pulsed laser deposition of oxides, for example working in low pressure condition of extremely oxidizing gases¹¹⁻¹³. The limitation in using RHEED technique in high pressure oxides deposition was overcome introducing a two stage differentially pumped e-gun¹⁴. That fulfilled both mentioned requirements: a low pressure in e-gun and minimum attenuation of e-beam intensity. Using this two-stage pumping system, the pressure in the deposition chamber can be increased up 0.5 mbar, maintaining the required vacuum in the electron source.

The High Pressure used on MODA system is shown in Figure 2.6. The electron source is mounted on a flange connected to a stainless steel extension tube with an inner diameter of 8 μm . An aperture with a size of diameter of 250 μm , separates the tube from the deposition chamber. The additional XYZ stage of the electron source is used to roughly direct the electron beam. There is an additional electrical deflection unit which allows that the electron beam can pass through the apertures inside the differential pumping unit and to enter in the deposition chamber. The fluorescent phosphor screen diameter 40 mm is mounted on a flange located less than 50 mm near the substrate. The screen is shielded from the plasma in order to minimize a coating. A minimum beam size of 100 μm can be obtained even at large working distances. The heater can be rotated in order to adjust the angle of incidence of the electron beam on the substrate. The azimuth angle can be changed by additional rotation of the heater. The diffraction pattern is monitored by a charge coupled device (CCD) camera.

2.1.2.2 Growth monitoring by RHEED

The wide used application of RHEED is growth rate monitoring and it is the consequence of finding that the intensity of any diffraction feature oscillates with a period corresponding to the growth of a single mono layer-ML¹⁵⁻¹⁷. Usually, the monitoring is via recording of the specular spot but in principle all of them can be

used. The oscillations of the spots are a manifestation of two-dimensional (2D) layer-by-layer, the Frank–van-der-Merwe, growth mode. The oscillating intensity can be explained by the changing surface morphology, alternating between completed layers and a rougher intermediate state. This principle is presented in Figure 2.7.

However, a more detailed understanding of the diffraction process generating the oscillations is complicated by strong multiple scattering effects. Meanwhile, an important remaining problem is the explanation of the RHEED oscillation phase dispersion measured at the specularly reflected position as a function of electron beam incidence angle ¹⁸.

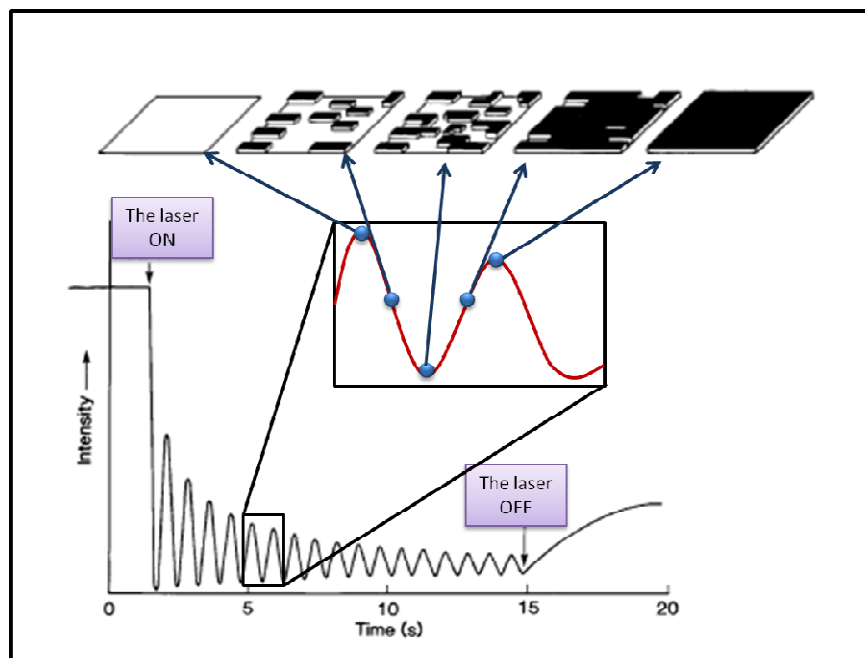


Fig. 2.7: The Intensity oscillations of the RHEED specular beam during growth. The maximums correspond to the complete layer while the minimums to the half coverage of the surface.

Furthermore, the phase of the oscillations depends on the overpressure during the rate-limiting deposition and F. Briones and et al. demonstrated that different surface reconstructions with cause different slopes for RHEED oscillation curves ¹⁹.

In the case of 3D growth mode, the step density on the surface increases in time and cause that the specular RHEED intensity decreases and moreover, the additional

spots in to the RHEED pattern appear. It is because the diffraction occurs due to island transparency for electrons. In case of 3D growth the recovery of the RHEED intensity, when deposition is stopped, takes no place while in 2D growth the process is obvious. In the case of a step-flow growth, characterized by the absence of periodic change in step density on the surface, no RHEED oscillations are expected. Nevertheless, the lack of RHEED oscillations is not always a clear signature of pure step flow growth. Even when a stable RHEED intensity is observed, the second layer nucleation may occur causes a constant step density and, therefore, a constant RHEED intensity.

2.2 THE ANALYTIC CHAMBER

All of the analytic techniques are placed in a separated chamber where it is possible to transfer a sample with system of manipulators without braking vacuum conditions. The chamber is equipped with three levels of pumping system, turbo molecular ion and titanium sublimation pumps enabling that vacuum is in the range of 10^{-11} mbar. This extremely high vacuum allows quit long duration of sample measurements without contamination from the environment. For monitoring of the residual gasses the gas spectrometer is installed. In the analytic chamber is a main manipulator with five degrees of freedom where a heater is placed, which can give temperature of the back side of a sample up to 1000 °C. Also, the chamber can be under oxygen atmosphere, controlled manually with the leek valve and monitored by gas spectrometer.

In the next sections all techniques used in sample analysis are described shortly.

2.2.1 X-ray Photoemission Spectroscopy-XPS

A chemical analysis is crucial for almost every research in surface science. Even many techniques exist which can provide that, XPS is one of mostly used because it is non-destructive technique. XPS, besides the major answer about which elements are present on the surface, allows the identification of the different chemical compounds that is possible to find on the surfaces. For example, the XPS

spectroscopy is easily able to distinguish if the element is in ionic or covalent state, or, for many metallic elements, if they are oxidized or reduced.

Generally speaking, XPS is based on the photoelectric effect. The process is shown schematically in Figure 2.8. Photon interacts with an electron, in a way that its energy ($h\nu$) is transferred and the electron is photo-emitted with a kinetic energy (E_K) provided that it is greater than its binding energy (E_B).

The energy in the process is conserved and can be described with following equation:

$$h\nu = E_B + E_K + \phi \quad (2.4)$$

The photon energy must be high enough for the electrons to overcome the work function (ϕ) of the solid. As the results of the measurements the XPS technique produces a spectrum of emission intensities versus electron binding or kinetic energy. The analysis of the spectrum is quite complicated and is explained below which information can be taken from the spectra.

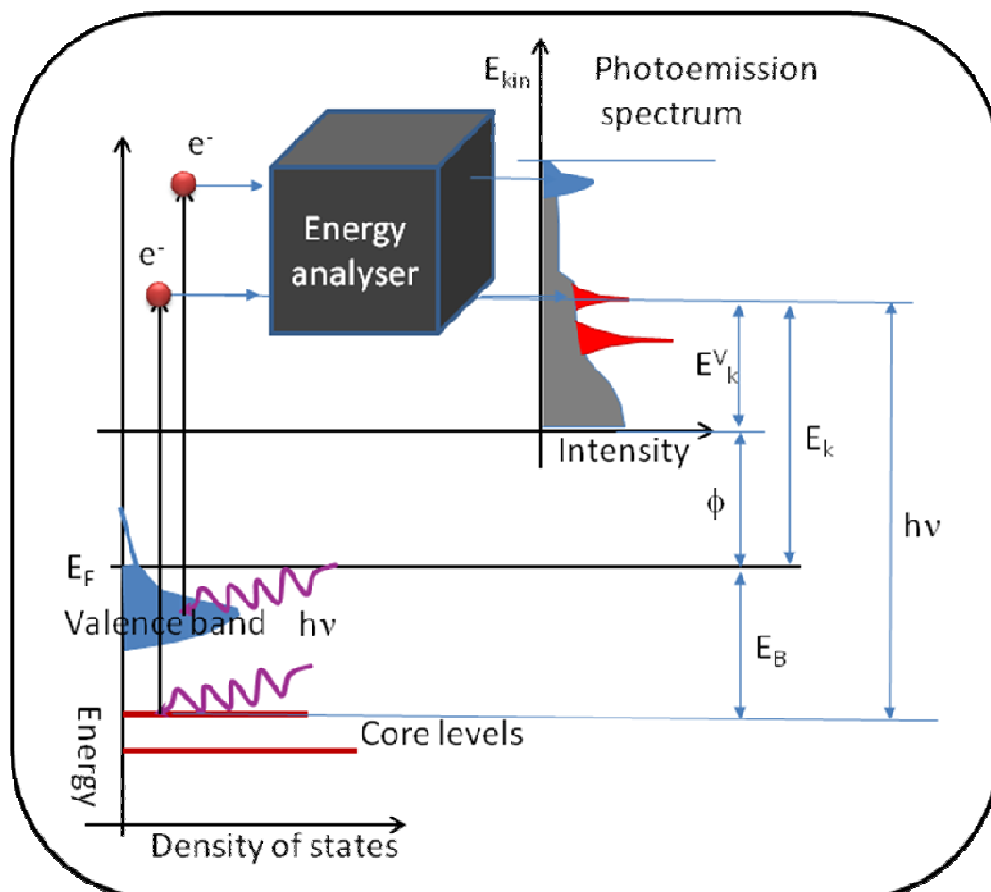


Fig. 2.8: The basic principal of XPS technique.

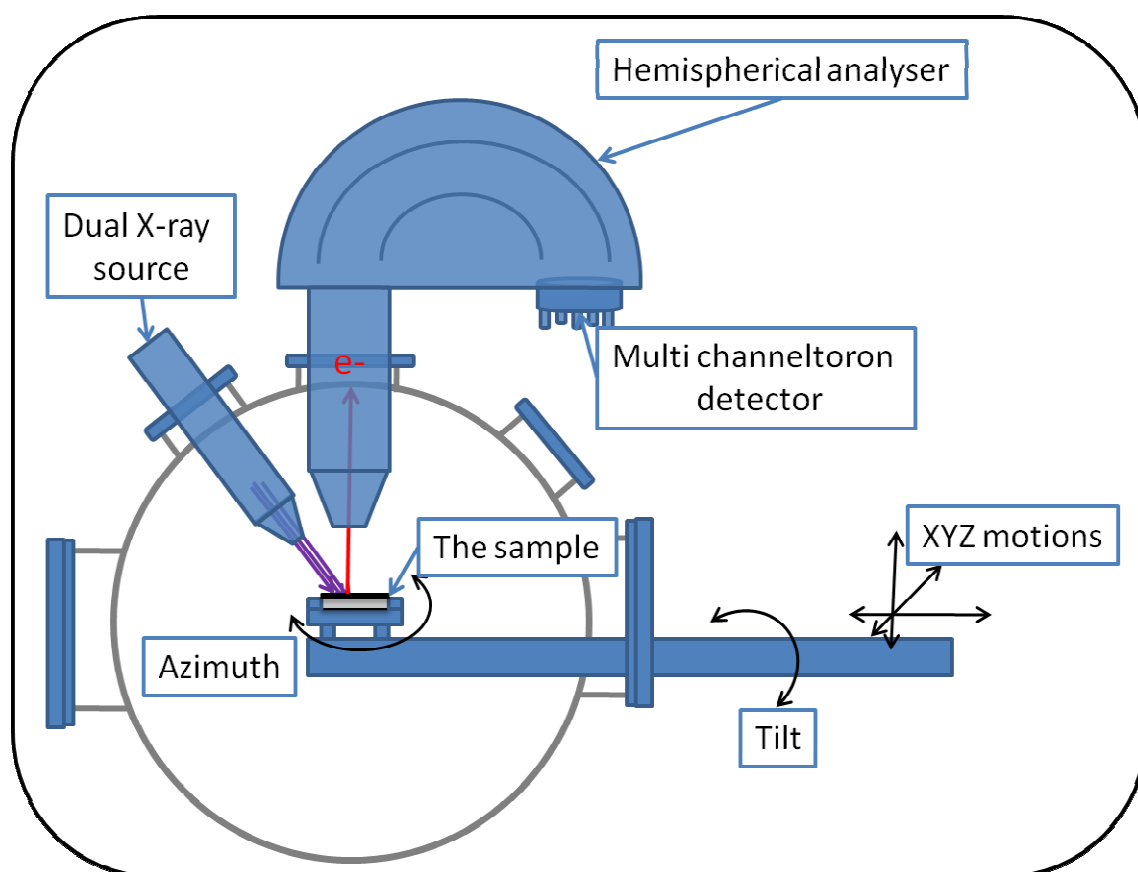


Fig. 2.9: The scheme of XPS instrument.

The source is standard Omicron X-ray dual anode unmonochromatic sources that operate with two emitted lines: Al $K\alpha$ (1486.6 eV) or Mg $K\alpha$ (1253.6 eV). The analyzer, consisting of two hemispherical electrodes, allows a selection of energy of the photoelectrons. The potential difference between these two electrodes defines the path energy of the electrons. Only the electrons having a kinetic energy included in an interval of energy centered on this path energy will arrive at the detector placed at the end of the analyzer. The multiplying detector contains 5 channeltrons and produces a spectrum of emission intensity versus electron binding or kinetic energy.

2.2.2 Low Energy Electrons Diffraction-LEED

Low Energy Electron Diffraction (LEED) is one of the first and one of the most successful surface science techniques for structure determination. This technique has been the dominant method to study the structure and morphology of two dimensional plane surfaces. The technique was invented in 1927 by Davison and

Germer ²⁰ and in last decades the technique was significantly developed. The analytic part of MODA system includes one special type of LEED instruments called Spot Profile Analysis LEED (SPA-LEED). With special electronic parts inside of the instrument, recording and analyses of the diffraction spot is possible.

For a technique, which uses the electron diffraction, to be in a class of surface sensitive techniques the electrons must satisfy two conditions:

1. the wavelength of the electrons must be of the order of the lattice spacing ($\lambda_e \gg a$);
2. the electrons must be sensitive only to the surface, i.e. they must not penetrate deep into the sample.

LEED is typically done in the range 20-1000 eV, where the de Broglie wavelength ($\lambda = h/p$) in the range of few Å. Since crystal lattices have typical spacing on the order of a few Angstroms, diffraction should be observable using low-energy electrons. Consequently, LEED electrons penetrate only in few atomic layers of the sample, enabling the technique to be quite sensitive to the surface structure of the studied material ^{21, 22}.

The simplest theoretical explanation of LEED is in terms of kinematic theory. This theory assumes that electrons are scattered only once from the sample and that each scattering event is elastic so that no energy is lost. Dynamical LEED theory includes multiple scattering, inelastic scattering, and other effects and presents more complete theory. However, the kinematic theory is able to describe basic LEED patterns, such as spot positions, and can even account for the appearance of extra spots in the pattern due to superstructures or reconstructions ²³.

$$\Delta \vec{k}_{||} = \vec{g} = h \vec{a}_1^* + k \vec{a}_2^* \quad (2.5)$$

Here is given the short introduction of LEED kinematic theory.

The total electron wave function $\Psi_{\text{tot}}(\vec{r})$ must obey Schroedinger's equation

$$\left[-\frac{\hbar^2}{2m} \nabla^2 + V(\vec{r}) - E \right] \Psi_{\text{tot}}(\vec{r}) = 0 \quad (2.6)$$

The total wave function consists of three parts: $\psi_i(\vec{r})$ of the incident electron, $\psi_{\text{in}}(\vec{r})$

of the electron inside the crystal, and $\psi_0(\vec{r})$ of the diffracted electron. The incident electron is not in any potential so its wave function is as for free electron, so the function can be expressed as:

$$\psi_i(\vec{r}) = A_i e^{i(\vec{k}_i \cdot \vec{r})} \quad (2.7)$$

Inside the crystal, the electron is in to the crystal potential. Since the crystal lattice is periodic in two dimensions on the surface, the potential is also periodic.

$V(\mathbf{r}) = V(\mathbf{r} + \mathbf{t})$, where \mathbf{t} is a lattice translation vector of the crystal. According to Bloch's theorem, the wave function inside the crystal can be expressed as a function with the same periodicity as the potential, $U_{\vec{k}_{||}}(\vec{r})$.

$$U_{\vec{k}_{||}}(\vec{r}) = U_{\vec{k}_{||}}(\vec{r} + \vec{t}) \quad (2.8)$$

Thus inside the crystal the wave function can be described as:

$$\psi_m(\vec{r}) = U_{\vec{k}_{||}}(\vec{r}) e^{i(\vec{k}_{||} \cdot \vec{r})} \quad (2.9)$$

$\vec{k}_{||}$ is the component of the incident wave vector parallel to the surface. Since the Bloch function is periodic, it can be expanded in a Fourier series as:

$$U_{\vec{k}_{||}}(\vec{r}) = \sum_{\vec{g}} A e^{i(\vec{k}_{||} \cdot \vec{r})} \quad (2.10)$$

Because of space periodicity: $\vec{t} = m_1 \vec{a}_1 + m_2 \vec{a}_2$, the exponential part must satisfy the following condition: $e^{i(\vec{g} \cdot \vec{r})} = e^{i(\vec{g} \cdot (\vec{r} + \vec{t}))}$.

This will give following consequences:

$$\vec{g} \cdot \vec{a}_1 = m \cdot 2\pi \quad \text{and} \quad \vec{g} \cdot \vec{a}_2 = n \cdot 2\pi \quad (2.11)$$

where m and n are integers.

Vector \mathbf{g} in this form is, actually, the reciprocal lattice vector:

$$\vec{g} = h\vec{a}_1^* + k\vec{a}_2^* \quad (2.12)$$

These equations show that the momentum transfer parallel to the surface must be equal to a reciprocal lattice vector. The resulting diffraction pattern is constrained by the reciprocal lattice of the material.

The SPA-LEED system installed in MODA lab is a commercial Omicron instrument, based on the one which Henzler et al. developed in 1986²⁴. Figure 2.11 shows the principal elements of the SPA-LEED system. The system has a glass phosphorus screen, which is observed from the back side. The screen gives a quickly available overview of the diffraction pattern. Due to the large distance between the crystal and the screen the spatial resolution is higher than with a normal optics, so more details can be recognized. On the other hand, the visible area of the reflex pattern is smaller. Behind holes in the screen the electron gun and the channeltron are mounted. In the main mode the intensity at a given position of the pattern is detected by the channeltron.

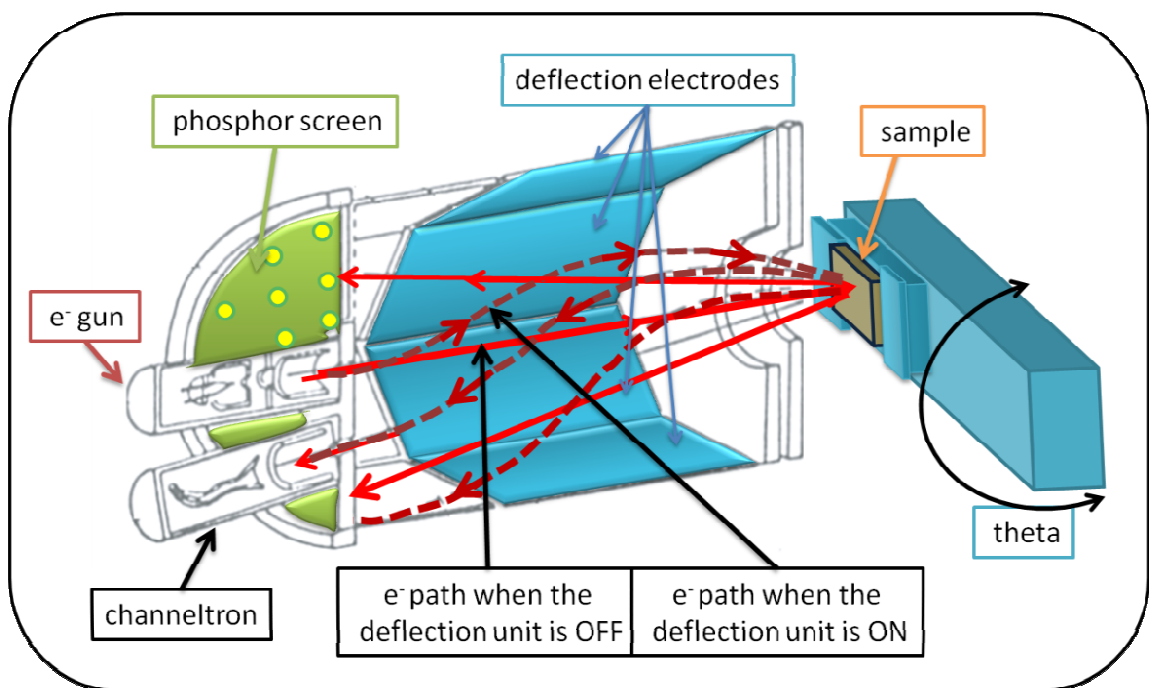


Fig 2.11: Schematic draw of set-up of the SPA-LEED system

The electron gun uses a commercial directly heated tungsten filament. The electron gun supplies an emission current up to 10^{-6} A and for the screen display even

though a fraction of it would be enough. When working with the channeltron a current of 10^{-10} to 5×10^{-8} A is sufficient. For that low current the electron source diameter is less than 0.1 mm for electron energy less than 100 eV. For such small diameter special efforts are needed with adjustment and design of a cathode, Wehnelt cylinder and an anode region.

The main concept of the system is to handle the reflex scanning with electrostatic deflection. No mechanical movement of the sample or the detector is needed during scanning which simplifies the instrument very much. Without voltages applied, the direct beam is reflected into the channeltron aperture for a crystal with its surface inclined by ± 4 degrees relative to the axis of the system.

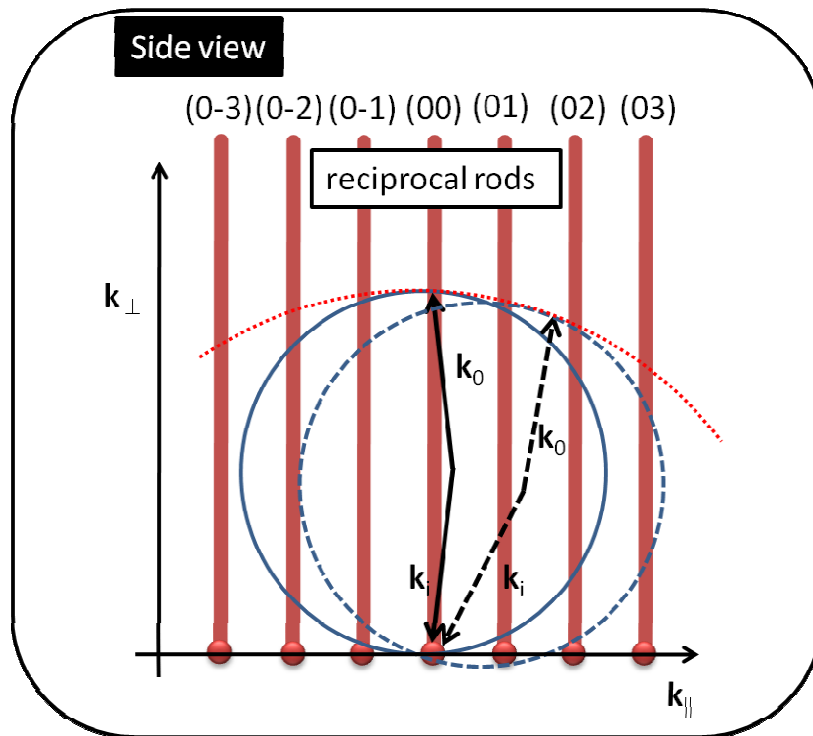


Fig. 2.12: Scattering geometry for the SPA-LEED instrument. The angle between the wave vectors \mathbf{k}_i and \mathbf{k}_o remains constant at ± 4 degrees. The condition is equivalent to a sample rotation with fixed positions of the detector and the source²⁵.

On Figure 2.12 is presented in which way is possible to obtain crossing of reciprocal rods with Ewald sphere in SPA-LEED instrument. The mechanical alignment of sample determines the angle between the incoming beam \mathbf{k}_i and the outgoing beam

\mathbf{k}_0 . For electrostatic scanning the opposite deflection plates are supplied with equal voltages of opposite polarity. The ratio of the voltages between the screen plates and the crystal plates is chosen to be close to 1, so that the position of the primary beam does not shift on the crystal. The angle between \mathbf{k}_i and \mathbf{k}_0 remains constant during scanning. Therefore, the absolute value of the scattering vector $\Delta\mathbf{K} = |\mathbf{k}_0 - \mathbf{k}_i|$ stays constant, only its orientation with respect to the surface varies during scanning.

At fixed primary electron energy the count rate of every scan position is recorded. The computer generates one dimensional line scans or two dimensional area scans. In the case of area scans the intensity can be presented as contour levels or a surface plot with different magnifications. Depending on the deflection voltages, the area scan gives overview of the whole Brillouin zone or detailed information of one or a few spots only. Mainly for area scans the aspect of measurement time becomes important. The total measurement time depends on the total number of channels and for each channel on the desired accuracy. With a maximum of channels an area of 400x400 points may be recorded. Linear scans of at least 2000 channels are used for accurate measurements throughout the Brillouin zone to enable reliable quantitative evaluation. Due to channeltron detection, the intensity can be measured over a range of six orders of magnitude. With this type of instrument the transfer width was increased up to 200 nm, i.e. periodic structures with a separation up to this length can be resolved. Important information which can be directly extracted from the spot profile is the average terrace length of an atomically rough surface. In this case, the important quantity is the Full Width at Half Maximum (FWHM) measured at an "out-of-phase" scattering condition ²⁶.

On Figure 2.13 is depicted the physical explanation of LEED sensitivity due to the morphology. On the figure, electrons scatter from two levels separated by a single atomic step and interfere with a phase difference of $2\pi S$. The phase depends on the wavelength, i.e. on the electrons' energy as $S = 2d \cos \theta / \lambda_{\text{electron}}$. For half integer values of S the electrons interfere destructively and the sharp LEED spot disappears. For integer values of S the interference is constructive and the electrons are insensitive to surface roughness. M. Horn-von Hoegen showed also that using SPA-LEED is possible to observe very precisely variations of surface morphology ²⁶. Some of the examples are presented in Figure 2.14.

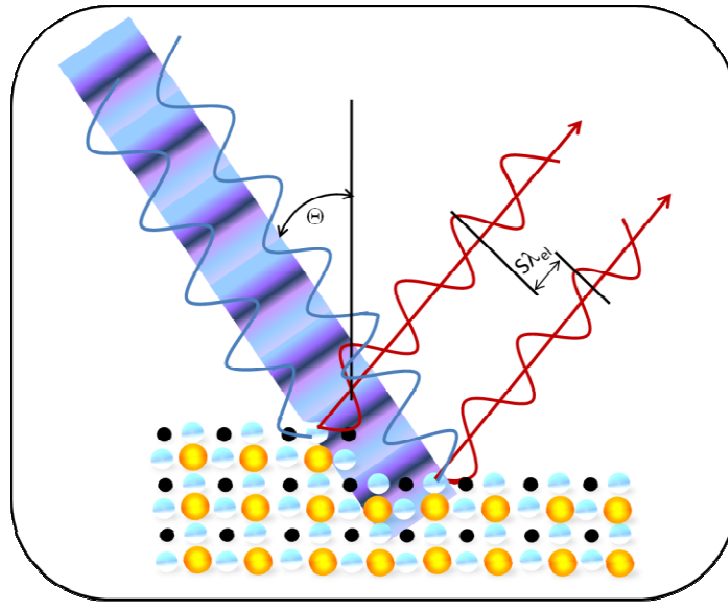


Fig. 2.13: Phase contrast at a step edge.

Type of surface	The reciprocal rods	Spot profile in Bragg condition ($S=n$)	Spot profile in anti Bragg condition ($S=n+1/2$)
<p>flat surface</p>			
<p>vicinal surface</p>			
<p>surface with two level roughness</p> <p>island with ML height</p>			
<p>multilevel rough surface</p>			

Fig. 2.14: Examples how to use SPA LEED for surface morphology observation.

2.2.3 SPM microscopy

In the 1980's Binnig and Rohrer, from IBM research center, developed a new technique for studying surface structure named Scanning Tunneling Microscopy-STM. Their invention was motivation to the development of a whole family of linked techniques which are classified in the general category of Scanning Probe Microscopy (SPM) techniques. Of these later techniques, the most important is Atomic Force Microscopy (AFM).

There is a huge literature about SPM-technology and application and few textbooks provide a good introduction^{27,28}. Therefore, here is given only the short introduction about two SPM techniques used during course of this study.

STM

The principle of the STM is remarkably simple, it uses a sharpened, conducting tip with a bias voltage applied between the tip and the sample (Figure 2.15). When the tip is brought within about 10\AA of the sample, electrons from the sample begin to "tunnel" through the 10\AA gap into the tip or vice versa, depending upon the sign of the bias voltage.

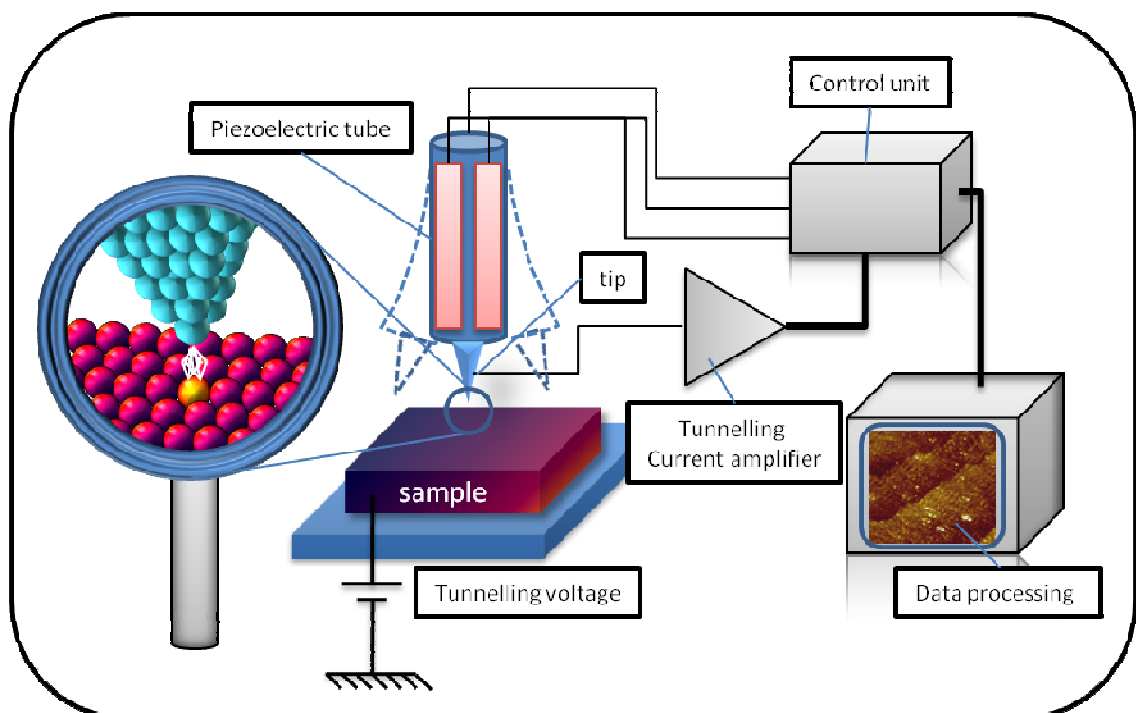


Fig.2.15: The scheme of STM instruments.

The resulting tunneling current varies with tip-to-sample spacing, and it is the signal used to create an STM image. The tunneling current depends very critically on the precise distance between the last atom of the tip and the nearest atom or atoms of the underlying specimen. When this distance is increased a little bit, the tunneling current decreases strongly. For tunneling to take place, both the sample and the tip must be conductors or semiconductors. Unlike AFM, which is shortly explained in the next section, STM cannot image insulating materials.

AFM

The second scanning probe microscope, which was developed soon after the STM, is the Atomic Force Microscope - AFM. The scheme of AFM is shown in Figure 2.14. The key difference between the AFM and the STM is that in the AFM, the tip gently touches the surface. The AFM does not record the tunneling current but the small force between the tip and the surface is registered.

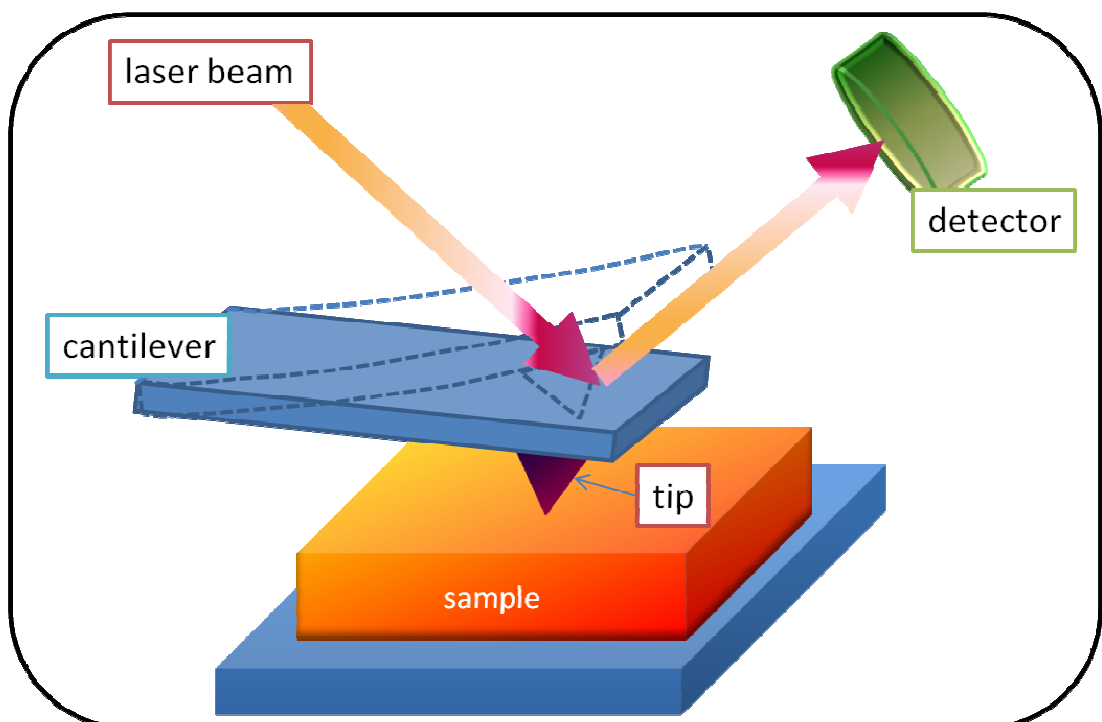


Fig. 2.14: The scheme of AFM measurement.

To enable this, the AFM tip is attached to a tiny leaf spring, the cantilever, which has

a low spring constant. The bending of this cantilever is detected, often with the use of a laser beam, which is reflected from the cantilever. Actually, the AFM measures contours of constant attractive or repulsive force. The detection is very sensitive so the detected forces can be as small as a few pN. In principle, forces below 1 nN are satisfactorily low to avoid damage to either the surface or the tip. Since the AFM does not depend on the presence of a tunneling current, the technique is suitable for using on non-conductive materials. In the SPM chamber installed on MODA facility is a commercial Omicron UHV system which includes STM and AFM instruments.

References

- ¹ H. M. Smith and A. F. Turner, *Applied Optics* **4**, 147 (1965).
- ² P. R. Willmott, R. Herger, C.M. Schleputz, D. Martoccia, and B. D. Patterson, *Phys. Rev. Lett.* **96**, 176102 (2006).
- ³ G. J. H. M. Rijnders G. Koster, D. H. A. Blank, H. Rogalla, *Applied Physics Letters* **74**, 3729 (1999).
- ⁴ Alessia Sambri, "Pulsed laser deposition of complex transition metal oxides: plume expansion and film growth"-PhD Thesis, Università degli Studi di Napoli Federico II, 2007
- ⁵ F.C. Frank and J.H. Van der Merwe, *Proc. Roy. Soc. London A* **198**, 216 (1949).
- ⁶ M.Volmer and A. Z .Weber, *Phys. Chem.* **119**, 277 (1926).
- ⁷ I.N. Stranski and L. Krastanov, *Acad. Wiss. Math.-Naturw.Klasse IIb* **146**, 797 (1938).
- ⁸ M.Huijben, " Tuning electronic properties by atomically controlled growth"-PhD Thesis, University of Twente 2006.
- ⁹ G.Rijnders, " The initial growth of complex oxides: study and manipulation"-PhD Thesis, University of Twente, 2001.
- ¹⁰ Ayahiko Ichimiya and Philip I. Cohen, *REFLECTION HIGH-ENERGY ELECTRON DIFFRACTION* (Cambridge University Press, Cambridge, UK, 2004).
- ¹¹ M. Kanai, T. Kawai, and S. Kawai, *Jpn. J. Appl. Phys.* **Part 2 31**, L331 (1992);
- ¹² M.Y. Chern, A.Gupta, B.W. Hussey, *Appl. Phys. Lett.* **60**, 3045 (1992);
- ¹³ T. Terashima, Y. Bando, K. Iijima, K. Yamamoto, K. Hirata, K.Hayashi, K.Kamigaki, and H. Terauchi, *Phys. Rev. Lett.* **65**, 2684 (1990).
- ¹⁴ G. Rijnders, G. Koster, D. H. A. Blank and H. Rogalla, *Appl. Phys.Lett.* **70**, 1888 (1997).
- ¹⁵ J.J. Harris, B.A. Joyce, P.J. Dobson, *Surf. Sci.* **103**, L90 (1981);
- ¹⁶ J.H. Neave, B.A. Joyce, P.J. Dobson and N. Norton, *Appl. Phys. Lett.* **A31**, 1 (1983);

- 17 J.M. Van Hove, C.S. Lent, P.R. Pukite, P.I. Cohen, J. Vac. Sci. Technol. **B1**, 741 (1983).
- 18 J. Zhang, J. H. Neave, P. J. Dobson and B. A. Joyce, Appl. Phys. Lett. **A 42**, 317 (1987).
- 19 D. Golmayo F. Briones, L. Gonzalez and J. L. De Miguel, Jpn. J. Appl. Phys. **24**, L478 (1985).
- 20 C. Davisson and L. H. Germer, Phys. Rev. Lett. **30:6**, 705 (1927).
- 21 C. J. Powell, Surf. Sci. **44:1**, 29 (1974);
- 22 M. P. Seah, W. A. Dench, Surf. Interface Analysis. **1:1** 2(1979).
- 23 M. A. Van Hove, W. H. Weinberg, C. M. Chan, *Low Energy Electron Diffraction: Experiment, Theory, and Surface Structure Determination*. (Springer-Verlag, New York, 1986).
- 24 U. Scheithauer, G. Meyer, and M. Henzler, Surf. Sci. **178**, 441 (1986).
- 25 M. Horn-von Hoegen, Z. Kristallogr. **214**, 684 (1999).
- 26 M. Horn-von Hoegen, Zeitschrift für Kristallographie **214**, 591 (1999).
- 27 R. Wiesendanger, *Scanning Probe Microscopy and Spectroscopy: Methods and Applications*. (Cambridge University Press, Cambridge, UK, 1998);
- 28 D. Bonnell, *Scanning Probe Microscopy and Spectroscopy: Theory, Techniques, and Applications*. (Wiley-VCH, New York, 2001).

RESULTS OF STO

CHAPTER 3.1: THE SURFACES TERMINATIONS OF STO (001) SINGLE CRYSTAL, AND HOMOEPITAXIAL FILMS

Thin films and heterostructures based on perovskite oxides, in last years, became an extensive topic area for research and technological development. These materials may create strongly correlated systems such as High Temperature Superconductors-HTC, Colossal Magnetoresistance-CMR ferromagnetics or some ferroelectrics. If these materials are fabricated with deposition techniques, in order to have the full control on their structure on atomic scale the basic condition is layer by layer epitaxial growth.

On the other hand, the substrate plays the crucial role in achieving the high quality films. A surface morphology of substrates affects strongly the growth mode and the structures of the film. Moreover, the surface terminated layer is very important starting condition for a growth. Having in mind perovskite oxide materials, the surface of ABO_3 single crystals truncated in 001 direction is either AO or BO_2 terminated or can be considered as the mixture of both terminations. Consequently, the type of termination will affect the overall stacking of the hetero epitaxial perovskite thin film, thus the final termination of the film ¹.

Considering the fact that STO is most frequently used perovskite as the substrate, in this subchapter is shown our modification of the recipe for obtaining TiO_2 terminated STO, none terminated STO and TiO_2 terminated STO influence to the homoepitaxial thin film growth and finally our way to get SrO terminated surface of STO.

$SrTiO_3$ is composed of SrO and TiO_2 -alternative layers with the distance of $a_{STO}/2$ ($a_{STO} = 0.3905$ nm) in the [001] direction, hence the surface can be terminated by either SrO- or TiO_2 - domains. The morphology of the commercially available substrates depends on polishing method ². Usually, the substrates are polished mechanically with silica particles in alkaline solution ³. Polished STO surfaces are reasonably flat and have intrinsically mixed termination of TiO_2 and SrO, with SrO percentages ranging from 5 to 25% ⁴⁻⁵.

Results: STO

In my research done on STO (001), the substrates were purchased from Surface Net, GmbH, Germany. The surface measured by AFM of as received substrate is shown on Figure 3.1.

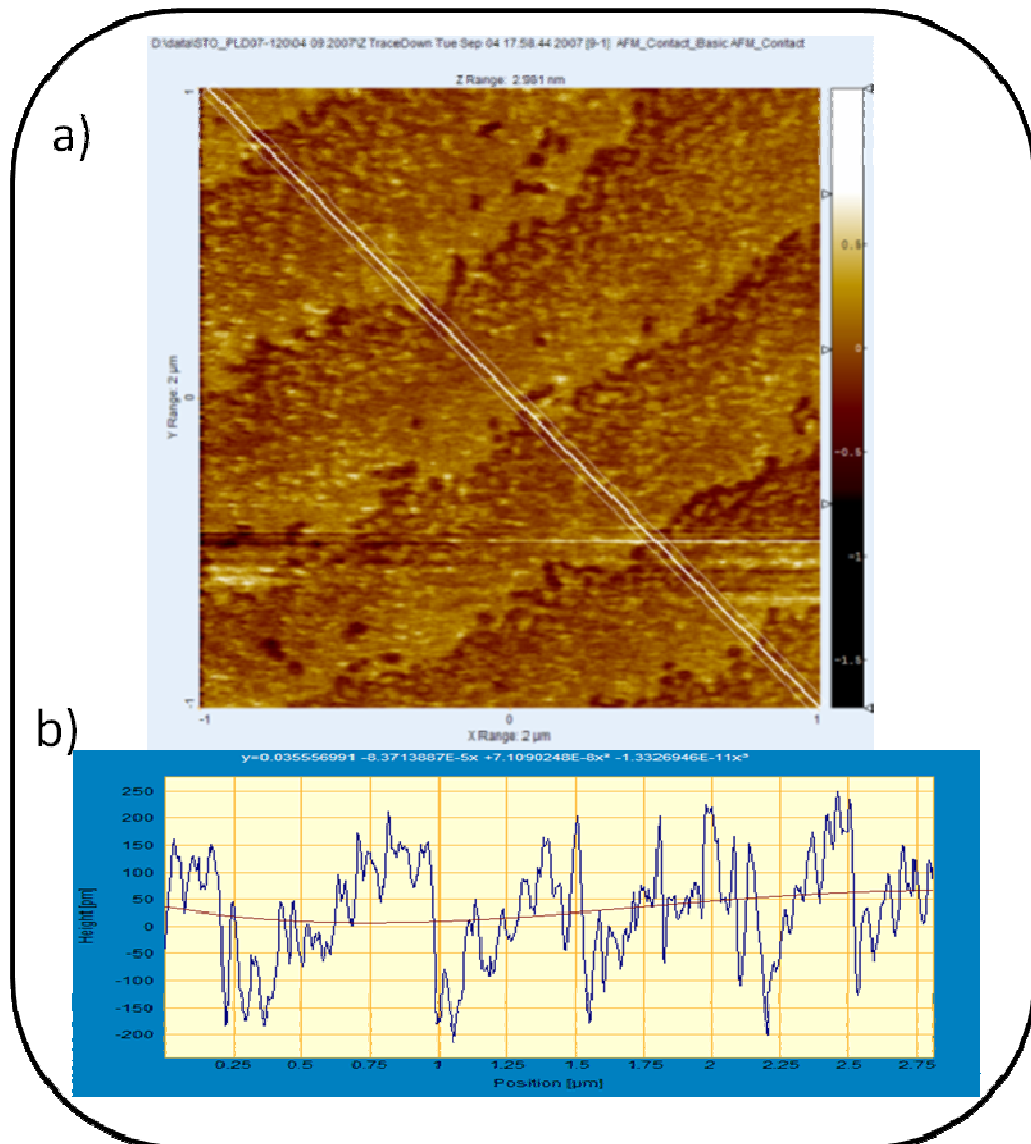


Fig. 3.1: AFM image of as received STO (001) substrate: a) 2D image (2 μm x 2 μm), b) the linear scan.

On the Figure 3.1, 4 Å high terraces on the surface are clearly notable, with additional 1.5 to 2 Å high islands on them. These heights indicate the double termination of the surface. This surface cannot be suitable for distinct properties materials growth in a controlled way.

The, as received, STO sample was also analyzed with RHEED instrument and the obtained results suggests that the surface is reconstructed. The superstructures are ordered as C (2x2) and this occurrence could be connected with presence of Sr atoms.

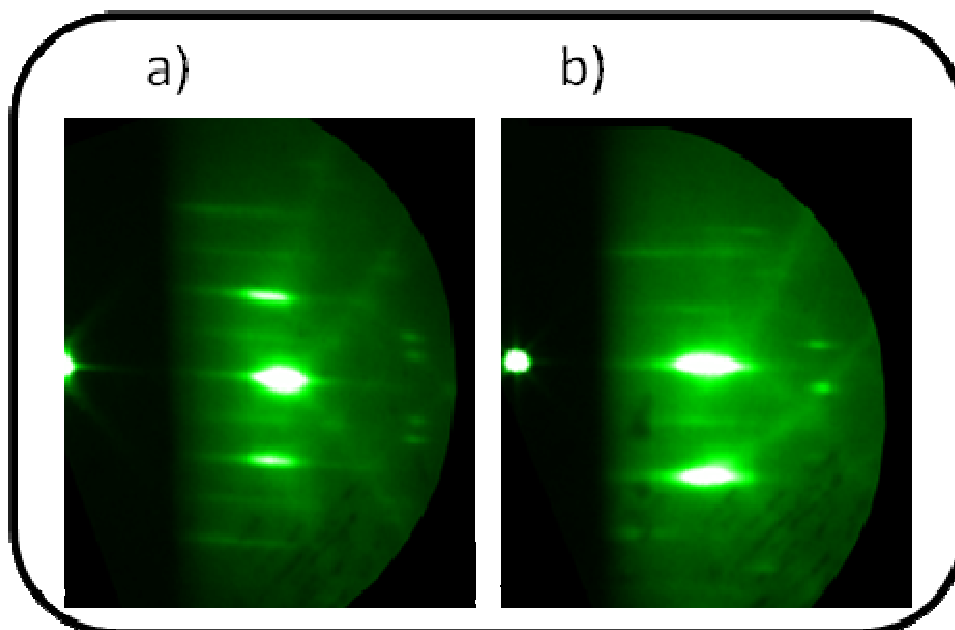


Fig. 3.2: RHEED pattern of a received STO (001) surface taken in [010]-(a) and [110]-(b) directions of the incident beam.

It is in agreement with previously published observations ⁶. Moreover, from the chemical point of view, as received substrates could also contain impurities like carbon, water molecules, strontium hydroxide or strontium carbonate which may form in contact with environment. However, annealing at the high temperatures removes impurities from the surface and improves the surface crystallinity. The deposition conditions of 800 °C, 0.1-0.5 mbar of Oxygen or vacuum and pre-annealing of 1-2 h used in this experiment was enough to clean the surface but it still contained intrinsically double termination.

3.1.1 Homoepitaxial STO film on as received STO (001)

To determine the growth mechanism on this surface I performed homoepitaxial growth of STO. The PLD growth was performed by resorting to a 248 nm KrF-excimer laser, with typical fluence $\sim 2.5 \text{ J cm}^{-2}$ at the target. STO deposition was carried at 800 °C, 0.1 mbar of flowing O_2 and at a laser repetition rate in the range 1-2 Hz. In the Figure 3.3 is depicted the RHEED oscillation during this homoepitaxial growth. Oscillations are very clearly visible with the same period of about 16 seconds. Also, the final RHEED 2D pattern indicates smooth surface without additional strikes which can be a sign of some kind of reconstructions.

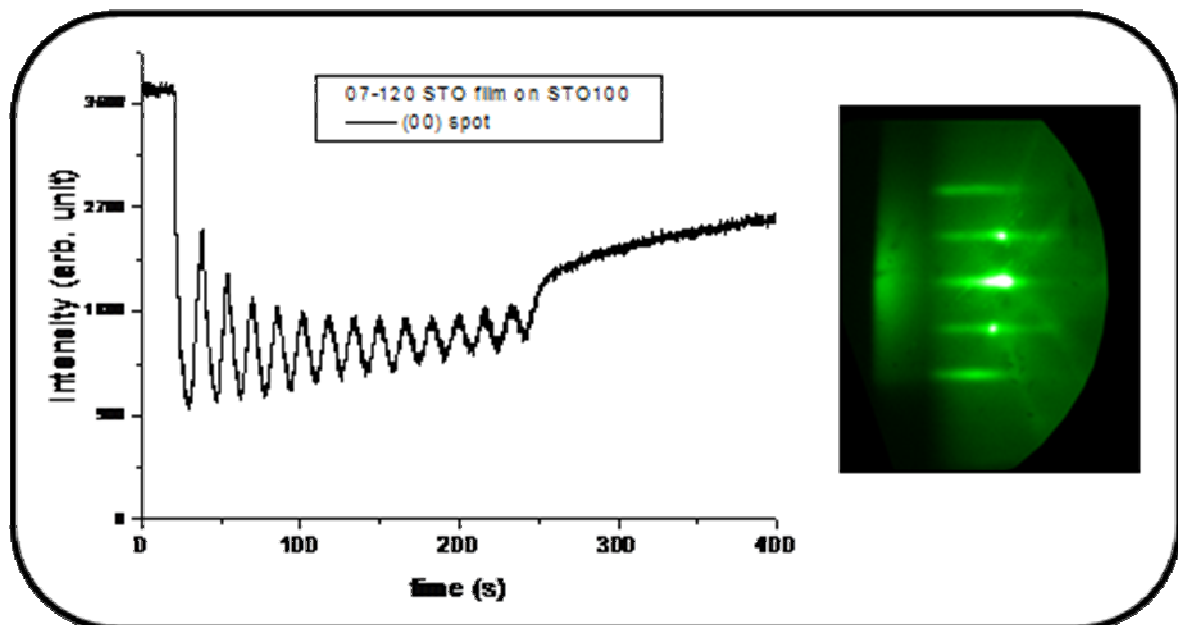


Fig. 3.3: The RHEED oscillations during growth and final RHEED pattern of the film.

After cooling down the film was transferred *in situ* in to the analytic chamber where was measured by AFM. Figure 3.4 shows AFM image of the film surface. Analysis of the 1D scan image show that there are still terraces, but their height is more 2 \AA than 4 \AA . This indicates that the surface surely has two terminations, TiO_2 and SrO . This was the proof that without the clear procedure of the termination the surface of the films cannot be with only one type of termination.

In other words, the film surface is replica of the interfaces (the surface substrate).

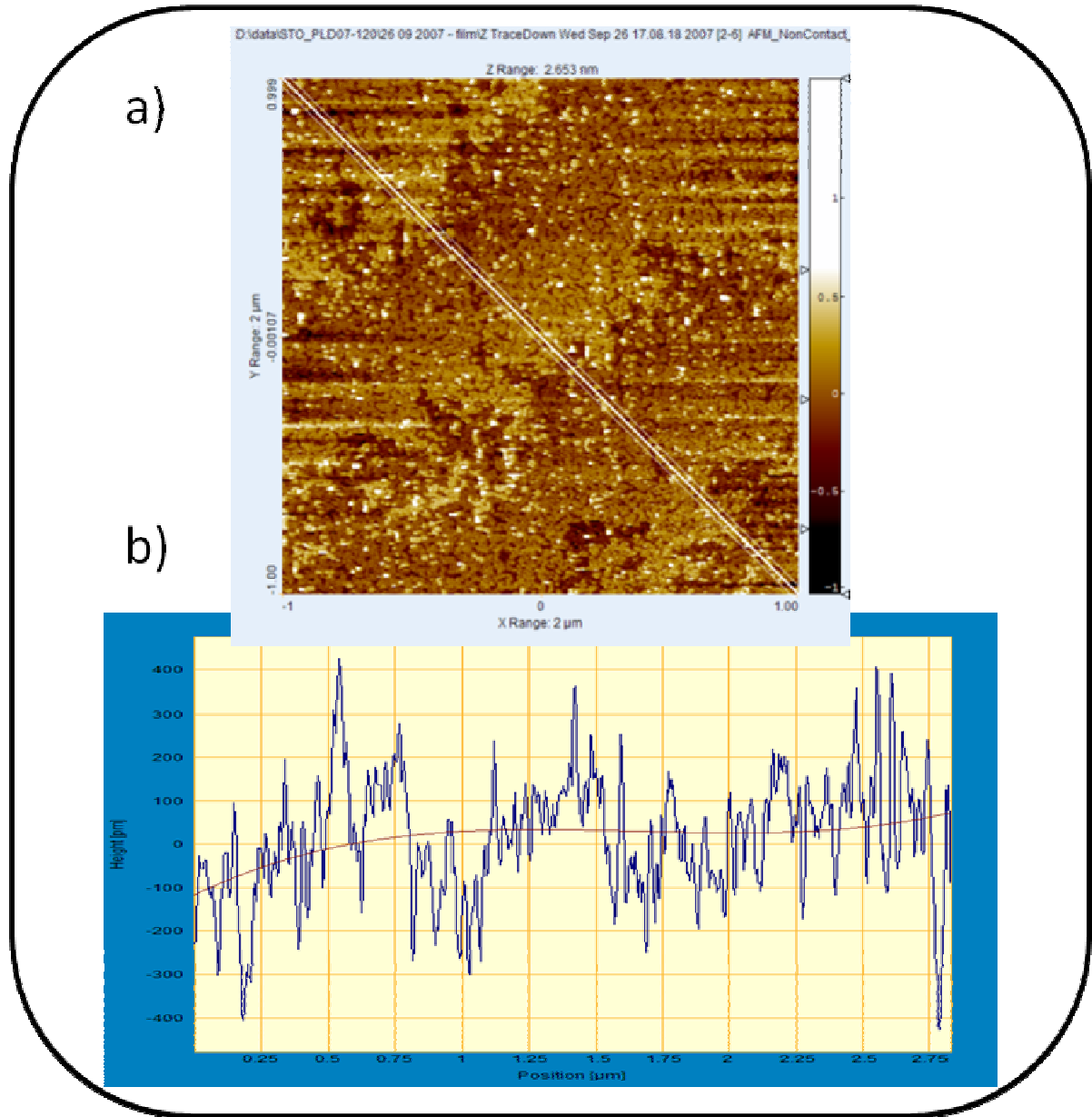


Fig. 3.4: AFM image of the STO film grown on as received STO (001) substrate: a) 2D (2 μm x 2 μm) image, b) the linear diagonal scan.

3.1.2 Homoepitaxial STO film on TiO₂ terminated STO (001)

The chemical etching joined with thermal annealing is one of the methods which give rise to the very well defined and terminated surface. The initial attempt was done by Kawasaki et al.³ and the method was improved by Twente group⁷. The different solubility between SrO and TiO₂ in acids is the base to get TiO₂ terminated surface. The chemical etching in our experiments is done in four steps:

1. Cleaning the substrates in acetone using ultrasonic bath for 10 min followed by N₂ draying,
2. Additional substrate cleaning in ethanol using the ultrasonic bath for 10 min followed by N₂ draying,
3. Soaking of the substrates in clean deionised water for 30 minutes using the ultrasonic bath also followed by N₂ draying. During this step SrO on the surface reacts with water and forms Sr(OH)₂, SrCO₃, SrO₂, etc^{1,7,8}.
4. Soaking of the substrates in BHF for 30 seconds (20 seconds using the ultrasonic bath and 10 seconds by manual shaking). During this step hydroxide complex dissolves. Contrary, TiO₂ is very stabile in the acid. Finally, substrate is washed with clean water and N₂ dried.

In the Figure 3.5, the AFM image of STO (001) surface after chemical treatment is presented. Height of the terraces is 4 Å, the terraces are flat and in comparison with STO as received substrate surface (Fig. 3.1) there are no signs of double termination. The chemically treated STO surface may contain holes as the consequence of etching treatments and are called "etch pits". To recover surface, improve crystallinity, close etch pits and to straighten terrace edges, thermal annealing is next step. The annealing is usually performed in Oxygen at normal pressure and at high temperature, up to 1000 °C. The annealing time depends on terrace step size, where for larger terraces the time is considerably longer. In any case the annealing time is in order of few hours.

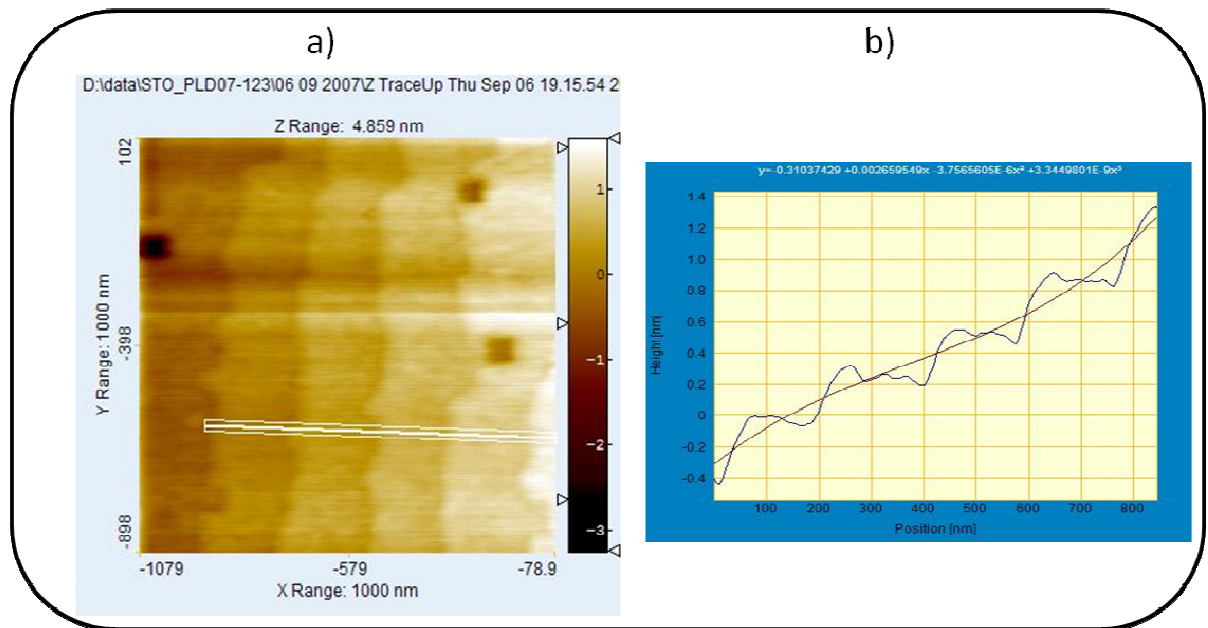


Fig. 3.5: AFM image of etched STO (001): a) 2D image, b) linear scan.

Regarding the high temperature annealing of STO, I would like to point out very important physical effect which is caused by the thermal treatment, Sr surface segregation. T. Ohnishi and al. claimed that the Sr surface segregation may appear at relatively low temperatures during annealing⁸. They proposed to do re-etching of the surface in order to remove Sr phases and to stabilize TiO₂ termination. K. Szot and co worker proved, by AFM study, that the extensive thermal treatment causes the formation of a regular SrO-rich surface⁹. Taking into account that, before the deposition, the substrate remains in the growth chamber quite long time (could be more the one hour) at high deposition temperature (about 800 °C) we were concerned that the additional annealing in the PLD chamber can cause Sr segregation. To avoid this we modified the recipe for obtaining TiO₂ terminated surface in sense that the *in situ* annealing of the substrate in the PLD chamber is performed right before the deposition. The parameters used for this step are: 950 °C and O₂ partial pressure of 0.5 mbar.

In the Figure 3.6 is shown AFM image of STO (001) surface prepared as described above. From the figure is possible to conclude that the terrace edges are now straight and flat with 4Å height, indicating full TiO₂ termination. Additionally, the RHEED patterns are free of any signs of a reconstruction.

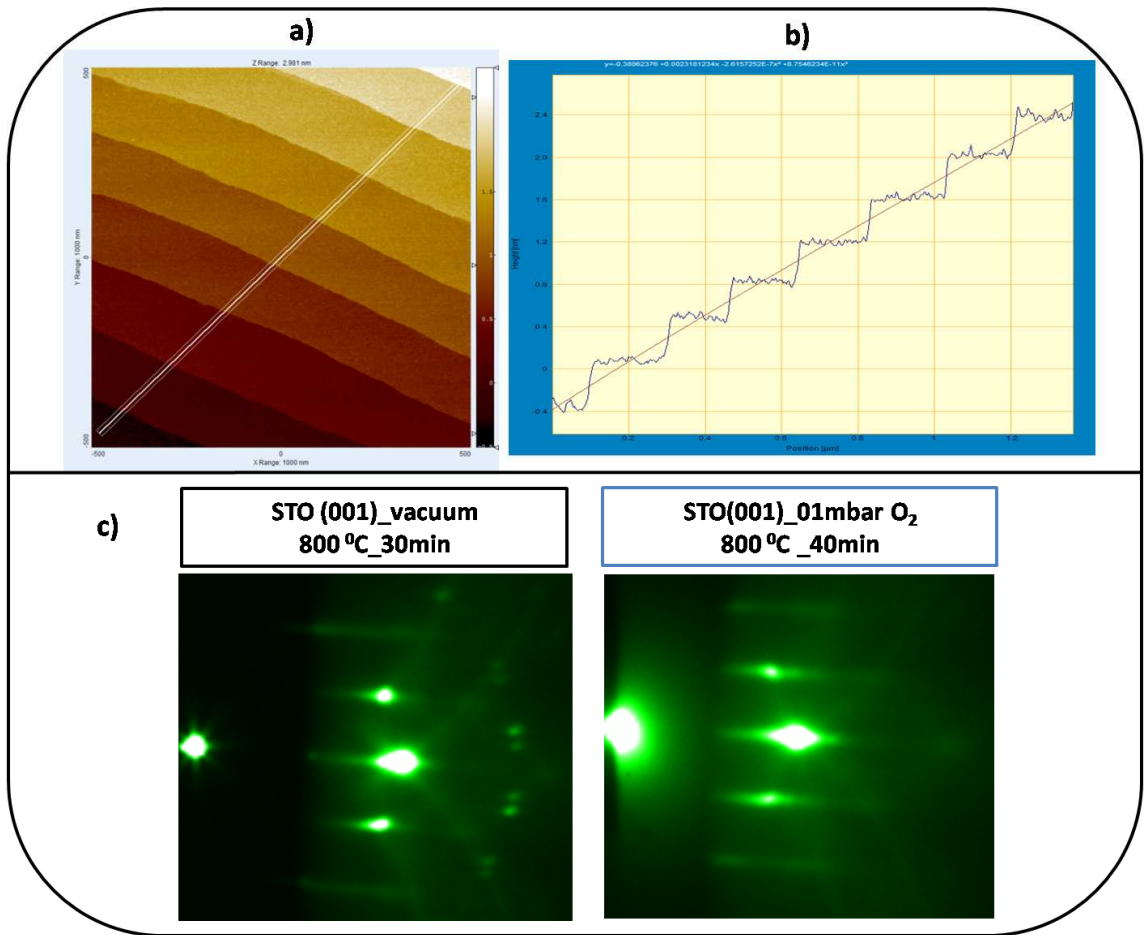


Fig. 3.6: The chemical etching with MODA thermal treatment. The AFM ($1\ \mu\text{m} \times 1\ \mu\text{m}$) image of the etched and annealed STO (001): a) 2D image, b) linear scan and c) the RHEED patterns of the substrate under different conditions.

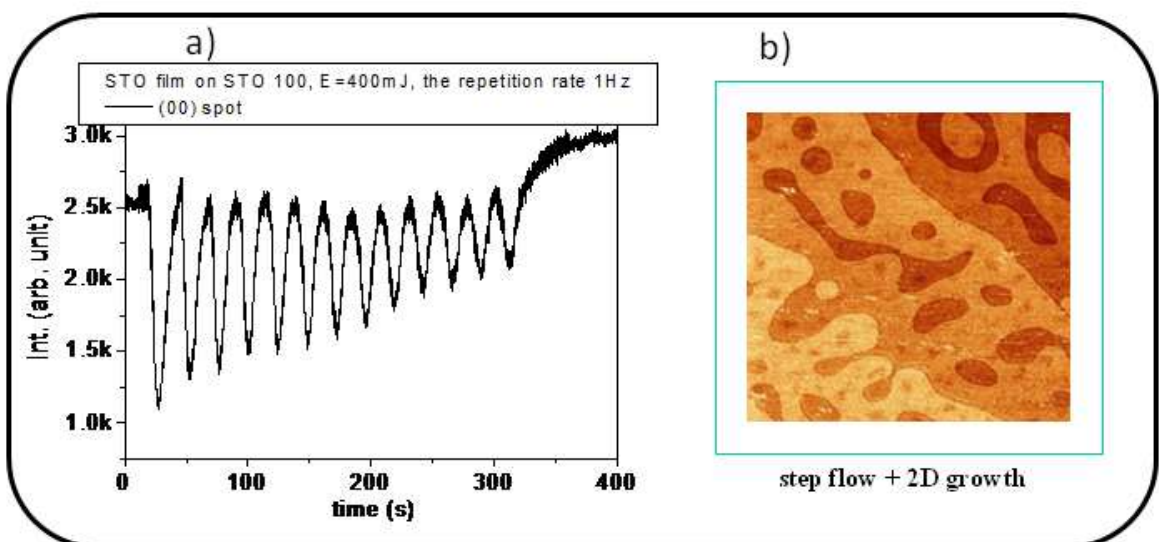


Fig. 3.7: The STO film on TiO₂ terminated STO: a) RHEED Intensity oscillations of 00 diffraction spot during the growth, b) STM image of the film.

On the TiO₂ terminated substrate homoepitaxial STO film was grown. The deposition parameters were the same as described above. The deposition was monitored by RHEED and the clear oscillations (Fig. 3.7a), sign of 2D growth, were visible. The film was measured by STM and the obtained image is depicted in Figure 3.7b. On the clearly visible terraces there are nucleated 2D islands as the consequence of the mixed growths, 2D and step flow. The height of the islands and terrace steps are the same, about 4 Å indicating one termination film surface. To confirm that the film has TiO₂ termination as the substrate itself has, qualitative analysis of XPS data were performed. The XPS measurement for this and for the other analysis presented in next subchapters was done in the following way:

- The measurements were performed in two geometrical configurations of the sample and the spectrometer. First configuration is when the XPS spectrometer collects emitted electrons perpendicular to the sample and the second where collected electrons are emitted from 35 degrees angle in respect to the surface. With the second configuration the measurement is more surface sensitive since escape depth ($t_d = d_e \sin 35^\circ$) is smaller than in the perpendicular configuration. The comparison of data from both configurations can give us indication of the presences of different elements in the bulk and the surface. The configuration of the XPS measurements is depicted in Figure 3.8.
- The chemical character of sample surfaces was qualified by XPS analyses. The spectra of the 3d_{5/2} 3d_{3/2} Sr peaks (Figure 3. 9) are normalized to the intensity of the corresponding 2p_{3/2}-2p_{1/2} Ti peak (obtained from the same spectrum and after removal of the background).

In Figure 3.9, the data from three deferent samples are presented. The left spectrum is Sr 3d doublet obtained, as previously described, from STO where surface in not controlled. Actually, the sample was annealed couple of times in oxygen and UHV environments in order to cause Sr segregation. The data indicates that there is no deference in Sr presences between the bulk and the surface (perpendicular and shallow geometry), since the peak intensities in both measurements configurations are similar.

Results: STO

The central spectra are from TiO_2 terminated surface what was confirmed by AFM measurements (see Fig. 3.6).

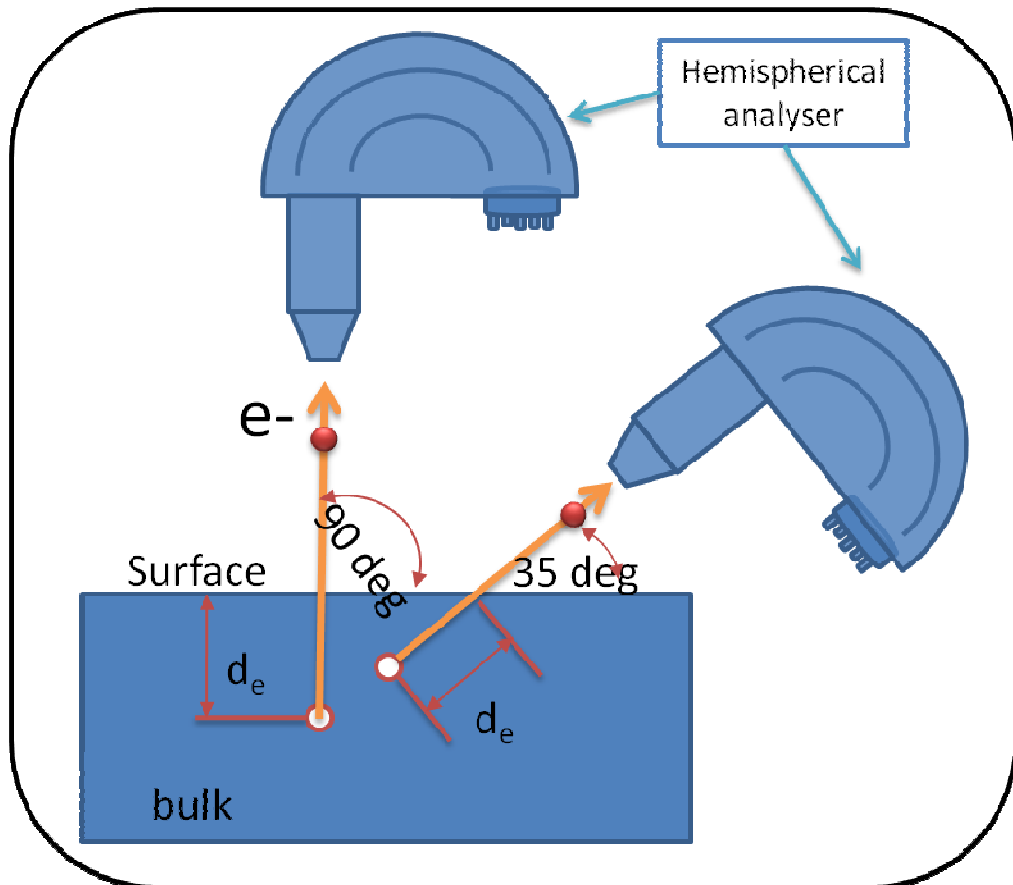


Fig. 3.8: two XPS configurations for the measurements.

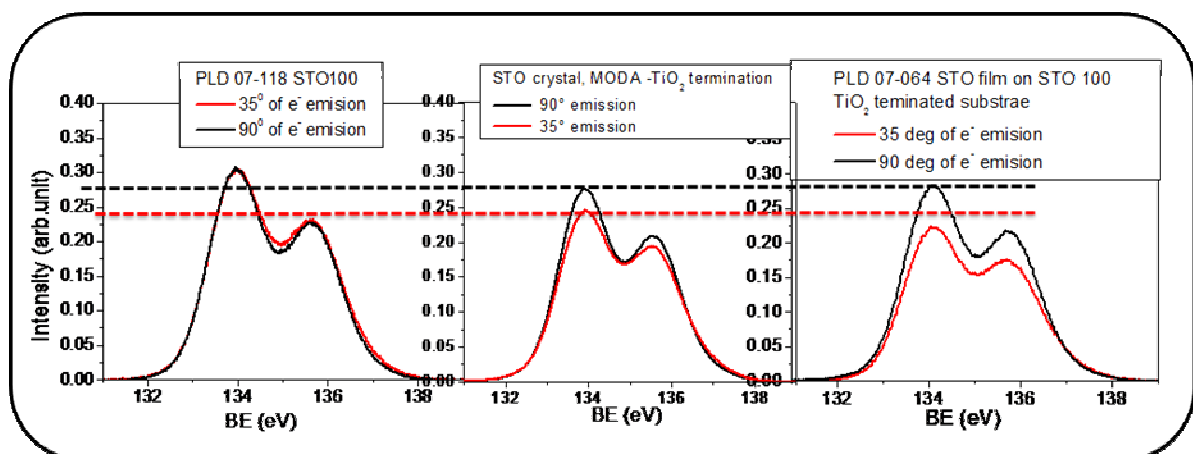


Fig. 3.9: XPS data of: left-STO annealed several time at high T , center- TiO_2 terminated STO, and right-STO film on TiO_2 terminated STO substrate

This spectrum clearly shows that the surface contains less Sr atoms respect to the bulk. It is to be expected if the surface is terminated by TiO₂ layer. The spectrum shown on the right is from STO homoepitaxial film on TiO₂ terminated STO. The presence of the strontium is slightly deferent in the shallow configuration respect to the TiO₂ terminated STO, while in the perpendicular geometry the intensities of the peak are identical.

General conclusion from the performed experiments of the TiO₂ termination control, according to the STM and the XPS measurements are:

1. The TiO₂ termination of STO commercial substrates with our modification was very successful. Therefore, the starting condition for the growth of the controlled surface was satisfied.
2. The parameters for homoepitaxial growth of STO film on TiO₂ terminated STO substrate are optimized in a way that provide conditions for 2D growth. Moreover, the termination of the film is also TiO₂ as well as the substrate is.

References:

- ¹ G. Rijanders G. Koster, D.H.A. Blank and H. Rogalla, *Physica C* **339**, 215 (2000).
- ² G. Rijanders V. Leca, G. Koster, D.H.A. Blank and H. Rogalla, *Materials Research Society Symposium* **587 (C)** (2000).
- ³ K. Takahashi M. Kawasaki, T. Maeda, R. Tsuchiya, M. Shinohara, O. Ishiyama, T. Yonezawa, M. Yoshimoto, and H. Koinuma *Science* **266**, 1540 (1994).
- ⁴ T. Maeda M. Yoshimoto, K. Shimozono, H. Koinuma, M. Shinohara, O. Ishiyama, and F. Ohtani, *Appl. Phys. Lett.* **65**, 3197 (1994);
- ⁵ Z. Y. Liu M. Kawai, T. Hanada, M. Katayama, M. Aono, and C. F. McConville, *Appl. Surf. Sci.* **82** (1994).
- ⁶ G. M. De Luca A. Fragneto, R. Di Capua, U. Scotti di Uccio, M. Salluzzo, X. Torrelles, Tien-Lin Lee and J. Zegenhagen, *Appl. Phys. Lett.* **91**, 101910 (2007).
- ⁷ B.L. Kropman G. Koster, G. Rijanders and D.H.A. Blank, *Appl. Phys. Lett.* **73**, 2920 (1998).
- ⁸ K. Shibuya T. Ohnishi, M. Lippmaa, D. Kobayashi, H. Kumigashira, M. Oshima and H. Koinuma, *Appl. Phys. Lett.* **85**, 272 (2004).
- ⁹ W. Speier K. Szot, *Phys. Rev. B* **60**, 5909 (1999).

3.2 GROWTH AND CHARACTERIZATION OF STABLE SrO-TERMINATED SrTiO₃ SURFACES

A simple technique for the growth of SrO-terminated SrTiO₃ surfaces is reported. High quality SrTiO₃ epitaxial films were grown by reflection high energy electron diffraction assisted pulsed laser deposition on suitably prepared NdGaO₃ (110) substrates. The surface properties, analysed within a growth/characterization multi-chamber UHV system, by photoemission spectroscopy performed on the core-level spectra of Sr and Ti, low energy electron diffraction and scanning tunnelling and atomic force microscopy, are fully consistent with a single Sr oxide termination. The availability of such high quality Sr-terminated SrTiO₃ surfaces is of major importance for the controlled growth of oxide epilayers and interfaces.

The technology of epitaxial oxide film growth has been continuously progressing during the last decades, resulting in the capability to control structures, morphologies, surfaces and interfaces at the highest level. It was soon realized that a prerequisite for achieving samples with a high degree of perfection is the availability of atomically smooth substrates. As a matter of fact, the demonstration of suitable procedures for obtaining SrTiO₃ (STO) crystals with flat, single terminated, (001) terraces, contributed to the success of this material as a substrate for the growth of countless types of functional oxides. The STO lattice consists of an alternating stack of SrO (A-site) and TiO₂ (B-site) atomic layers along the [001] direction. In their pioneering work, Kawasaki et al.¹ showed that a simple chemical etching can remove SrO at the STO surface, so that a single TiO₂ terminating surface layer is obtained. Further improvements were achieved by the same authors and by others²⁻⁵, demonstrating the feasibility of the TiO₂ termination with high crystallinity and straight step edges. A spectacular effect of the importance of surface termination is provided by the formation of a high mobility 2D electron gas at the LaAlO₃/STO interface, which only takes place on B-site terminated STO⁶.

While control of the B-site termination of STO may be regarded nowadays as a standard protocol in many laboratories, the control over the A-site termination is by far more difficult. Such termination has been obtained by the deposition of a SrO monolayer onto a previously prepared B-site STO⁷⁻⁹ The control of film thickness is achieved by monitoring Reflection High Energy Electron Diffraction (RHEED) during

the growth, and by calibrating the rate, with due care to achieve a complete layer¹⁰ while avoiding SrO precipitate formation. Only under very specific growth conditions (i.e., the so called "interval deposition" technique) the surfaces of these samples are smooth⁸ as demonstrated by AFM analyses, and well suited for successive layers growth¹¹. A SrO terminated surface was also prepared in a different way by G. Rijnders, et al.¹², who observed that the expected RuO₂ termination of SrRuO₃ deposited onto B-site STO was in fact unstable, due to the volatility of the ruthenium oxide¹³.

The A-site termination of STO is by far less investigated, in spite of the potential interest for catalytic processes¹⁴ and for the realization of specific functional heterostructures and interfaces. The main idea is that the terminating layer determines the stacking sequence in the heteroepitaxial growth of perovskites¹⁵, according to the law that A- and B-sites are generally alternated. In principle, the properties of the deposited film may be sensitively affected by the interface properties, through e.g. charge transfer¹⁶. In a recent work¹⁷, some of the authors studied the crystallographic and morphological properties of both A- and B-site terminated STO single crystals, resorting to Atomic Force and Scanning Tunnelling Microcopies (AFM and STM) and to Grazing Incidence X-Ray Diffraction (GIXRD). The results demonstrated the stability of the B-site termination against thermal treatments, also confirming the observation⁴ that SrO precipitates are formed during annealing. On the other hand, the nominally A-site terminated samples after long exposure to air appeared as not fully covered by SrO and more disordered, probably due to a greater sensitivity of such surface to the interaction with the atmosphere¹⁸.

In this subchapter, our further investigations on this issue, showing that a high quality SrO termination can be achieved by resorting to STO heteroepitaxial growth on (110) NdGaO₃ (NGO) substrates are reported. This procedure has one fundamental advantage: the A-site termination of NGO is prepared through a thermodynamic equilibrium process, that is, a thermal treatment¹⁹, which in our case was performed in a constant flow of pure oxygen, at 1200 °C for 20 hours (Figure 3.10). The crystal structure of NGO belongs to the space group Pbnm, with $a = 0.54333$ nm, $b = 0.55036$ nm, and $c = 0.77157$ nm²⁰. It is deduced that a STO cell on (110) NGO has to match an effective in-plane rectangular lattice of

Results: STO

0.3867x0.3858 nm². The misfit with respect to the relaxed STO lattice parameter ($a_{\text{STO}} = 0.3905$ nm) is therefore as small as 1.2 %.

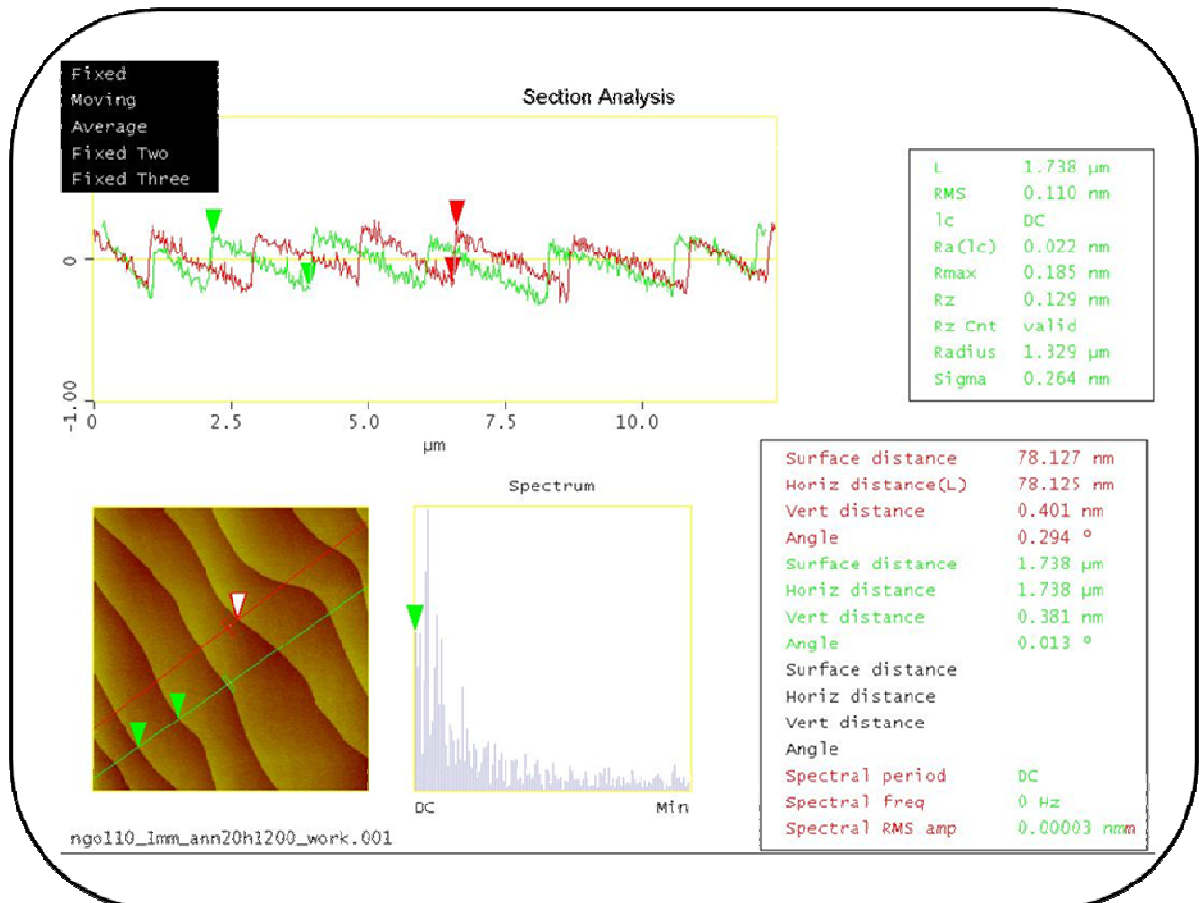


Fig 3.10: The AFM data of A site terminated NGO (110).

The RHEED images reported in Figure 3.11, collected after introduction of 0.1 mbar O₂ in the chamber, demonstrates the high crystal quality of this surface. The PLD growth was performed using the recipe as for the homoepitaxial STO growth on STO 001 substrate. The sharp 2D like diffraction patterns, collected at the end of depositions, confirm the excellent crystallinity, both in the case of thin, and for relatively thick films. The RHEED specular spot oscillations are regular (Fig.3.10).

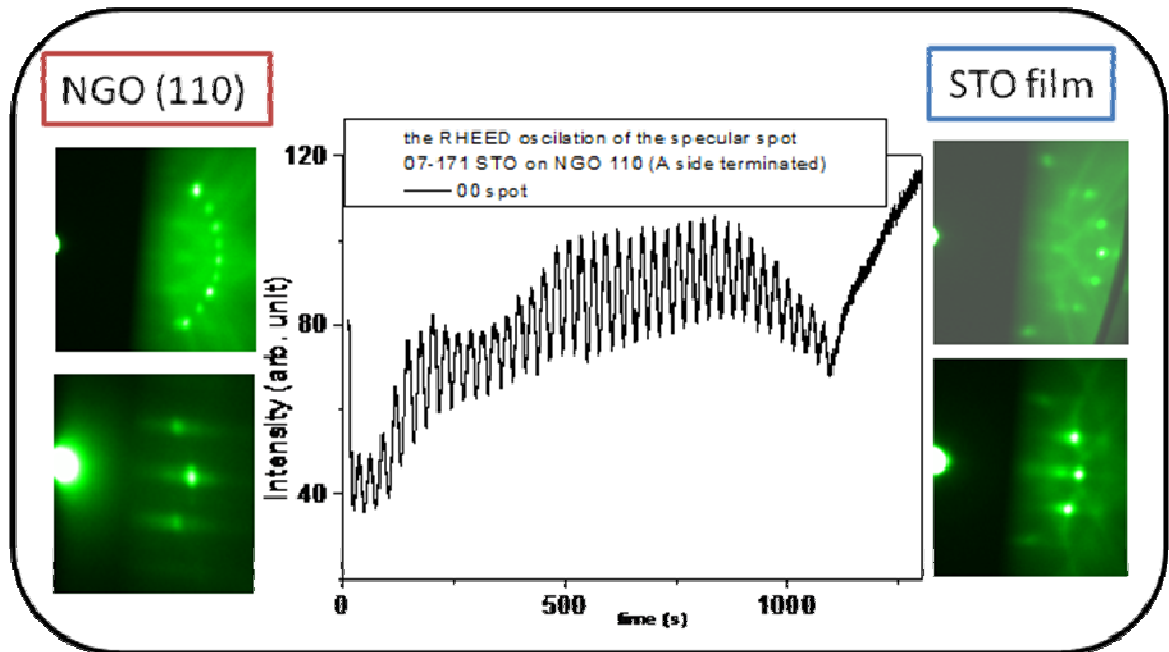


Fig.3.11: High pressure RHEEDs measurements of: the (110) NdGaO_3 surface before film deposition at 800 °C (left), the RHEED oscillations of the specular reflection during the film growth (centre) and of the STO film after cooling down (right). The RHEED images are taken with different angle of e^- incident beam.

The behaviour is indicative of a growth that proceeds by nucleation and lateral expansion of grains. In a steady state regime, the delay between RHEED maxima indicates the time needed to complete a unit cell (u.c.) stack and hence the growth rate, that we varied in the range 0.02 – 0.06 u.c. per laser pulse. After interrupting the deposition, the RHEED signal increases, suggesting an ordering of the surface. The homoepitaxial growth of STO on such surface proceeds with improved regularity. As an example, the pattern in fig. 1d shows oscillations that persist over more than 40 cycles. After a brief annealing in vacuum at 800°C, the SPA-LEED patterns of the STO films deposited on (110) NGO show sharp and clean signature of a $c(2 \times 2)$ reconstruction (Fig. 3.12d). This differs from the $p(2 \times 1)$ reconstruction, that is often observed in the case of STO single crystals with TiO_2 termination, and that has been ascribed to the ordering of oxygen vacancies²¹.

In situ non-contact atomic force microscopy (NC-AFM) performed on as-grown samples (Fig. 3.12a) shows flat surfaces covered with islands, confirming that STO grows by 2D nucleation.

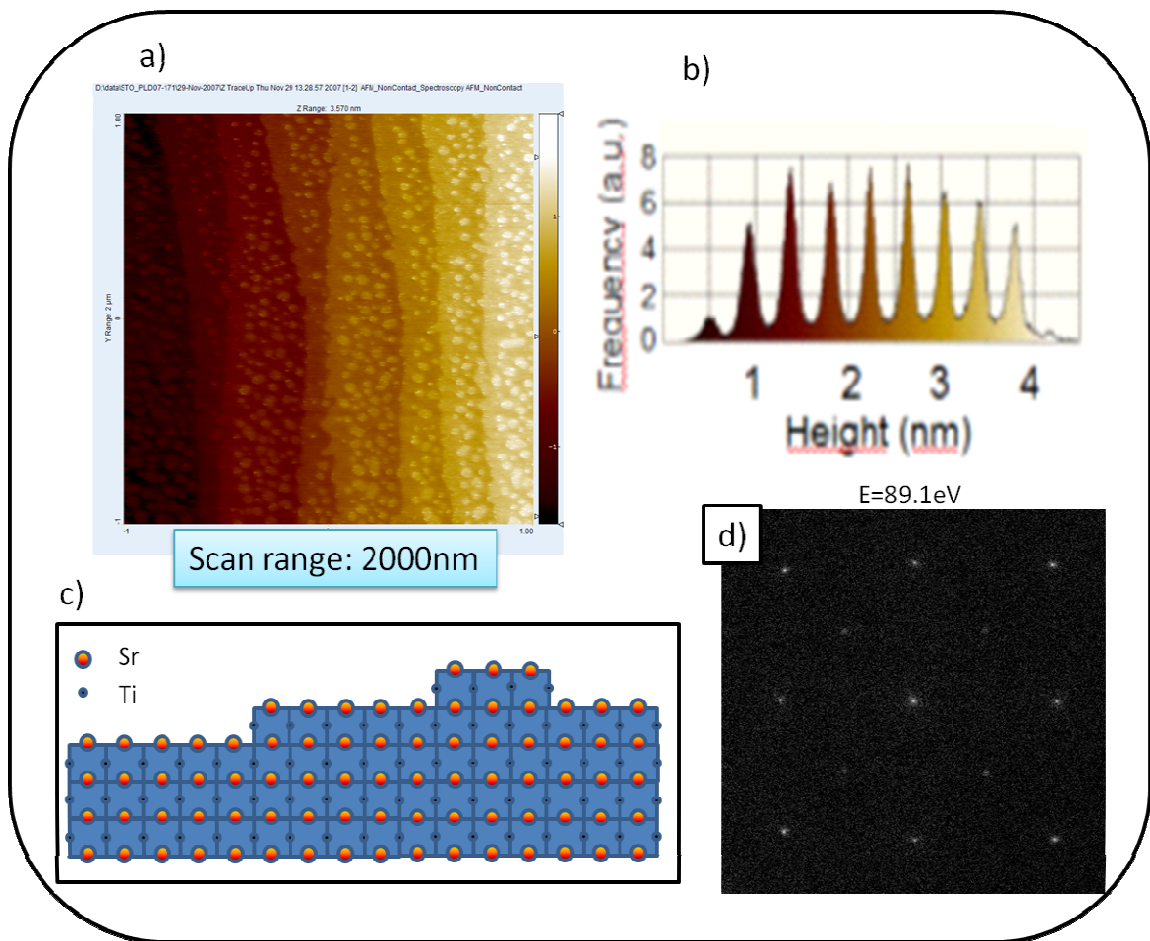


Fig. 3.12: a) Morphology of a 18 nm STO film obtained by in situ NC-AFM (it shows ~15% islands coverage), b) The histogram shows 0.39 nm high steps only, c) the scheme of the film surface, d) SPA LEED image shows c 2x2 reconstructed surface.

Strikingly, the annealing in UHV (800 °C in 10^{-10} mbar for 75 min) of air-exposed samples (Fig. 3.13a) preserves the terrace smoothness and the step height of 0.39 nm (i.e., 1 u.c.). Even very thin STO films (6 u.c.) are very stable against annealing in different environmental conditions, including high oxygen pressures (up to 1 mbar) and high temperatures (800°C) (Fig. 3.13b).

Each STM map was quantitatively analyzed. As a typical result, the heights histogram is presented in Figure 3.12b, revealing the occurrence of peaks separated by 0.39 nm. Both such data and the maps morphology confirm that the samples have one termination, excluding half-cell steps at edges or at pits.

It is worth mentioning that areas with double termination are instead easily detected by our setup in STO crystals that undergo suitable thermal treatments.

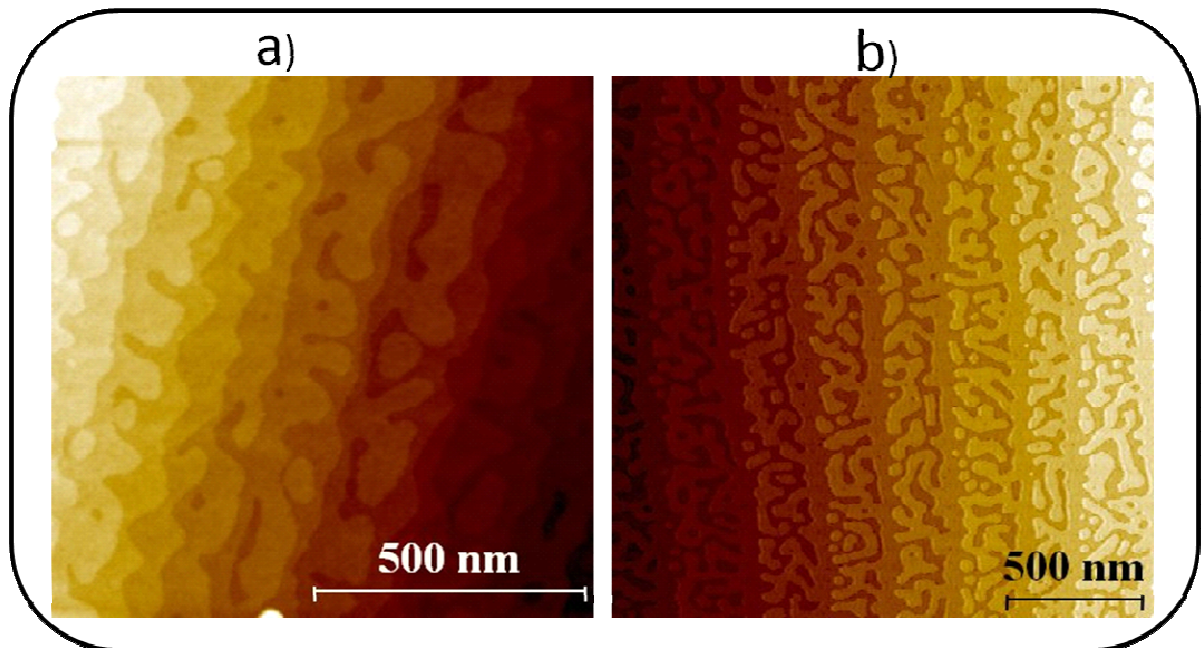


Fig. 3.13: Morphology of STO films: a) STM after air exposure followed by thermal treatment at 800°C in UHV. c) NC-AFM on a 6 u.c. STO after overnight annealing at 800°C in 0.1 mbar O₂.

The chemical nature of sample surfaces was qualified by XPS analyses, that we performed on an as-grown STO film deposited on NGO and on a TiO₂-terminated crystal (prepared as in ref. 3) as a reference. The spectra of the 3d_{5/2} 3d_{3/2} Sr emission (Fig. 3.14) are normalized to the intensity of the corresponding 2p_{3/2}-2p_{1/2} Ti peak. The spectra are collected from electrons emitted at normal and at shallow angle (35° to the surface), the latter being most sensitive to the surface chemical composition because of the short mean free path of the photoelectrons; the spectra at normal emission are compared in Figure 3.13-left. The spectrum of normal-emitted photoelectrons is more intense in the case of the TiO₂-terminated crystal. The opposite happens for the STO film, as expected for different crystallographic terminations. We also mention that the spectra of our STO homoepitaxial films grown on TiO₂-terminated crystals (see Fig. 3.9) closely resemble those of the substrate²². The quantitative evaluation²³ of the XPS data fully supports our claim that a complete SrO layer terminates STO films on NGO.

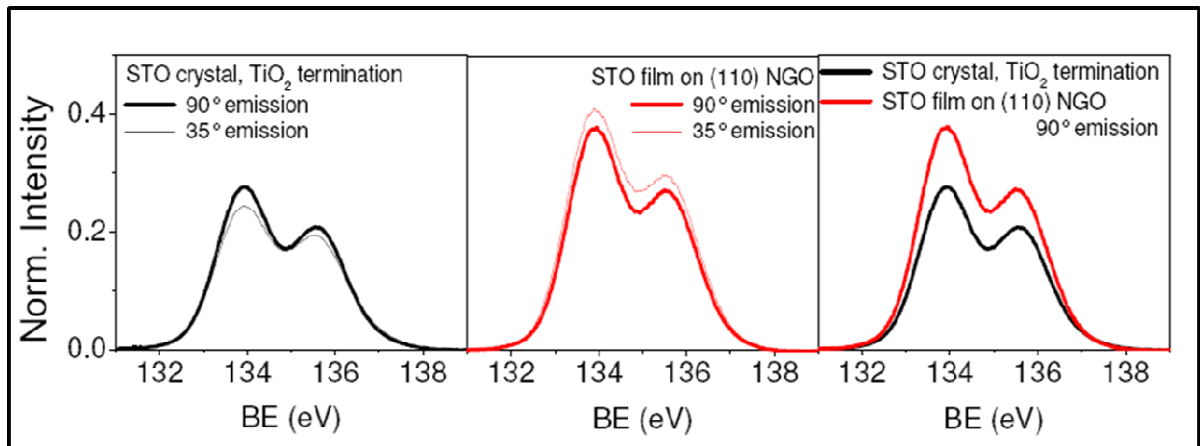


Fig.3.14: Spectra of the 3d_{5/2}-3d_{3/2} Sr emission normalized to the intensity of the 2p_{3/2}-2p_{1/2} Ti peak. Left: STO film on NGO, normal vs. shallow emission angle; centre: TiO₂-terminated STO crystal, normal vs. shallow emission angle. Right: the comparison between the two (normal emission angle).

It is worth mentioning that NGO is typically a much more perfect crystal than STO is, as also confirmed by our preliminary structural characterization by synchrotron light. It has been shown that STO films grown on substrates with a comparable degree of perfection, such as perovskitic scandates²⁴, even exceed the quality of commercial STO single crystals.

The x ray diffraction measurements (Figure 3.15) confirm the expectation of high structural quality. The STO epilayer is under in-plane compressive stress to match NGO, and the vertical spacing is elongated up to 0.393 nm.

The reported preparation method for a SrO terminated STO buffer on (110) NGO is a self-controlled process. Although described experiment was performed in a highly advanced system, that was needed to perform the reported in-situ analysis, the growth technique of A-site terminated STO can be easily replicated in other simpler systems. The key point is that, in contrast to the usual deposition of a SrO monolayer that requires a special deposition technique (see, e.g., ref. 8) and the RHEED control to interrupt the process at 1 layer completion, the process that we propose can be interrupted at any time, always resulting in a SrO termination. This does not mean, however, that the physics of the reported growth process is trivial.

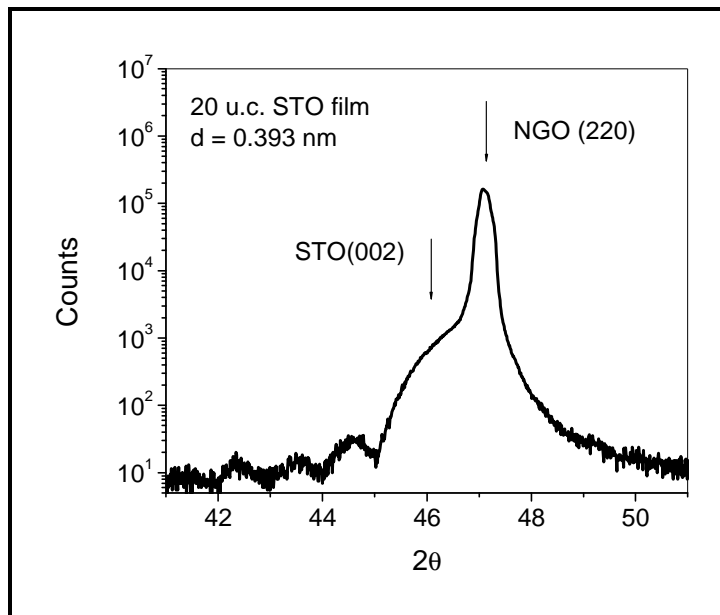


Fig.3.15: X ray θ - 2θ measurements for the STO film on (110) NGO.

In conclusion, we grew high quality STO epitaxial films on A-site terminated (110) NGO substrates by PLD assisted by high pressure RHEED. The reported data strongly support our initial guess, that a single, A-site (i.e. SrO), termination is obtained. This statement is based on the following observations:

1. In situ AFM and STM measurements demonstrate steps with integer unit cell height and smooth terraces surface.
2. The chemical composition of the surface layer determined by XPS confirms that the terminating layer is SrO. Therefore, the STO films grow on NGO keeping the stacking sequence ...A-B-A-B... through the interface.
3. Finally, the LEED indicates that the SrO surface has a high crystallinity and, after UHV annealing, a peculiar c (2×2) reconstruction, thus indicating that a well ordered surface lattice is realized, and that such a structure is stable, as ab-initio calculations anticipate²⁵.

This termination is also perfectly suitable for successive growth process, as demonstrated by our data of STO homoepitaxy that is characterized by a coherent growth with large RHEED oscillations over tens of unit layers. On the contrary, the occasionally reported instability of the SrO termination could be related to the presence of incomplete or of multiple-layer SrO coverage, or to the formation of non-crystalline, or polycrystalline, or disordered SrO islands.

References

- 1 M. Kawasaki et al., *Science* **226**, 1540 (1994).
- 2 M. Kawasaki et al., *Appl. Surf. Sci.* **107**, 102 (1996).
- 3 G. Koster et al., *Appl. Phys. Lett.* **73**, 2920 (1998).
- 4 T. Ohnishi et al., *Appl. Phys. Lett.* **85**, 272 (2004).
- 5 D. Kobayashi et al., *Journal of Electron Spectroscopy and Related Phenomena* **144–147**, 443 (2005).
- 6 A. Ohtomo and H. Y. Hwang, *Nature* **427**, 423–426 (2006).
- 7 S. Migita, Y. Kasai, S. Sakai, *J. Low Temp. Phys.* **105**, 1337 (1996).
- 8 G. Rijnders et al., *Applied Surface Science* **168**, 223 (2000).
- 9 R. Takahashi et al., *Appl. Surf. Science* (2002); R. Takahashi et al., *J. Cryst. Growth* **234**, 505, (2002).
- 10 Clear evidence that the maximum of diffracted intensity doesn't guarantee layer completion was provided, e.g., by J. Z. Tischler et al. *Phys. Rev. Lett.* **96**, 226104 (2006), by resorting to a x ray probe, but the same may be expected for RHEED.
- 11 See, e.g., R. Tsuchiya et al., *Appl. Phys. Lett.* **71**, 1570 (1997).
- 12 G. Rijnders, D. H. A. Blank, J. Choi & C. B. Eom, *Appl. Phys. Lett.* **84**, 505 (2004).
- 13 U. Scotti di Uccio et al., *Eur. Phys. J. B* **41**, 3–9 (2004).
- 14 Y. Matsumoto et al., *Thin Solid Films* **486**, 11 (2005).
- 15 G. Rijnders, D. Blank, *Nature* **433**, 370 (2005).
- 16 H. Zenia, G.A. Gehring and W.M. Temmerman, *New J. Phys.* **9**, 105 (2007).
- 17 A. Fragneto et al., *Appl. Phys. Lett.* **91**, 101910 (2007).
- 18 The different reactivity of A-site and B-site surfaces with water is just the principle on which the selective etchings are based. See also R.A. Evarestov, A.V. Bandura and E.N. Blokhin, *J. Phys. Conf. Series* **93**, 012001 (2007).
- 19 T. Ohnishi et al., *Appl. Phys. Lett.* **74**, 2531 (1999).
- 20 W. Marti et al., *J. Phys.: Condens. Matter* **6**, 127 (1994); L. Vasylechko et al. *J. of Alloys and Compounds* **297**, 46 (2000).
- 21 The STO surface presents a large variety of reconstructions, depending on the preparation. The p(2x1) reconstruction is described, for instance, by K. Johnston, M.R. Castell, A.T. Paxton, and M.W. Finnis, *Phys. Rev. B* **70**, 085415 (2004).
- 22 Some authors (see J. M. Huijbregtse, J.H. Rector, B. Dam, *Physica C* **351**, 183 (2001) for a brief review) reported on a single SrO termination of their homoepitaxial STO films. This is not the case for our samples. The complex dynamics of Sr during homoepitaxial growth and of its effect on the surface structure will be discussed elsewhere.
- 23 We compare the experimental data for normalized intensities R after background subtraction (CASA® software) with theoretical evaluations for line intensity from a perfect stacking of alternate A – B – A... layers (in parenthesis): R = () at normal emission; R = () at 35° emission.
- 24 M. D. Biegalski et al., *Appl. Phys. Lett.* **88**, 192907 (2006).
- 25 R. I. Eglitis and David Vanderbilt, *Phys. Rev. B* (2008), in press.

3.3 THE TiO₂ TERMINATED (001) STO SURFACES UNDER THERMAL TREATMENTS

Thermally and chemically treated STO surfaces have been extensively investigated due to the induction of surface terminations and many different varieties of their reconstructions and relaxations¹. Based on the literature, it can be concluded that STO surface is very sensitive to the preparation and processing conditions. As mentioned in the Introduction, several concepts have been used to explain the experimental observations of STO surface reconstructions and relaxations. Explanations, mostly present in a literature, are referring to lateral displacements including rumpling of the surface atoms²⁻⁴, oxygen deficiency⁵⁻⁷, Sr ad-atom model⁸ and formation of non-perovskite phases containing nanostructures based on either of SrO or TiO⁹⁻¹⁰.

Here, in this chapter, I present my study on one type of reconstruction which is widely observed, p(1x2)^{6, 7}. This type of reconstruction is already theoretically described¹¹ and according to the published studies, it is due to the creation of oxygen vacancies and their ordering on the surface. Since STO develops conducting properties when oxygen deficient and its surface can even have more enhanced conducting behavior, it is really important to understand the processes of creation and annihilation of oxygen vacancies on the surface. Moreover, there is still a debate regarding the reason for the presence of a quasi two-dimensional electron gas at the interface of STO with LaAlO₃, which are both insulators. The electron gas is only present in the case of TiO₂-terminated STO, while in the case of SrO-termination, no such effect is observed¹². This fact suggests that the appearance of the quasi two-dimensional electron is tightly connected to the preparation and a treatment of the surface.

3.3.1 High temperature UHV (1x2) reconstructed surface of TiO₂-terminated STO

SrTiO₃ single crystals with epi-polished (001) surfaces were supplied by SurfaceNet GmbH, Germany. The TiO₂ terminated STO (001), processed as described in this thesis, was mounted on the OMICRON sample holder, introduced in the analytic chamber of MODA system and placed on the manipulator above the heater. Before

any *in situ* thermal treatment the sample was measured by XPS to ensure that the sample is an intrinsic insulator. After that, the sample was annealed at 800 °C for 1h. The temperature was gradually increased, at 20 °C per minute. The temperature was also monitored by the thermocouple and the pyrometer. The pressure in the chamber, during annealing, was lower than 1×10^{-9} mbar. After the annealing the sample was cooled down at same rate and then measured by XPS again. The XPS data before and after the annealing are presented in Figure 3.16.

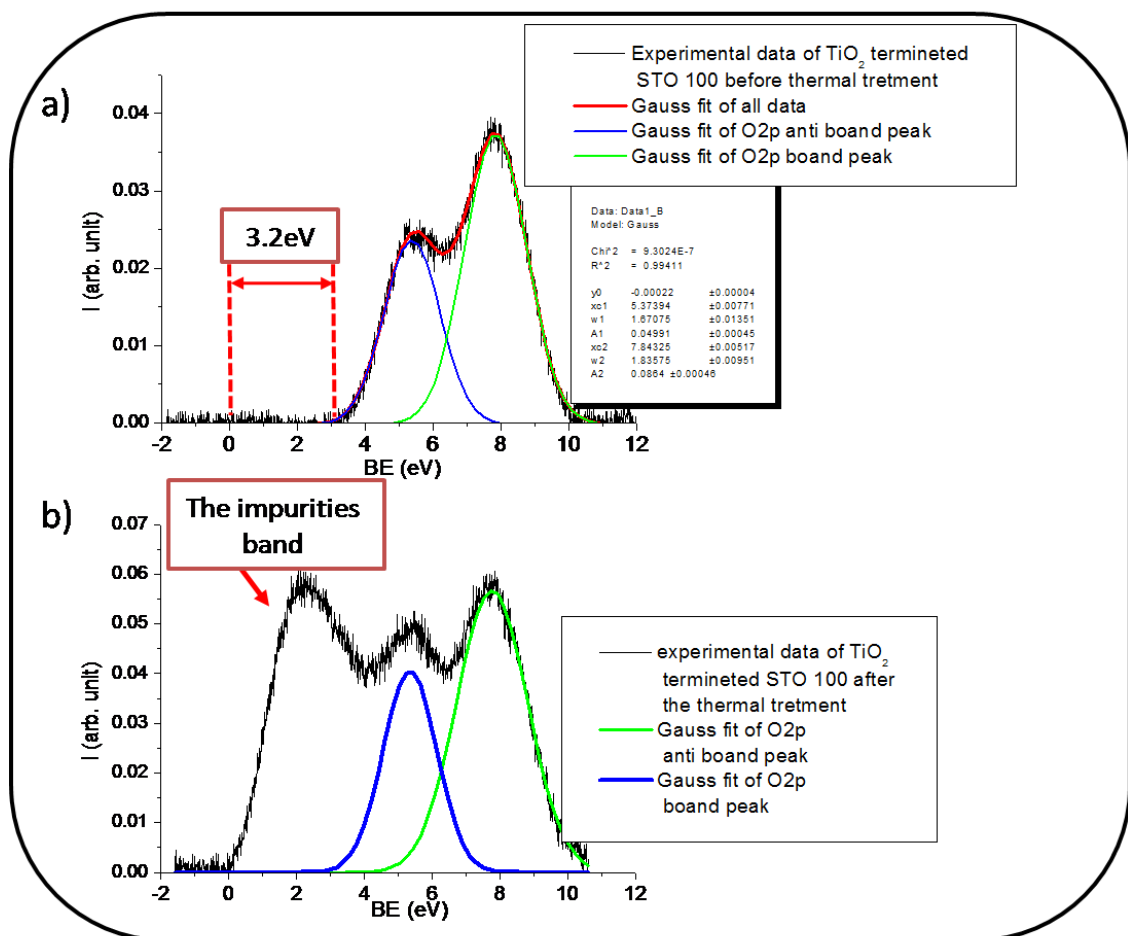


Fig. 3.16: The XPS data of TiO_2 terminated STO: a) before thermal treatment, b) after 1h at 800 °C in UHV condition.

Our observation of the insulator gap of 3.2 eV is in good agreement with the previously reported values^{13, 14}. In addition, the fit of oxygen 2p peaks, bonding and non bonding, on two Gaussians is very satisfactory (Figure 3.16a).

Results: STO

After the annealing, as a consequence, the valence region of the sample is drastically altered. The new band appeared in the gap (Figure 3.15b) and the sample turned from a transparent into the black-colored material. The newly appeared band crosses the Fermi level and causes the STO sample to become the conductor.

Due to this fact, it was possible to apply the LEED technique in order to study the sample surface. In MODA system the LEED instrument is Spot Profile Analysis modification of the conventional instruments (see the chapter about Instruments) and it is placed in same chamber where the XPS instrument is.

Using the same manipulator the sample was moved on the front of SPA-LEED. The results are showed in Figure 3.17a.

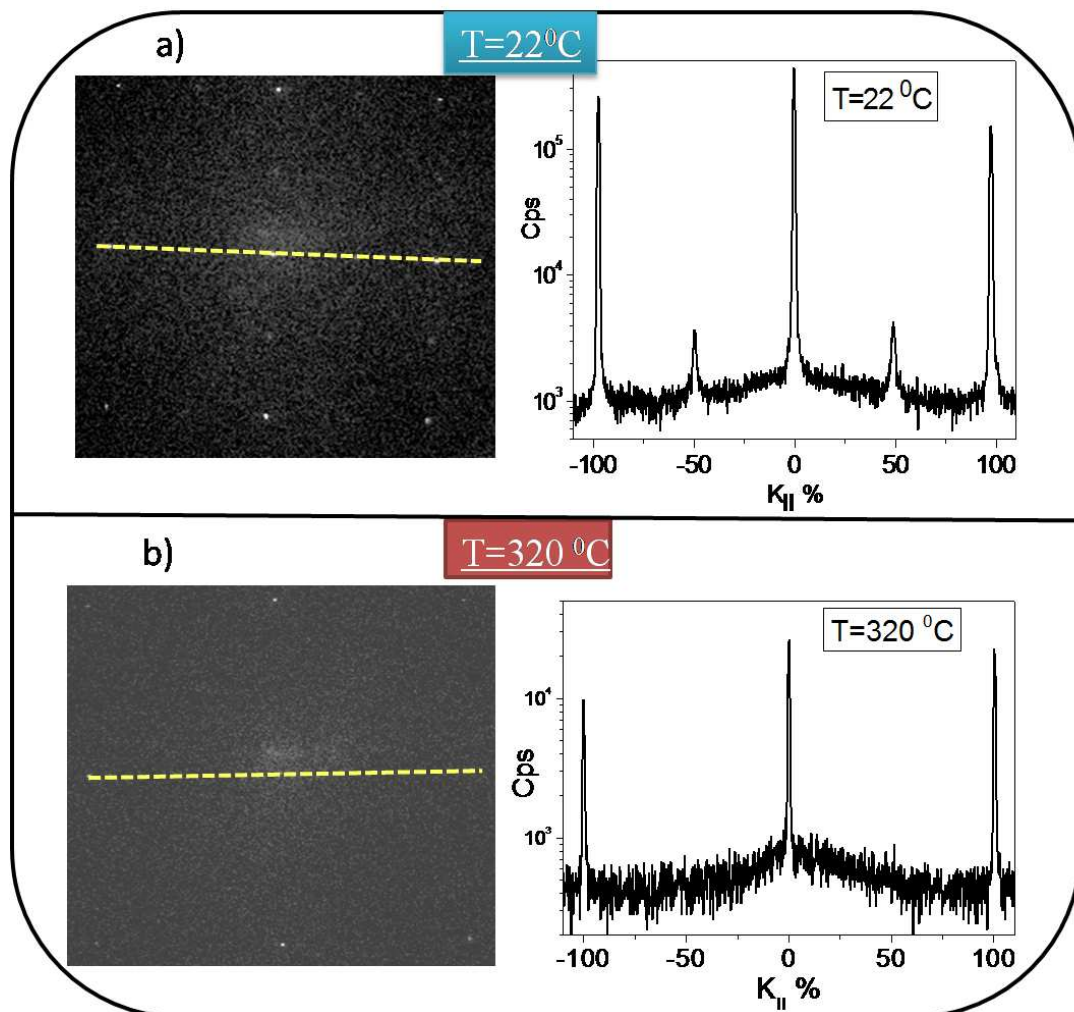


Fig. 3.17: SPA LEED images of STO taken: a) after 1h of UHV annealing at 800 °C, b) after 4.5h of UHV re-annealing at 320 °C.

The results obtained by the SPA-LEED suggested that the (001) surface is (1x2) reconstructed in two domains because of the plane equivalency in 010 and 100 directions. This result is in agreement with some research groups ^{6, 7} which use similar conditions of the annealing, but the data obtained by some other groups are sometimes contradictory. However, only a few of the studies have attempted to support their results with a practical model for the (2x1) surface structure.

Four structure models are candidates to explain this (2x1) reconstruction. The first one is based on the idea that alternate rows of oxygen removed from the TiO₂ terminated (1x1) surface cause creation of (2x1) ordered surfaces. As a consequence, the surface has reduced stoichiometry of Ti₂O₃ ⁷. This model is schematically presented in Figure 3.18.

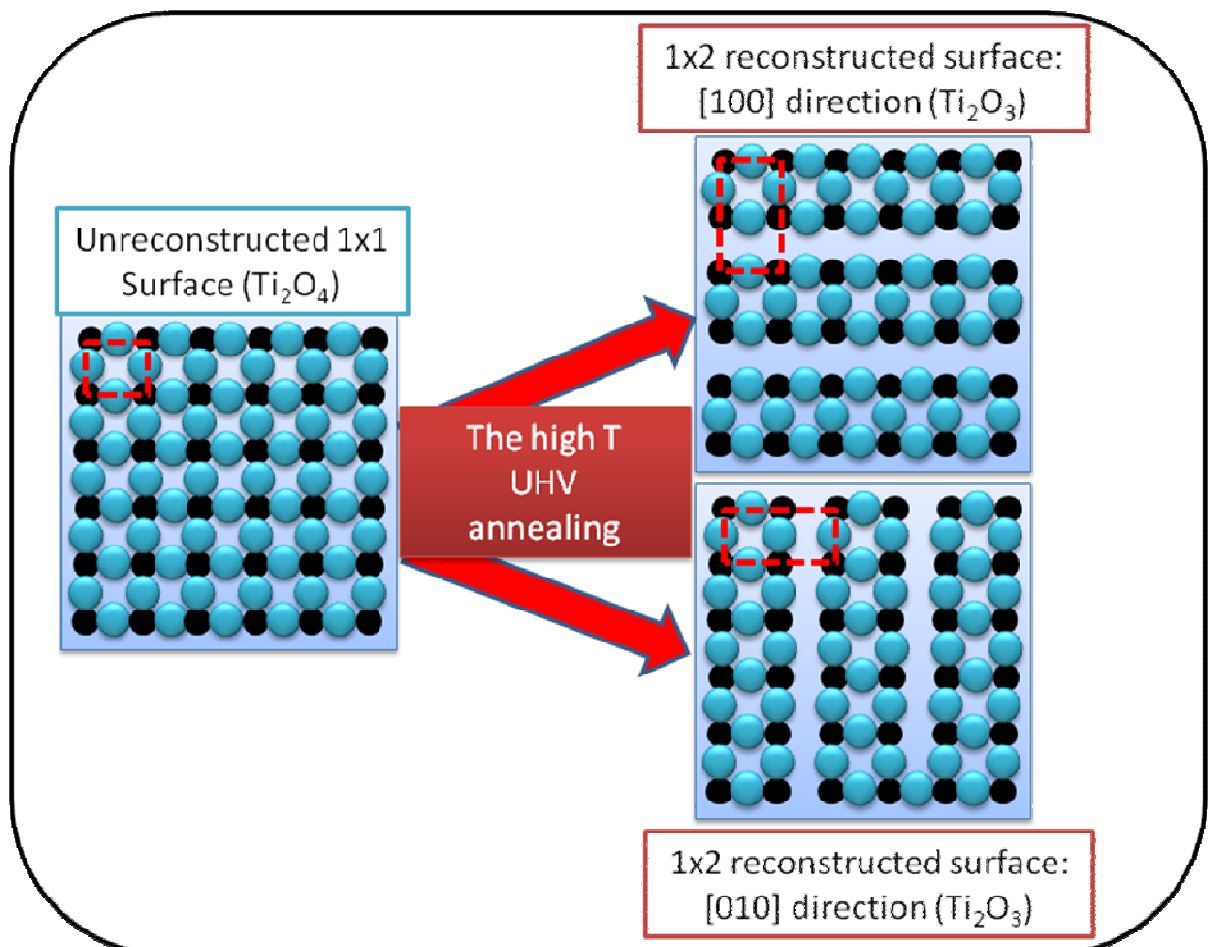


Fig. 3.18: The scheme of the formation of (1x2) reconstructed domains.

Second one suggests that (2x1) structure reduces surface coverage of Ti but maintains the TiO₂ stoichiometry⁷. The third model was proposed by Erdman et al¹⁵. In this model the surface has a double TiO₂ terminated layer and they named it the (2x1) DL-TiO₂ surface. Finally, Kubo and Nozoye have proposed that the observed reconstruction can be explained as arising from the patterns of Sr ad-atoms on a TiO₂ terminated (1x1) surface¹⁶.

Based on the described models, one could conclude that **causes of the reconstruction can be different**. According to this, my goal was to determine the reasons for (1x2) reconstruction in our experimental conditions.

In order to do that the experimental plan was as following:

1. Checking of the stability of (1x2) reconstruction by thermal re-annealing at a low temperature in UHV and *in situ* monitoring of the sample by LEED. Why the low temperature annealing? If the (1x2) reconstruction is due to Sr ad-atoms, it means that the Sr coverage is 50% while some authors which proposed the low temperature segregation of Sr reported that the maximum of Sr coverage is less than 20% at 400 °C¹⁷. Because of that, if the temperature of re-annealing is below 400 °C it will be difficult to interpret that the possible disappearance of reconstruction is due to additional segregation of Sr.
2. Prepare the second sample by the annealing at the same conditions (UHV, 800 °C, 1h) but using vicinal STO, cut of 4 degrees in [010] direction and TiO₂ terminated (obtained from Surface Net GmbH, Germany) and checking of the stability of (1x2) reconstruction on this sample.

The reason of choosing vicinal STO is to see the influence of step edges on (1x2) reconstruction. If the reconstruction is due to oxygen vacancies, according to Zhu et al., the excess oxygen vacancies in the monolayer are reduced by vacancy diffusion into the bulk through step edges¹⁸. This means that we could see it by LEED following stability of the reconstruction in both directions, parallel and perpendicular to the step edges.

The obtained results are as following:

1. The non vicinal (1x2) reconstructed SrTiO₃ substrate was re-annealed in three steps: 90 min at 120 °C, 90 min at 250 °C and 90 min at 320 °C. The sample was monitored by SPA-LEED after each sequence using both modes of measurement, 2D and 1D scans. The surface showed the reconstruction stability until final

temperature when it vanished. The results are presented in Figure 3.17b. From the SPA-LEED scans it was possible to see that there are not any additional spots. Judging from the profiles of the main spots, the surface is still very well ordered since they are very sharp.

2. The vicinal substrate used in the experiment was TiO_2 terminated, then annealed in same conditions as the previous sample: $800\text{ }^\circ\text{C}$, 90 min, UHV. After thermal treatment the sample was slowly cooled down and measured by SPA-LEED at room temperature. The results are depicted in Figure 3.18.

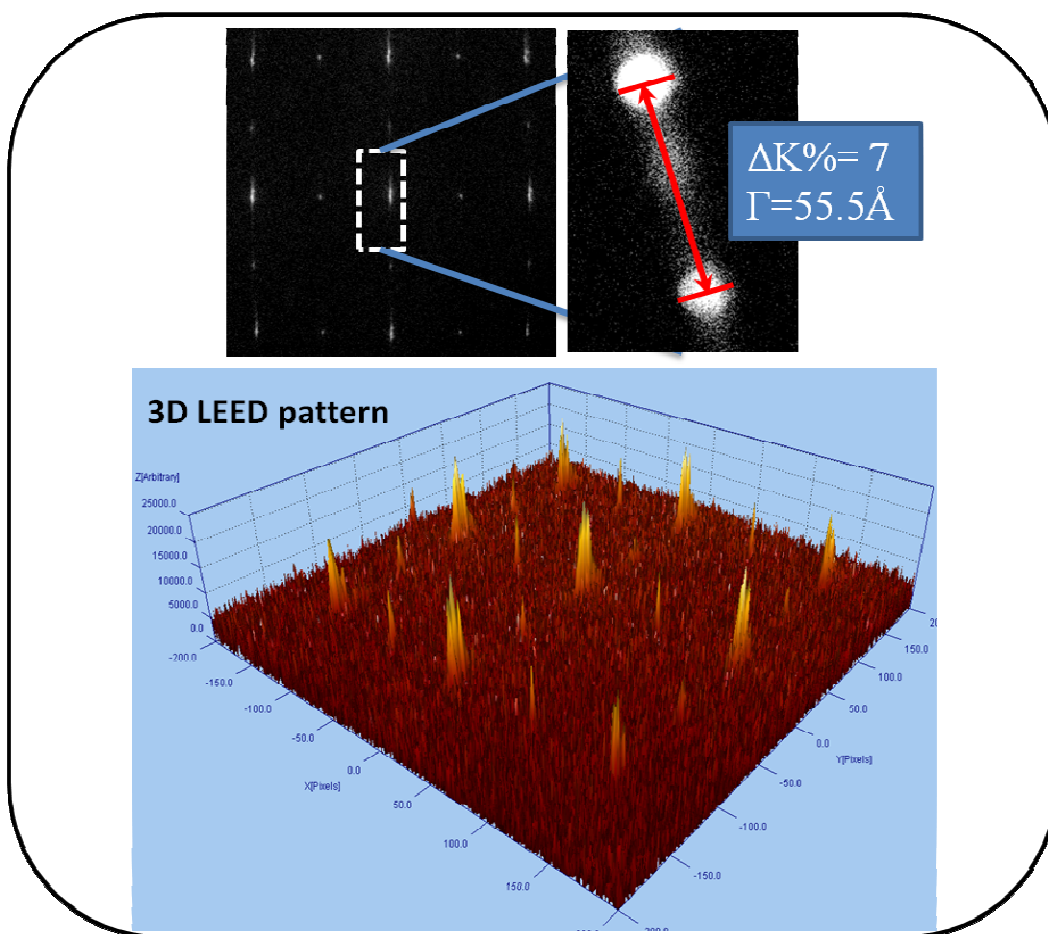


Fig. 3.19: 2D and 3D SPA-LEED images of 4° vicinal (001) substrate after 1h of UHV annealing at $800\text{ }^\circ\text{C}$.

The sample was with vicinal cut of exactly 4 degrees in $[010]$ direction. According to this fact, the terrace width has to be about 55.8 \AA which is in very good agreement with the LEED measurement. From these data, the steps are oriented to $[010]$

direction, following the direction of the cut (because of the splitting of the spots is in [010] direction). The distances between split spots are about 7% of the STO reciprocal lattice unit which in the real space correspond to the distance of 55.5 Å. It is known that the splitting is due to the terrace surface structure and it corresponds to the terrace width (see the introduction about SPA-LEED).

Furthermore, the sample is (1x2) reconstructed in both [100] and [010] directions as previously analyzed non vicinal sample. In the Figure 3.19 are presented 2D and 3D SPA-LEED images and from them is clear that the reconstruction peaks are not split indicating that reconstruction domains on the terrace are mixed.

The evolution of the (1x2) reconstruction, followed by SPA-LEED during re-annealing at low temperatures, is depicted in Figure 3.20.

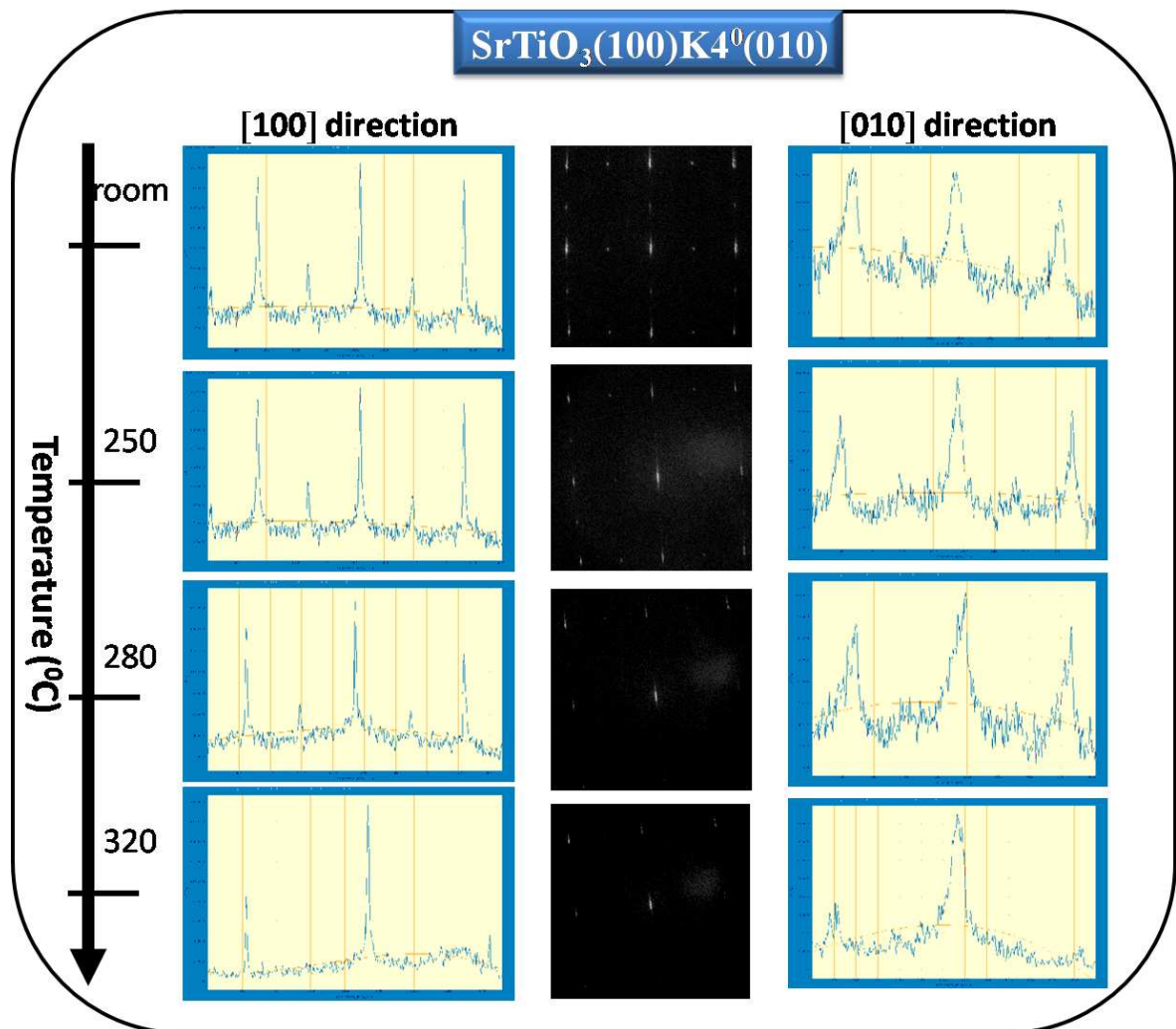


Fig. 3.20: The evolution of the (1x2) reconstruction pattern of the vicinal (001) STO followed by SPA-LEED.

The re-annealing was done in five steps: 120, 210, 250 and 320 °C. The sample was exposed to each temperature between 1 and 1.5 hours. The existence of reconstruction spots are checked in both directions using the linear scan mode. From the measurements it was possible to conclude that the reconstruction is less stable in direction perpendicular to the steps ([010] direction) since the spots vanished between 250 and 280 °C. After further annealing at 320 °C the remained (1x2) reconstruction spots, in 100 direction, disappeared. The value of the temperature at which the reconstruction spots disappear is in surprising coincidence with the temperature for the non vicinal STO substrate.

The fact, which is experimentally observed, is that the activation energy for the reduction is 1.0 eV¹⁸. The energy, which corresponds to 300 °C, is about 0.4 eV. Bearing in the mind these data, the possibility that the filling of the oxygen vacancies on the surface is due to the reduction of the bulk and the vacancies inter-diffusion has to be considered.

This inter-diffusion of oxygen atoms from the bulk to the surface causes that number of the vacancies density decreased from 25% ((1x2) reconstruction). Considering the experimentally supported idea that the filling of the vacancies starts from the steps¹⁸, the (1x2) reconstructed domains which are due to missing of oxygen rows parallel to the steps disappeared earlier.

3.3.2 Low temperature annealing of TiO₂ terminated (001) STO

In order to confirm this interpretation for the disappearance of the reconstruction, next experiment was performed. Following the idea that oxygen atoms can leave the bulk at low temperature in our conditions, the conclusion that naturally emerges is that **if the bulk can be reduced at low temperature in several hours, reducing of the surface should happen too.**

For this experiment we used non vicinal STO (001), TiO₂ terminated (obtained from Surface Net GmbH, Germany). The sample was measured by XPS before and after low temperature annealing (200 °C, 14 hours, UHV P_{base}<1x10⁻⁹mbar).

The XPS data are depicted in Figure 3.21. The presented data showed us that the sample was insulator initially, but it turned to conductor after the annealing. This behavior is in full agreement with the hypothesis that the oxygen atoms' leaving the surface causes the reduction of the surface. Also, I would like to point out that the

sample was still optically transparent, which suggests that the density of oxygen vacancies in the bulk is much lower than in case of the strong UHV annealing.

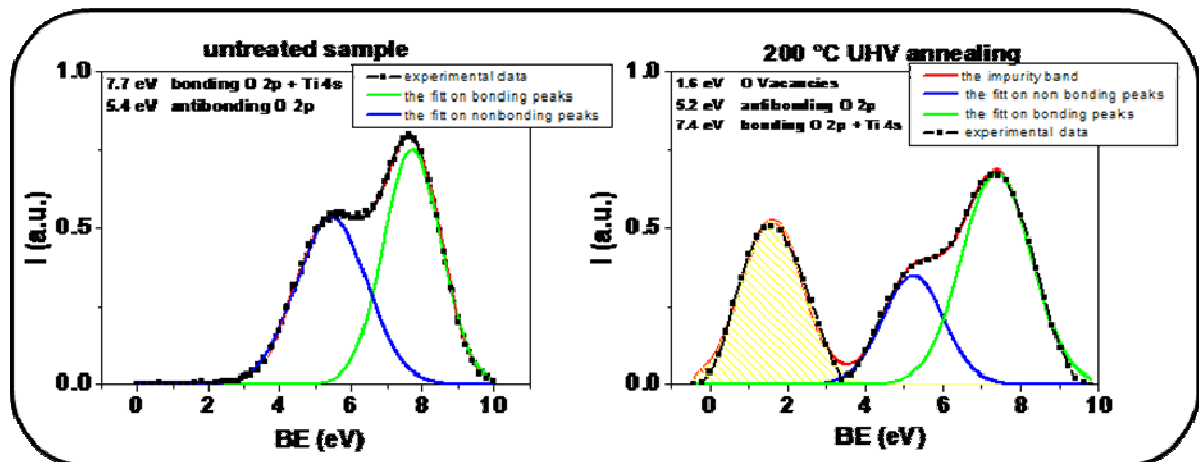


Fig. 3.21: The XPS measurements of TiO_2 terminated STO (001) before (left) and after the low thermal treatment.

Generally, the XPS data are very similar with the data obtained on the sample annealed at high temperature. It suggests that the creation of new bands, which takes place in the gap, has the same cause in both varieties of the annealing, that is, the creation of complexes $Ti^{3+}-V_o$. The reactions which can describe the processes of the vacancies creation on the surface and their refilling are schematically presented in Figure 3.22.

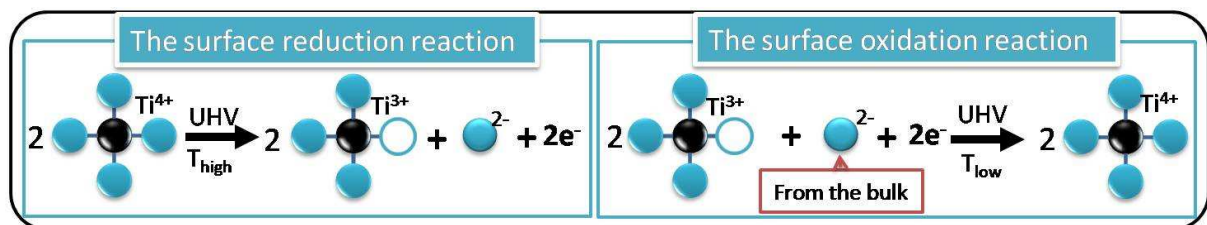


Fig. 3.22: The reactions of the surface reduction and re-oxidation.

The refilling is, actually, due to the creation of the vacancies in deeper levels inside of the bulk and inter-diffusion of the oxygen atoms from the bulk toward to the surface.

The sample was also measured with STM, which is very charge sensitive technique, without any problem with a stabilization of the tunneling current. The obtained images are showed in Figure 3.23.

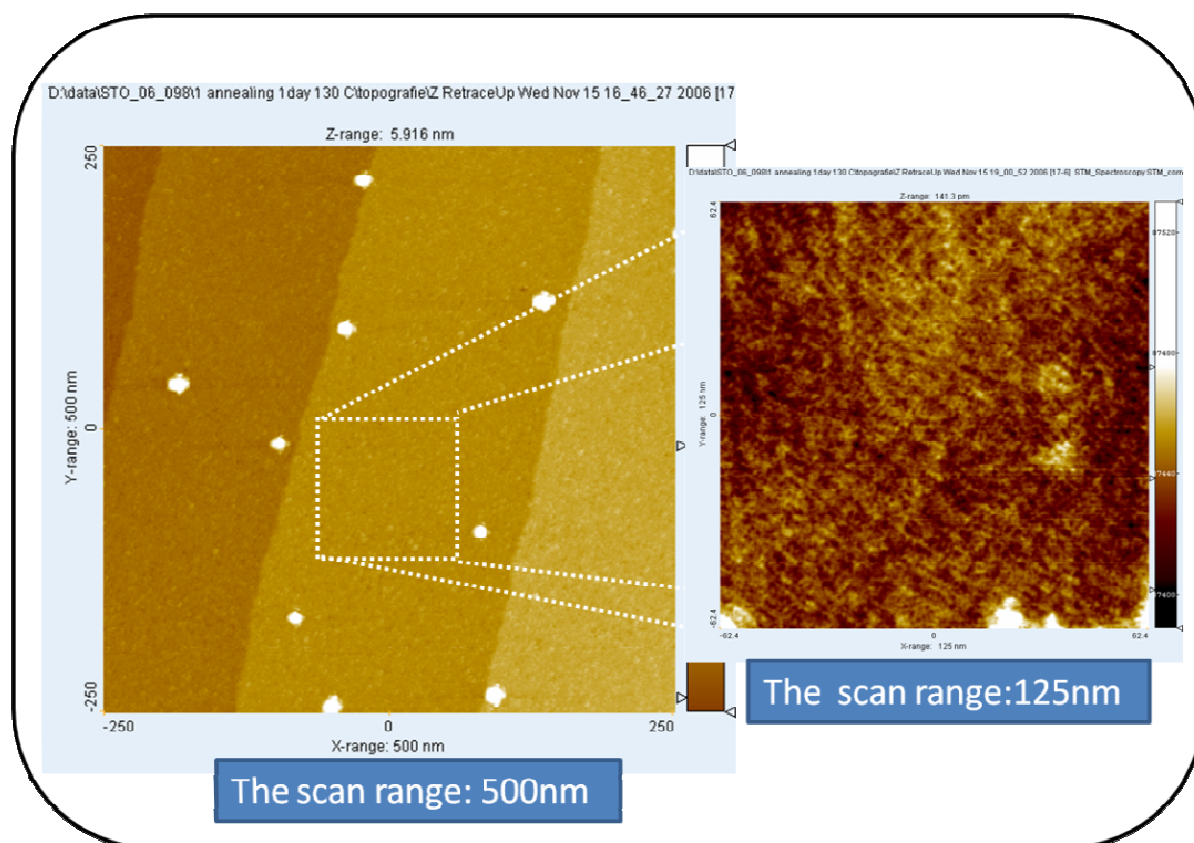


Fig. 3.23: The STM images of low temperature annealed (001) STO.

3.3.3 The model of (1x2) reconstruction

The processes of the oxygen vacancies vanish is modeled and depicted in Figure 3.24. The high temperature annealing causes creation of complexes $Ti^{3+}-V_o$. When the density of these complexes reaches 25% ($N(Ti^{3+})/ N(Ti^{3+})+ N(Ti^{4+})$), due to repulsive forces between them, they will preferentially order in the parallel row-like structure and surface will be 1x2 reconstructed. In this way, the structure maximizes the attractive energy while minimizing the repulsive energy¹⁹. The parallel surface structures may have two orientations, [100] and [010] because of planar crystal symmetry.

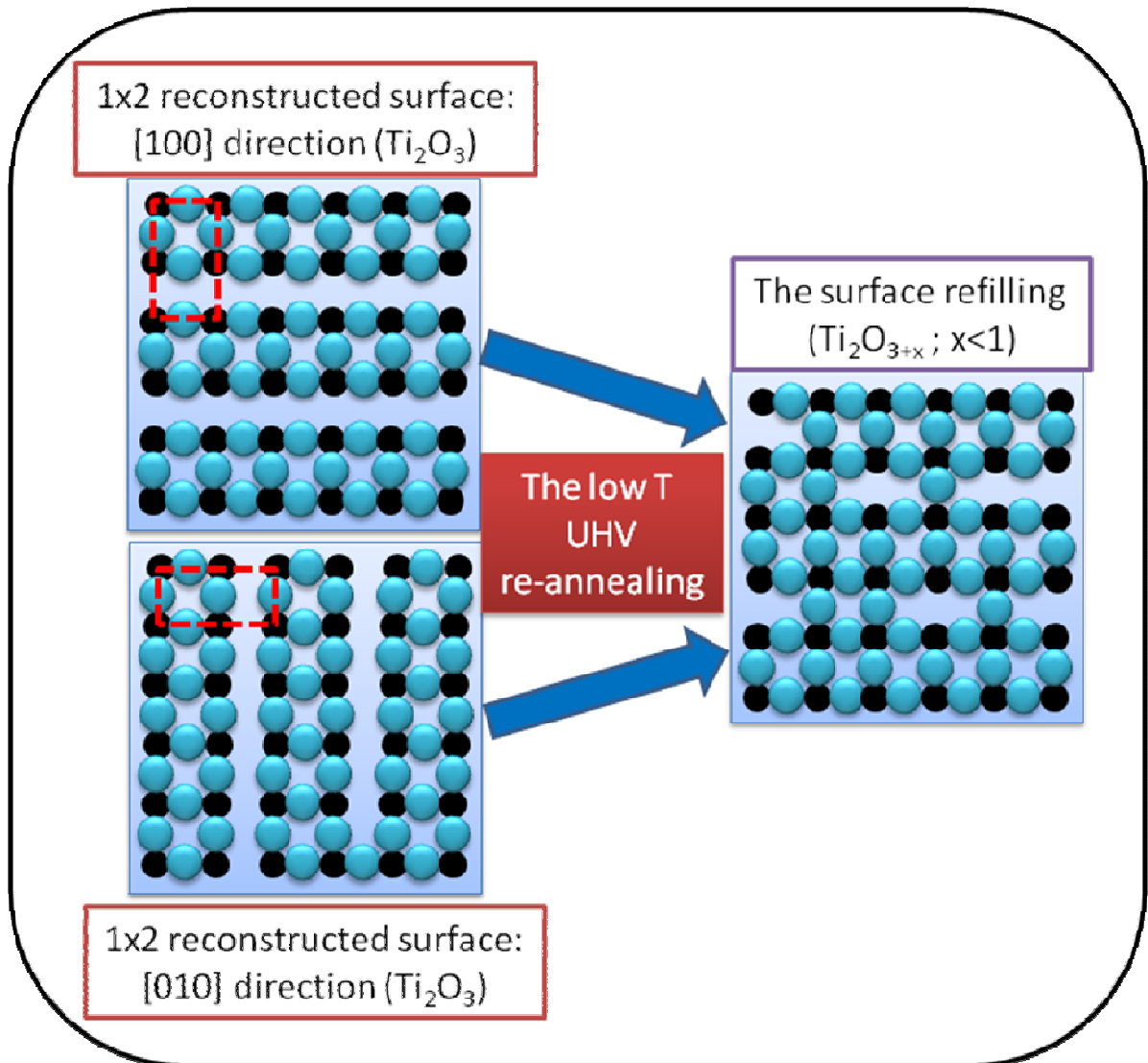


Fig. 3.24: The scheme of the canceling of the (1x2) reconstruction due to the decreasing of oxygen vacancies.

When the surface is already (1x2) reconstructed, the stoichiometry (Ti_2O_3) is changed very much compared to native state (Ti_2O_4) and thus, it could be considered as the different material above STO. Along these lines, we can divide the sample in three regions: the reconstructed surface, the subsurface and the bulk. The subsurface has a lot of characteristics of unreconstructed STO surface before annealing, since its stoichiometry is closer to the ideal. This modeled sample is schematically depicted in Figure 3.25-left. From our surprising result that the TiO_2 terminated STO surface, can lose oxygen, causing conducting surface at low temperature, we can assume that the subsurface can behave in the same way. The main difference is that between vacuum and the subsurface is one layer which is

strongly deficient in oxygen. It can look like a trap for oxygen atoms, those present in the environment (however, not present in this case, since the work is done UHV), as well as those that are leaving the crystal. This process is schematically shown in Figure 3.24-right.

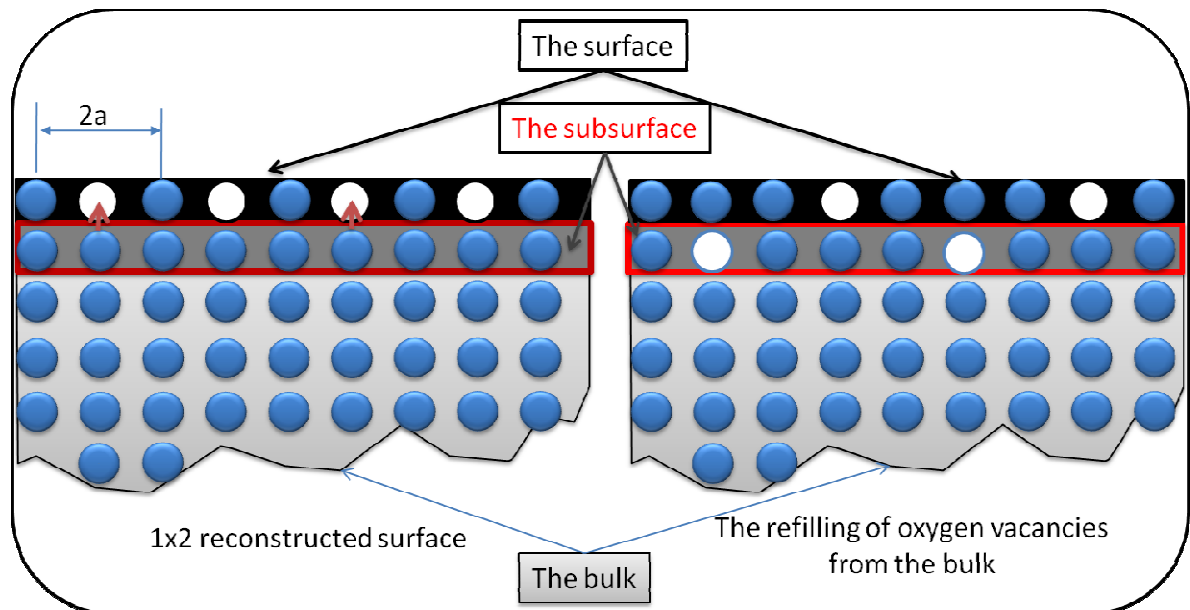


Fig. 3.25: The model of the vacancies refilling from the subsurface.

Based on the observations described above, I would like to conclude:

1. The (1x2) reconstruction of TiO₂ terminated STO 001 surface in our preparation conditions (800 °C, 1-2 hours, UHV) is very often present.
2. The low temperature annealing (200-300 °C, 14 hours, UHV) of TiO₂ terminated STO 001 causes unexpected effect that the surface turn from insulator to conductor. It can be explained as that the surface can lose oxygen even at low temperature under UHV conditions.
3. The (1x2) reconstruction can disappear after re-annealing of the sample under the same UHV conditions at low temperature (320 °C) for several hours. Concerning the effect that at low temperature the lattices can lose oxygen I proposed model that suggests that the refilling of the reconstructed surface is through the exchange of oxygen between the surface and the subsurface. It can be

suggested that initial (1x2) reconstruction in our conditions was due to the creation and ordering of oxygen vacancies.

References:

- 1 R. Hergert, P. R. Willmott, O. Bunk, C. M. Schlepütz, B. D. Patterson, B. Delley, V. L. Shneerson, P. F. Lyman, and D. K. Saldin, *Phys. Rev. B* **76**, 195435 (2007).
- 2 N. Bickel, G. Schmidt, K. Heinz, and K. Müller, *Phys. Rev. Lett.* **62**, 2009 (1989);
- 3 V. Ravikumar, D. Wolf, and V. P. Dravid, *Phys. Rev. Lett.* **74**, 960 (1995));
- 4 G. Charlton, S. Brennan, C. A. Muryn, R. McGrath, D. Norman, T. S. Turner, and G. Thornton *Surf. Sci.* **457**, L376 (2000).
- 5 Matsumoto, H. Tanaka, T. Kawai, and S. Kawai *Surf. Sci.* **278**, L153 (1992).
- 6 Q. D. Jiang and J. Zegenhagen, *Surf. Sci.* **425**, 343 (1999).
- 7 M. R. Castell, *Surf. Sci.* **505**, 1 (2002).
- 8 Kubo and H. Nozoye, *Phys. Rev. Lett.* **86**, 1801 (2001).
- 9 K. Szot, W. Speier, *Phys. Rev. B* **60**, 5909 (1999).
- 10 A. Kazimirov, D.M. Goodner, M. J. Bedzyk, J. Bai, and C. R. Hubbard, *Surf. Sci.* **492**, L711 (2001).
- 11 Karen Johnston, Martin R. Castell, Anthony T. Paxton, and Michael W. Finnis, *Phys. Rev. B* **70**, 085415 (2004).
- 12 A. Ohtomo, H. Y. Hwang, *Nature* **427**, 423 (2004).
- 13 M. Cardona, *Phys. Rev. A* **651**, 140 (1965);
- 14 Myriam H. Aguirre Maria S. Martín Gonzalez , Emilio Moran , Miquel A . Alario-Franco, Virginia Perez-Dieste, Jose Avila , Maria C. Asensio *Solid State Sciences* **2**, 519 (2000).
- 15 N. Erdman, K. R. Poeppelmeier, M. Asta, O. Warschkow, D. E. Ellis, and L. D. Marks, *Nature* **419**, 55 (2002).
- 16 T. Kubo, H. Nozoye, *Surf. Sci.* **542**, 177 (2003).
- 17 T. Ohnishi, K. Shibuya, M. Lippman, D. Kobayashi, H. Kumigashira, M. Oshima, H. Koinuma, *Appl. Phys. Lett.* **85**, 272 (2004).
- 18 X. D. Zhu, Y. Y. Fei, H. B. Lu, and G. Z. Yang, *Appl. Phys. Lett.* **87**, 051903 (2005).
- 19 H. Tanaka, T. Matsumoto, T. Kawai, S. Kawai, *Surface Science Lett.* **278**, 153 (1992).

3.4 THE STUDY OF (6X4) RECONSTRUCTION OF (110) SrTiO₃ SURFACES

The SrTiO₃ surface in the [110] direction consists of a sequence of alternating charged SrTiO and O₂ planes. Equivalent (110) layers are separated by the distance of $a\sqrt{2}/2=0.276$ nm where a (0.3905 nm) is the length of the cube of the SrTiO₃ unit cell. Therefore, the SrTiO and the O₂ layer are separated by $a/2\sqrt{2}= 0.138$ nm in the [110] direction (Figure 3.26).

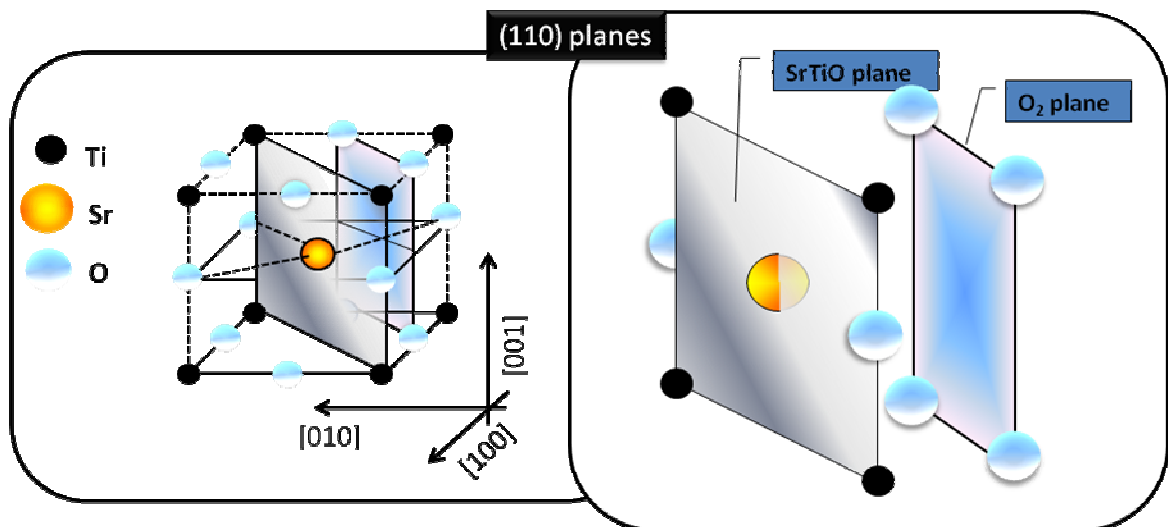


Fig. 3.26: STO unit cell and (110) planes

It is also well known that such a surface is unstable owing to an dipole moment produced by the charged planes perpendicular to the surface. The polar SrTiO₃ (110) surfaces have not been extensively experimentally investigated as (001) surface. Nevertheless, some important SrTiO₃ (110) surface behaviours were reported. If the SrTiO₃ (110) is annealed in ultrahigh vacuum at 800 °C¹ or at 960 °C for 2 h² the surface exhibits the (1x1) LEED pattern. (1x2) reconstruction was observed after the surface was heated at 1000 °C for 1 h in ultrahigh vacuum³. In contrast, a (nxm) periodicity is observed when the SrTiO₃ (110) surface is annealed at temperatures higher than 900 °C or when annealing is combined with ion sputtering^{2,4}. These reconstructions are observed regularly and are dependent on heating temperature and duration. Brunen and Zegenhagen studied undoped SrTiO₃ (110) single-crystal surfaces heated up to 1000 °C². By using Scanning Tunnelling Microscopy (STM) techniques, they concluded that the surface reconstructs forming (100) and (010) TiO₂ microfacetted planes. A. Gunhold et al. performed similar

experiment on STO (110) and their results confirmed the coexistence of two periodicities, (1x1) and (1x2)³. Also, the same authors claimed that under oxidizing conditions SrO islands may form on the top of (110) surfaces.

However, a smooth homogeneous surface of SrTiO₃ (110) is important for the growth of high-quality film in general. Specially this substrate is commonly used for (110) or (103)/(013)-oriented RBa₂Cu₃O_{7-x} thin films⁵. These types of films are of special importance for the fabrication of Josephson junctions and Grain Boundary Josephson Junctions^{6,7}. La_{0.7}Sr_{0.3}MnO₃ grown on STO (110) is strained inducing an in-plane anisotropy with easy axis along the (001) direction which can be used in planar spin valves⁸.

Since a preparation of a STO (110) surface is not developed as well as for STO (001) I analyzed the initial properties of STO (110) surface and the status of the surface after the thermal treatment similar to the condition of deposition.

The experiment

Commercially available 10x10 mm² SrTiO₃ monocrystals cut in the (110) directions were purchased from Crystal, Germany. One, as received, sample was annealed in 0.1mbar oxygen atmosphere at 800 °C for less than 1 hour to simulate pre-grown treatment. The RHEED measurements indicated that the sample surface is reconstructed as (6xn) superstructures. The results are shown in Figure 3.26.

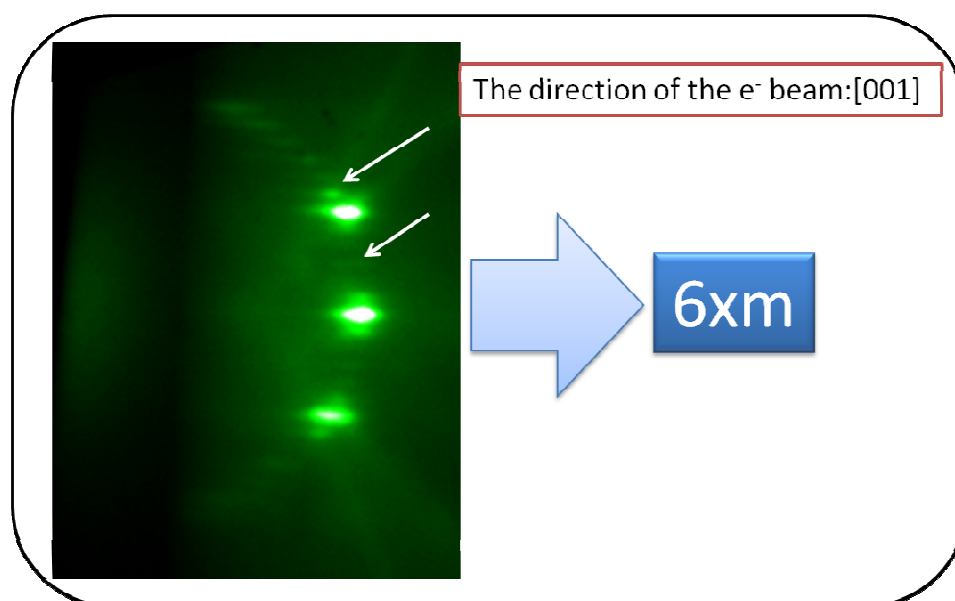


Fig. 3.27: The RHEED pattern of STO (110) after annealing in 0.1 mbar of O₂ about 1h. The RHEED pattern showed (6xm) surface reconstruction.

The second sample was specially prepared in the analytic chamber. In order to remove surface contaminants, the crystals used in the experiments were annealed in the Analytic chamber using the irradiative heater, at 800 °C in UHV condition (the pressure during the annealing was below 1×10^{-9} mbar). The temperature was controlled by a thermocouple and a pyrometer. The final temperature was reached gradually with the rate of about 30 °C per minute. After UHV annealing the samples were cooled down in the same manner.

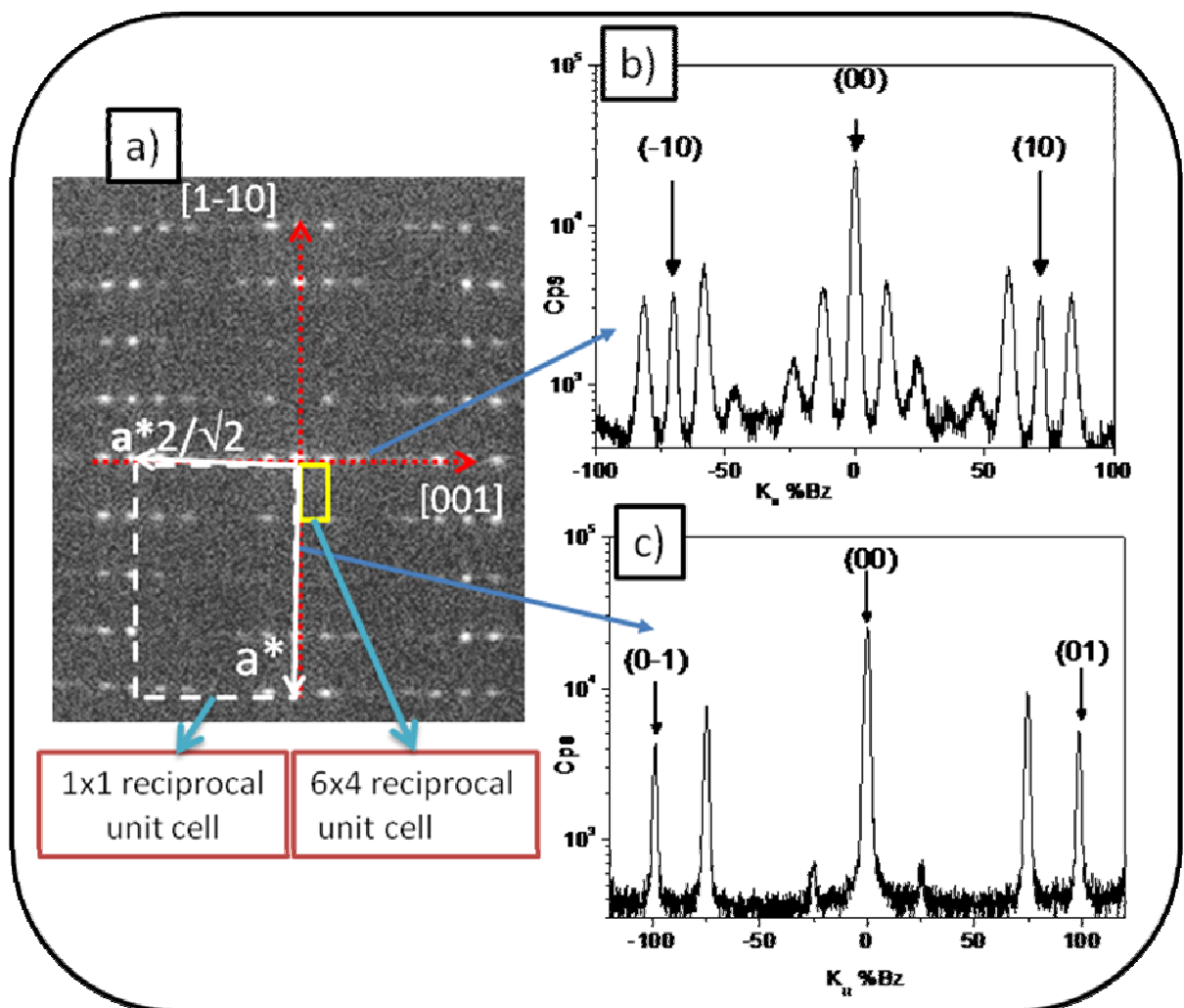


Fig. 3.28: SPA-LEED data of STO (110) surface after the UHV thermal treatment (1h, 800 °C): a) 2D pattern, b) the liner scan in $[1-10]$ direction and c) the liner scan in $[001]$ direction (the scale of a liner scan is calibrated on STO (001) 2D reciprocal lattice).

Results: STO

The STO (110) samples, after this thermal procedure, turn from a transparent insulator into a black colored conductor. The samples were measured with Spot Profile Analysis-Low Energy Electrons Diffraction (SPA-LEED) and Scanning Tunnel Microscopy (STM) instruments. The SPA-LEED results showed that (110) surface of the p(6x4) reconstructed. The obtained results are presented in Figure 3.28.

The SPA-LEED linear scan was calibrated on STO (001) 2D reciprocal lattice. The distances between main spots in one direction showed $\mathbf{a}^*2/\sqrt{2}$ of STO (001) reciprocal lattice while in the other the distance is about \mathbf{a}^* . These results correspond to expected values.

The STO (110) sample after SPA-LEED measurements was transferred in to SPM chamber (part of the Analytic chamber of MODA facility) where was performed STM morphology measurement. The STM measurements of the sample are depicted in Figure 3.29. The clearly defined terraces with the height about 2.7 Å indicate that the surface has one termination, either O₂ or SrTiO termination.

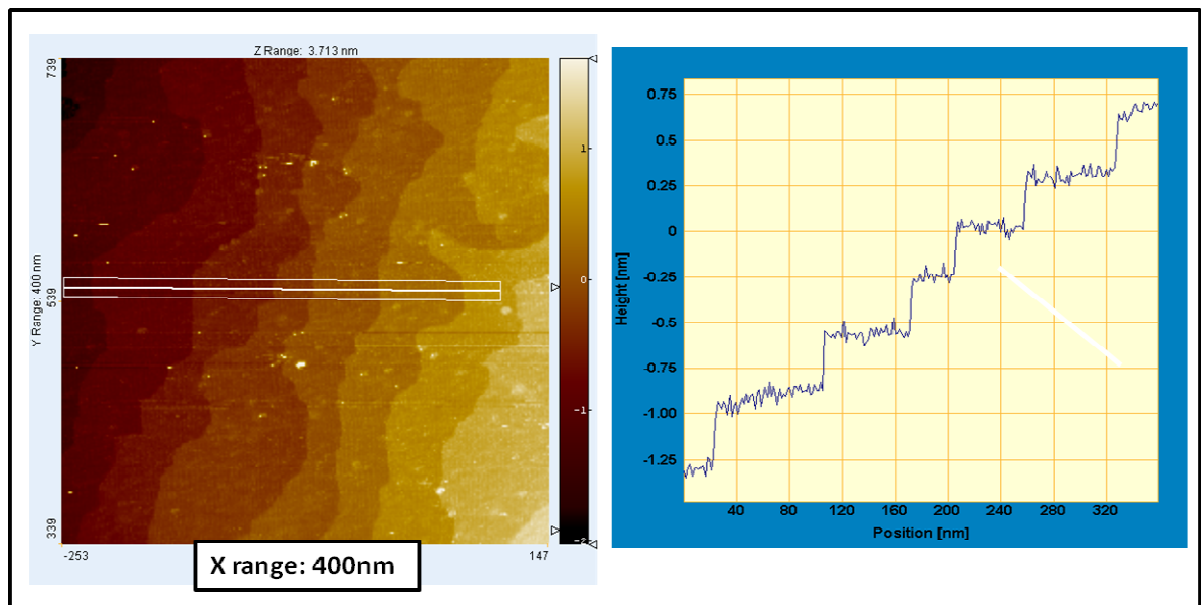


Fig 3.29: The STM image and the liner scan of STO (110) surface after the thermal treatment.

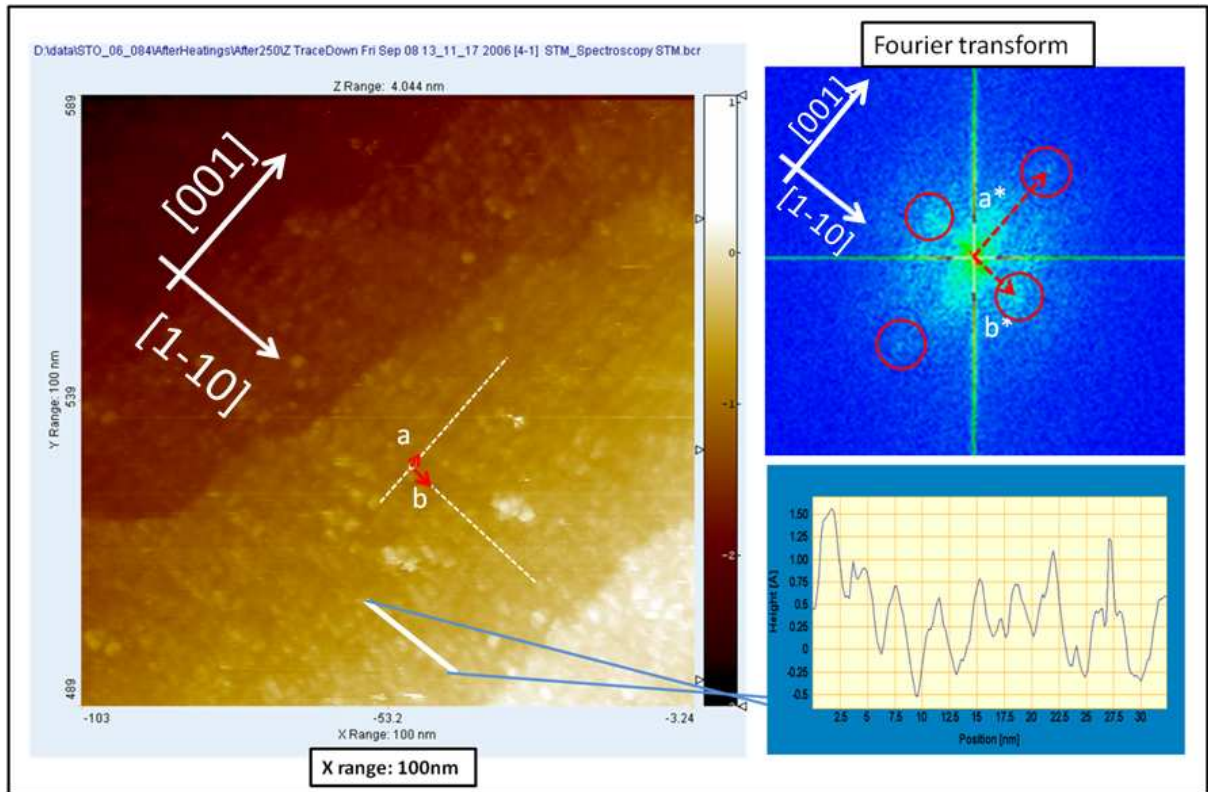


Fig. 3.30: The STM image, its Fourier transform and the liner scan taken perpendicularly to the rows.

The higher magnification of STM measurements (Figure 3.30) proved that the surface is reconstructed since the “row like” structures are visible. Fourier transform of the image (Figure 3.20) showed two pairs of peaks (marked by red cycles) which are perpendicularly oriented. The modulus of the reciprocal vectors \mathbf{a}^* and \mathbf{b}^* correspond to the modulus of vectors \mathbf{a} and \mathbf{b} which represent $\mathbf{6}\times\mathbf{4}$ superstructures ($\mathbf{6}\times\mathbf{0.55nm}=3.3\text{nm}$ and $\mathbf{4}\times\mathbf{0.4nm}=1.6\text{nm}$). The STM profile shows that the corrugation of the surface is very low, on the range of 1 \AA . It may indicate that the reconstruction involves just one monolayer.

In order to check stability of the surface and also of the reconstruction the sample was further annealed in three steps in UHV: 1 hour at $250\text{ }^{\circ}\text{C}$, 1 hour at $420\text{ }^{\circ}\text{C}$ and finally 1 hour at $550\text{ }^{\circ}\text{C}$. After each heating sequence the sample was measured by LEED and STM at room temperature. The SPA-LEED profiles are depicted in Figure 3.31. In both directions, [010] and [001] of the SPA-LEED scans, ($\mathbf{4}\times\mathbf{6}$) reconstruction was stable.

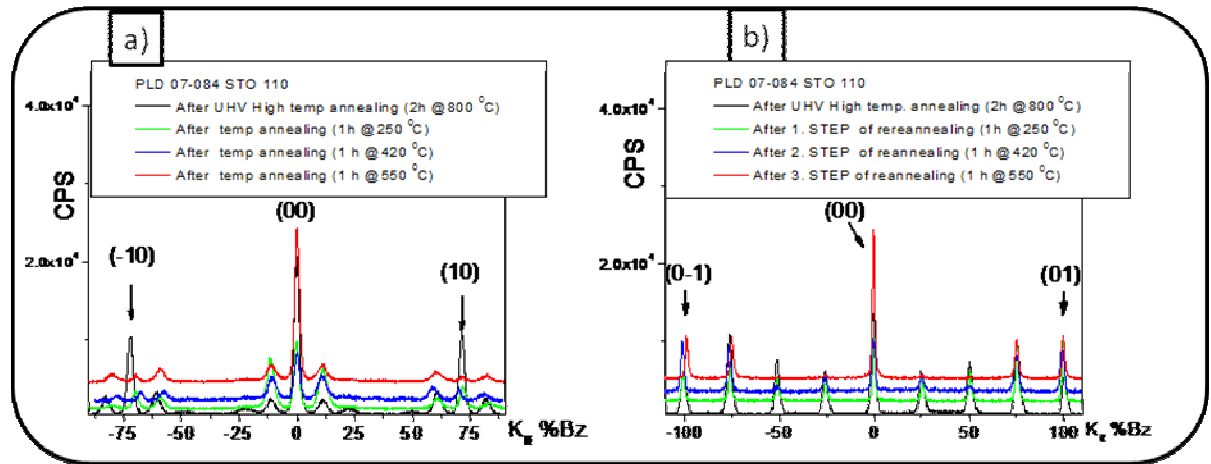


Fig. 3.31: The SPA-LEED liner scans of STO (110) surfaces versus annealing temperature.

If the annealing is performed in oxygen-rich environment (Figure 3.26) it is reasonable to infer that the annealing could give rise to O_2 surface termination. On contrary, during annealing in the oxygen-poor condition (UHV) it is expectable that O_2 termination disappears during the early stages of annealing. In other words, the “starting” surface, in this case, can be accepted as the stoichiometric $SrTiO_3$. The surface has periodicity in $[1-10]$ direction which is 6 times larger than unreconstructed surface (The RHEED measurements showed this). On the other hand, the annealing at the same temperature but in the UHV condition provokes the same type of the surface reconstruction in $[1-10]$ direction. The STM measurements confirmed this reconstruction and showed that it is caused by “row like” structure formed on the surface. The corrugation of these structures is very low, between 1\AA and 1.5\AA . This could mean that the reconstruction is connected to the mixed termination (O_2 and $SrTiO_3$) of the surface. Additionally, Brunen and Zegenhagen noticed that during the annealing and sputtering processes a change in the concentration of oxygen is not detectable, while concentration of strontium on the surface increases with the annealing temperature². This is in disagreement with their micro-faceted model² of the annealed $SrTiO_3$ (110) surface because it suggests that the strontium is completely removed from the surface.

Taking into account the facts described previously one simple explanation could be also considered. If the starting termination is O₂ the observed reconstruction could be due to the missing oxygen rows (Figure 3.32). If so, according to the obtained experimental results (LEED and STM), the O₂ coverage in this surface could be between 1/12 and 11/12 of complete layer. The second layer starts to be “open” which may be the reason why the Auger measurements in Brunen and Zegenhagen experiments² showed more strontium after the annealing.

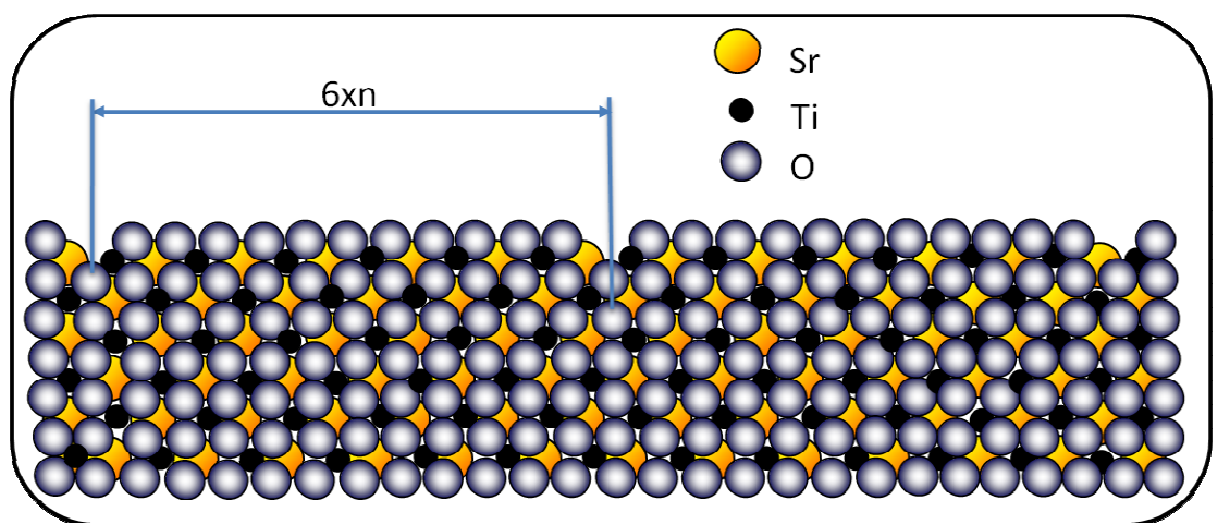


Fig. 3.32: the (6xn) reconstruction due to missing oxygen rows.

In the cases when the annealing and the reannealing were performed this reconstruction seems to be thermodynamically very stable. Maybe the oxygen coverage change but the reconstruction periodicity remains the same.

Surfaces prepared in this way were used for the deposition of complex materials such as Pr_{0.7}Ca_{0.3}MnO₃. The successful deposition is proofed by RHEED monitoring (Figure 3.33). The first part of the growth was 2D (layer by layer) which changed in to step flow growth.

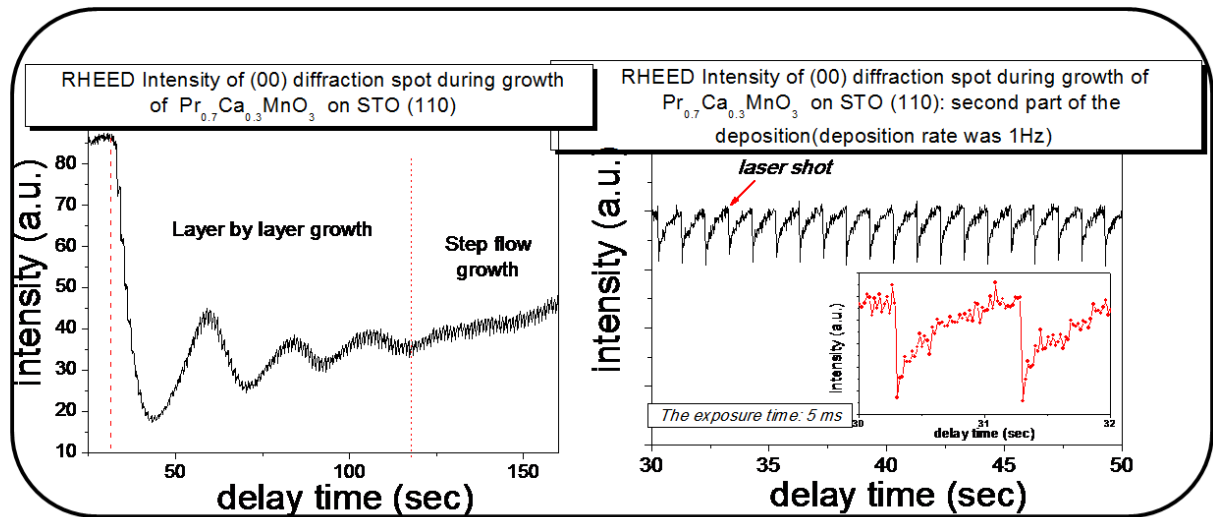


Fig. 3.30: The RHEED Intensity versus deposition time of $\text{Pr}_{0.7}\text{Ca}_{0.3}\text{MnO}_3$ film grown on STO (110).

Conclusion:

Short-time heating of SrTiO_3 (110) at the temperature of 800 °C results in (4x6) reconstructed surface as observed by LEED. STM measurements confirmed that surface is covered by the rows with the same periodicity. The reannealing of the sample showed that (6x4) reconstruction is very stable. The above described results show that the used annealing treatment of the SrTiO_3 (110) gives suitable flat surface.

References:

- 1 H. Bando, Y. Aiura, Y. Haruyama, T. Shimizu, and Y. Nishira, J. Vac. Sci. Technol. B **13**, 1150 (1995).
- 2 Brunen J, Zegenhagen J. , Surf. Sci. **389**, 349 (1997).
- 3 A. Gunhold, L. Beuermann, K. Gomann, G. Borchardt, V. Kempter, W. Maus-Friedrichs, S. Piskunov, E. A. Kotomin and S. Dorfman Surf. Interface Anal. **35**, 998 (2003).
- 4 Francois Bottin, Fabio Finocchi, and Claudine Noguera, PHYS. REV. B **68**, 035418 (2003).
- 5 F. Miletto Granozio, F. Ricci, U. Scotti di Uccio, and J. C. Villegier, PHYS. REV. B **57**, 6173 (1998).
- 6 F. Tafuri, F. Miletto Granozio, F. Carillo, A. Di Chiara, K. Verbist and G. Van Tendeloo, PHYS. REV. B **59**, 11523 (1999);
- 7 Thilo Bauch, Tobias Lindstrom, Francesco Tafuri, Giacomo Rotoli, Per Delsing, Tord Claeson and Floriana Lombardi, SCIENCE **311**, 57 (2006).
- 8 A. Ruotolo, A. Oropallo, F. Miletto Granozio, G. P. Pepe, P. Perna, U. Scotti di Uccio and D. Pullini, Appl. Phys. Lett. **91**, 132502 (2007).

IV RESULTS OF TiO₂-ANATASE THIN FILMS

Titanium dioxide as anatase, is the material of large importance in a number of technological applications including photocatalysis, gas sensors, solar cells, and memory devices¹⁻⁵. Almost all of anatase applicable behaviours are strongly connected to its surface, thus understanding surface properties including: morphology, termination, stoichiometry, impurity levels (if present), electrical properties, etc. became very important. The problem of anatase availability for some commercial application, such as gas sensors, memory devices, etc., was overcome by TiO₂ films grown on suitable substrates⁶⁻⁸.

This chapter presents my study of the anatase TiO₂ (001) thin films grown on SrTiO₃ (001), SrLaAlO₄ (001) and LaAlO₃ (001) and occurrence of (1x4) surfaces reconstruction during the growth and its stability during annealing in UHV environment. The film surfaces were analyzed by: Low Energy Electron Diffraction (LEED), Scanning Tunnelling Microscopy (STM), X-ray Photoelectron Spectroscopy XPS, Transmission Electron microscopy (TEM) and X-ray Diffraction techniques.

The studies were performed in three different steps:

Step 1: Optimization of anatase thin films growth on different substrates and characterization their structure,

Step 2: Testing of the structural stabilities and chemical composition of anatase films under annealing in UHV conditions.

Step 3: Study of the first growth steps of TiO₂ on TiO₂ terminated STO (001).

4.1 THE STABILIZATION OF TiO₂ ANATASE THIN FILMS GROWN ON DIFFERENT SUBSTRATES: STO(100), SLAO (100) AND LAO (100) AND THEIR CHARACTERISATION

The experiments were performed in two separated UHV chambers, the growth chamber and the analytic chamber, respectively. UHV transfer of the samples from the growth to the analytic chamber was through UHV distribution chamber. The characterization chamber is supplied with XPS (X-ray Photoelectron Spectroscopy), SPA-LEED (Spot Profile Analysis-Low Energy Electron Diffraction) and SPM (Scanning Probe Microscopy) setups. The base pressure of the characterization chamber was in low 10⁻¹¹ mbar.

As already mentioned, the phenomenon of anatase surface (1x4) reconstruction was already reported on as grown films without any special treatment of the surface^{9, 10}. Moreover, this reconstruction occurs during growth⁹. On the contrary, on the anatase monocrystals (1x4) reconstruction appears after specific preparation of the surface¹¹. The surface preparation, usually, includes a number of combined cycles of ion sputtering (by Ar⁺ or Ne⁺ ion guns) and annealing process. The sputtering strongly modifies surface and causes disordering of the atoms, hence is necessary to perform the annealing in order to recover and recrystallize the surface. Principally, the annealing may be recognized as "quasi" growth which means that disordered layers will follow matrix of the bulk. Consequently, it may seem as homoepitaxial growth. If so, (1x4) reconstructed surface could be natural consequence of the anatase growth. The film surface has to be reconstructed in this way always when stable growth allows reasonably flat surface. In the literature is reported that anatase surface is (1x4) reconstructed during thin film growth on LAO (001) and even STO (001) substrates^{9, 12, 13}.

In order to try to understand the appearance of (1x4) reconstruction during the anatase growth the following steps were planned:

1. The optimization of the growth parameters which can give high quality single anatase thin film on three different substrates (STO, SLAO, LAO).
2. The UHV annealing of the samples. This annealing allows getting a conducting surface thus making the application of XPS, LEED and STM, for surface studies.

3. The further UHV annealing. This step facilitates evaluation of the surface stability.

The TiO₂ anatase thin films have been grown on polished single crystal substrates of (001) oriented SrTiO₃, SrLaAlO₄, LaAlO₃, (5x5 mm²) purchased from SurfaceNet GmbH (Germany). Substrates were fixed or clamped, on the standard Omicron holder plates, by the conducting silver paste or steel strips respectively. The deposition temperature of the substrate was 800 °C and was continuously monitored by thermocouple. The laser operated at a rate of 1 or 2 Hz, with energy densities at the target of 2.5 J/cm². The target-to-substrate distance was maintained at ≈40 mm in all depositions.

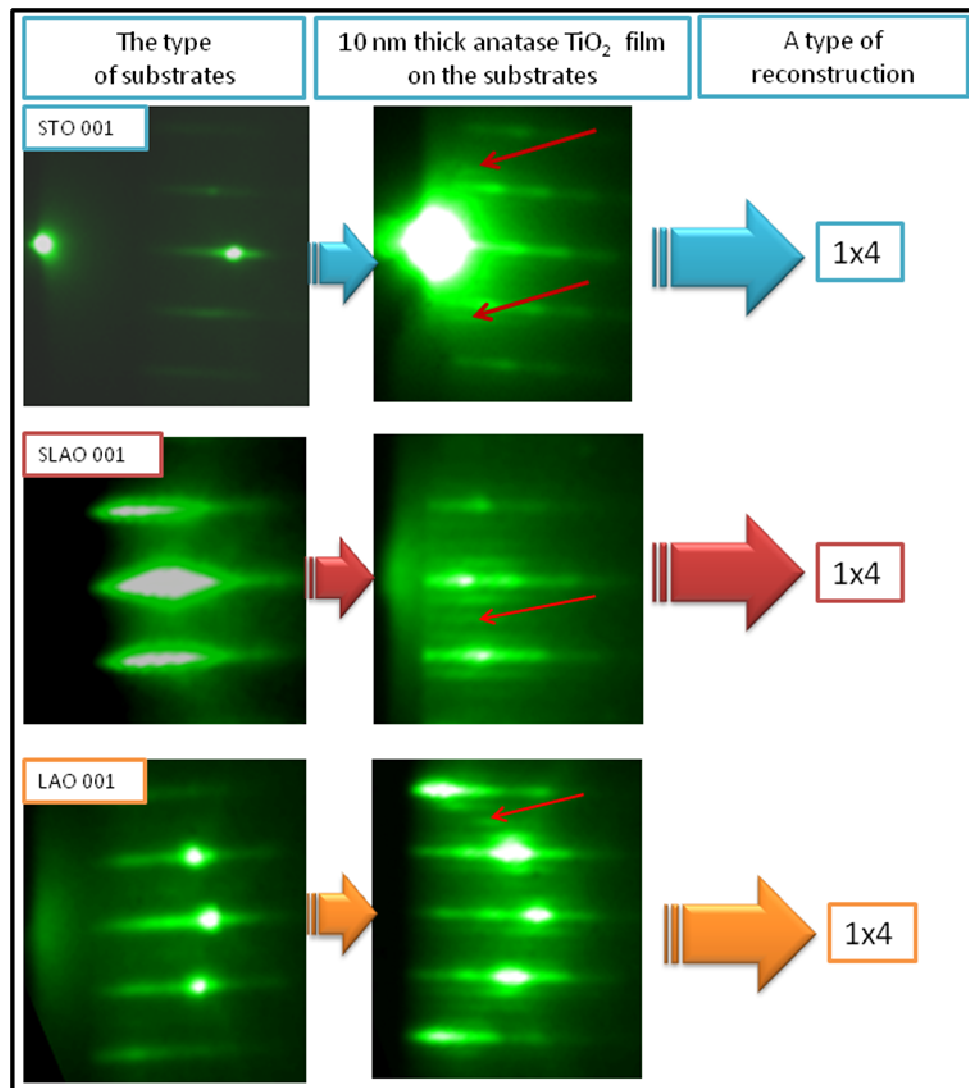


Fig. 4.1: The RHEED images of anatase thin films during growth on different substrates. The RHEED patterns show that the film surface is smooth.

Results: TiO₂

The RHEED instrument was used to follow the growth along the [010] direction in respect to the plane substrate axis. The patterns of the substrates and the films during the growth are presented in Figure 4.1.

Apart from the primary (1x1) diffraction pattern, (1x4) diffraction features (marked by red arrows) consisting of three additional streaks are also seen, confirming that 1x4 reconstruction already appears during the growth. The RHEED patterns are 2D suggesting that the film surfaces were very flat. Similar results of the RHEED pattern were published previously^{9, 12, 14}.

The crystal quality of the anatase films grown on all of the mentioned substrates was confirmed by XRD measurements. As an example, the XRD data of anatase films grown on STO, SLAO and LAO (001) oriented substrates are depicted in Figure 4.2.

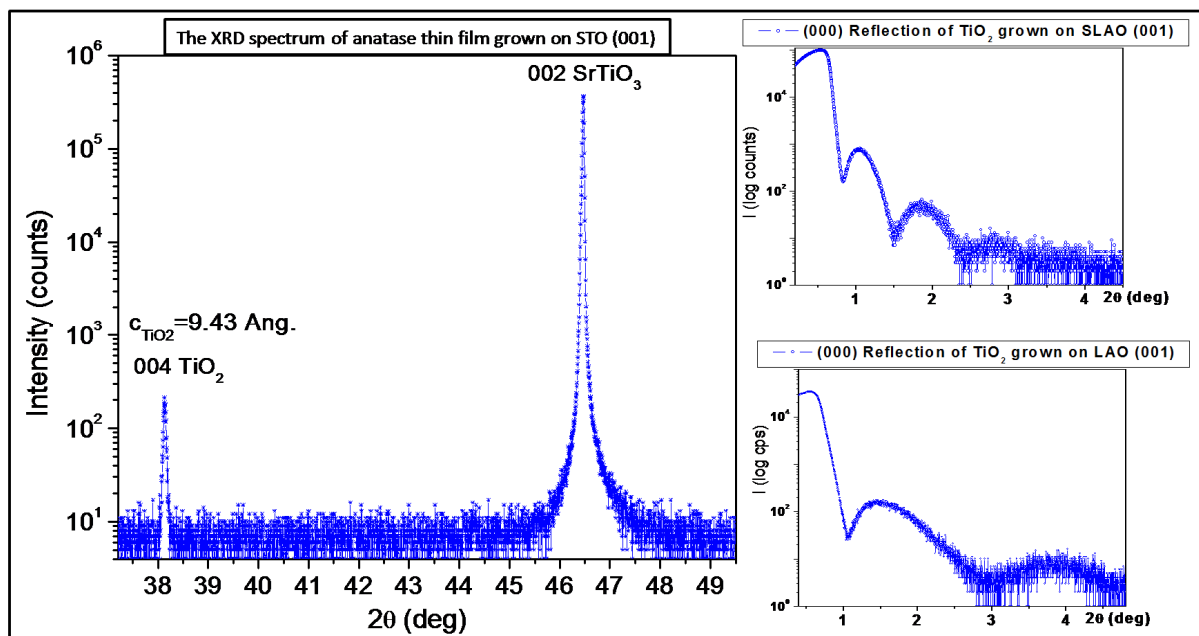


Fig. 4.2: XRD data of anatase thin films grown on different substrates.

The XRD spectrum, shown on the upper graph in Figure 4.2, of the film grown on STO (001), shows no sign of the other TiO₂ phases such as rutile, suggesting that the film is pure anatase. Additionally, the reflectivity data, depicted in Figure 4.2, ascertain the smoothness of the film.

Results: TiO₂

The TEM data of anatase film grown on STO (001) are presented in Figure 4.3. The red line marks the interface between the substrate and the film. The crystallinity of the film is very high since the planes of the film are clearly visible.

Since the RHEED oscillation were absent during the growth, the estimation of the growth rate was done by the analysis of the reflectivity XRD data and TEM cross section images. The estimated growth rate was approximately, 0.12 Å/shot.

After deposition, the samples were cooled down in the same pressure of the deposition (0.1mbar). The anatase thin film grown on STO (001) was further carefully analyzed since my goal was also to understand compatibilities between the substrate and the film.

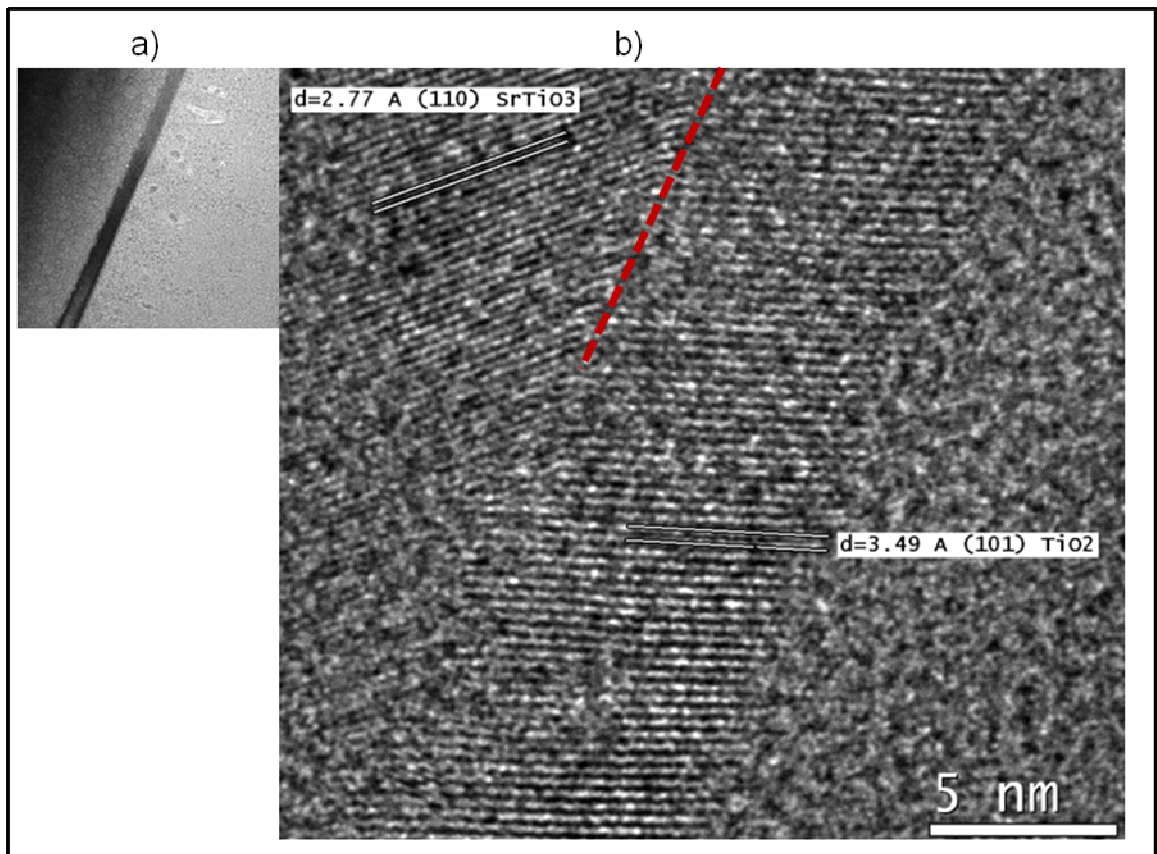


Figure 4.3: The TEM cross sections of the anatase thin film grown on STO (001):
a) lower magnification, b) bigger magnification.

After the deposition the samples were transferred into the analytic chamber where the films were annealed in UHV condition ($P < 1 \times 10^{-9}$ mbar) at 800 °C for 1h. After

sample cooling at room temperature SPA-LEED, XPS and SPM measurements were performed.

XPS analysis was performed to qualify the chemical and electrical nature of the sample surface. The XPS was performed using Mg K α at 1253.6 eV in two configurations of the set up, in the perpendicular and the shallow angles (35 degrees) of photoelectron emission.

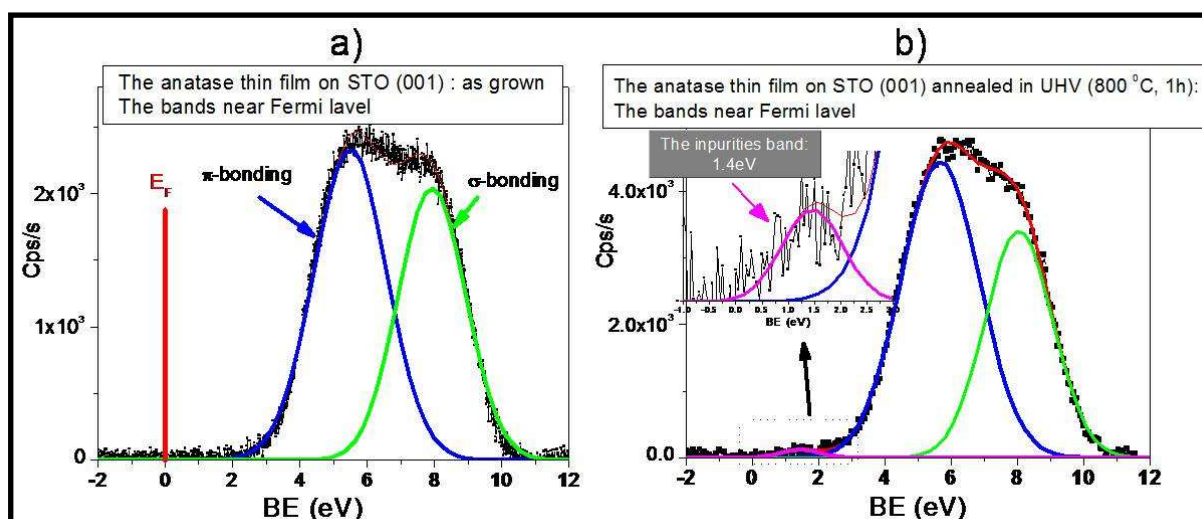


Figure 4.4: XPS data of anatase thin film grown on STO (001): a) as grown film, b) after the annealing in UHV at 800 °C for 1h.

After normalization of the spectra on the integrated values of Ti 2p peaks, the region of the valence band of as grown sample showed a band gap respect to Fermi level of about 2 eV. The XPS measurements of the valence band of anatase thin film annealed at 800 °C for 1hour in UHV condition showed appearance of a small peak in the gap on 1.4 eV (Figure 4.4). Contrary to the results of XPS spectrum near the Fermi level of TiO₂ terminated STO surface, the new band is very weak. It seems that the creation of Oxygen vacancies is more difficult in case of the reconstructed anatase surface.

The sample, at the room temperature, was studied with the LEED instrument using electron's beam energy of 105 eV. The observed results confirmed that the surface is 1x4 reconstructed in two directions, [010] and [100] respects to the orientation of the substrate. The 2D LEED pattern and the profiles of the spots taken in two directions, [100] and [010], are presented in the Figure 4.5.

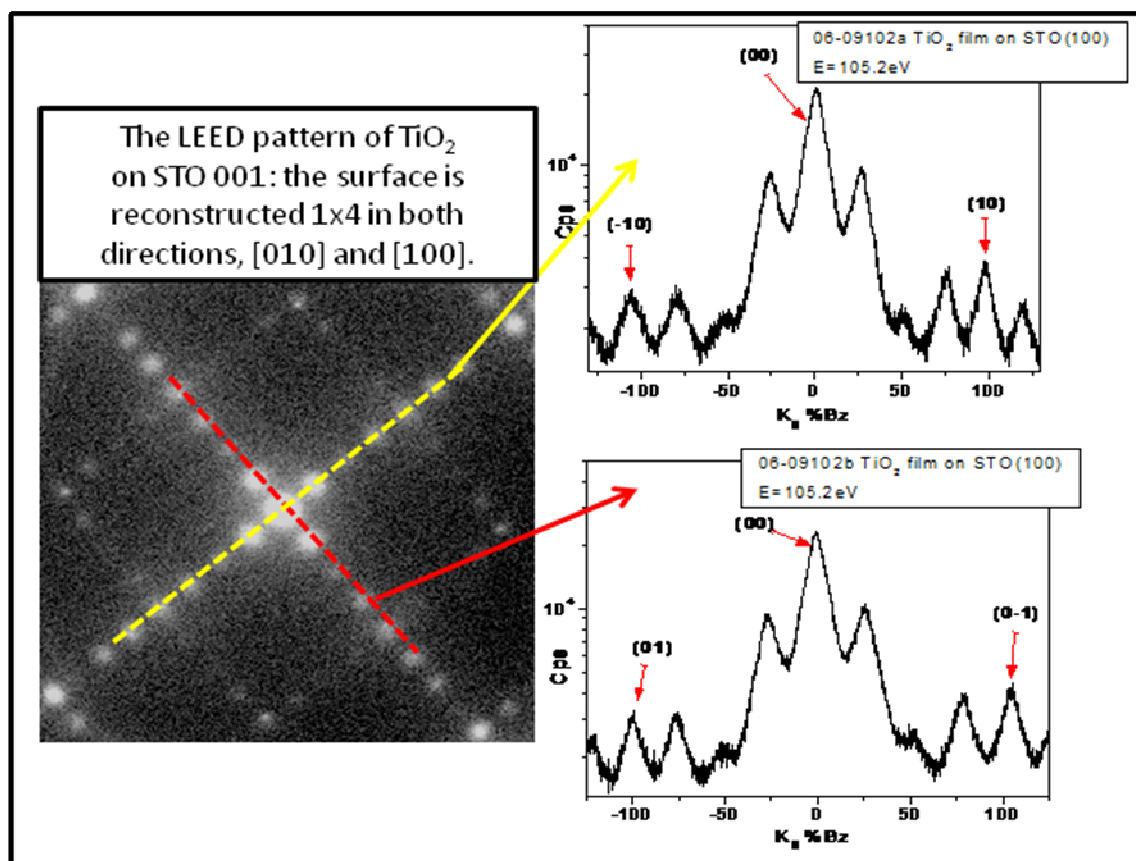


Fig. 4.5: LEED pattern of TiO₂ grown on STO (100): 2D SPA LEED image of (1x4) reconstructed surface (a), profiles of the LEED spots taken in [100](b), and [010] direction(c).

The careful analysis of the distances between the main and the reconstructed spots showed that the film is fully relaxed in the plane since the average distance between main spots is 103 % of STO (001) 2D reciprocal lattice. This corresponds to 3.78 Å which is in good agreement with the bulk values of anatase lattice.

The sample, after LEED measurements, was *in situ* transferred on the STM instrument and the morphology measurements of the film are presented in Figure 4.6. Analysis of the STM images showed that the surface is composed from square shaped blocks rotated by 90 degrees one to the other. The higher magnification of the STM measurements indicated that these blocks are, actually, domains with the row like structures orientated in [100] and [010] directions. The formation of two domains may be explained by the bulk crystal structure of anatase. The top layers in the anatase unit cell are essentially twofold symmetric for the (001) surface plane.

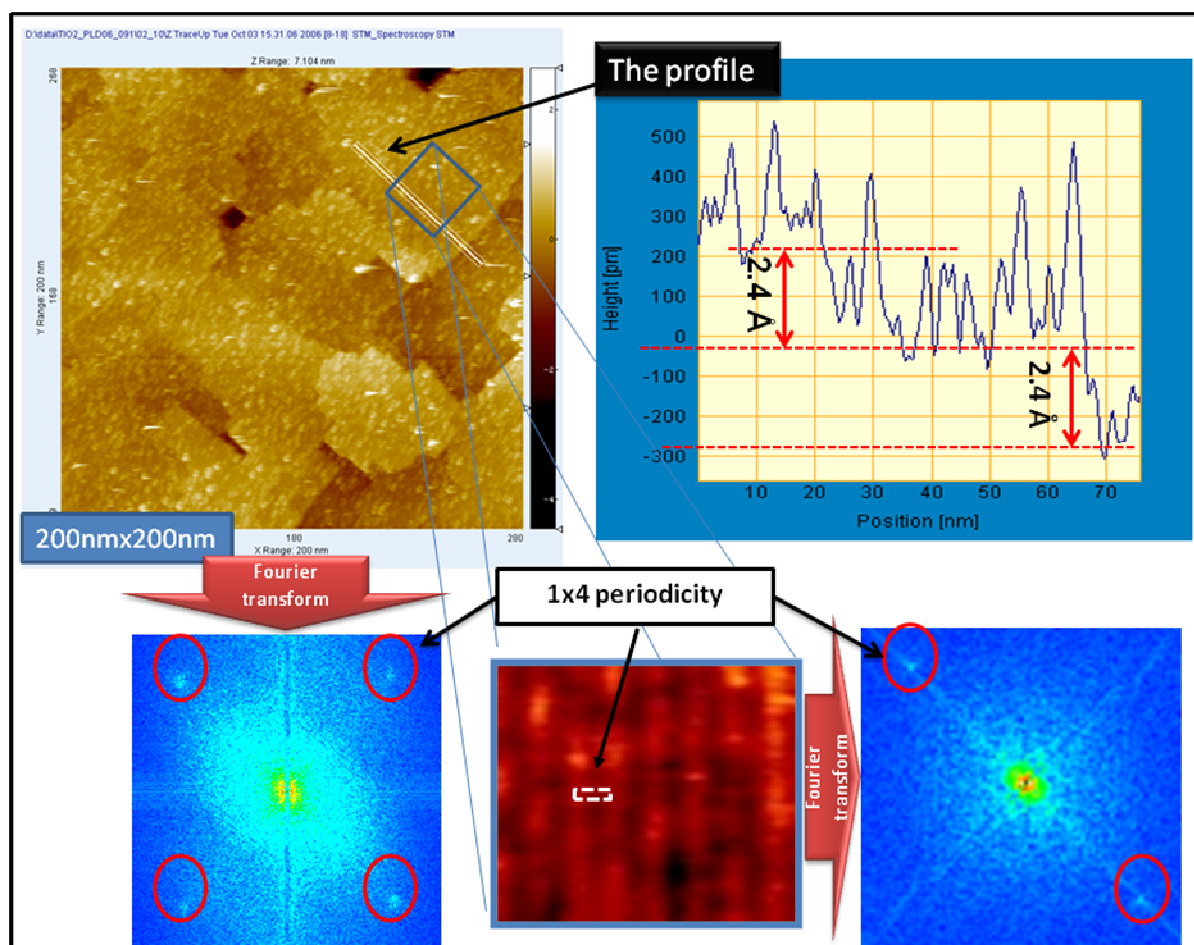


Fig. 4.6: STM morphology measurements of anatase thin film grown on STO (001) with corresponding Fourier transforms of the images and the linear scan.

The step, 2.4 Å high, results from the vertical translation of the surface and 90 degrees rotation. In studied case, exactly this kind of the growth seems to be responsible for the observed morphology. Additionally, the linear scan shows that the surface corrugation could be 2.4 Å or, approximately, two times higher. Fourier transformation of the STM images results exactly in the (1x4) LEED pattern. A distance between the spots is equivalent, in real space, to 15.1 Å which is four times 3.78 Å. The STM zoom of the square terrace near the edge is presented in the same figure (4.6). Fourier transformation of this STM image has the maximums in one direction which is perpendicular to the step. Distances between spots, in the real space, correspond also to 15 Å.

The stability of the (1x4) reconstruction was checked with the additional UHV annealing step performed at 800 °C for 2h. After the additional thermal treatment

the film was measured again by SPA LEED instrument. These results are showed in Figure 4.7. The (1x4) reconstruction was still present but less ordered than in previous case. This can be explained by the fact that the further annealing caused some intra-diffusion of surface materials which are responsible for the reconstruction.

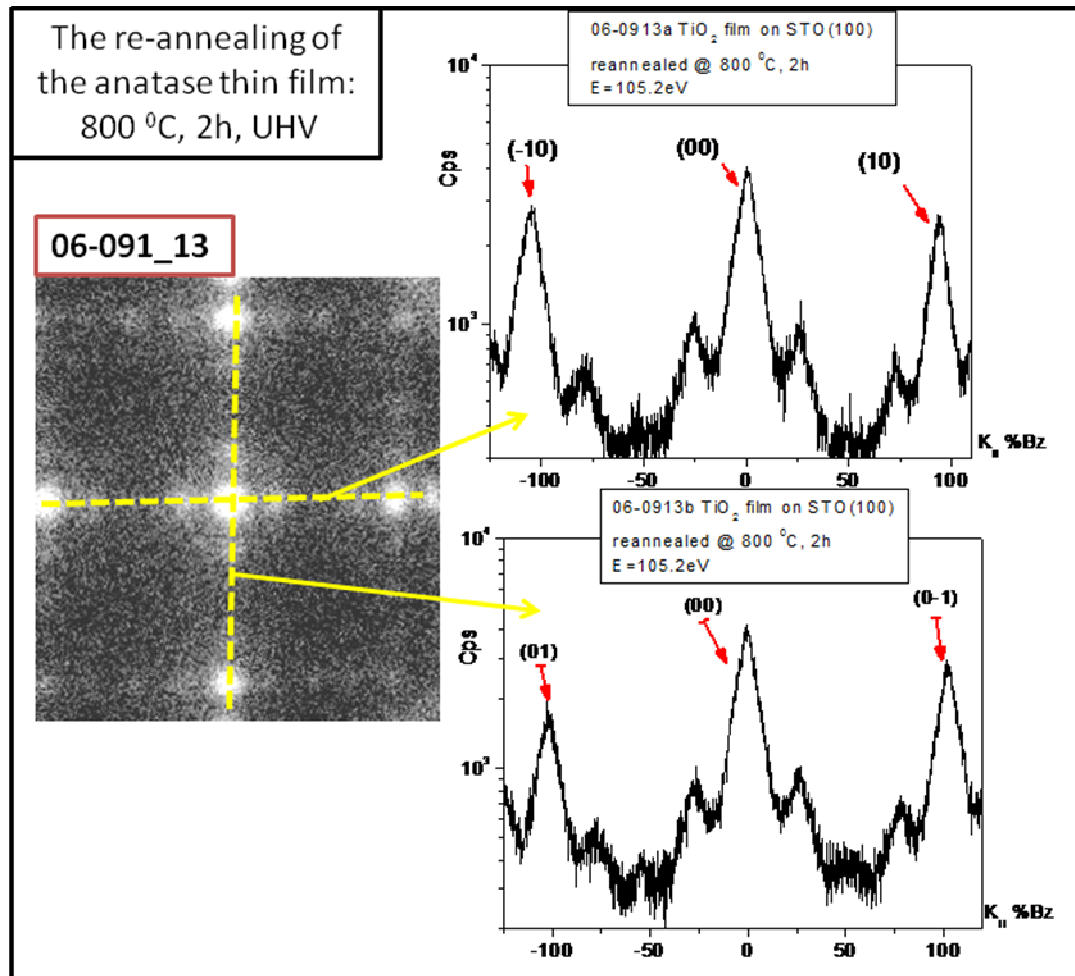


Fig 4.7: SPA-LEED 2D pattern with the spot profiles taken in 100 and 010 direction of TiO₂ grown on STO after second UHV annealing (800 °C, 2h).

Summary of the obtained results:

1. (1x4) reconstruction **appeared during the growth** and is stable under the growth conditions.

2. The appearance of the reconstruction during the growth **does not crucially depend on substrate types used.**
3. The UHV annealing **cause creation of weak new bands** in the insulator gap.
4. The STM measurement confirmed that the surface is (1x4) reconstructed in two domains. The reconstructed surface, morphologically, looks as **rows structured surface.**
5. (1x4) reconstruction **is stable** after further UHV annealing.

The explanations of (1x4) reconstruction appearance during the growth

One of the first successful experimental measurements of the anatase surface has been performed by Durinck et al.¹⁵ They reported results obtained by low-energy electron diffraction -LEED technique which showed that (001) orientated surface from the mineral anatase is (1x1) reconstructed. On contrary, Herman et al. reported that the thin-film anatase TiO₂ (001) surface is reconstructed as (1x4) type¹⁰. The explanation, based on angle-resolved mass spectroscopy of recoiled ions, attributed the (1x4) reconstruction to the formation of micro facets toward [103] and [-103] surface planes. Hengerer et al.¹¹ also, reported the (1x4) reconstruction on anatase (001) surfaces while their suggestion was that this reconstruction might be due to ordered oxygen vacancies. Herman et al. proposed that the reconstruction could be based on added rows¹⁰. According to this model, rows are placed on the surface with the periodicity of 4 times the lattice constant while the surface consists of twofold coordinated oxygen and fivefold coordinated titanium atoms.

Based on STM, RHEED, LEED, and XPS results Liang et al. developed this model further. Their model is based on the (1x1) surface structure, involving "added" and "missing" rows⁹. (For detailed description of mentioned models see the Introduction about TiO₂).

In order to explain appearance of (1x4) reconstructed surface during the growth on the high temperature in relatively rich oxygen environment, I proposed the model that is based on ad-row models with the variation that takes into account stabilities of the reconstruction during the growth. This model is schematically presented in Figure 4.8.

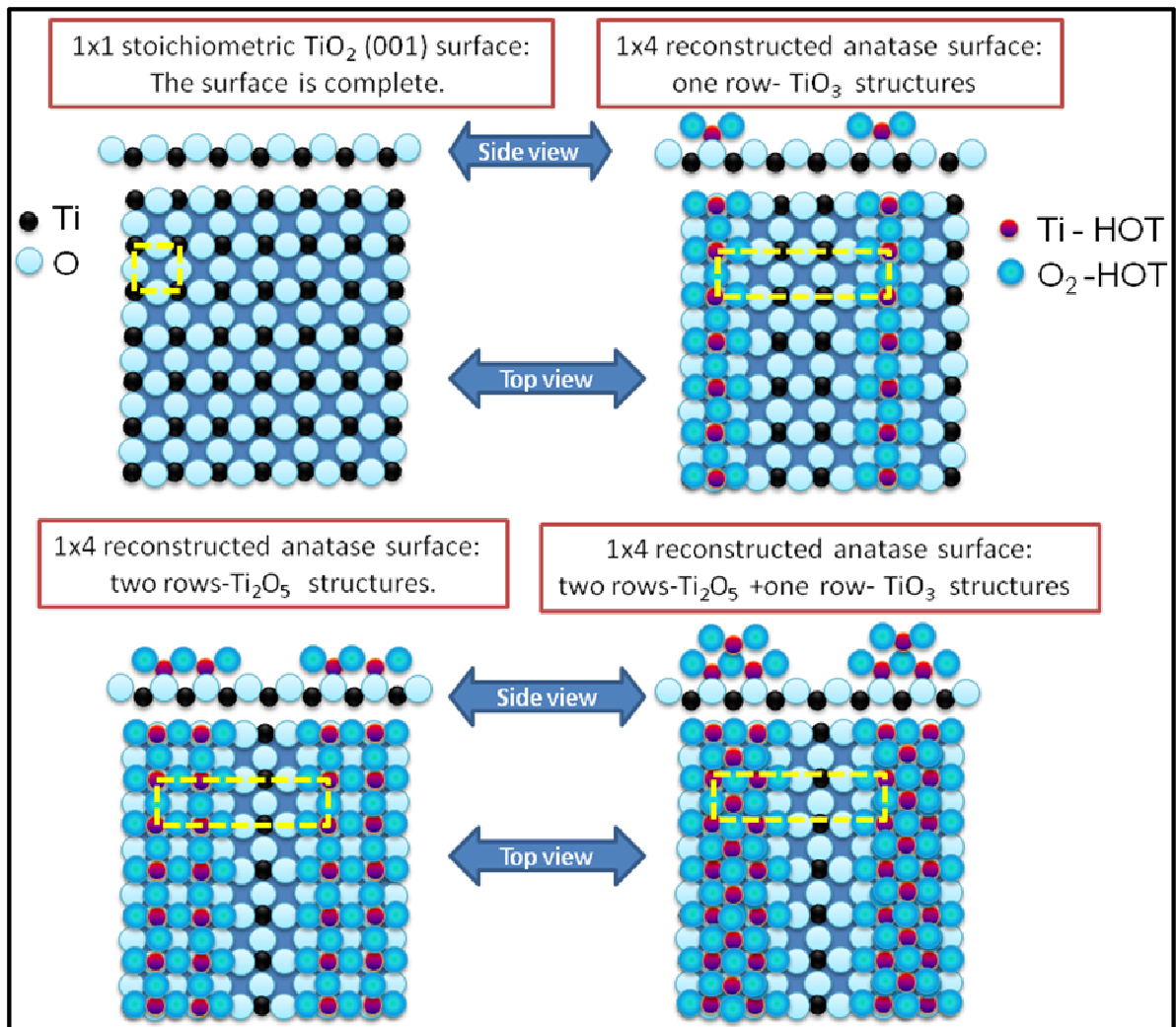


Fig. 4.8: The dynamic ad-row model of (1x4) reconstructed anatase (001) surfaces.

Considering the fact that *ab initio* calculations predict that an “ad-molecule” model is energetically favoured in comparison to the unreconstructed (1x1) surface¹⁶ similar way of thinking could be implemented to explain (1x4) reconstruction formation. Following oxygen rumpling of completed layer the oxygen atoms, which are deposited (in the Figure 4.8 represented as hot O₂), form the network where Ti cations, which are smaller than oxygen ions, arrange in their correct sites. Formation of the interface in this way is common model for hetero epitaxial growth of metal oxides¹⁷ and this model is used to describe the formation of new layers. The coverage of deposited atoms is 25% in the **one row** type of (1x4) reconstruction. With additional deposition of the material, the oxygen network extends laterally creating **the two rows** structure while (1x4) periodicity remains. After that, newly arrived material can be arranged in two ways: it can be laterally attached on existing rows or placed

on the two rows structures. In the case of the first scenario the oxygen network will be complete while the second causes formation of micro facets toward [103] and [-103] surface planes. Because of the high stability of the microfaceted surface the second scenario is more favourable. After that, the new material will complete lower layer causing the surface change in the **one row** structure. By applying this model appearance and steadiness of (1x4) reconstruction (confirmed by RHEED measurements) during anatase growth could be explained. This model predicts that in any moment of the deposition entire anatase surface is covered either with one row, two rows structures or their combination. Additionally, it has been already reported that surfaces are covered by rows with (1x4) periodicity⁹ which is in accordance with our STM data.

Having in a mind that, in the case of STO (001), the UHV annealing condition causes the creation of oxygen vacancies on the surfaces and the appearance of the strong new bands into the insulator gap, the above proposed model of the reconstruction may explain weakness of these bands in case of anatase thin film. The oxidative states of Ti atoms according to the model are: for the one row structure- Ti⁺⁶, for the two rows structure- Ti⁺⁵, for the three rows structure- between +4 and +5. It means that the additional free electrons caused by creation of the oxygen vacancies, will fill atomic Ti4sp orbital, acquired through the hybridization, which are involved in the bond formations of row structures. The same density of oxygen vacancies on the reduced (1x1) and (1x4) reconstructed surfaces causes the same number of the "free" electrons. For (1x1) reduced surface these electrons will fill the empty 3d Ti levels. In the case of (1x4) reconstructed reduced surface there are additional Ti4sp orbital which have to be filled first while remained "free" electrons will fill 3d Ti levels. This interpretation and presented XPS measurement of a region near Fermi level are in agreement with some reported photoemission spectroscopy data which showed that the (1x4) reconstructed anatase (001) surface has weaker new band between the Fermi level and the valence bands¹⁸ then in case of rutile (110) or anatase (101) surfaces.

4.2 Sr DIFFUSION AND SEGREGATION DURING UHV ANNEALING IN ANATASE THIN FILMS GROWN ON STO (001) AND SLAO (001) SUBSTRATES

Almost all research groups, which have studied TiO₂ films grown on STO, noticed that during the sample deposition or the sample preparation Sr diffusion occurs^{8,10}. The diffusion of atoms from the substrate into the film during growth or the annealing is an expectable phenomenon since the growth takes place at high temperature (700-800 °C). In order to understand strontium diffusion and the strain effect on diffusion I studied anatase thin films grown on two different substrates, STO and SLAO, since both substrates contain Sr atoms. The rationale of using the two different substrates, which contain Sr, aimed at understanding of the stress influence caused by the lattice mismatch between the film and the substrates. In the case of SrTiO₃ (001) substrate the mismatch is about -3% and the strain is expansive, while for the film grown on SLAO (001) the mismatch is less than 1% and causes the compressive strain. The data about the lattice mismatches between anatase and used substrates are presented in Table 4.1.

The substrate	SrTiO ₃ (001)	LaAlO ₃ (001)	SrLaAlO ₄ (001)
The lattice parameter (nm)	0.3905	0.379	0.375
The mismatch: $(a_{\text{anatase}} - a_{\text{substrate}}) / a_{\text{substrate}}$	~-3%	~-0.3%	~+1%

Table 4.1: The lattice mismatch between anatase and the substrates

The experiment was designed in the following way:

1. The two TiO₂ anatase 10 nm thick films, grown on STO (001) and SLAO (001), were measured by XPS as grown sample;
2. The same samples were annealed at 590 °C for 2 hours, 4 hours and additional 6h. After each annealing sequence the samples were measured by SPA LEED and XPS at room temperature. As the reference sample was used the film was grown on LAO (001). This is naturally choice since the LAO (001) has good lattice match with anatase, then it cannot be oxygen donor during UHV annealing and finally this substrate does not contain Sr.

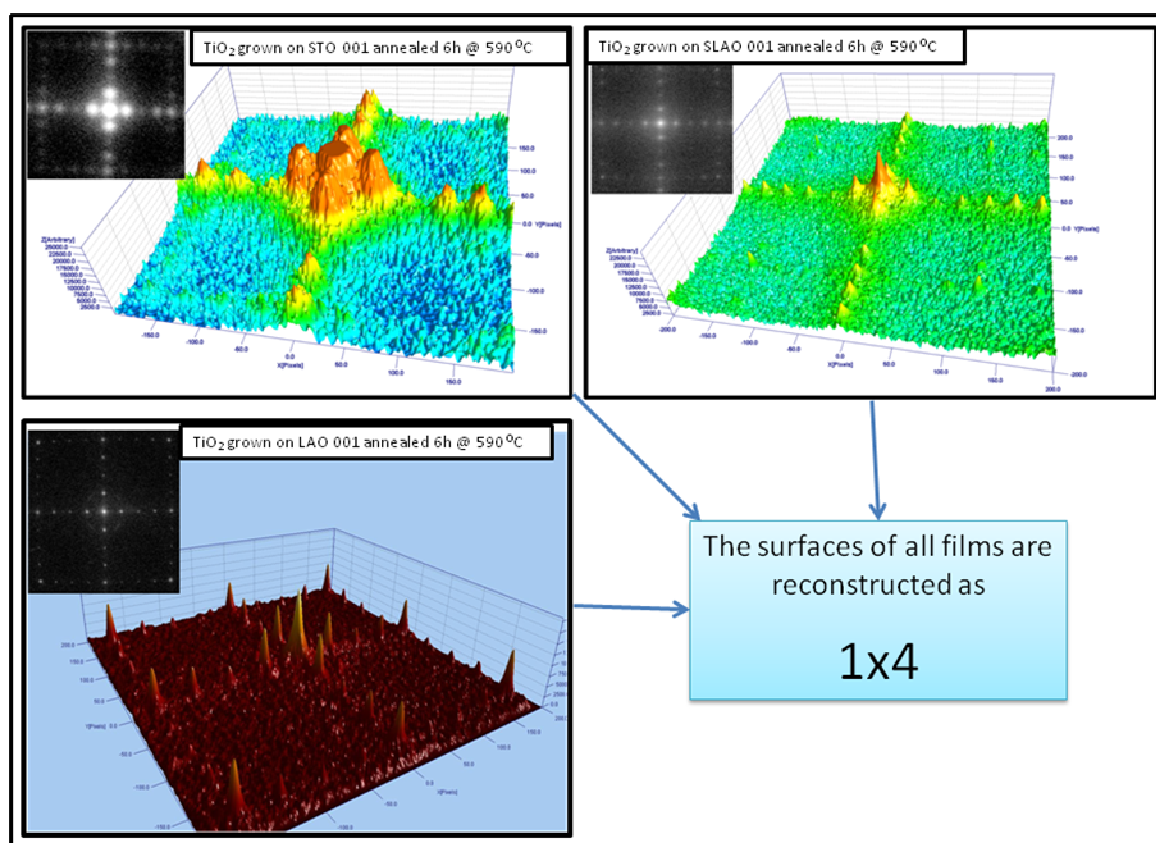
Results: TiO₂

3. After these first sequences of the annealing the films were reannealed again at the higher temperature, 750 °C. After cooling down the samples were again measured by XPS and SPA LEED.

In order to follow Sr contents in the film I measured, by XPS, the evolution of the 3d_{5/2}-3d_{3/2} Sr peaks and 2p_{1/2}-2p_{3/2} Ti peaks emissions versus temperature and time. The spectrum of the Sr emission was normalized to the intensity of the corresponding Ti peaks. The spectra were collected from the emitted electrons at the perpendicular (normal) and the shallow angle (35° to the surface).

The 590 °C annealing temperature was selected for two reasons. One was to follow the suggestion of Yong Liang and co-workers⁹. They used the deposition temperature of 550 °C to avoid Sr contamination from the substrate. Also, my experimental work done on another anatase samples (grown on STO) showed that the Sr segregation effect starts at the temperatures higher than 600 °C.

The 2D and 3D SPA-LEED patterns of anatase thin films grown on three different substrates are depicted in Figure 4.9.



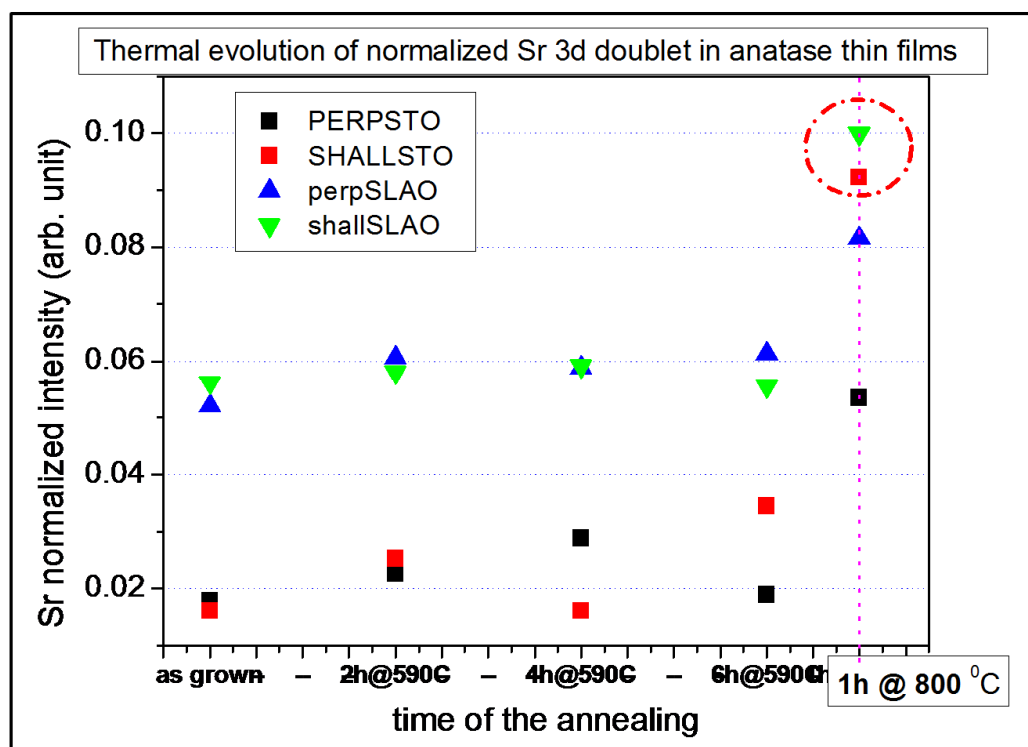
4.9. SPA-LEED 2D and 3D images of diffraction patterns of anatase thin film grown on different substrates.

Results: TiO₂

All patterns were obtained after the same annealing conditions: the pressure less than 1×10^{-9} mbar and 6 hours annealing at 590 °C. The data showed that the surfaces are (1x4) reconstructed.

The XPS data of two anatase thin films, grown on STO (001) and SLAO (001) substrates, treated in the way as described above, are shown in Figure 4.10.

From the XPS spectra analysis it was possible to conclude that Sr atoms are present in both films before any annealing. This could be due to the diffusion of Sr from the substrate to the film since the deposition temperature during the growth of the substrates was at 800 °C. Also, there are the same amounts of Sr in both configurations of the measurements, perpendicular and shallow. This fact indicates that Sr atoms are homogeneously distributed in the films. Throughout the annealing at 590 °C the Sr amount in the film grown on SLAO did not change significantly, while in the case of STO substrate the Sr presence started to change. The observed change was not radical. Nevertheless, after 6 hours of annealing the amount of Sr, measured in shallow configuration, is higher in comparison with the perpendicular configuration of the XPS measurement.



4.10: XPS monitoring of normalized Sr 3d doublet in anatase TiO₂ (001) films grown on STO (001) and SLAO (001) during UHV annealing.

Conversely, the notable increasing of Sr presence occurred in the both samples after the UHV annealing for 1 hour at 800 °C. In this case, besides the diffusion process, new effect occurs, **the segregation**, since Sr presence in both films is higher in the shallow configuration of the measurements.

By observing the graph depicted in Figure 4.10, the Sr diffusion is clearly visible. The amount of Sr in the film grown on STO, when measured in perpendicular condition increased about 250%, while in the shallow configuration it was increased about 300%. In the case of the film grown on SLAO the increase was lower but still significant. Interesting fact is that for both samples Sr amounts measured in the shallow configuration after the final annealing are very similar (marked with red cycle).

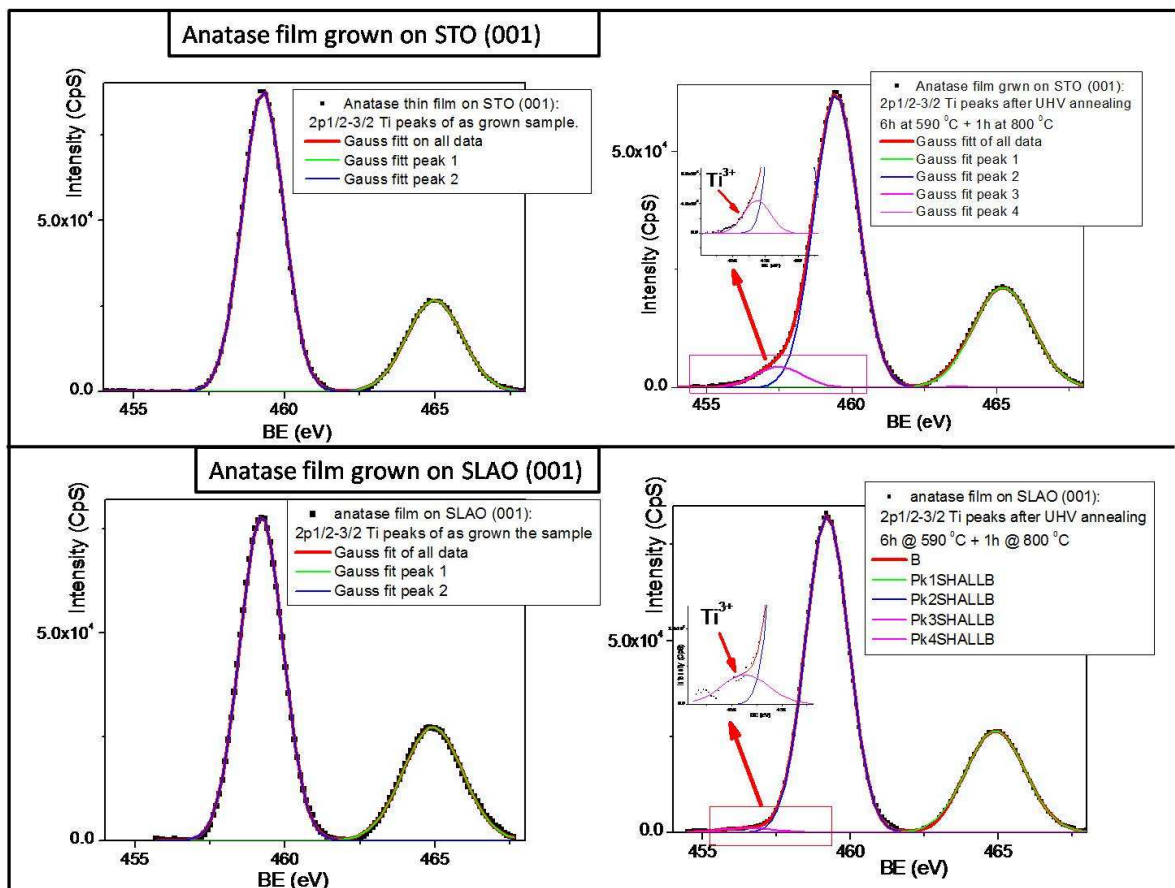


Figure 4.11: XPS data of 2p_{1/2-3/2} Ti emission of anatase thin films before and after the thermal treatment grown on STO and SLAO.

The increase of Sr amount in the films during the annealing up to 800 °C, could be explained in the following way. If Sr atoms are present in the films after the growth, it means that they move in to the films even the oxygen reach environment. During the UHV annealing this effect is more significant because the time of the annealing (1h) is longer in comparison with time of the deposition which was in these cases about 10 minutes.

The segregation may be explained as the influence of oxygen vacancies creation. Since the annealing generates oxygen vacancies, their densities must be higher near to or in the surfaces. The indication that the high temperature annealing creates oxygen vacancies could be in the appearance of the small shoulders on the 2p_{1/2}-3/2 Ti peaks. These shoulders, which may be due to existence of Ti³⁺ states, are depicted in Figure 4.11. Regarding the facts that the shoulder of Ti peak and the segregation effect (see Fig. 4.10) are more visible in the case where the substrate is STO, they could be consider as *cause and effect*. Having in mind that Sr atoms tend to diffuse trough the defects it is reasonable to assume that the atoms will accumulate where the density of vacancies is higher, which means near to or in the surface.

Conclusions:

1. The optimization of parameters for high quality anatase thin film growth was successful. The growth condition allows that the film quality does not depend significantly on the type of substrates.
2. The film surface is (1x4) reconstructed during the growth and does not depend on the substrates' type and the strain effects.
3. (1x4) reconstruction can be explained as the consequence of the natural way of anatase growth as ad rows model.
4. Sr diffusion from the substrates is very significant effect if growth or annealing temperature is around 800 °C. Sr inter-diffusion seems to be intrinsic property of anatase since it does not depend on the substrate type or the strains.
5. The Sr segregation is the effect which occurs during the UHV annealing at 800 °C. It could be connected with creation of oxygen vacancies.

References:

- 1 A. Fujishima and K. Honda, *Nature* **238**, 37 (1972);
- 2 J. T. Remillard, J. R. McBride, K. E. Nietering, A. R. Drews, and X. Zhang, *J. Phys. Chem. B* **104**, 4440 (2000);
- 3 A. I. Kingon, J. P. Maris, and S. K. Steiffer, *Nature* **406**, 1032 (2000);
- 4 B. O'Regan and M. Gratzel, *Nature* **353**, 737 (1991);
- 5 U. Diebold, *Surf. Sci. Rep.* **48**, 53 (2003).
- 6 S. Chen, M. G. Mason, H. J. Gysling, G. R. Paz-Pujalt, T. N. Blanton, T. Castro, K. M. Chen, C. P. Fictorie, W. L. Gladfelter, A. Franciosi, P. I. Cohen, and J. F. Evans, *J. Vac. Sci. Technol. A* **11**, 2419 (1993);
- 7 G.S. Herman, Y. Gao, T.T. Tran, J. Osterwalder, *Surf. Sci.* **447** 201 (1999).
- 8 G.S. Herman, Y. Gao, *Thin Solid Films* **397**, 157 (2001).
- 9 Y. Liang, S. Gan, S.A. Chambers, E.I. Altman, *Phys. Rev.B* **63**, 235402 (2001).
- 10 G. S. Herman, M. R. Sievers, and Y. Gao, *Phys. Rev. Lett.* **84** 3354 (2000).
- 11 R. Hengerer, B. Bolliger, M. Erbudak, and M. Gratzel, *Surf. Sci.* **460**, 162 (2000).
- 12 Patrick Fisher, Oleg Maksimov, Hui Du, Volker D. Heydemann, Marek Skowronski, Paul A. Salvador, *Microelectronics Journal* **37**, 1493 (2006).
- 13 S.A. Chambers, C.M. Wang, S. Thevuthasan, T. Droubay, D.E. McCready, A.S. Lea, V. Shutthanandan, C.F. Windisch Jr, *Thin Solid Films* **418** 197 (2002).
- 14 R. Shao, C. Wang, D. E. McCready, T. C. Droubay, S.A. Chambers *Surface Science* **601**, 1582 (2007).
- 15 G. Durinck, H. Poelman, P. Clauws, L. Fiermans, J. Vennik, and G. Dalmai, *Solid State Commun.* **80**, 579 (1991).
- 16 M.Lazzeri, A. Selloni, *Phys. Rev. Lett.* **87** 266105 (2001).
- 17 D.S. Lind, *Phys. Rev. B* **45**, 1838 (1992).
- 18 A. G. Thomas, W. R. Flavell, A. K. Mallick, A. R. Kumarasinghe, D. Tsoutsou, N. Khan, C. Chatwin, S. Rayner, G. C. Smith, R. L. Stockbauer, S. Warren, T. K. Johal, S. Patel, D. Holland, A. Taleb and F. Wiame, *PHYSICAL REVIEW B* **75**, 035105 (2007).

4.3 IN SITU INVESTIGATION OF THE EARLY STAGES OF TiO₂ EPITAXY ON SrTiO₃

The growth of ultrathin TiO₂ epilayers of nominally TiO₂-terminated SrTiO₃ substrates and homoepitaxial SrTiO₃ films is analysed in-situ by reflection high energy electron diffraction, low energy electron diffraction, x-ray photoemission spectroscopy and scanning probe microscopy, complemented by ex-situ analyses. It is shown that, in highly controlled deposition conditions and on very clean surfaces, a quite unusual growth mode, which is inconsistent with the formation of the expected anatase layer, takes place. On the base of a thorough characterization, we *show* that in suitable conditions the TiO₂ deposition can activate a Sr migration from the substrate to the film, resulting in the growth of a "SrTiO₃-like", cubic film. We argue that Sr migration is not only thermally induced, but it is activated by strain minimization. Above a critical thickness, the anatase phase nucleates.

Introduction

The interface of an epitaxial (001) anatase film with a SrTiO₃ (STO) substrate is recognized, from the simple observation of the crystal structures, to be an intriguing problem. A (001) oriented STO crystal is a stack of alternating SrO and TiO₂ planes. Unlike the underlying TiO₂ planes in STO, the TiO₂ planes stacked along the (001) direction of anatase are strongly buckled and each of them is in-plane shifted. A "upper" layer can be reproduced from a lower layer by a single-height vertical translation of 2.4 Å, accompanied by a 90° rotation along the 001 axis, and followed by a 1.9 Å horizontal translation. Once growth starts, and a (001)TiO₂/(001)STO interface is created, epitaxy poses strong constraints to the anatase layer, due to the relatively large (~ 3%) lattice mismatch. In order to match the in-plane lattice parameters of STO, anatase will have either (a) to stretch the O-Ti-O equatorial bond angle from the equilibrium value of about 156°, or (b) to lengthen the Ti-O equatorial bond length d from an equilibrium value of about 0,1934 nm. Actually, both mechanisms can be assumed to be at play. The straightening of the angle can be expected to have a reduced energy cost, since the O-Ti-O bending mode is the softer phonon mode of anatase (144 cm⁻¹)¹, but even a full straightening cannot allow, alone, to match the 0.3905 nm STO lattice parameter. As a matter of fact, the

Results: TiO₂

TiO₂ planes within the STO structure are in tensile strain themselves, due to the intercalated SrO planes, a circumstance that makes of STO an incipient ferroelectric. The stability of such a strongly deformed structure, composed of "straightened" and stretched TiO₂ planes is obviously questionable. Several possible relaxation mechanisms can be imagined, including dislocation formation, induction of oxygen non-stoichiometry, cation inter-diffusion, or others.

TiO₂ ultrathin film were grown on (001) STO, SLAO and LAO substrates and analyzed in situ, resorting to several surface science techniques, within our modular system for oxide deposition and analyses (MODA). Film growth was performed with a KrF excimer, with a typical fluence of 2.5 J cm⁻² on the target and a typical growth temperature of 800°C. Some samples were grown at other temperatures in the interval 600°C - 800°C yielding substantially similar results to the ones discussed below.

Films grown on LAO and SLAO show very similar properties, exhibiting a high degree of crystallographic perfection and relatively smooth surfaces. As a very typical signature which is easily recognised in surface electron diffraction (both RHEED and LEED), and in agreement with previous reports, the films show a strongly visible (4x1) reconstruction. Data regarding the films grown on LAO and SLAO are reported in Subchapter 4.1.

Data regarding the growth on (100) STO showed a strikingly different behavior, and a marked variability from case to case, seemingly as a function of the crystal quality and atomic termination of the substrate surface. In this subchapter, I reported data obtained either on high quality surfaces (as checked by RHEED, LEED and AFM) of nominally TiO₂ terminated substrates or of homoepitaxial STO thin films. STO substrates were etched according to and annealed in situ within the PLD chamber at 950°C for 2h right before deposition. This procedure reduces the risk of any possible surface contamination during and after the annealing.

The first striking feature that was regularly observed was a steady RHEED pattern that remained unchanged during the very first nm of TiO₂ deposition. At contrast to the case of TiO₂ growth on LAO, where a sudden changing of the pattern could be observed, the typical initial RHEED pattern of the STO surface was marginally affected, only manifesting a decrease in the intensity which took place on a relatively slow scale.

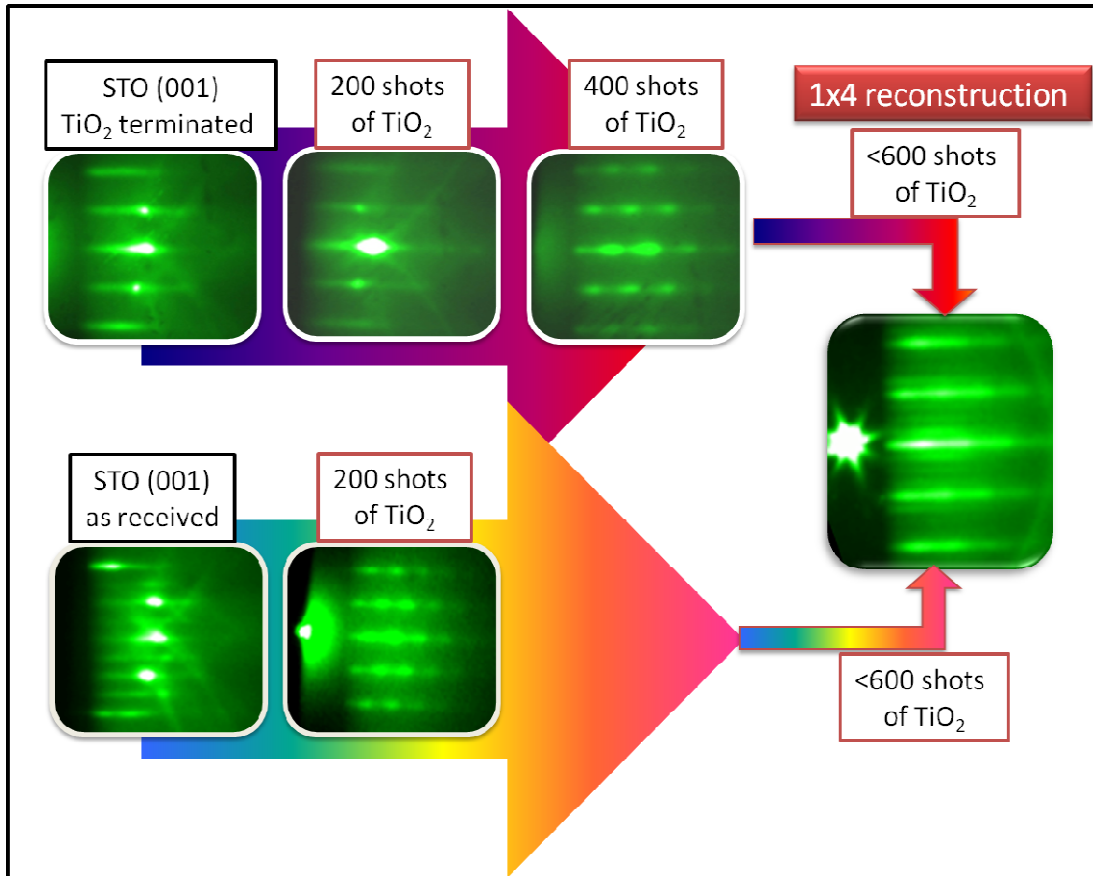


Fig. 4.3.1: The evolution of the RHEED patterns during TiO₂ growth on TiO₂ terminated (up) and as received (down) STO (001).

The RHEED pattern two TiO₂ films grown on highly TiO₂ terminated SrTiO₃ and non prepared substrates are shown in Figure 4.3.1. From this data is possible to conclude that the appearance of the typical RHEED pattern of TiO₂ grown on the terminated surface is in delay in comparison with the film grown on as received substrate.

A quantitative representation of the qualitative difference that we observe in RHEED patterns, for growth on 001 oriented LAO, SLAO, as received STO and TiO₂ terminated STO respectively, is given by the plots the intensity of the specular spot versus time. In all cases, the RHEED intensity decreases after the start of the deposition with a behavior that can be empirically fitted by the exponential decay law:

$$I(t) = I_o + Ke^{-\frac{t}{\tau}} \quad (4.3.1)$$

Results: TiO₂

Here the value t corresponds to the time in seconds, but also to the number of laser shots, since all reported experiments were performed at a 1Hz repetition rate, with a typical deposition rate of 0.012 nm/shot.

While for samples grown on LAO and SLAO the typical τ value is of the order 7-8 seconds, as received STO has slightly higher the value, 13seconds. On contrary in the case of the deposition on highly TiO₂ terminated STO or on STO films, τ values is much higher, up to 40 seconds or more.

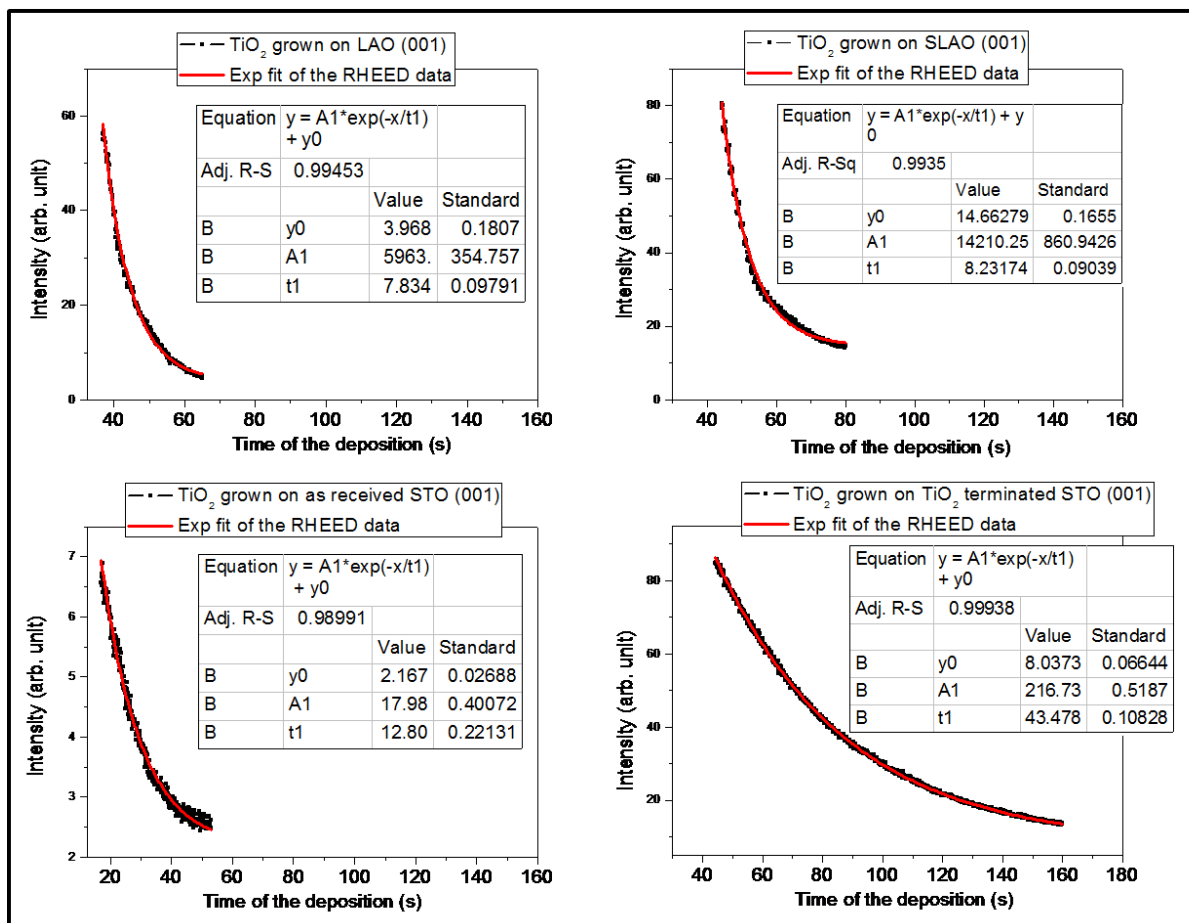


Fig. 4.3.2: The decay of RHEED intensities during first part of TiO₂ growth on different substrates and exponential fits.

This “intermediate phase”, where the reciprocal lattice of the TiO₂ films surface remained substantially isomorphous to the reciprocal lattice of a perfect STO surface as apparent from RHEED patterns, typically lasted 200-250 shots, corresponding to 2.4-3 nm. It ended with the abrupt appearance of 3D like pattern, as witnessed by

Results: TiO₂

the sudden development of a scattered intensity in a formerly empty region of the reciprocal space, shown in Figure 4.3.1.

The nature of such "intermediate phase" and observed variability as a function of the STO surface preparation are the main subjects of this subchapter.

The nature of the intermediate phase was investigated by resorting to the joint application of a number of different techniques, including LEED, STM, AFM, XPS and TEM.

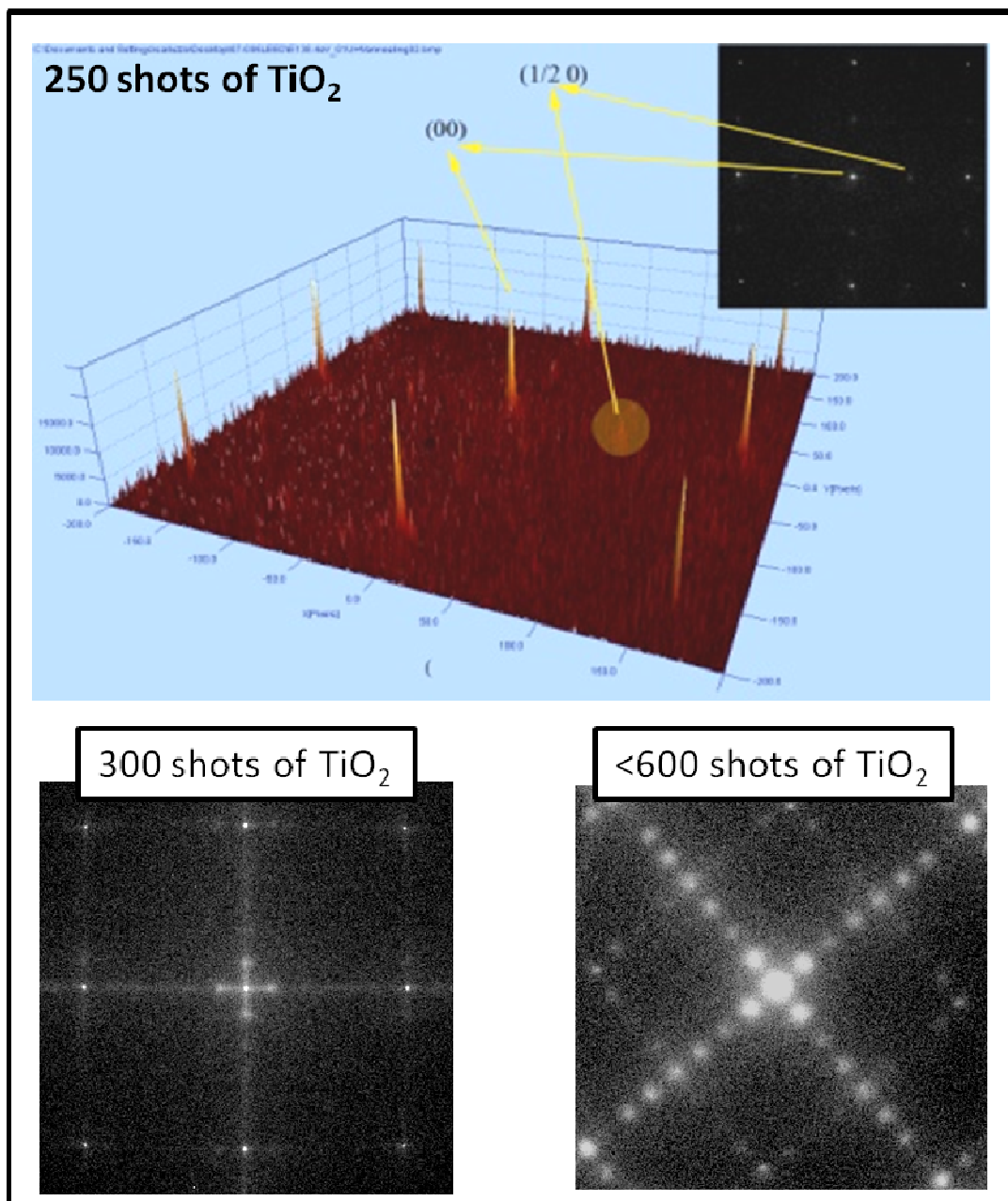


Fig.4.3.3: The LEED patterns of TiO₂ films grown on TiO₂ terminated STO (001) with different thickness.

Results: TiO₂

LEED patterns and AFM/STM images were collected by transferring the samples in-situ into the analytical chambers of the system. The films were annealed in vacuum (750-800 °C for 1-2 h) in order to make them conducting enough for LEED and STM analyses. LEED patterns fully confirm the trends reported for the RHEED. The film surfaces showed the same square pattern with a (1x1) or a weak (2x1) surface reconstruction, as usually found on the STO substrates, also depending on the details of the thermal treatment. Until a thickness of about 2-3 nm, the films were strained on the STO substrate, as proved by the distance of the reciprocal lattice spots after calibration on the STO (001) surface. With increasing the TiO₂ thickness, the LEED patterns shows a lattice relaxation to the smaller TiO₂ lattice parameter, and the appearance of new features until a typical 4x1 pattern, similar to the ones obtained on LAO and SLAO, but with much broader spots, appears. The SPA-LEED data of three different samples are depicted in Figure 4.3.3. The thickness of the first film is 2-3nm, the second with 5-6 nm and the thickness of the third is 10 nm.

AFM and STM images also confirmed the peculiar nature of the so called "intermediate phase" of the TiO₂ films. Rather than presenting the typical aspect of (001) anatase surface, with a multilevel terrace structure and a row structure on terraces corresponding to the (4x1) reconstruction, the films show remarkably flat terraces that reproduce the underlying STO surfaces. Even more interestingly, the terrace steps are 0.4 nm high, just as STO and unlike anatase, which is characterized by a unit cell with a c-axis of 0.95 nm and an interplane distance of 0.24 nm. The peculiar aspect of the anatase surface is instead recovered in thick films.

X-ray diffraction scans performed (ex situ) on these samples do not show measurable peaks at the characteristic XRD peaks of (001) anatase, providing indirect evidence that the film resulting after short ablation of the TiO₂ target are not anatase.

The same effect (or even stronger) was noted during TiO₂ deposition, using the same deposition parameters, on homoepitaxial STO (001) film. In this case, the special preparation of the substrate is not necessary to be done. One sample was monitored after each sequences of the growth (STO film then 10 shots of TiO₂, additionally 20 shots, additionally 30 shots, additionally 120 shots and finally

Results: TiO₂

additionally 120 shots of TiO₂, by LEED and XPS (Figure 4.3.4). After each deposition, the film was UHV annealed at 800 °C for 1hour.

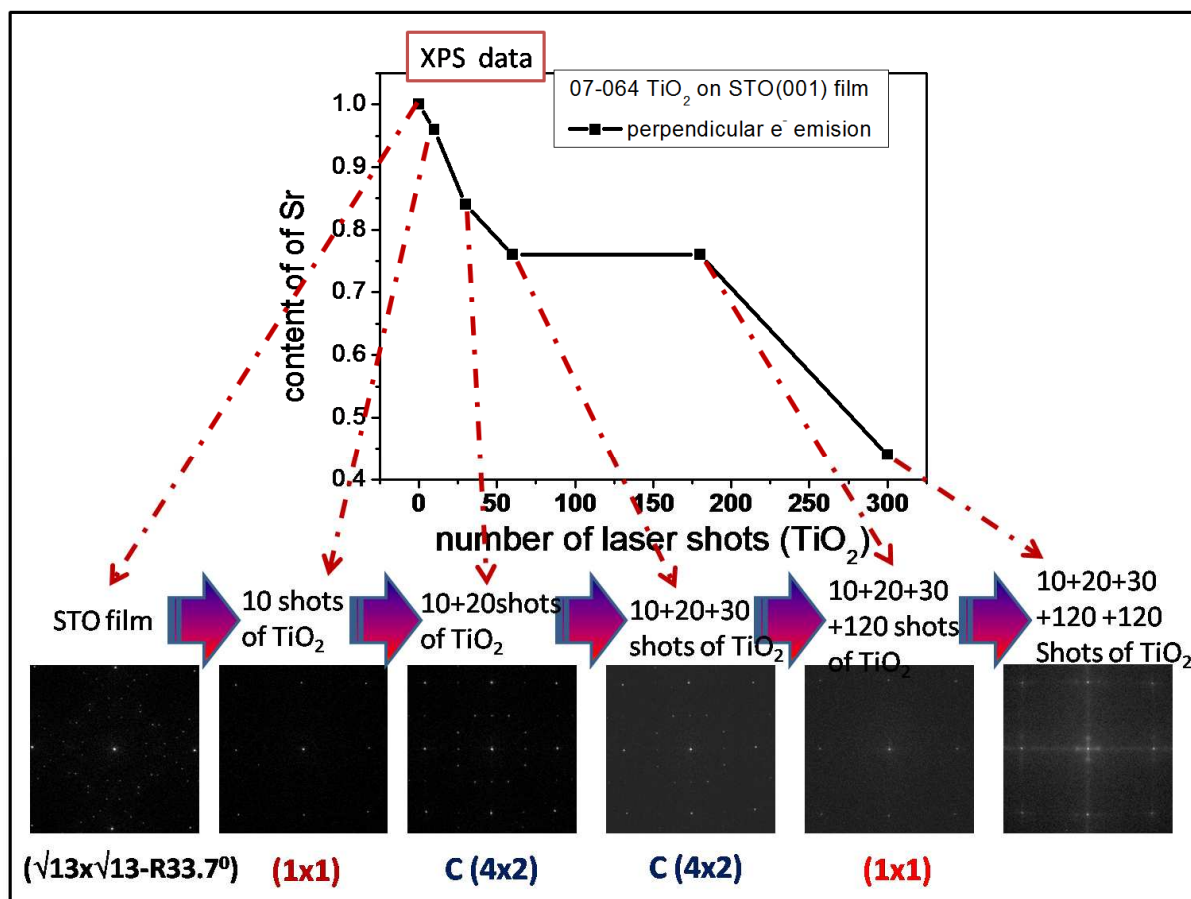


Fig 4.3.4: XPS and LEED data evolution of the sample thickness (number of laser shots on TiO₂ target).

The XPS data showed that Sr content, measured at the perpendicular geometry, decreased in first sequences of deposition (in total 60 shots of TiO₂) then the amount was constant (180 shots of TiO₂) and after that is again of Sr amount decreased. In same time the LEED patterns, beside of reconstructions, showed no change until the final deposition. Moreover, the distances between main spots showed that the reciprocal lattices corresponded to STO 2D reciprocal lattice.

In order to investigate the chemical nature of the intermediate layer, the XPS measurements of films grown on TiO₂ terminated and none terminated substrates were done. In Figure 4.3.6 the X ray photoemission spectra of the Sr 3d doublet for a) a SrTiO₃ film; b) a 3 nm thick TiO₂ film deposited on SrTiO₃ are compared.

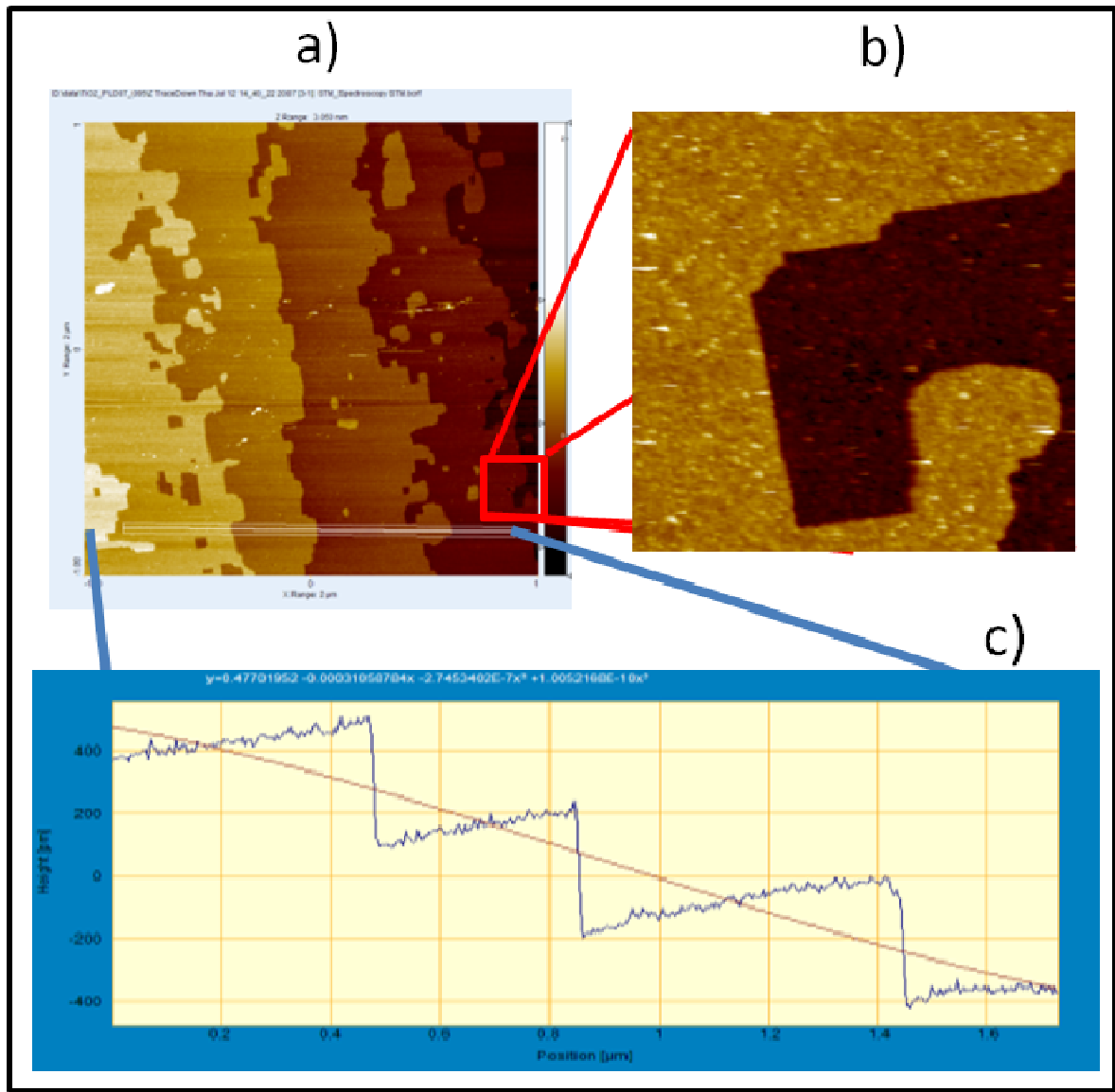
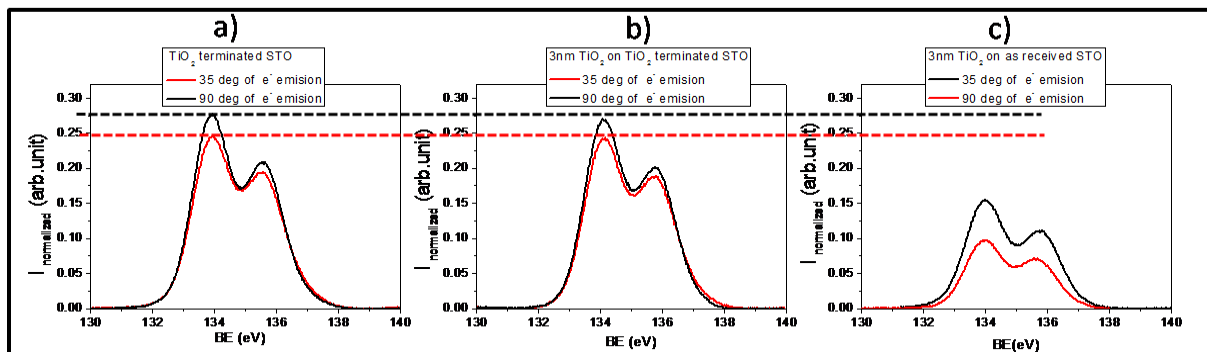


Fig. 4.3.5: The STM morphology images of TiO₂ "intermediate phase".



4.3.6: XPS of the Sr 3d doublet in perpendicular emission and in shallow angle emission configurations.

Results: TiO₂

The vertical scale in each measurement is normalized to the intensity of the corresponding Ti 3d doublet recorded at the same conditions. The measurements were performed both at perpendicular emission (P) and at smaller angle of emission, which was 35° (in following text referred as S) of photoelectrons. Escape depth of Sr 3d electrons with about 1100 eV kinetic energies in solids are generally reported as about 3 nm at most, which is expected to be independent of kinds of materials. Therefore, the S configuration probes a depth of the order of ≈ 1.5 nm, that is, at list, double less than the film thickness for measurements b and c, while the P configuration senses the body of the film and may bear the contribution from the substrate. The striking evidence in Figure 4.3.6 b indicates a high Sr content (with a stoichiometric ratio $[\text{Sr}]/[\text{Ti}] \approx 0.7$) within the over-layer that was supposed to be pure TiO₂. For comparison, we remark that the Sr 3d doublet (Figure 4.3.6 c) is almost double less for TiO₂ film grown on as received STO (001) with same number of the shots (the thickness about 2.5nm).

The one growth on TiO₂ terminated STO was dedicated to ketch the moment where the "intermediate phase" will turn into "normal" anatase growth.

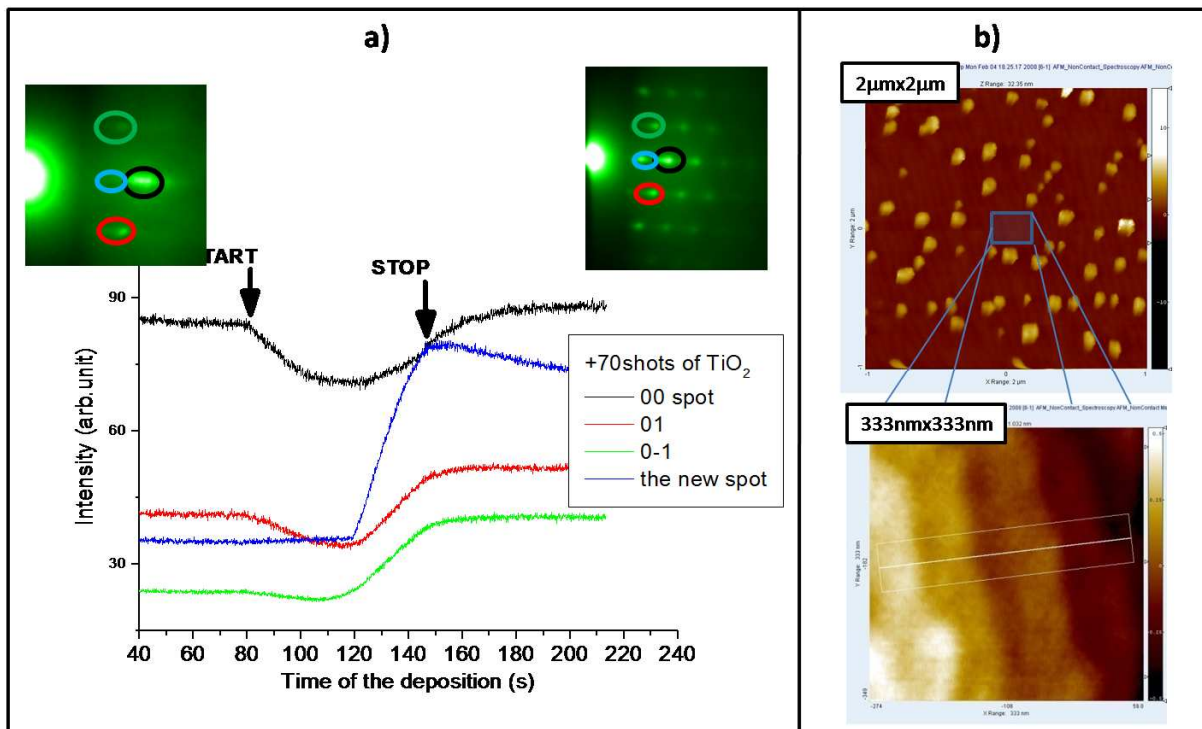


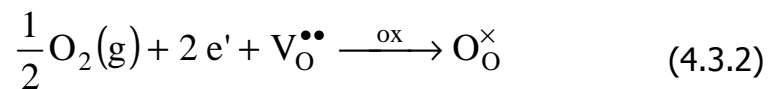
Fig. 4.3.7: a) The RHEED Intensity dependence on the deposition time, b) AFM images of ultra thin film after 190 shots.

Results: TiO₂

The deposition was done in two steps: first 120 shots of TiO₂ caused exponential decay of the RHEED intensity with τ about 40 s, while second deposition step caused also the exponential decay but just during additional 40 shots. After that the further 30 shots provoked drastically changed in the RHEED pattern (Figure 4.3.6 a). The new spots appeared (the one is marked with blue cycle) and the intensity of all spots started to increase. The deposition was stopped after these 70 shots of TiO₂ while all deposition contents 190 shots. After the cooling down in oxygen atmosphere the sample was *in situ* transferred in the Analytic chamber where was measured by AFM. The AFM images are presented in Figure 4.3.6 b. The image with the scan 1 μ m x 1 μ m shows the clear evidence of the early stage of the nucleation. The second image was taken on three time smaller scale (333nm x 333nm) then the first image. Between the islands the surface is still terraced. This confirmed the hypotheses that the film is created from two kind of the growth: the first, 2D growth caused the formation of the "intermediate phase" while the second, which appeared after the critical thickness of the first phase, was 3D growth.

The model of the "intermediate phase" growth

It is widely acknowledged that under reducing conditions the STO undergoes several complex chemical reactions involving defect formation and diffusion. In brief, two main processes take place. The first one is the creation of oxygen vacancies, according to the defect reaction ²:



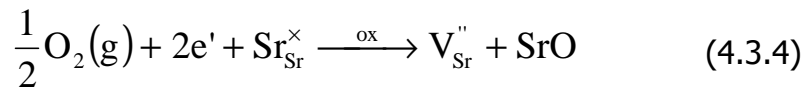
Involving oxygen vacancies ($\text{V}_\text{O}^{\bullet\bullet}$), electrons (e'), and regular oxygen sites (O_O^\times). The kinetics of transition is limited in this case by oxygen vacancy migration ³. At lower temperatures, the surface reaction (4.3.2) becomes the rate-limiting step ⁴.

At the same time, a slower reaction involves the Sr cations. It was at first proposed that this is achieved by the establishment of rocksalt intergrowth ⁵ layers (the Ruddlesden-Popper phases $\text{SrO} \cdot (\text{SrTiO}_3)_n$), following the defect reaction of regular metal ions ($\text{Sr}_\text{Sr}^\times$) and regular oxygen ions:



Results: TiO₂

However, no experimental evidence of intergrowth in SrTiO₃ has ever been found. On the contrary, an overwhelming evidence indicate an alternative defect mechanism, where strontium vacancies and the SrO-rich second phase can be exclusively created at the surface of single crystals⁶⁻⁸. Then, the equilibration kinetics is limited by cation *diffusion*. The point defect reaction of the cation sublattice may then be written as follows:



Once the Sr migration at the STO surface is acknowledged, it is possible to propose a model that accounts for the whole body of our results. At the deposition conditions, Sr vacancies are formed close to the STO surface and Sr adatoms appear. We believe that the growing front of the TiO₂ film incorporates them in a very efficient way during the growth process, according to the following scenario.

When Sr enters the lattice of TiO₂ layer, the film stoichiometry is transformed into Sr_{1-x}TiO_{3-x}. Since no defect free crystal structure is available in the STO phase diagram for x<1, this Sr deficient compound will crystallize in the form of a defective perovskite structure. Such phase is strain stabilized in thin film form, since, unlike anatase, it matches the STO substrate. The TiO₂ adatoms impinging on the terraces and condensing at the edges during the step-flow growth, feel a driving force to crystallize in such a form that allows lattice matching, not only to the substrate in plane parameter, but also to the step height. Such a matching is accomplished by resorting to the incorporation of available Sr atoms and the formation of the defective perovskite. This in turn allows for the formation of a fresh shifted step edge, where segregated Sr atoms and Ti adatoms can react. Although the STO substrate can be considered as an infinite Sr reservoir, the limited mobility will cause the Sr content to decrease with thickness. The process will stop abruptly with the nucleation of unstrained anatase islands which will cover the surface giving rise to the TiO₂ film. The sketch of the final situation of the growth is presented in Figure 4.3.7. In the figure is presented that the growth causes Sr diffusion from STO substrate giving the situation that the interface doesn't exist. Before that the arriving material reaches amount which corresponds to "critical thickness", Sr distribution in

top layers follows exponential law. This law can be expressed in very simple way following the chemical formula of the "intermediate phase"- Sr_{1-x}TiO_{3-x}:

$$x = 1 \exp(-d/d_c) \quad (4.3.5)$$

where **d** is distance from the layer which has correct stoichiometry, SrTiO₃, while **d_c** is critical thickness where Sr_{1-x}TiO_{3-x} structure is still perovskite (Figure 4.3.8).

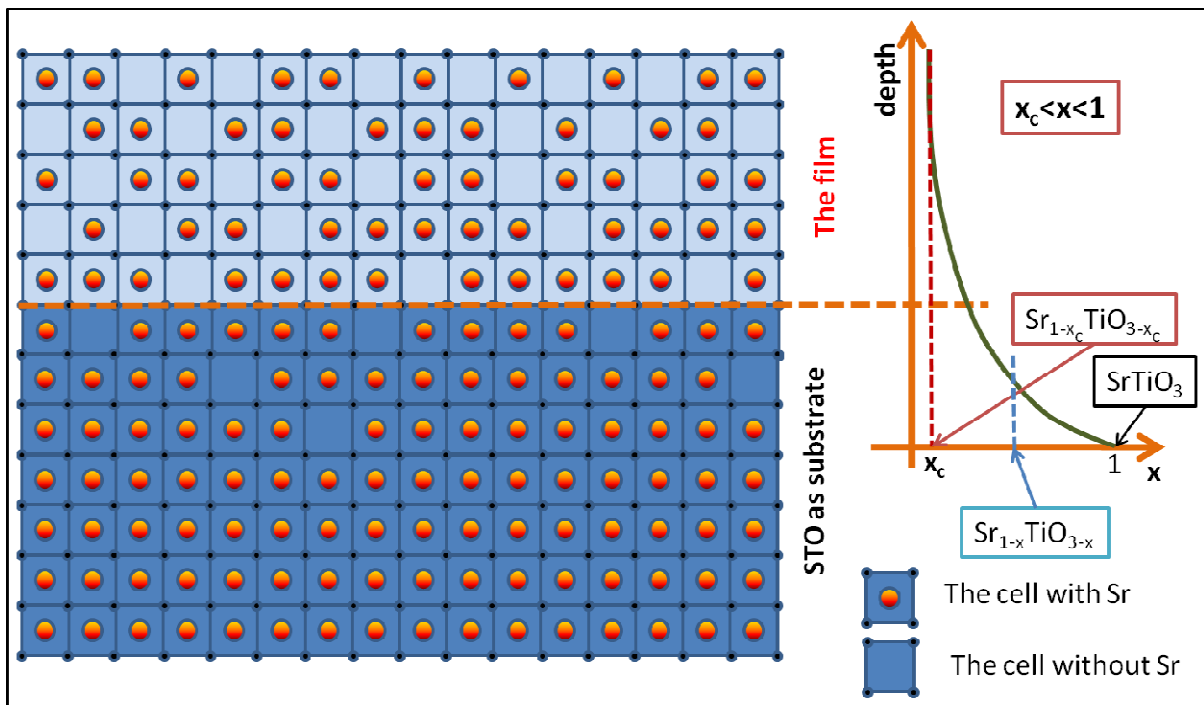


Fig.4.3.8: The scheme of the "intermediate phase" of TiO₂ film grown on STO (001).

The RHEED Intensity following kinematic theory of diffraction can be described as:

$$I(\vec{K}, \vec{k}_i) = F(\vec{K}, \vec{k}_i)G(\vec{K}) \quad (4.3.6)$$

where $F(\vec{K}, \vec{k}_i)$ is the dynamical form factor while $G(\vec{K})$ represents the lattice factor. The dynamical form factor can be expressed as function of electrons number which

Results: TiO₂

are involved in elastic scattering processes or in simplified form as function of all electron, Z:

$$F(\vec{K}, \vec{k}_i) = f(Z) \quad (4.3.7)$$

Considering the facts that the growth is, in the presented model described above, step flow growth, and that the crystal structure (perovskite) remain constant, the RHEED intensity of the diffracted spots will depend only on the form factor. It can be expressed as:

$$I(\vec{K}, \vec{k}_i) = f(Z) = kZ \quad (4.3.8)$$

In a dynamical situation of the growth, the intensity of the diffraction points will decrease since the new layer will have fewer electrons (more Sr vacancies). The number of the vacancies is directly proportional with deposition time thus the decrees of intensity can be described with the equation.

$$dI = -kI dZ = -KI dt \quad (4.3.9)$$

The solution of the equation 4.3.9 has same form of the equation 4.3.1 which fits experimental RHEED data.

$$I(t) = I_0 + Ke^{-\frac{t}{\tau}} \quad (4.3.10)$$

This observed and described effect can be used as way to improve TiO₂ termination of STO (001) *in situ* since there is clear evidence that Sr excess (which can appear during pre-annealing or already exist on STO surface) can be incorporated during first stage of TiO₂ deposition.

Conclusion:

1. The **strain** effect between STO (001) and anatase causes strong **inter-diffusion** of Sr.
2. The consequence of the strain and the Sr inter-diffusion is growth of "**intermediate phase**" with perovskite crystal structure and Sr_{1-x}TiO_{3-x} chemical formula.

References:

- 1 T. Ohsaka, S. Yamaoka, O. Shimomura, Solid State Communications **30**, 345 (1979).
- 2 F. A. Kroger and H. J.Vink, Solid State Phys. **3**, 307 (1956).
- 3 R.Waser, T. Baiatu, and K. H. Hardtl, J. Am. Ceram. Soc. **73**, 1645 (1990).
- 4 J. Claus, M. Leonhardt, and J. Maier, J. Phys. Chem. Solids **61**, 1199 (2000).
- 5 R. Moos and K. H. Hardtl, J. Am. Ceram. Soc. **80**, 2549 (1997).
- 6 K. Szot, W. Speier, U. Breuer, R. Meyer, J. Szade and R. Waser, Surf. Sci. **460**, 112 (2000).
- 7 Karsten Gomann, Gunter Borchardt, Micha Schulz, Anissa Gomann, W. Maus-Friedrichs, Bernard Lesage, Odile Kaitasov, Susanne Hoffmann Eiferte, T. Schneller, Phys . Chem. Chem. Phys. **7**, 2053 (2005).
- 8 T. Ohnishi, K. Shibuya, M. Lippmaa, D. Kobayashi, H. Kumigashira, M. Oshima, and H. Koinuma, Appl. Phys. Lett. **85**, 272 (2004).

Appendix: Properties of STO/LAO interface

The importance of technological method developed sufficiently to produce highly terminated and controlled surfaces of the STO, as substrate, is illustrated in the next paragraph.

Ohtomo and Hwang ¹ reported the existence of a conducting electron layer at the heterointerface between two nominal insulators, SrTiO₃ and LaAlO₃. This significant result motivates many research groups to contribute to the understanding of this effect and to try to implement it. Ohtomo and Hwang demonstrated that the terminations at the interface of nonpolar STO with polar LAO play a crucial role in the formation of a quasi-two-dimensional electron gas (Q2-DEG). The SrO-AlO₂ interface is insulating, while the TiO₂-LaO interface produces a Q2-DEG.

Although it is generally agreed that this phenomenon is induced by delicate changes at the interface, interpretations of the mechanisms are still under debate. According to Noguera hypothesis ² (see Chapter 1.2.4) in order to prevent the potential divergence in LAO films, electrons are transferred from the LAO layer into the TiO₂ bonds of the STO layer through the interface. Consequently, the "electrondoped" STO layer in the surrounding area of the heterointerface begins to conduct.

However, to produce the conducting interface two necessary conditions must be fulfilled: perfect TiO₂ termination of STO (001) and the perfect layer by layer LAO growth. We used two ways to achieve highly TiO₂ termination: one, the chemical etching joined with *in situ* annealing (described in Chapter 3.1.1) and second, deposition of 1-2 layers of TiO₂ on STO (001) (Chapter 4.3). LAO, 10 unit cells thick, thin film grown on chemically etched and *in situ* annealed (0.5 mbar of oxygen) STO (001) was monitored by RHEED during growth and these data are depicted in Figure a1. The oscillations of (00) diffraction spot during the growth indicated 2D (layer by layer) growth while the final 2D RHEED pattern of the film proved that the surface is flat. One LAO film was grown on STO (001) prepared by 15 shots of TiO₂ deposition (this amount of TiO₂ should correspond to formation of 1-2 TiO₂ layers).

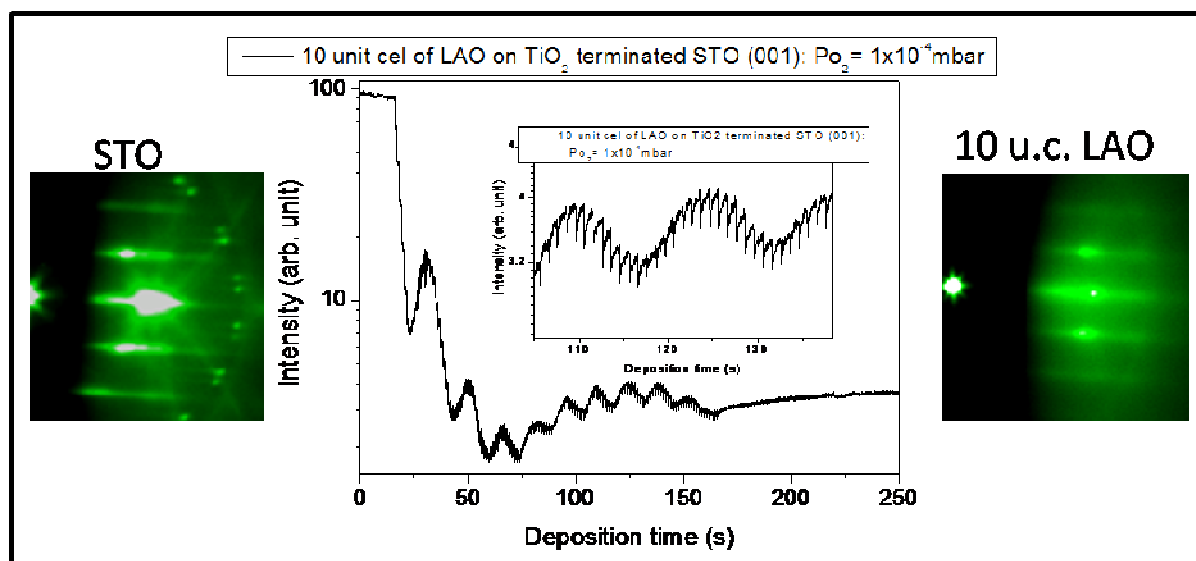


Fig. a1: The RHEED data during growth of 10 unit cells of LAO on TiO₂ terminated STO (001).

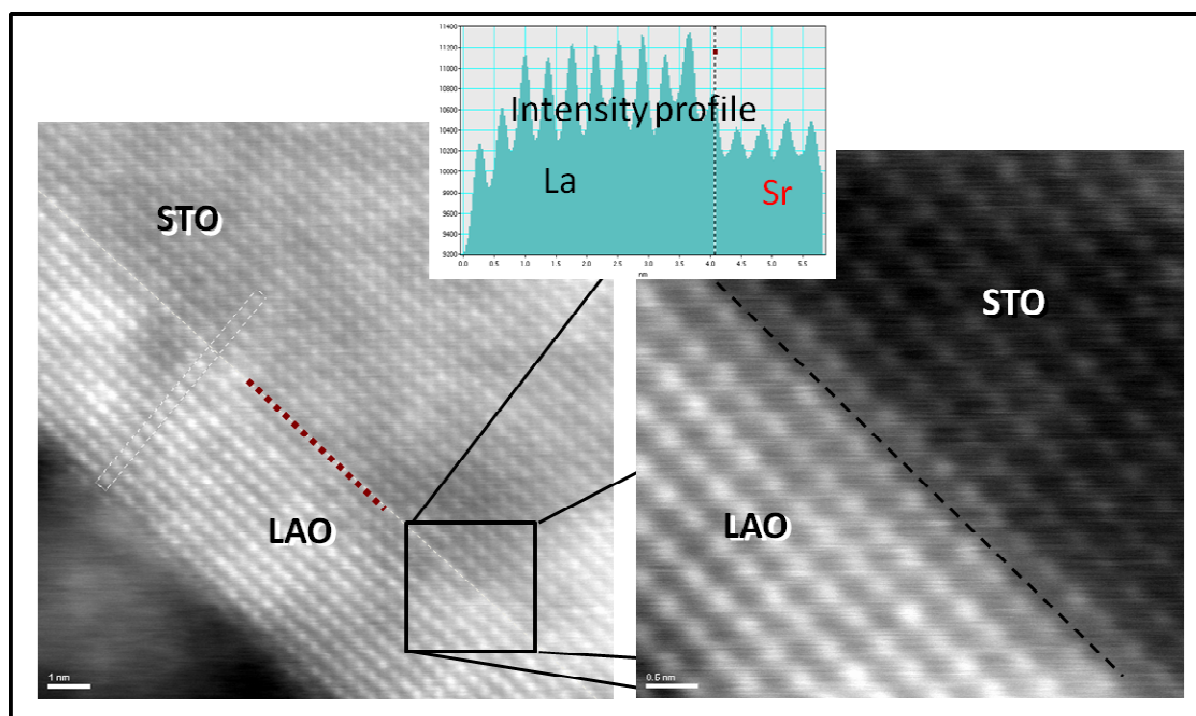


Fig. a2: The TEM cross section of the LAO/STO interface together with the intensity profiles of Lanthanum and Strontium in the region near the interface.

Transmission electron microscopy (TEM) cross-sections of the sample are presented in Figure a2. The interface is without any defects indicating that these 15 shots of TiO₂ are sufficient to the creation of the fully TiO₂ terminated STO.

Appendix: Interface STO/LAO

Formation of a quasi-two-dimensional electron gas (q2-DEG) at the interface between SrTiO₃ (001) and LaAlO₃ was confirmed by the measurements of the electronic properties of the structure. This data are presented in Figure a3.

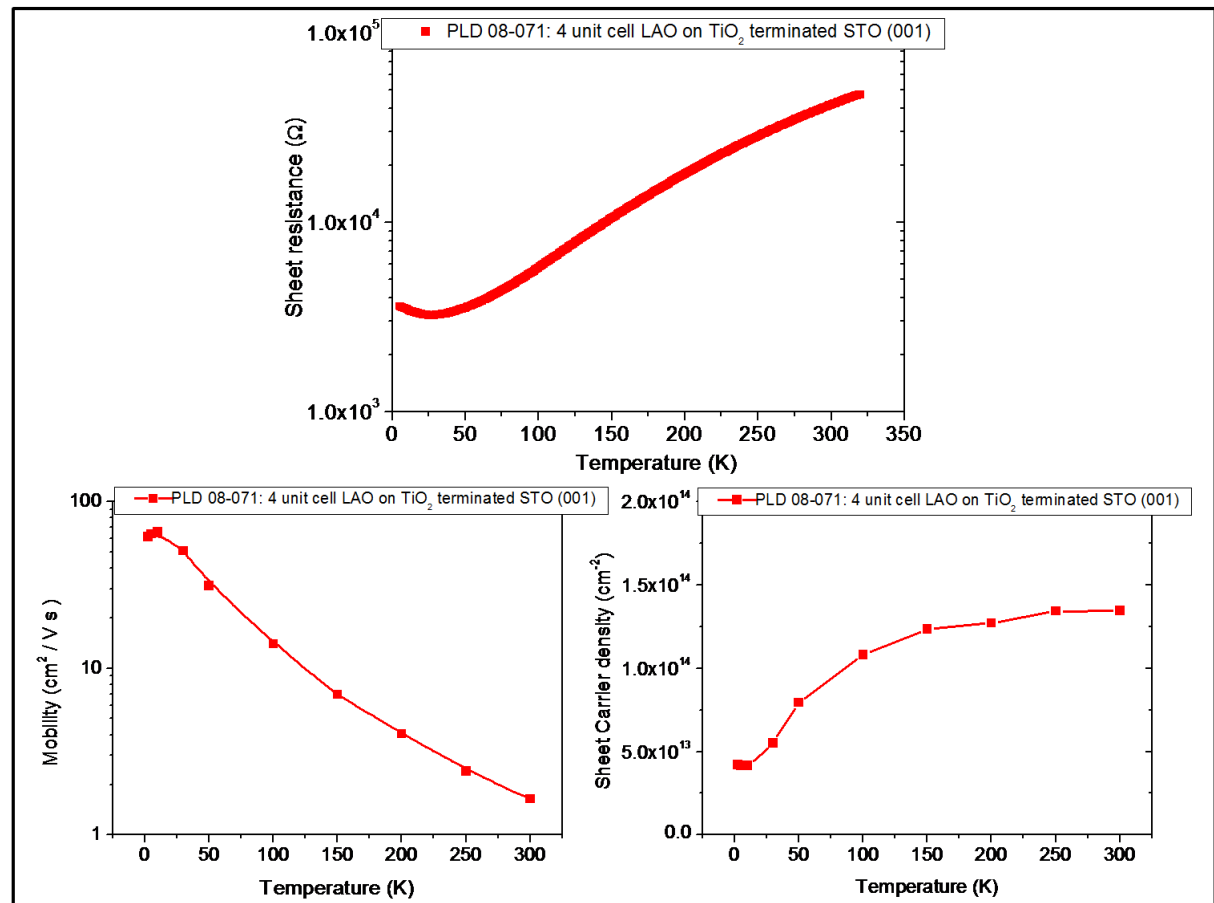


Fig. a3: Sheet resistivity, Sheet-carrier density and carrier mobility for 4 unit cells thick LAO film grown on TiO₂ terminated STO (001)

The charge that is necessary to prevent the polarization catastrophe is equal to half an electron per unit cell³ or $3,2 \times 10^{14} \text{ cm}^{-2}$ and the measured Sheet-carrier density is very near to the theoretical value.

References:

- 1 A. Ohtomo and H.Y. Hwang, Nature **427**, 423 (2004).
- 2 Claudine Noguera, J. Phys. Condens. Matter **12**, R367 (2000).
- 3 Wolter Siemons, Gertjan Koster, Hideki Yamamoto, Walter A. Harrison, Gerald Lucovsky, Theodore H. Geballe, Dave H. A. Blank, and Malcolm R. Beasley, PHYSICAL REVIEW LETTERS **98**, 196802 (2007).

V GENERAL CONCLUSION

Subject of this thesis are studies of two materials from Transition metal oxides (TMO) family:

- 1. Strontium titanate** - SrTiO_3 (STO),
- 2. Anatase** polymorphous of titanium dioxide - TiO_2

All examples and results which exist in the literature (some of them are presented in this thesis) about STO and anatase, pointing out to the necessity of investigating in detail the crystal, chemical and electronic properties of STO surfaces, triggered my interest in facing the problem of controlling and understanding the surface properties by resorting to a novel approach.

- 1.** My study has been confined to the **(001)** and **(110)** surfaces of undoped SrTiO_3 . The study highlights the importance of an appropriate pre-treatment of SrTiO_3 substrates in order to obtain smooth and well-defined surfaces. The presented results indicate the importance of the details of the preparation process, the history of the crystals in terms of the chemical and thermal treatments.

Since STO (001) has the two possible terminations, both of them were subject of presented studies. For homo-epitaxy, the termination mainly determines the kinetics of the deposited material. In the case of heteroepitaxy (YBCO, PCMO, LSMO etc.), the stacking sequence is determined by the terminating layer; thus, the process for obtaining of the termination and the reproducibility are as crucial as starting condition for a deposition.

- The TiO_2 termination of STO (001)** commercial substrates with presented modification is very successful. The smoothest and most reproducible surface morphology is obtained after the optimal treatment, consisting of the chemical etching with the HF buffered solution followed by *in situ* annealing at high temperature (900 -1000 °C) in oxygen environment similar to an usually deposition pressure (0.5 mbar). TiO_2 -terminated surface, with superior properties with respect to stability and morphology is obtained. Furthermore, it is suggested that the composition of the surface can be controlled, yielding single termination, provided

that the deposition rate of the constituents is known. Therefore, the starting condition for the growth of the controlled surface was satisfied.

ii. **The parameters for homoepitaxial growth of STO film on TiO₂** terminated STO (001) substrate are optimized in a way that provide conditions for 2D growth. Moreover, the termination of the film is also TiO₂ as well as the substrate is. In general, I conclude that the thin film growth on these substrates results in highly ordered surface.

iii. **The growth of high quality STO** epitaxial films on A-site terminated (110) NGO substrates using PLD assisted by high pressure RHEED was proofed. The reported data strongly support the initial assumption, that a single, **A-site (i.e. SrO), termination is obtained.**

iv. **The low temperature annealing** (200-300 °C, 14 hours, UHV) of TiO₂ terminated STO (001) causes unexpected effect of the surface turning from insulator to **conductor**. It can be explained as that the surface can lose oxygen even at low temperature under UHV conditions.

This study confirmed that prolonged UHV annealing for 1 hour at 800 °C of an HF etched SrTiO₃ (001) (TiO₂ terminated STO) sample gives rise to the formation of a new band between the Fermi level and the valence bands – VB (the conduction band) and appearing of a (1x2) reconstruction. The (1x2) surface reconstruction can disappear after several hours of re-annealing at low temperature (320 °C) under UHV conditions. Concerning the effect that at **low temperature** the lattices can **lose oxygen**, I proposed model that suggests that the refilling of the reconstructed surface occurs through the exchange of oxygen between the surface and the subsurface. It can be suggested that initial (1x2) reconstruction, in our conditions, was due to the creation and ordering of oxygen vacancies. On a Ti–O-terminated surface, the competition between bulk oxygen diffusion and the escape of oxygen from the surface causes that the (1x2) TiO₂ reconstruction is unstable under the used conditions of re-annealing (very low pO₂).

v. **Short-time heating (~1h) of SrTiO₃ (110)** at the temperature of 800 °C results in **(6x4) reconstructed surface** as observed by LEED. STM measurements confirmed that surface is covered by the rows with the same periodicity. The reannealing of the sample showed that (6x4) reconstruction is very

stable. The described results show that the used annealing treatment of the SrTiO₃ (110) gives suitable flat surface.

2. Anatase as TiO₂ phase, although is more efficient for several applications, including catalysis, has technological difficulties in implementations because of its instabilities, compared to the other polymorphous.

i. **The optimization** of parameters for a **high quality anatase thin film** growth was successful. The growth conditions allow that the film quality does not depend significantly on the type of substrates. The quality of epitaxial films was characterized using RHEED monitoring during growth, LEED, STM, XRD and TEM measurements. The presented result clearly indicate that the anatase thin films fabricated on STO (001), LAO (001) and SLAO (001) by laser MBE have crystal quality equivalent to bulk single crystals.

The surfaces of anatase films are (1x4) reconstructed during the growth and do not depend on the substrates' type and the strain effects. (1x4) reconstruction can be explained as the consequence of the natural way of anatase growth as ad rows model.

ii. **Sr diffusion** from the substrates to anatase films is very significant effect if growth or annealing temperature is around 800 °C. Sr inter-diffusion does not depend on the substrate type or the strains since similar effect is observed in both case of used substrates, STO (001) and SLAO (001).

iii. **The strain effect between** STO (001) and anatase causes strong inter-diffusion of Sr. The consequence of the strain and the Sr inter-diffusion is growth of "intermediate phase" with perovskite crystal structure and Sr_{1-x}TiO_{3-x} chemical formula. It is proposed that these structures have fully TiO₂-terminated surface which is thermodynamically stable. According to obtained RHEED, STM, SPA-LEED, and TEM results, additional deposition of few layers of TiO₂ could be used as way to obtain fully the TiO₂-terminated STO surface. As a demonstration of proposed approach, a few unit cell thick LaAlO₃ film was grown on specially prepared STO surface on which, between one and two layers, TiO₂ were beforehand deposited. The TEM measurements show clearly the interface indicating that the growth was entirely heteroepitaxial.

ACKNOWLEDGEMENTS

I would like here to express my thanks to the people who have been very helpful during the time of my stage at University "Federico II".

First of all I would like to thank my supervisor Dr. Fabio Miletto Granozio for having welcomed me in his lab and for his supervision during the past three years and for enabling me to be a part of the amazing MODA group. I am grateful to Fabio for encouraging me to always learn more and never to give up.

Also, I would like to express my thanks to Professor Umberto Scotti di Uccio for his support and helpful discussions which were not only about science.

I owe my special gratefulness to Professor Giancarlo Abbate, the coordinator of the PhD program, for strong support and for leading us through these three years.

I wish to express my sincere thankfulness to Professor Ruggero Vaglio, the director of Coherentia Institute, for his support in difficult moments.

I warmly thank and owe my deepest gratitude to my colleagues and at same time friends, past and present members of MODA lab: Marco, Zoran, Gabriela, Nathascia, Roberto, Paolo, Alessia and Davide. Their constant support kept me going and gave me strength during the hard times.

My special thanks are to Guido Celentano for help in fight against administrative problems.

Finally, my loving thanks go to Dragana, my beloved soul, who has shown great understanding and patience towards this work as well as everything else I do.

This work was financially supported by the National Fellowship of Italian Government.